FLUID LOADING AND HYDRO-ELASTIC RESPONSE OF TOWED PIPELINES

by

Young Sik Jang

A thesis submitted for the degree of Doctor of Philosophy
in the Faculty of Engineering, University of London

Department of Mechanical Engineering
University College London

August 1996

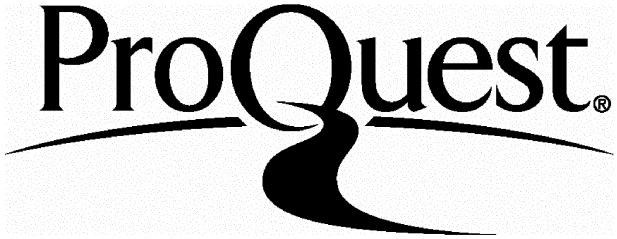

ABSTRACT

As oil production moves to deeper water and marginal fields, it is necessary to critically consider the merits and drawbacks of different subsea pipelaying techniques. The pipeline tow method is one of these. The basic concept of the tow method is to tow and lay the pipeline at an off-shore location after joining and testing the system at an on-shore fabrication site. This method, therefore, assures improved production quality of pipelines and can be applied economically and easily to all kinds of pipe. It does, however, pose a greater risk of failure due to ocean wave loads during its towing phase.

As a consequence, the tow method requires very careful design to achieve a very small submerged weight and maintain a nearly horizontal catenary that is then directly exposed to wave action. The physical problem of towed pipelines in currents and waves is exceedingly complex. The static component of the problem has a significant structural nonlinearity whereas the dynamic component is complicated by the quadratic nonlinearity of the hydrodynamic drag force and the unusual nature of the inertia force under a high near-tangential flow. Such an inertia force was first identified by Sir James Lighthill as applicable to circular cylinders with near-tangential incident flow in waves. The analysis must also account for the axial dynamics of the pipeline, towlines and the tow vessels. The research described in this thesis is aimed at investigating these issues and to obtain a quantitative understanding of their effects on the responses of typical towed pipelines.

Initially, the governing equations for towed pipelines and the analytical solutions for simplified cases are presented. In order to tackle a full, representative problem, the finite element method (FEM) is used both for static and dynamic analysis. For the static analysis, full nonlinear algorithms are implemented for the pipeline with simple support boundary condition at each end. To improve convergence performance during this nonlinear analysis, an enhanced catenary equation, which can consider the effect of a uniform normal component of current load, is used to obtain an initial

configuration for the nonlinear analysis. To consider deformation-dependent loading from currents and hydrostatic pressure, an improved version of the direct iteration method is applied using a conventional inner iteration approach with constant external load and an outer iteration to ensure that the residual forces resulting from the deformation-dependent loading are equilibrated. Both tow vessels and towlines are added to the static analysis model to form a dynamic analysis model with the initial stiffness method being employed during a direct integration procedure. The dynamic analysis is done in the time domain for regular waves with either the Morison equation or Lighthill's inertia loading formulation. The results from this complete FEM are verified by comparison with those from another finite element package (ABAQUS) for simplified models.

The results show that towed pipelines are highly influenced by external loads because their submerged weight must be kept very small. Therefore, an accurate application of deformation-dependent loading and hydrostatic pressure force is essential during the static analysis. In dynamic cases, high lateral responses are concentrated around the ends of the pipeline due to their proximity to the water surface and the soft constraints from towlines. The dynamic bending moment is mainly influenced by wave forces on the pipeline and increases rapidly as the pipeline approaches the water surface. The axial interaction between tow vessels and a pipeline is highly influenced by the property of the towline. Therefore, too stiff towlines may induce large dynamic axial force and give transient compressive axial force. The Morison formulation gives slightly less inertia force and response than that obtained from Lighthill's approach. Considering this slight difference and the uncertainties in wave kinematics and drag forces, it can be said that the Morison formulation still provides reasonable results for towed pipelines.

ACKNOWLEDGEMENTS

I am very grateful to my supervisor, Professor Minoo H. Patel, for his excellent guidance and continuous encouragement throughout this research. Without his advice, this thesis would not have been written.

My appreciation is extended to Dr. Joel A. Witz, Dr. Geoff J. Lyons , Dr. David T. Brown and Dr. Jie Fang for their valuable discussion and advice on this tough topic.

It has been a pleasure being with colleagues of the Santa Fe Laboratory for Offshore Engineering. I want to especially thank Mr. Renato Silva and Mr. Mark Dixon for their friendship and help.

The author expresses deep appreciation to Hyundai Heavy Industries which supported this research. I also want to extend my deep gratitude to directors and colleagues of Hyundai Heavy Industries for their encouragement.

Finally, I wish to give warm and special thanks to my family, Myoung Ok, Yong Jun and Hye Jin, for their patience and support over the last three and half years.

CONTENTS

LIST OF FIGURES

LIST OF TABLES

LIST OF PRINCIPAL SYMBOLS

normal characters Constants or variables

bold characters Vectors or matrices

a Wave amplitude

a_0 and a_1 Parameters for Rayleigh damping

$\boldsymbol{a}_b$ Acceleration vector of a pipe element

$\boldsymbol{a}_f$ Acceleration vector of fluid

c Propagation speed of wave profile

$\boldsymbol{C}$ Assembled damping matrix

C_a Added mass coefficient

$\boldsymbol{C}_a$ Added mass coefficient matrix

C_d or C_{dn} Normal drag coefficient

C_{dt} Tangential drag coefficient

C_M Inertia coefficient

D Diameter of a pipe

E Young's modulus

EA Axial rigidity

EI Bending rigidity

$\boldsymbol{F}$ Assembled load matrix

g Acceleration of gravity

h Water depth

k Wave number

$\boldsymbol{K}$ Assembled stiffness matrix

$\hat{\boldsymbol{K}}$ Effective stiffness matrix

$\boldsymbol{M}$ Assembled mass matrix

N_i Shape functions

P Pressure

$\boldsymbol{R}$ and $\boldsymbol{T}$ Transformation matrix, whose size is (3×3) and (12×12) respectively

s Arc length

t Time

T Tensile force

U Tow speed, current speed or relative fluid velocity

$\boldsymbol{U}$ Displacement vector of the finite element assemblage

$\boldsymbol{U}_t^{(k)}$ Displacement of k-th iteration at time t

u Horizontal displacement of a fluid particle

v Vertical displacement of a fluid particle

$\boldsymbol{v}_b$ Velocity vector of a pipe element

$\boldsymbol{v}_f$ Velocity vector of fluid

v_t Tangential component of fluid velocity

w Weight per unit length of a cable or pipeline

α and δ Newmark's integration parameters

γ Specific weight

ξ Damping ratios

λ Wave length

ρ Density

ω Wave frequency

$\boldsymbol{\omega}_b$ Angular velocity vector of a pipe element

ω_e Frequency of encounter

ϕ Velocity potential

Σ Summation

Δt Time interval (step) for numerical integration

$\Delta \boldsymbol{U}$ Incremental displacement vector

$\Delta \hat{\boldsymbol{F}}$ Effective incremental load vector

$\dot{\cdot}, \ddot{\cdot}$ First and second derivatives with respect to time

$'$, $''$, $^{(4)}$ First, second and fourth derivatives with respect to space

1. INTRODUCTION

The development of the on-shore and off-shore oil and gas industry has gone hand in hand with the use of steel pipelines for the transportation of liquids and also as structural elements of offshore jackets and assorted oil field structures (see Figure 1.1). In particular, steel pipelines laid on the seabed or buried underneath it play a crucial part in the transportation of produced fluids from satellite well heads to the platform and the export of processed oil and gas to on-shore terminals. Thus the technology of installing and operating subsea pipelines plays a big part in the success of most offshore field developments. There are various methods for pipeline installation, including lay-barge, reel-barge and tow methods - some of these being more suitable for a particular application than others. The lay-barge method is the most common although it is expensive in operation, mobilisation and demobilisation. Moreover, this method has many drawbacks for bundles and insulated pipelines as well as for deep water applications.

As oil production moves to deeper water and marginal fields, it is necessary to develop alternative methods that are able to economically lay various kinds of pipeline. The pipeline tow method is one of them. The basic concept of the tow method is to tow and lay the pipeline at an off-shore location after joining and testing the system at an on-shore fabrication site. This method, therefore, assures improved production quality of pipelines and reduces offshore work significantly. Also, towing requires relatively small vessels for transportation of pipelines to the installation site. Consequently, the tow method can be applied economically and easily to all kinds of pipe including pipelines, bundles, umbilicals, and tension leg platform (TLP) tethers regardless of pipe size, pipe type and water depth. However, the tow method also has many inherent drawbacks. The selection of shore based fabrication sites with long lengths and moderate surf action is very difficult. This along with environmental conditions along the tow route, consequently, limits length of pipelines. Also the tow method requires a special design for laying operation and extremely careful buoyancy and weight control. Moreover, such towed pipelines

may be exposed to severe wave action during its towing phase that can cause damage or a total write off of the pipe. Therefore, detailed analysis for the tow condition is necessary to check the influence of waves and currents. Since there have been relatively few detailed studies on towed pipe analysis, this has led to conservative design. At the same time, all of the physics of towed pipeline behaviour in currents and waves has not been completely resolved. Two factors that continue to introduce uncertainty are the changes in fluid loading caused by incident flow on a towed pipeline at a small angle to the horizontal and the dynamic axial interaction of pipeline tension with the wave induced horizontal motion of the towing vessels. The present research is, therefore, aimed at investigating these uncertainties and thereby improving the accuracy of towed pipeline analysis.

Initially, a summary of pipeline types, lay-barge, reel-barge and tow methods, a tow system and tow history are described in the following sections. It also includes an overview of this thesis. A review of previous work is summarised in Chapter 2. It includes material directly or indirectly related to tow analysis and experiments for pipelines and TLP tethers. The governing equations for the tow system are described in Chapter 3. They include the equilibrium equations for slender structures and fluid-induced loads on the tow system. Chapter 4 describes a finite element formulation together with a solution procedure for nonlinear static and dynamic analyses. The results are compared in various ways and together with a sensitivity analysis are presented in Chapter 5. Finally, important items found from this research are summarised in Chapter 6.

1.1 Pipeline Types

Based on their cross-sectional properties, pipelines can be classified as conventional pipelines, insulated pipelines and bundles (see Figure 1.2).

Conventional pipelines consist of a steel pipe, corrosion coating and concrete coating (see Figure 1.2.a). The steel pipe is designed to resist hydrostatic pressure and the

tension and bending moment induced during pipelaying. The concrete coating, sometimes known as the weight coating, provides on-bottom stability and negative buoyancy during laying.

Insulated pipelines are used for hot fluids to reduce heat transfer over long routes. The structure of such pipelines becomes complex (see Figure 1.2.b) to protect insulation material during laying by the lay-barge method.

The structure of bundles consists of the outer carrier pipe, inner flowlines or service lines, and transverse bulkheads (see Figure 1.2.c). The carrier pipe provides protection against external hazards and is an initial barrier against leaking product. The submerged weight of the flooded bundle provides on-bottom stability and resistance to upheaval buckling without trenching or burial. The carrier pipe together with two end bulkheads provides a closed container, which when filled with inhibited sea water gives a corrosion free environment. This reduces or avoids the need for individual corrosion coating of each of the flowlines. Thermal insulation of the flowlines, when required, can easily be accommodated in the carrier pipe design.

1.2 Lay-Barge and Reel-Barge Methods

Purpose-built barges with special equipment are necessary to lay pipelines using the S-lay, J-lay or reeling methods. The selection of lay method depends on pipe properties, water depth and environmental conditions.

The Lay-Barge Method

The lay-barge method (see Figure 1.3.a and 1.3.b) is the most common for subsea pipeline installations. The technique operates as follows:

1. The pipeline is delivered to the lay barge in single or double length joints, of 20 or 40 feet, by a cargo barge.
2. A deck crane transfers the pipeline to storage racks on the lay barge.

3. During laying, the crane transfers the pipeline from the storage racks to an automated conveyor for feeding the pipeline to the line-up table.
4. After welding, the pipeline's field joints are radiographically examined and coated with corrosion coating and, if necessary, weight coating.
5. The pipeline laying operation is continuous with the barge slowly moving forward as the jointed pipeline moves on rollers, onto a stinger and then onto the seabed.

Conventional lay barges require additional vessels to support a laying operation. The spread generally includes one or more anchor handling boats, cargo barges and tug boats.

The stinger is an articulated ramp over which the pipeline is fed off the side of the barge. The stinger controls the bending of the pipeline around the surface whereas a tensioner provides a hold-back force to limit the sag-bend curvature of the pipeline. According to the method of tension application and stinger position, two pipeline laying configurations are possible and called respectively S-lay and J-lay. In the S-lay method (see Figure 1.3.a), the tension is applied horizontally and the welded pipeline is lowered over a stinger at a specific departure angle. However, if the water is deep and the pipeline is heavy, very high tension is required to keep the sag-bend area within acceptable bending moment levels. In the J-lay method (see Figure 1.3.b), pipeline joints are welded and tensioned on a vertical or near-vertical stinger to minimise the bending moment at the clamped end. This mode reduces suspended pipeline length and, consequently, the required tensioner force. Therefore, the J-lay method is chosen to install heavy pipelines in deep water - generally beyond the limit of the S-lay method.

The Reel-barge Method

The reel-barge method (see Figure 1.3.c) uses a continuous length of pipeline coiled onto a reel. Pipeline installation is accomplished by uncoiling and straightening the pipeline as the barge moves forward. Pipelaying can take place at relatively high

speeds and dynamic positioning can be used as opposed to multipoint anchor systems. This method has been used extensively to install small diameter pipelines in relatively shallow water depths. Because of coiling, no concrete coating can be used and a relatively heavy wall thickness is required to avoid pipe flattening and, in some cases, to provide additional weight for on-bottom stability.

Two configurations of the reel are in use, the vertical reel and the horizontal reel. Use of the vertical reel is advantageous in deep water applications, since it can be loaded for discharging from the top and requires a short stinger or no stinger at all.

1.3 Tow Methods

The basic concept of the tow method is to tow and lay the pipeline after joining and testing the system at a fabrication site. This means that the tow method can improve pipeline quality and reduce offshore work significantly. Also, towing requires relatively small vessels to transport pipe strings to the installation site.

There are various tow methods suitable for pipe property and tow routes and they can be classified as surface, sub-surface, mid-depth, off-bottom and bottom tow methods (see Figure 1.4). Installation procedure common to all tow methods and characteristics of each tow method are summarised in this section.

Procedure of Installation

The sequence of pipeline installation by the tow method is fabrication, launch, tow, and positioning and the usual procedure for each step is as follows:

- Fabrication

1. Short pipeline segments are assembled to design length by butt welding, radiographic testing, wrapping and coating.
2. Buoyancy tanks, buoys or chains are attached.

3. Towheads or special pipeline termination units for subsea connection are fitted to each end of the long pipeline. Completed bundle layout and details of sub parts used in the East Frigg Field are shown in Figure 1.5.
4. The pipeline is cleaned and pigged.
5. The pipeline is hydrostatically tested.
6. After dewatering the pipeline, it is filled with pressurised nitrogen to prevent ingress of water in the event of a leak during the tow.

- Launch

1. A high capacity pull-barge is anchored at sea in line with the pipeline.
2. The pipeline is then pulled with cables attached to the towhead and bogies.
3. The acoustic telemetry system is checked.

- Tow

1. Tow vessels pick up tow pendants.
2. Tension is applied on the pipeline and the tow proceeds to the installation field.
3. The towhead position, internal pressure, and strains of the pipeline are continuously measured.

- Positioning

1. An array of acoustic transponders is deployed on the seabed to assist accurate positioning.
2. Anchor blocks are positioned at strategic locations along the pipeline route corridor and end target areas. These are used to secure the pipeline and towheads in their final positions.
3. The pipeline is flooded and lowered to the seabed and secured in place using the pre-installed anchor blocks.

The Surface Tow

The pipeline is kept floating (see Figure 1.4.a) with self buoyancy or additional buoyancy tanks. Detailed analysis is required because the pipeline is very sensitive to the influence of surface waves. Generally this method is limited to sheltered areas.

Its advantage is that it requires a relatively low tow force. However, it has major disadvantages - it is very susceptible to waves and is exposed to marine traffic during the tow. This tow method also requires special considerations for positioning the pipeline.

The Sub-Surface Tow (The Near-Surface Tow)

Sub-surface tows use flotation devices to support negatively buoyant pipelines below the significant wave active zone (see Figure 1.4.b). Generally cylindrical spar buoys are used because they experience relatively small hydrodynamic loads. The advantages and disadvantages of this technique are similar to those of the surface tow.

The Mid-Depth Tow (The Controlled Depth Tow)

Combining the advantages of the surface and off-bottom tow methods, this method is particularly suitable for the transportation of bundles in more highly developed offshore areas with congested seabeds. Chains are attached to the pipeline at specified intervals for additional weight and lift force. At rest or at low tow speeds, this method is the same as the off-bottom tow in that chains are in contact with the seabed. As the tow speed increases, the resultant flow around the system generates a net lift force that reduces system weight allowing the entire system to be towed free of the seabed (see Figure 1.4.c). Careful control of tow speed and tension applied by the tow vessels enables the pipe configuration and deflection to be maintained within the required tolerances.

Its advantages are that the pipeline is below the most severe wave loading regime at the sea surface and can be laid on the seabed rapidly in worsening weather conditions. However, this technique requires very careful control of weight and buoyancy.

The Off-Bottom Tow

The total buoyancy of the system is determined so that the pipeline floats above the seabed with a part of the drag chains remaining in contact with the seabed (see Figure 1.4.d). For this purpose chains and/or buoyancy tanks are attached to the pipeline at specified intervals. If the tow route includes areas where lateral currents might affect the stability of the pipeline, the length of chain pulled on the seabed can be designed to provide a force to stabilise the line.

Its advantages are that it requires a relatively low tow force and a towed system is less exposed to other marine traffic. Also such a towed system is more stable against wave and current action. However, this technique requires a smooth sea bed and special design of the buoyancy tanks both for towing and releasing.

The Bottom Tow

In this bottom tow method, the pipeline is in contact with the seabed during towing (see Figure 1.4.e). This makes the nature of the tow route one of the most critical design factors. Seabed conditions along the route affect coating design for abrasion criteria, stability during tow, tow vessel size and optimum pipeline length. The on-bottom weight of heavy pipelines, however, can be reduced by the addition of buoyancy tanks.

The major advantages of this method are that a towed system is the least exposed to wave conditions and it can be temporarily parked on the seabed at any time if sea

conditions become bad. Also this technique requires only one tow vessel although it needs higher tow forces. The major drawback is that there are limitations to the tow routes so as to avoid obstructions. Also a careful design of a pipeline coating is essential to avoid damage.

1.4 System for Mid-Depth Tow

The tow system for mid-depth tow consists of a pipeline, chains, pipeline termination units, tow spread, towlines, and subsea telemetry instrumentation (see Figures 1.4.c and 1.5). The function and requirement of each item are summarised in the followings.

The Pipeline

The pipeline provides buoyancy during the towing and installation phases so that it is nearly horizontal and friction forces on the seabed are minimised during the offshore pull-in phase. In the case of bundles, the carrier pipe provides sufficient on-bottom stability to the pipeline during the production life of the field since it is flooded with inhibited water at completion of the offshore pull-in. In order to prevent collapse during the tow due to hydrostatic pressure, the annulus between the sleeve and outer carrier pipe is filled with nitrogen.

Chains

Chains are attached (see Figure 1.6) to provide additional weight to any system with limited submerged weight. During tow, these chains also create a lift force, reducing the system submerged weight and thus the pipeline deflection. Usually the first and last chains are longer than the others for checking the final submerged weight of the system by measuring their lengths on the seabed before tow out. Chain intervals along the pipeline are decided by considering pipeline trim and its final positioning on the seabed.

Pipeline Termination Units

A towhead, a connection unit and a buoyancy tank are prepared at each end of the pipeline (see Figure 1.5). Each connection unit incorporates special facilities for convenient mechanical or hydraulic connection with other structures such as wellheads and other pipelines. Because towheads or connection units are somewhat heavy, their design must satisfy the concept that the entire flowline would be suspended in neutral buoyancy when the connections are made. For this, buoyancy tanks are arranged to compensate the unbalanced weight from towheads or connection units.

The Towspread

The towspread generally consists of four vessels. The leading primary vessel has a high bollard pull and is fitted with a navigation system and, in some special cases, a constant-tension winch. The trailing vessel is generally smaller than the leading vessel as it only requires to exert a relatively small tension force for the control of the pipeline. A third vessel is equipped with an acoustic telemetry system to monitor position, depth, internal pressure and the loads on the pipeline. It also serves as a back-up vessel for the leading or trailing vessels. A fourth vessel is used to warn-off other ships around the tow route.

Towlines

Towlines are usually composite systems that have chain bridle and/or pendants at the end of the pipeline and a synthetic fibre rope between the end of the chain and the vessel. Most synthetic ropes are made of polyamide (nylon) or polyester (dacron) and their properties are quite different (see Table 1.1 and Figure 1.7). Because nylon is over twice as extensible as polyester and thus absorbs more energy for a given load, it is preferred in applications where extension and energy absorption are

of prime importance. However, nylon loses strength rapidly when wet, whereas polyester does not (see Figure 1.7), so polyester offers better performance than nylon in wet cyclic loading. Both nylon and polyester ropes are quite extensible and their densities exceed that of water.

Subsea Telemetry Instrumentation

A subsea navigation transponder is mounted at each end of the pipeline to aid the navigation of the pipeline into a predetermined position on the seabed and to monitor the position of the ends of the pipeline with respect to the tow vessels. It is usual to mount strain gauges and depth-indicating pressure transducers near the middle of the pipeline with their output transmitted to the surface by an acoustic telemetry package. The strain gauge package measures the horizontal and vertical strains at the middle or, if necessary, other special parts of the pipeline.

1.5 History of Towed Pipelines

Before the oil industry developed offshore fields, tow methods had been frequently used to install pipelines in sheltered seas or lakes. However, its application to offshore fields was considered so risky that the lay-barge method was generally used. As the most productive fields in shallow to moderate water depth were discovered and exploited, the remaining fields found in deeper water became increasingly economically marginal. At this time, despite its technical and operational risks, tow methods for laying pipelines became increasingly more attractive compared to the expensive lay-barge approach. An additional factor was that as the oil price became low in the mid 1980s, there was an urgent need for alternative lay methods to reduce installation cost. The tow method offered one low cost solution. Pipeline installations by tow methods since 1980 are summarised in Table 1.2. It shows that the tow method is applicable regardless of pipe types, pipe size and installation sites.

In the case of the North Sea, the mid-depth tow method has been primarily used since its first application in the Murchison field in 1980. The largest of the bundles installed in the Murchison field had a diameter of 12.75 inches, a weight of 250 tons and a length of 2 km.

In 1988, a diverless installation technique was applied in the Elf East Frigg field. Two flow line bundles of 24 inches in diameter and 1.6 km in length were installed by the mid-depth tow method to connect its satellite manifolds to the gathering manifold. A remote control pull-in technique was applied from a dynamically positioned diving support vessel.

In 1990, the scope and scale of bundle installations increased greatly with the development of the Shell Expro Osprey field. The vital statistics for this project included a bundle diameter of 38 inches, a weight of 3,500 tons and a length of 3.5 km.

In 1991, two pipeline bundles were installed in the Occidental Piper field, the largest of which had a diameter of 40.5 inches, a weight of 6,700 tons and a length of 6.7 km. Both ends of the bundle incorporated towhead structures of over 100 tons each, which included the emergency shutdown valve assemblies.

In 1994, bundles and pipelines of 34 km in total length were installed in a Western Australian field by the bottom tow method. For this, a new 4.5 km long on-shore fabrication site was established and successive pipe strings were towed along the seabed to their offshore location using a high powered vessel spread. Once in place the pipe strings were joined together by divers, then stabilised on the seabed by a combination of trenching and anchoring. The total length of the lines was about 26 km of bundled 20 inches diameter pipeline plus a further 8 km of 6.7 inches diameter pipeline.

The tow method was also applied to the installation of mooring tethers of a tension leg platform (TLP).

In 1995, 16 tethers of Conoco's Heidrun TLP were towed out from a Norwegian fjord after a series of inshore towing and upending trials. Each tether had a length of 270 m, a diameter of 1.1 m and a wall thickness of 38 mm. For towing, tethers were

fitted with foam-filled buoyancy units near each end to offset the weight of the threaded section at the tether top and the bottom connector assembly. In the towed configuration, a tether had a displacement of 320 tons, with a draught of around 2 m at the ends and 4 m in the middle. After undergoing a 17 hour tow at 8 knots, the tethers arrived at the Heidrun field and were upended and slotted into concrete foundations placed on the seabed.

1.6 Overview of Thesis

Although the tow method offers many merits for the installation of pipelines, it requires very careful design due to the high risk of damage to the pipelines that are directly exposed to severe wave action. The review of previous literature reveals that very little work has been performed for towed pipelines and, moreover, the analysis schemes do not seem to have been firmly established. Generally the analysis scheme was imported from riser analysis.

From a structural point of view, the behaviour of towed pipelines, however, may be quite different to that of risers considering the typical configuration of each structure, that is, near-horizontal configuration of towed pipelines compared to the near-vertical one of risers. Also the tow vessels may have an influence on the behaviour of the pipeline via very flexible towlines because, in the case of long pipelines, the mass of the tow vessels is comparable with that of the pipelines.

From a hydrodynamic point of view, Morison equation that was originally developed for vertical piles has a fundamental flaw for towed pipelines which are exposed to a relatively high incident flow (due to towing) at small angles between tow direction and pipe centre line.

The above two features indicate that the physics of towed pipelines has not been completely established as yet. The research described in this thesis is mainly aimed at investigating the above two issues and to obtain a quantitative understanding of their effects on towed pipeline responses. The physical problem of towed pipelines in currents and waves is exceedingly complex. The static component of the problem

has a significant structural nonlinearity compounded by the quadratic nonlinearity of the hydrodynamic drag force and the unusual nature of wave-induced fluid loading. This is further complicated by the axial dynamics of the pipe, its towlines and the towing vessels. All of this means that the finite element method (FEM) is the only feasible way of tackling the problem. The work here uses the FEM for both static and dynamic analysis. For the static analysis, full nonlinear algorithms are implemented for the pipeline with simple support boundary condition at each end. To improve convergence performance during this nonlinear analysis, an enhanced elastic catenary equation, which can consider the effect of a uniform normal component of current load, is used to obtain an initial configuration for the nonlinear analysis. Both tow vessels and towlines are added to the static analysis model and an initial stiffness solution technique is employed during direct integration procedure. The dynamic analysis is done in the time domain for regular waves with either Morison equation or Lighthill's fluid loading formulations. Since a typical towed pipeline is designed to have very small submerged weight, external forces significantly influence structural behaviour. Therefore, particular attention is paid to considering the accuracy of loads from currents, waves and hydrostatic pressure. Deformation-dependent loading is applied to both static and dynamic analysis.

One of the problem associated with such complex FEM is that it is difficult to formulate simple analytical cases for comparison and verification of the FEM results. This difficulty is circumvented to some extent by using two finite element formulations - one based on specifically written code and the other using the ABAQUS finite element package.

Table 1.1 Comparison of properties of nylon and polyester fibers (Flory et al., 1988)

Property	*Nylon*	*Polyester*
Specific Gravity	1.14	1.38
Extension at Break, *%*	19~25	11~19
Extension at 50*%* of Break	9~14	5~11
Breaking Length, *km*	67~75	73~84
Water Absorbtion, *%*	0~12	0~0.82
Softening Point, ℃	170~180	230~240
Dry Melt Point, ℃	213~219	256~260
Wet Melt Point, ℃	170	213

Table 1.2 Pipeline installation by tow methods

Operator	*Field*	*Year*	*Length* (m)	*Mass* (ton)	*Diameter* (inch)	*Remarks*	*Method*
WAPET	West Australia	1994	26,000		20.00	Bundle segments are joined by divers	Bottom
Chevron UK Ltd.	Alba	1993	3,000	1,328	28.50	12" flowline within a 16" sleeve pipe + 4" fuel oil line	Mid-Depth
Phillips Pet.Co. Norway	Embra	1992	5,200	1,578	24.00	14" duplex flowline	Mid-Depth
Occidental	Piper	1991	6,700 2,250	5,900 830	40.00 26.00	2 off 16", 10"+8" ESV's integrated on both ends 3 off 6"+8" umbilical	Mid-Depth
Shell	Gannet	1990	3,600 3,200 2,600 2,200		37.24 37.24 29.37 29.37	14×50, 100 and 150mm lines 8×50, 100 and 150mm lines	Mid-Depth
Shell Expro	Osprey	1990	3,500 3,100	2,468 2,383	38.00 38.00	2 off 8" insulated 10" mid field tie-in As above intermediate manifold, 10" plus umbilical	Mid-Depth
Elf Aquitaine Norge A/S	East Frigg	1988	1,600 1,600	555 555	24.00 24.00	10"+4" umbilical. Diverless installation and pull-in.	Mid-Depth
Occidental Pet. Cal.	Scapa	1986	4,394 4,390	1,811 1,809	28.25 28.25	10" plus 6" insulated, 3 off 3" insulated	Mid-Depth

Operator	*Field*	*Year*	*Length* (m)	*Mass* (ton)	*Diameter* (inch)	*Remarks*	*Method*
Placid Oil Co.	Green Canyon	1986	16,000 16,000		14.00 16.00	Oil export line Gas export line	Bottom
Bohai Oil Co.	Bohai, China	1985	1,600		12.75	4 segments of 400m insulated pipeline	Sub-Surface
Shell Expro	Central Cormorant	1984	3,343 3,343	1,250 1,250	26.00 26.00	8" insulated	Mid-Depth
Shell Expro	Central Cormorant	1982	3,345 3,343 3,310 3,310	1,250 1,250 1,065 1,065	26.00 26.00 24.00 24.00	8" insulated, mid field tie-in 2 off 4" insulated, mid field tie-in	Mid-Depth
Occidental Pet. Cal.	Claymore	1981	2,053 3,206	591 1,152	14.00 26.25	8" insulated, 5 hydraulic lines 10" insulated, 2 off 8" insulated, 10 hydraulic lines	Mid-Depth
Conoco UK	Murchison	1980	2,005 1,242 800	255 149 102	12.75 12.75 12.75	2 off 3" insulated, 5 off hydraulic control lines	Mid-Depth

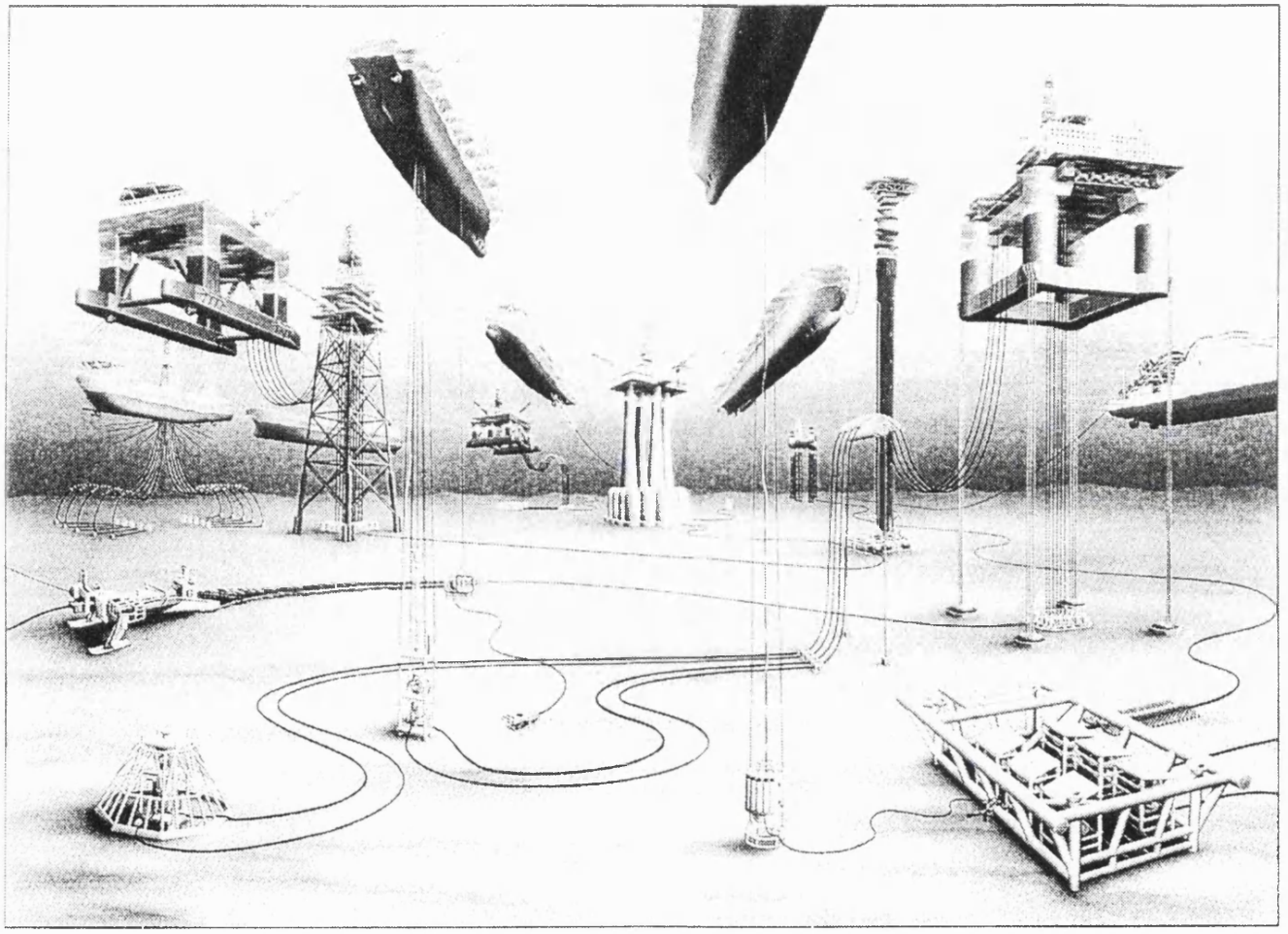

Figure 1.1 Various applications of pipe elements for subsea development (Hart's euroil, Sept. 1993)

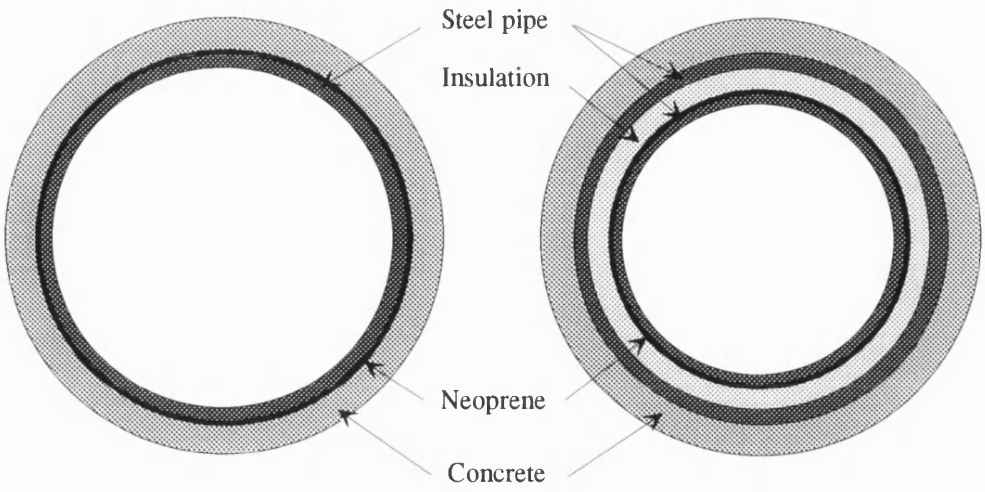

(a) Conventional pipeline (b) Insulated pipeline

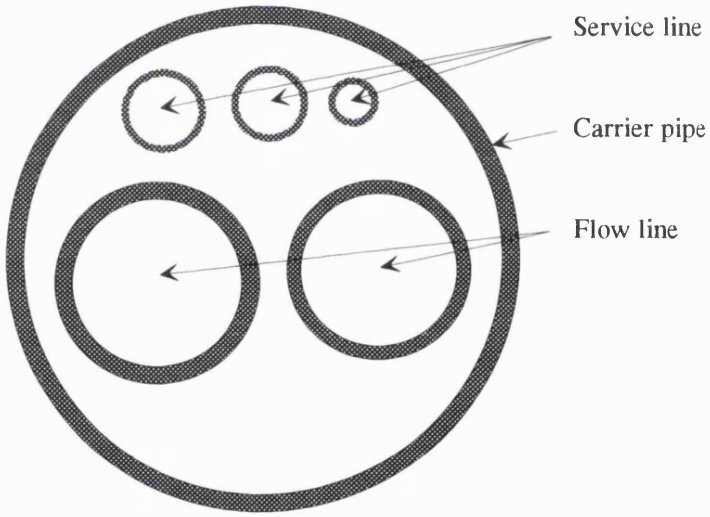

(c) Bundle

Figure 1.2 Pipeline types

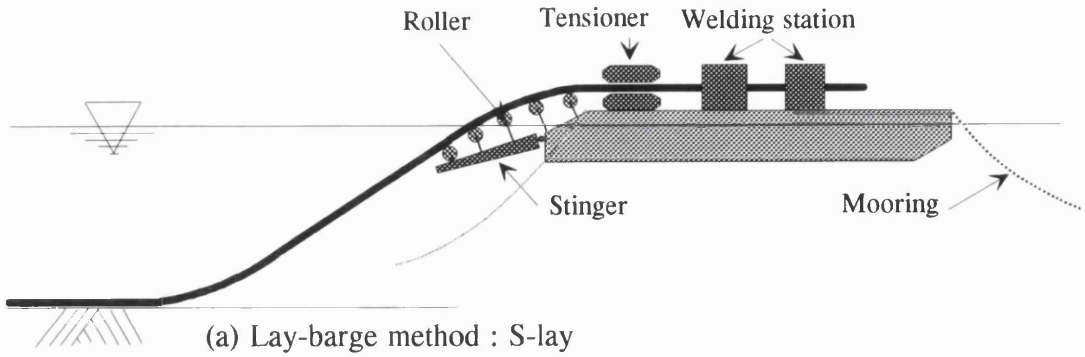

(a) Lay-barge method : S-lay

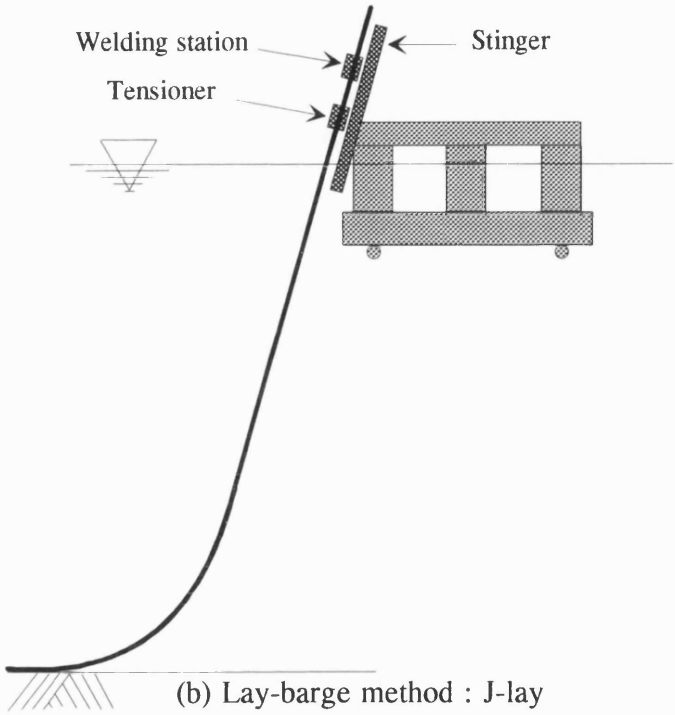

(b) Lay-barge method : J-lay

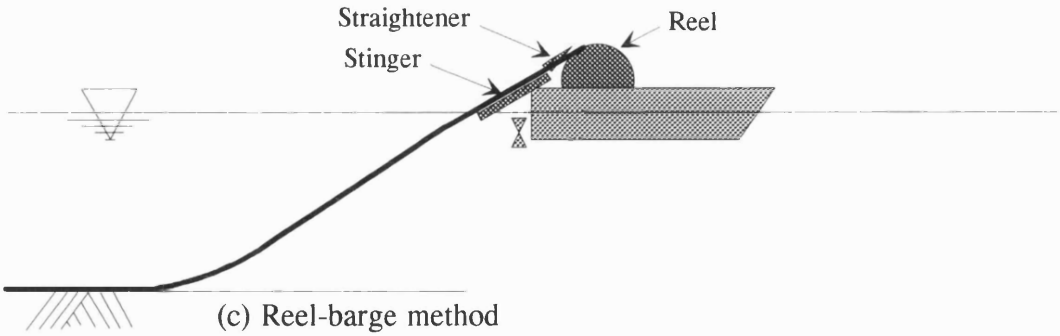

(c) Reel-barge method

Figure 1.3 Lay-barge and reel-barge methods

(a) Surface tow

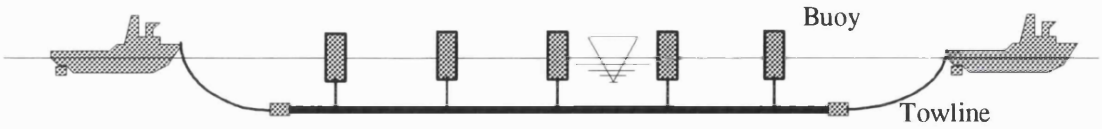

(b) Sub-surface tow

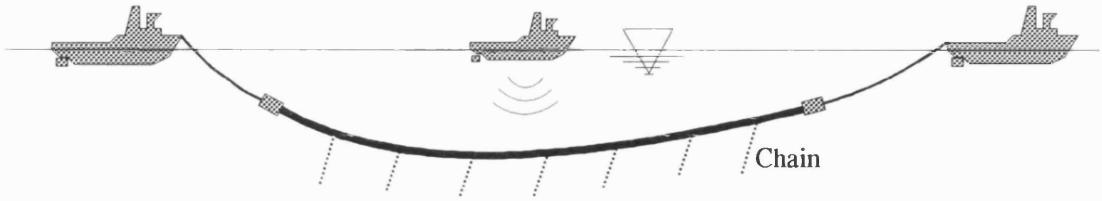

(c) Mid-depth tow

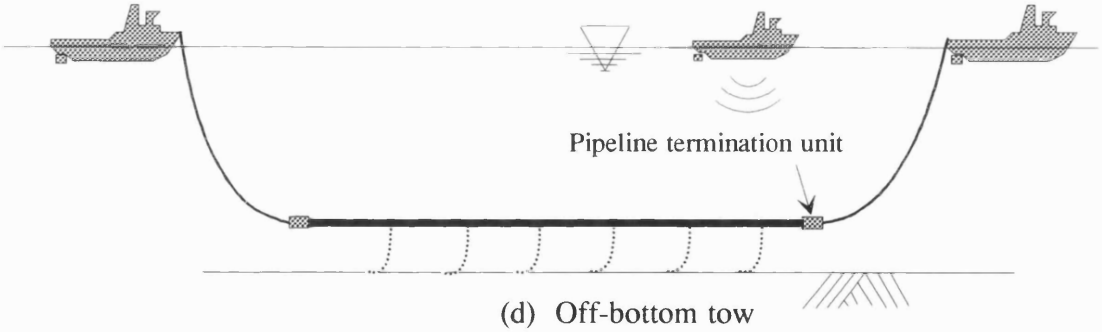

(d) Off-bottom tow

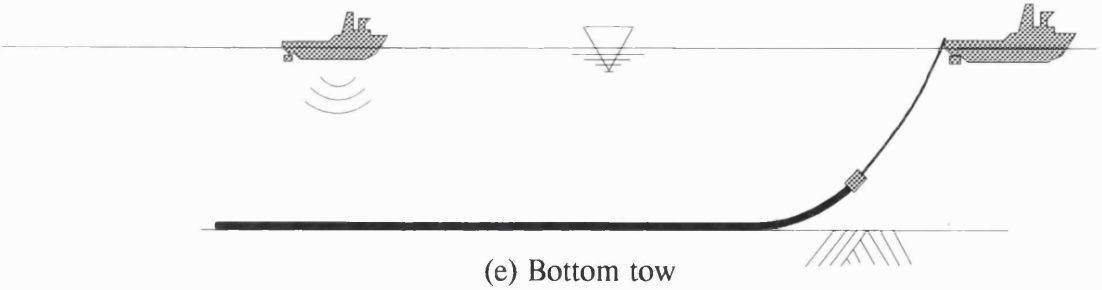

(e) Bottom tow

Figure 1.4 Tow methods

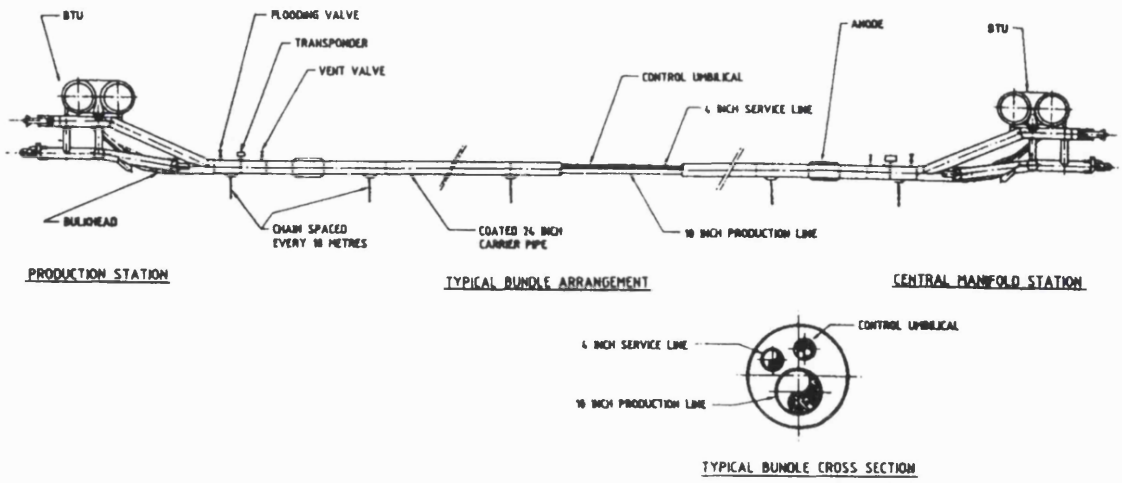

(a) Layout of bundle

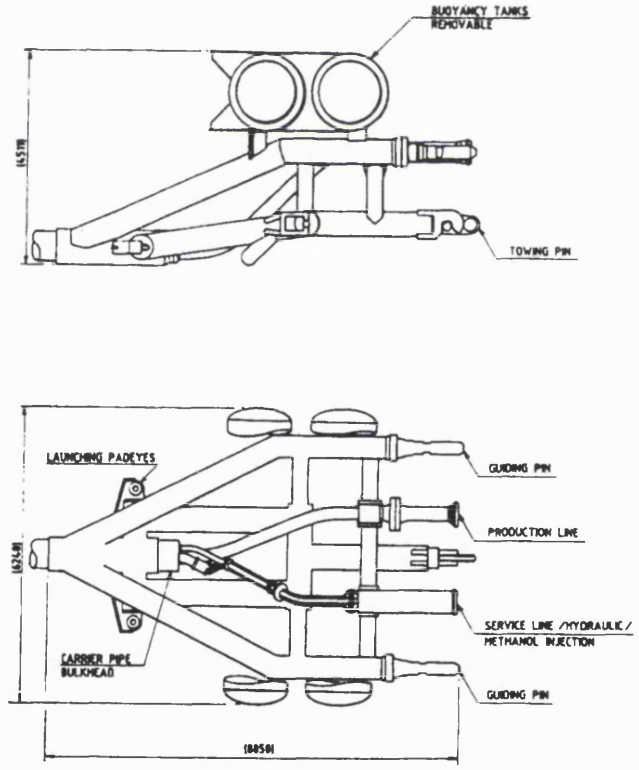

(b) Bundle termination unit

Figure 1.5 Layout of bundle and termination unit (Pelleau et al., 1988)

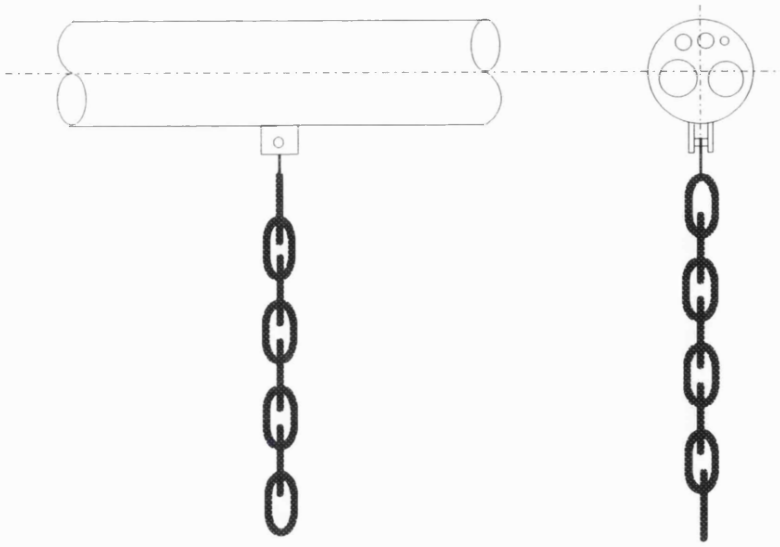

Figure 1.6 Layout of connection of a bundle and a chain

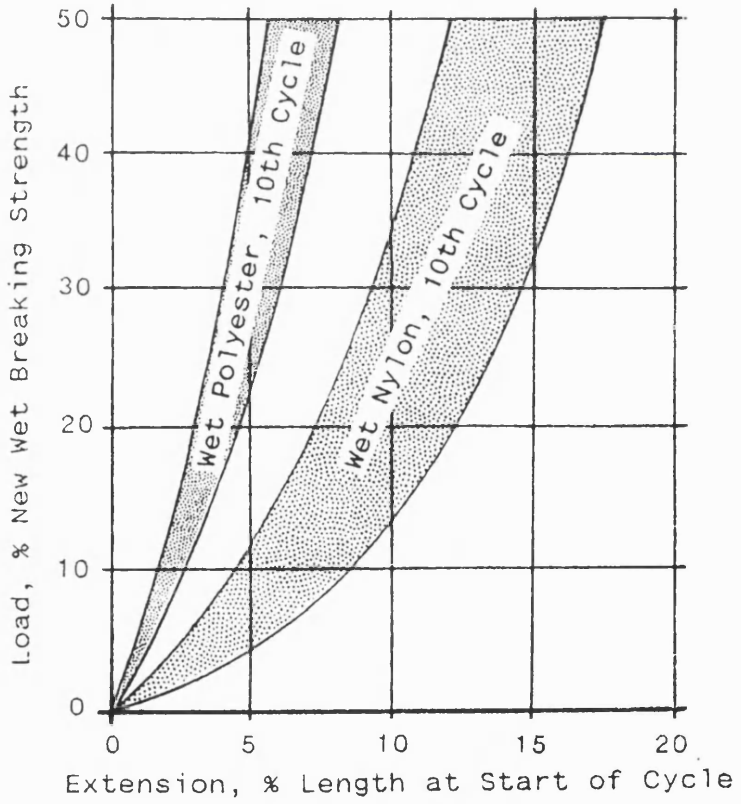

Figure 1.7 Load-extension curve bands, broken-in wet nylon and polyester ropes (Flory et al., 1988)

2. REVIEW OF PREVIOUS WORK

Although a towed pipeline is a simple structure, the effects of waves, currents, vessel motions, buoys and chains are such that it requires a very complex analysis to predict its behaviour. This complexity has discouraged work to predict the behaviour of towed pipelines during their tow out and installation phase. This review of previous work on towed pipes presents the work that has been done and summarises the relevant analysis methods.

2.1 Towed Pipes

A pipe is exposed to static and dynamic actions during towing which can cause extensive damage including complete destruction requiring abandonment of the pipe. So detailed analysis for the tow condition is necessary to check the influence of waves and currents. In particular, the dynamic behaviour of towed pipes is very important because the motion and load under the towed condition are dominated by large deflection dynamic responses. There has been, however, very little work to predict the behaviour of pipe during towing because of the considerably complicated phenomena resulting from its interaction with wave, current, tow vessels, and attachments such as buoys or chains.

Kan and Healey (1981) have studied a towed pipeline using a transfer matrix method. The transfer matrix is based on the Bernoulli-Euler beam model with large deflections included for the two-dimensional static case. The large deflection non-linear two-point boundary value problem is successively linearised and an element structural state transfer matrix method is utilised for the solution of an equivalent linearised system. This method is convenient rather than the more conventional stiffness matrix method since all operations are performed through matrices of small size. The authors have checked the sensitivity of a static pipe configuration due to changes in tow speed and number of fully submerged buoys with the same horizontal tow force and have presented results for both cases. They show that the higher the tow

speed, the larger the maximum vertical deflection and the more buoys there are, the less the deflection is. Therefore, higher tow force or more buoyancy must be added to maintain safe stress levels at higher tow speeds.

Morton (1981) has analysed and monitored the behaviour of a bundle in a mid-depth tow. Even though this paper did not include analysis results, it showed real phenomena during tow. The report said that as the speed increased to seven knots, the bundle approached too near the surface due to the increase of lift force. Under six knots, the bundle was visible from the surface. In some cases, the pipeline had a 'snaking' characteristic which was not evident during model tests. The reason for this is not clear - possibly due to a malfunction in the monitoring system or due to as yet unknown phenomena.

Costello et al. (1983) have presented detailed procedure for the mid-depth tow of an insulated bundle. The annulus between the sleeve and outer carrier pipe was filled with nitrogen to prevent collapse due to hydrostatic pressure. The external carrier pipe was designed to provide adequate buoyancy during towing and required sufficient wall thickness to withstand beach-pull break-out load and towing loads. Studies were performed to determine wave forces acting directly on the bundle, varying forces in the towline due to vessel motions and vortex shedding due to currents perpendicular to the bundle.

Verner et al. (1984) have presented a manoeuvring simulation technique for long towed pipelines. The authors claim that even though this technique specifically addresses surface towing, it is generally applicable to other tow methods as well. For the towing technique, a simulation procedure should be capable of simulating a flexural member undergoing tension with large deformations and interaction with waves or currents. Numerical simulation has been done using the finite difference method for inextensible rods. The authors have described the detailed procedure of their finite difference scheme and compared the results of numerical simulation with those of model test performed using pipeline models with buoyancy tanks and spar

buoys. Four manoeuvring cases were simulated during testing; lateral towing, circular towing, hand-over and alignment, and loss of tow vessel service during laying. Results show good correspondence between the numerical analysis and the model tests although the global behaviour of the pipeline is different between pipelines with buoyancy tanks and spar buoys. However, the authors have considered current only - they have not considered the effects due to wave action that may be very severe for surface tows.

Tatsuta and Kimura (1986) have performed model testing, numerical analysis and fatigue analysis to predict the influence of waves on a pipeline undergoing sub-surface and surface tows. A finite difference method for inextensible rods has been used. Hydrodynamic force and buoyancy on the pipe's supporting buoys have been calculated under the assumption that the buoy moves with the pipeline. Model tests and analyses have been performed for three types of model of relatively short length (see Figure 2.1.a), 200 m, under longitudinal regular and irregular waves; a pipeline with five buoys (Type I), a pipeline with seven buoys of smaller size (Type II) and a pipeline without buoys (Type III). The strains in the pipeline and the tensions of the cables connecting the pipeline and buoys have been measured.

Test results in regular waves show that larger strain responses are obtained as the measured position approaches closer to the centre of the pipeline (see Figure 2.1.b). This trend is common to all types of model and most wave periods. For short period waves, the response of the pipeline with buoys, Type I or II, is larger than that without buoys, Type III, due to resonant vibration arising from the relationship between wave length and buoy spacing. For long period waves, however, the trend is the opposite to this because the buoys cause a damping effect. If the pipeline has large buoys, the response becomes non-linear with the wave height and if smaller buoys or no buoys are used, the response becomes more linear. This suggests that the non-linear motion of buoys significantly affects the motion of the pipeline. It is interesting to note that excellent agreement between analysis and test results is obtained for Type III (see Figure 2.1.c), especially in waves of small amplitude. The detailed analysis scheme for this case has not been described.

Nedergaard et al. (1989a, 1989b) have produced two numerical methods for dynamic simulation of long pipelines undergoing off-bottom tow, sub-surface tow and positioning. They have used a finite element model and a modified modal integral equation technique. The finite element model is based on the incremental method in which the solution of each time increment is obtained by an iterative secant stiffness method. They include methods for modelling applied forces from the tow vessels, buoys and stabiliser chains. Their modified modal analysis model works in the time domain and is based on the impulse response method. The solution is based on the overdamped solutions of the free oscillating problem and numerically stable solutions for the large deformation problem of hydrodynamically damped pipelines are obtained. The authors have recommended that the finite element model is useful for the detailed analysis of problems with large deflection or special boundary conditions whereas the modal analysis model is useful for large scale simulations such as positioning. The authors have considered normal drag force only on the buoys and neglected bending stiffness and longitudinal drag forces of pipelines.

Langley (1989) has proposed an analytical solution scheme of towed pipelines for the general case of random spreading seas. Initially, the dynamic response of an infinite pipeline is calculated and it is modified to incorporate relevant boundary conditions. During the development of the scheme, the author has made many assumptions to simplify the formulation although these allow the application of this scheme to very limited cases. The author has disregarded a static component and, instead, used a straight line directly for the dynamic analysis although the static equilibrium profile significantly influences dynamic responses. Also the effect of buoys or chains has been distributed along the pipeline. This scheme, therefore, may be used only to obtain an initial estimate of dynamic responses in gently curved pipelines with small buoys or chains.

den Boer et al. (1990) have presented the concept of an integrated towed flowline bundle production system using the mid-depth tow method. This system has a tow

head, manifold and a remotely operated vehicle (ROV) docking facility. The authors have claimed that by using this concept, diverless installation can be readily extended to waters of more than 1,000 m depth.

McNamara and Lane (1991) have performed frequency and time domain analysis for the sub-surface tow, installation and operation of TLP tethers. During the time domain analysis, an optimum time increment is automatically calculated in response to ambient conditions of loads and structural response. The overall scheme is extremely robust and accurate and is unconditionally stable with respect to time step size. In the case of tow analysis, a two-dimensional condition has been considered in both time and frequency domain and the results have shown good agreement.

Ishikawa et al. (1992) have performed analysis and model tests for TLP tethers subjected to sub-surface towing and up-ending. Their analysis was done in time domain to include non-linear effects and model tests were done in regular waves. The authors have suggested that for partially submerged buoys, additional forces resulting from the pressure distribution on these must be considered. These forces have a negligible effect on the total structural response although their dynamic behaviour due to wave action and their water depth dependency plays an important role in evaluating forces on the buoy. Buoys were modelled as springs whose stiffness constant is the same as the vertical restoring coefficient of buoy (Type 1) or buoy elements that are the same as used by Tatsuta and Kimura (Type 2), i.e., hydrodynamic force and buoyancy on the buoys are calculated under the assumption that the buoy moves with the pipe. The analysis using Type 2 gave closer results to test results than using Type 1 (see Figure 2.2). The towed tether exhibited vibration in the second mode at some encounter frequencies and the maximum bending moment occurred at approximately a quarter of the length from the trailing end. The results of the analysis and model tests showed agreement in the form of variation but, there were large differences in absolute values, especially at high encounter frequencies. This may be due to inaccurate modelling of the buoys because buoy motions become complex at high frequencies and the precise estimation of the lift

force is difficult near the top part of the tether where the trailing angle is somewhat large.

Nihous (1995) has proposed an analytical solution scheme for the transportation of a very long and large diameter pipeline at surface or sub-surface tow. The pipeline under consideration was a cold water pipe used for ocean thermal energy conversion (OTEC). The pipeline was approximated as a straight beam with a free-free boundary condition corresponding to zero bending moments and shear forces at the ends of the beam. The analytical model determined vertical and horizontal transverse motion in a linear frequency domain framework and the results were compared with those from an experiment for a 1/50th scale model of a pipe with 9.1 m diameter and 922 m length. The agreement between theory and experiment appears to be satisfactory in trend, although not in value. This model, however, neglected the effects of tow speed and axial tension under the premise that, in the case of the considered OTEC pipe, tow speed and tension are negligible. The author, however, argues that the effect of axial tension can be accommodated in his model.

2.2 Hydrodynamic Loads on Pipes

Traditionally Morison's formula has been used by offshore engineers to predict wave and current forces on slender structures. The total hydrodynamic force is divided into inertia loads and drag loads. The latter must inevitably be calculated from experimental data while the former can be calculated analytically. The accurate estimation of this hydrodynamic force depends on the realistic values of drag and inertia coefficients, wave kinematics and its interaction with the structure. These force coefficients depend on parameters such as Reynolds number, Keulegan-Carpenter number, roughness ratio, etc. Because Morison equation was originally developed for vertical piles, it has a fundamental flaw for loading on pipes in near-tangential flow, which is typical in tow cases.

2.2.1 The Morison Formulation

The Morison formulation for hydrodynamic wave force is described fully in Section 3.4.2. This section presents some recent experimental evidence of its accuracy and robustness.

Sarpkaya (1977) has performed many experiments and presented extensive data for inertia and drag force coefficients as functions of Reynolds number, Keulegen-Carpenter number and roughness ratio. However, most results are for vertical cylinders in waves or for horizontal cylinders in planar oscillatory flow, for which only horizontal components of the wave particle velocity and acceleration are considered.

Teng and Nath (1985) have experimentally studied hydrodynamic forces on a horizontal cylinder in waves or in waves and current for a Reynolds number up to 5.0×10^5 and have shown differences of wave force coefficients between wave and planar oscillatory flow. The results show that force coefficients for horizontal cylinders in waves or in waves and currents are smaller than those for horizontal cylinders in planar oscillatory flow or vertical cylinder in waves, that is, conventional values given by Sarpkaya. The values of force coefficients with different velocity ratios, the ratio between maximum vertical velocity and maximum horizontal velocity of water particle, are shown in Figure 2.3 against Reynolds number. The results of Sarpkaya are from planar oscillatory flow, that is velocity ratio is zero, whereas those of Holmes/Chaplin and the present authors are 1.0 and between 0.42 and 0.93, respectively. This demonstrates that velocity ratios play a significant role in determining force coefficients in waves. The reason for this may be deduced from the fact that for planar oscillatory flow, the wake formed from a cylinder encounters the cylinder on the return half cycle and results in larger forces. However, for a horizontal cylinder in waves or in waves and current, where velocity ratio is sufficiently large, the wake will move around the cylinder in an elliptic or circular path due to the presence of the vertical velocity. Thus, because of the reduced wake

encounter effect, force coefficients will be smaller than for planar oscillatory flow. When the current velocity is large, the drag force is much larger than the inertia force because the drag term is proportional to the square of the velocity. Thus if the current velocity is large enough, the inertia component is negligible and the drag component represents the total force. In this case drag coefficients approach those for steady flow.

Moe et al. (1990) have experimentally investigated the forces acting on a weakly buoyant pipeline under tow in a reduced length scale of 1/13.55. The tests were performed on a stationary pipeline in head seas with regular and irregular waves. The results were analysed based on Morison equation plus a buoyancy term. The force coefficients were correlated with the Keulegan-Carpenter number because they may be strongly influenced by surface proximity. In the case of irregular waves, the results are unreliable due to the problem of test rig and pipeline size. In the case of regular waves, however, the displacement traces give reasonable agreement with set down predictions based on simple buoyancy considerations. This agreement becomes quite good if rocking motion effects due to short pipeline are included. The local force maxima consistently exceed the values obtained by the Morison equation with the buoyancy model, sometimes by a factor of two (see Figure 2.4). Therefore the authors claim that the analytical model needed to be refined by the inclusion of a ventilation effect. Ventilation occurs close to the water surface and has the effect of reducing local pressure down to the atmospheric pressure. This may occur on the down stream side of a strut connecting a hydrofoil and hull in steady flow. In the present case it will occur when the water level rises up after wave trough passes. Then the water surface must be well beyond the top of the cylinder before a dynamic pressure lower than zero can develop along the upper half of the cylinder. This negative pressure will be ventilated to air. When a trough approaches, the underpressure area is located one diameter deeper down in the water. Thus the force in the above two situations are quite asymmetric. This effect is not covered by the inertia or buoyancy term and it has the opposite effect to that of a positive fluid drag term, that is, reduction in force when vertical velocity is positive.

Bourget and Marichal (1990) have developed a scheme to account for the apparent increase in the drag coefficients of a submerged cylinder when it begins to vibrate. When the amplitude of vibration is low, the high frequency vibration may not be negligible compared with the normal component of tow velocity. The proposed scheme is based on consideration of the transverse component of relative velocity of the cylinder and fluid and obtaining the equivalent drag coefficient by equating the mean dissipated energy with and without vibration during the period of vibration. By this approach, the equivalent drag coefficient can be obtained if the drag coefficient without vibration and amplitude and frequency of vibration are known. This scheme also provides an explanation for the self-limitation of vibration during the locking-on of frequencies from vortex shedding and structure, i.e., if the vibration amplitude increases, it destroys vortex shedding and after that vortex shedding has no effect. The authors have applied their scheme to four cases to validate results and they have shown that the energy approach gives results consistent with those obtained by experiment.

2.2.2 The Lighthill Approach

Lighthill (1960) pointed out that the inertia load deserves more attention in those cases where drag force does not dominate and near-tangential fluid velocity is high. The author showed that the Morison equation omitted an important term in the inertia force as the flow approaches tangentially to a flexible pipe, that is, the tangential component of fluid velocity relative to the pipeline was not included. If a slender structure undergoes transverse deflection, it induces additional flow due to this deflection. The author derived this term for a two-dimensional case under tangential flow using a total (or convective) derivative and included it to derive an improved theoretical formula for inertia loads. He used two independent methods to derive the inertia term which gave the same result; the first was a rigorous solution of the potential theory problem, the second a slightly less-rigorous momentum method. The basic concept of the momentum method is that the force acting on the fluid due

to relative acceleration should equal the rate of change of momentum disturbance in the fluid due to relative motion. Lighthill's formulation, however, poses serious difficulties in many applications since it is only applicable to the special two-dimensional situation he considered, that is, small angle deflection and uniform flow. Section 3.4.3 gives a full mathematical formulation of the Lighthill's approach.

Rainey (1989) investigated circumstances in which the analytical formula by Lighthill gives a worthwhile importance over the Morison-type semi-empirical inertia forces for the analysis of towed arrays and flexible risers. The author showed that for towed arrays Lighthill's extra inertia loads are important if longitudinal water velocity along the array becomes comparable with the propagation speed of lateral waves along the array. He also showed that the Lighthill's formulation cannot be applied to tightly curved flexible risers since the analytical formulation itself breaks down due to the violation of assumptions used during the derivation.

Quiggin and Carson (1994) pointed out that the Lighthill's formulation is not a complete one because there is no obvious criterion for deciding how and where to switch between the Lighthill and Morison formulae, and there is no obvious way of putting the Lighthill's formulation into three-dimensional form. The authors expanded the Lighthill's momentum method to derive a three-dimensional generalisation of his formula, that is, they derived a generalised inertia term by calculating the rate of change of momentum disturbance as seen by the fluid. The authors compared their results with analytical ones of towed arrays and showed good agreement. The authors also expected that systems with a pronounced in-line flow component, especially where other forces are small, might be significantly affected by the new inertia terms whereas many flexible riser systems will be little influenced.

2.3 Static Analysis Methods

In the case of surface, sub-surface or mid-depth tows, the pipeline experiences large deflections due to static forces from current, tow speed, hydrostatic pressure and self

weight. Under given conditions such as the capabilities of tow vessels, current speed and direction, optimum and accurate equilibrium configurations are very important for manoeuvring plans and for subsequent dynamic analysis. In side currents especially, pipelines experience large current force and consequently, large tensions. In some cases, it may be beyond the capacity of the tow vessels.

In the analysis of continuous structures such as pipelines, differential equations govern the structural response whereas a discrete system can be described by a set of algebraic equations for the unknown state variables. The classical solution of the differential equation satisfying all boundary conditions is only possible for relatively simple structures, and in most cases, numerical procedures must be employed for a solution. These procedures, in essence, reduce the continuous structure to a discrete one that can be analysed in the same manner as a discrete structure. There are two such numerical procedures that are widely used in structural analysis; the finite difference method (FDM) and the finite element method (FEM).

The FDM is one of the most commonly used methods in the field of numerical analysis. It is a methodology for the differential relations of structural analysis to be approximated by their finite difference analogies and thus reducing the problem to that of solving a system of algebraic equations.

The FEM, on the other hand, gives a piece wise approximation to the governing equation. The key to the FEM lies in relating the primary unknown function to the individual element, rather than to the total system and in approximating an unknown function systematically. Hence the geometry of the overall body and boundary conditions are of no concern when choosing the unknown function. Since these elements can be assembled in several ways, they can be used to represent the total structure regardless of the complexity of geometry and boundary conditions. The details of a finite element formulation and solution are summarised in Sections 4.2 and 4.3.

Martin and Carey (1973) and Bathe (1982) have described the detailed procedures of finite element formulation. On the basis of the equilibrium equation as the starting point, applying certain mathematical calculations leads to an expression that can be interpreted as a work relationship. The principle of virtual displacements is used for this purpose and usefully interpreted that during any arbitrary virtual displacement from the equilibrium state, the work done by the true force system equals the increment in strain energy. In using the principle of virtual displacements, we begin by assuming interpolation functions such that internal continuity and compatibility between elements across common boundaries are assured. A power series is often used and the accuracy of the result depends on the careful choice of this function. Application of the variational principle to the virtual work furnishes external equilibrium in terms of generalised force and element stiffness matrices. Once these are known, the problem solution procedure follows the steps already established for the matrix stiffness method of analysis.

Because long towed pipelines experience large deflections, geometric non-linearity must be considered in the finite element formulations.

Martin and Carey (1973) and Clough and Penzien (1993) have described the concept and systematic finite element formulation of geometric non-linear problems for beam elements. Geometric non-linearity is ascribed to large deflection problems in which the deformed configuration must be used to write the equilibrium equation. Thus it depends not only on the configuration of the structure but also on its condition of loading. In general, two different levels of approximation can be established for the evaluation of geometric stiffness properties depending on interpolation functions; linear approximation and higher order approximation (for details, see Section 4.2.1). Each coefficient of a geometric stiffness matrix can be calculated by applying standard finite element procedures, that is by applying virtual displacements and equating the internal and external work components. The assembly of the element components is exactly the same as for the elastic stiffness matrix.

If the stiffness properties depend on the deformed configuration, the problem becomes non-linear. In this case, direct solution of simultaneous equations obtained from the finite element formulation is generally impossible and an iterative scheme must be adopted.

Owen and Hinton (1980) have summarised the procedures of various iteration methods. In the direct iteration method successive solutions are performed, in each of which the previous solution for the unknowns is used to predict the current values of the stiffness matrix. To commence the process, an initial guess for the unknowns is required in order to calculate the stiffness matrix and it is necessary to recalculate the stiffness matrix for each iteration until it meets a convergence criterion. The process is illustrated for a single variable in Figure 2.5.a. A disadvantage of the direct iteration method is that convergence of the solution scheme is not guaranteed and cannot be predicted at the initial solution stage. Therefore the Newton-Raphson method is more frequently used because it gives more rapid and stable convergence path than the direct iteration method. The Newton-Raphson method also needs an initial guess for the unknowns and afterwards tangent stiffnesses based on the previous step are used. An iterative approach must be followed, with the matrices of unknown and tangent stiffness being corrected at each stage, until convergence of the process is deemed to have occurred. The process is illustrated in Figure 2.5.b.

The iteration method is suitable for cases in which the problem is moderately non-linear or a rough starting geometry is available. Otherwise, incremental or hybrid methods are more reliable. Besides these methods, there are various schemes that are useful for specific problems and principally they are based on the combination of the iteration method and the incremental method.

Seyed (1989) has described the procedures and merits of each solution method. The incremental method involves loading the structure gradually using small increments of the total load at each stage and calculating its deformations and forces cumulatively (see Figure 2.5.c). If the loads are strongly deformation dependent, the force

increment at each stage is taken as the difference between the forces at the current and the previous stages. This method is popular for non-linear analyses as it does not suffer from convergence problems. For more accurate analysis of highly non-linear problems, equilibrium iterations are sometimes carried out at each step of incremental loading. A method obtained from a combination of the incremental method and the inner iteration method is called the hybrid method. Its procedure is shown in Figure 2.5.d. Seyed has also summarised several approaches to reduce ill-conditioning problems arising from the small ratio of bending rigidity to axial rigidity for long pipes.

Leira and Remseth (1985) have also recommended that for strongly non-linear problems the true equilibrium path should be followed closely and the most reliable procedure will then be to combine an incremental method with equilibrium iterations. For more moderate non-linearities, the equilibrium path may be traced with sufficient accuracy by pure increments or increments with equilibrium correction.

Huang and Chucheepsakul (1985) have presented the method of static analysis for a marine riser experiencing large displacements. A variational formulation is presented to find an equilibrium configuration. The functional representing the energy and work of the riser system is expressed in terms of the horizontal coordinate which is parameterised in terms of the vertical depth instead of arc length. For a two dimensional problem, two multipliers are included in the functional; one of the multipliers represents the variable tension along the length and the other corresponds to the strain energy per unit length due to bending. The Newton-Raphson iteration method is used to solve resulting equations.

Bernitsas and Vlahopoulos (1990) have studied the static pipelaying problem using a three-dimensional, non-linear numerical model with large deformations. The condensation process has been used for constrained degrees of freedom and an incremental method has been used to handle the non-linearities of the model. The

deformation dependent hydrodynamic load and all stiffness matrices have been updated within each increment.

Even though the above numerical methods are powerful, they require large computer resources. They are therefore very expensive for the early design stage and, in some cases, experience ill-conditioning problems.

Peyrot and Goulois (1979) have provided a reliable method and computer program for calculation of the profile of catenaries suspended between two arbitrary points. The program incorporates the linear effects of axial elongation. The formulation expresses all variables in terms of force components at the supports and the resultant algorithm is combined with a cable element formulation to provide a program for general cable systems in three dimensions. The method involves calculation of the stiffness matrix for each cable segment using small perturbations of the ends of the cable and computing the resulting increases in end forces using a catenary analysis sub-program. This is then used to compute the displacements for a given set of loads. The tangent stiffness matrix is then updated for the new profile and multiplied by the displacements in the previous stage to calculate the unbalanced force vector.

Seyed (1989) has also used the elastic catenary equations to obtain preliminary static configuration of pipes and used it for an initial design check or starting condition of a rigorous finite element analysis. Even though the catenary equation has drawbacks in its ability to handle external loads and various boundary conditions, the results are reliable and very efficient if self weight is dominant. Moreover, if this configuration is used as the initial condition of a non-linear finite element analysis, it provides rapid convergence and significantly reduces ill-conditioned problems.

2.4 Dynamic Analysis Methods

Towed pipelines experience various kinds of dynamic loads due to waves, vessels, or buoys. An analytical solution of the equation of motion is generally not possible and

a numerical technique must be utilised as in the static analysis. The standard procedures proposed for the solution of a general system of differential equations can become very expensive if the order of the matrices is large. Therefore, in practical finite element analysis, we use a few effective methods that take advantage of the special characteristics of the stiffness, damping and mass matrices. The primary methods used for dynamic analysis are frequency domain, modal superposition and direct integration methods. The first two methods are used for linear systems whereas the last one is essential for highly non-linear systems.

The dynamic response of a towed pipeline is dominated by higher modes and influenced by a wide range of wave periods. In using the finite element method for dynamic analysis, it is necessary to model high mode vibration and therefore, have reasonably small element length.

Seyed (1989) has used a simplified modal superposition method to predict the dynamic response of towed pipelines in regular waves. The pipeline is idealised as a uniformly distributed beam with lumped masses and springs at its ends. Initially, an eigenvalue analysis is carried out using a Rayleigh-Ritz method. Since a large number of modes are usually used in a dynamic analysis of pipelines and to maximise accuracy, a Fourier series is used to represent the deformed shape. Using natural frequencies and associated mode shapes from the eigenvalue analysis, modal participation parameters are calculated for specific wave forces. Finally, the dynamic response is obtained by summing contributions of all the excited modes. Even though the result is not so accurate due to the simplification of the model and analysis scheme, the relative magnitudes of the modal participation parameter provide a good guide for the minimum required number of modes in finite element analysis. Additionally, prior information of these parameters helps selecting the element size.

The Frequency Domain Method

The total motion is expanded as a sum of components and expanding the forcing function in a Fourier series, a closed form, algebraic solution can be achieved and the need for numerical analysis reduced. Steady state response is rapidly obtained because time variables are eliminated from the equation of motion under the assumption that all time-dependent terms are harmonic. However, the use of this method requires linear equations of motion. Nonlinearities cannot be accommodated by this method. In the case of offshore structures, hydrodynamic drag has a strong influence and creates the non-linearity in the equation of motion. Therefore its successful use depends on a reasonable linearisation scheme. In spite of this shortcoming, this method has been widely used because it is much faster than the direct integration method and is suitable for obtaining irregular wave statistics.

The general procedure for compliant pipes is as follows:

1. Solution of non-linear static problem in the presence of mean forces from currents.
2. Linearisation of the structural part of the nonlinear dynamic equation around the static configuration for small dynamic motions and angles.
3. Equivalent linearisation of the non-linear drag force assuming monochromatic three-dimensional excitation and response.
4. Solution of the resulting linear boundary value problem modelling compliant pipe dynamics.
5. Determination of mean forces under currents, waves and pipe motions.
6. Once these mean forces are obtained, iteration starting from the first step until convergent solution is reached.

Unless the nonlinear drag force is linearised, the equation of motion must be solved by time step integration which tends to be computationally expensive. This has led to study on an equivalent form of nonlinear drag force which will allow the frequency domain solution. Initially, the superposition method was frequently used. In this method, the total solution was obtained by summing the results from the wave only

and current only cases. This method therefore cannot consider the dependence between input parameters such as current, wave and pipe velocities.

Krolikowski and Gay (1980) have presented an improved linearisation procedure for regular waves and for regular and irregular waves with current using the describing function method from control theory. This method is a form of quasi-linearisation which minimises the mean-square error between the output of the original non-linearity and the linear replacement. The mean squared approximation error is minimised by expanding the nonlinear output in a Fourier series and neglecting higher harmonics. Neglecting the higher harmonics can be justified by noting that the higher harmonics have less amplitude than the fundamental. In addition, higher harmonics in the drag forces are filtered by the pipe dynamics. The application results are compared with those from a nonlinear drag model and a superposition model. It is shown that the improved method gives reasonable results. The authors have also summarised the procedure for frequency domain riser analysis for a random wave with no current.

Ertos and Kozik (1987) have performed time domain and frequency domain analyses for the riser to check the influence of current velocity on the linearisation results. The authors followed the same improved linearisation scheme as Krolikowski and Gay. The results show that both analyses show good agreement for a regular wave with height of 20 feet and period of 12 seconds. In the case of a regular wave with uniform current, both analyses give very close results if the current velocity is less than 0.7 knots. Above this velocity, the responses from the two analyses become widely different (see Figure 2.6). From these results it can be seen that the effect of high current velocity on the accuracy of the riser response is significant. Therefore special attention and a higher order linearisation scheme may be required to use the frequency domain approach for the analysis of towed pipes, especially for high tow velocity with relatively small wave height.

Even though the above linearisation method, based on minimum error in the mean squared sense, is widely used, it has some drawbacks for more general use as mentioned.

Chen and Lin (1989) have presented a general drag force linearisation technique for regular waves with current. In their study, the non-linear drag force is expressed by a Fourier expansion up to any desired (n-th) order. Applying the iterative calculation procedure, all the Fourier coefficients can be obtained easily by numerical integration. The authors performed frequency domain analyses for a riser using this method and compared the results with those from time domain analyses. Three values of tension ratio, the ratio of the top tension to the total weight of the riser system in water, were used for study. The results show that the first order Fourier expansion may not be adequately accurate for both the displacement and the stress at the same time. Especially in the high tension case, the first order Fourier expansion is no longer valid for displacement, but it may still be good for stress. This is due to the fact that the bending stress is small and the top tension dominates the total stress. However, the second order Fourier expansion gives very satisfactory results for both displacement and stress regardless of tension ratio (see Figure 2.7). Applying the second or third order Fourier expansion requires about four to eight cycles of iterative calculation to get a convergent solution instead of about three to six cycles in the first order case.

Linearisation methods were developed in one dimensional space and their application to three dimensions was done by the approximation of drag forces from each normal velocity component which is dependent on the chosen coordinate system. The linearised drag force is therefore not frame invariant and this approximation, sometimes called the empirical method, is not physically sound.

Langley (1984) has presented a frame invariant linearisation method for three dimensional drag forces in random waves with current. Initially, a coordinate system local to the element is introduced and the normal velocity components in the global system are decomposed into those in the local one. Following the equivalent

linearisation method and minimisation of the mean squared values, the coefficient matrices are obtained. Having linearised in the local coordinate system, the drag force can be transformed back to the three dimensional global system. This scheme is very sound because any interactions between the two flow directions can be considered during linearisation. Also it complies with the standard procedures of finite element analysis. Comparison studies show that linearisation based on this method provides very close agreement to exact drag force values whereas that on the empirical method can lead to a significant underestimation of the drag force, since coupling between perpendicular flow directions is neglected.

The Modal Superposition Method

Once the mode shapes and eigen frequencies of a vibrating system have been found, its equation of motion can be transformed into a modal space. The use of modal coordinates serves to transform the equation of motion from a set of N simultaneous differential equations, which are coupled by the off-diagonal terms in the mass and stiffness matrices, to a set of N independent normal coordinate equations. The dynamic response, thereafter, can be obtained by solving separately for the response of each normal coordinate and then superposing these to obtain the total response in the original coordinates. In the case of a damped system, it is generally more convenient and physically reasonable to define the damping by damping ratio for each mode than to try to evaluate the coefficients of the damping matrix. If Rayleigh damping is assumed, the modal coordinate transformation can serve to uncouple the damping matrix. Solution of the equation of motion in the modal space permits a considerable saving in computation time compared with the direct integration method.

The Direct Integration Method

The basic idea of the direct integration method is to divide the response history into a series of short intervals and to obtain the dynamic response which satisfies the

equilibrium equation at discrete time intervals only by a step-by-step integration procedure. Within each increment, the system is assumed to be linear and a variation pattern of acceleration is assumed according to various proposed schemes.

This method is the most powerful and accurate technique for non-linear analysis because it allows calculation of non-linear drag forces due to relative pipe and fluid motions and modification of the stiffness matrix according to instantaneous system response on the basis of geometric non-linearity. However, it requires much more computer time than frequency domain analysis and considerable amount of computer time for the computation of transient response, which is generally of little interest. In order to obtain meaningful statistics for random wave, even greater time is required. The method is useful for final design check but is generally too expensive.

Clough and Penzien (1993) have described the detailed procedures of the direct integration method - especially the linear acceleration method. Dynamic equilibrium is established at the beginning of each interval and incremental equilibrium equation is set up. By introducing an assumed variation type of acceleration, increments of acceleration and velocity can be expanded to unknown displacement increments and known initial conditions. The unknown displacement is obtained from the incremental equilibrium equation. The method is described further in Section 4.4.2. The nonlinear nature of the system is considered by calculating new properties at the beginning of the next time increment based on the deformed state of the present step. The complete response is obtained by using the displacement and velocity computed at the end of one computational interval as the initial conditions for the next interval. The accumulation of error due to the approximation of element properties at the beginning of each step can be avoided by imposing the total equilibrium condition at each step of the analysis. Thus the process may be continued step by step from the initiation of loading to any desired time, approximating the non-linear behaviour as a sequence of successively changing linear systems.

Even though the direct integration method is powerful, its stability and accuracy depend on the applied time step.

Bathe (1982) has summarised a step-by-step solution procedure of various implicit and explicit direct integration methods. The author has also discussed their stability and accuracy in detail. The topic of stability of integration is closely related to that of numerical damping, or numerical dissipation. The accuracy of integration can be characterised by two attributes, amplitude accuracy and period accuracy. The stability and accuracy are assured if the time step is small enough to integrate the response at the highest frequency component. However, this may require a very small time step and accurate integration of the high frequencies is in many cases not justified and not necessary. Since the primary response usually lies in only some modes of vibration, the time step is determined by considering the frequencies associated with these modes and the frequency content of loading. The author has recommended that the frequencies contained in the loading should be identified using a Fourier analysis if necessary.

Vlahopoulos and Bernitsas (1990) have studied the dynamic behaviour of pipelines in stinger and J-type pipelaying by numerically solving the three dimensional, non-linear, large deflection model. Integration of the governing equation is performed by the Newmark method. Since the equations simulated in time are nonlinear, the appropriate values of β and γ are not obvious whereas β is 0.25 and γ is 0.5 for linear equations. In the numerical applications, it was observed that low values of β and γ resulted in no convergence in the iterative scheme. High values, however, caused damping of the lateral waves propagating along the pipeline. The problem was solved by using different values of β and γ for pipe segments according to whether they are supported by a stinger. In both cases, the values were selected to allow convergence without causing long term damping of lateral pipeline oscillations.

It is a difficult task to choose a proper time step for integration of dynamic problems to give accurate results regardless of stiffness, mass, smallest element size, load history and response change during the solution process.

Bergan and Mollestad (1985) have discussed an automatic time-stepping algorithm for discrete integration of dynamic problems. The general criteria in the algorithm are that it should seek the largest possible time step while maintaining a prescribed accuracy and the adjusted time step should be the same regardless of the size selected for the initial step. Also, the time step should remain constant during a linear, stationary response and should not be influenced by the selection of physical units or by the actual number of degrees of freedom in the dynamic equations. The algorithm is based on the current characteristic frequency that is available using the principle of conservation of energy - potential energy is equal to kinematic energy if no damping acts to absorb it. This frequency is generally not any particular eigen frequency, but it reflects rather the modal composition of the current frequency. Because the current frequency expresses a dominant incremental response period, it is used to describe the preliminary time step. To avoid too frequent and too dramatic changes of the time step, a tuning function is introduced. The tuning function can be built to determine the sensitivity of the time-stepping algorithm considering the previous and preliminary current step. If this algorithm is used, the necessary input parameters are the first time step and the step-length parameter. It is better that the first time step is given a value that is smaller than what is thought to be proper because it costs very little extra. The recommended step-length parameter is larger than ten. The authors have presented several examples of applications and demonstrated the efficiency and accuracy of this algorithm.

Jacob and Ebecken (1992) have summarised more general and efficient numerical strategies to the non-linear dynamic analysis of compliant structures for deep water oil exploration and production. These include an automatic determination of both the time step for direct integration and the time instants for recalculation of stiffness matrix. The automatic time-stepping algorithm is the same as that of Bergan and

Mollestad, that is, the time step is automatically adjusted according to the modal composition of the response and to the non-linear behaviour of the structure at each time instant. For the determination of the time instants with stiffness evaluation, it is considered that the variation of the dominant frequency reflects not only the variation of the modal composition of the response, but also the variation of the stiffness. The recalculation is therefore triggered if there is an alteration of the time step or if the number of iteration exceeds an optimum number, typically three. The reduced integration method is based on the coordinate transformation of the equation of motion, that is, the unknown displacement vector is expressed as a linear combination in terms of a generalised displacement vector. Some applications in the non-linear dynamic analysis for flexible risers and compliant guyed towers have been performed to demonstrate the computational efficiency and reliability of results. These show significant reductions of computer time without convergence problems even though the results are almost the same as those obtained from conventional methods.

2.5 Treatment of Tow Vessels

The tow system consists of a pipeline, tow vessels, towlines, etc. as described in detail in Section 1.4. Considering that the mass of a tow vessel is generally small and consequently comparable with that of a long pipeline, the interaction between tow vessels and a pipeline may be significant. Surprisingly, however, all previous works on the towed pipes in Section 2.1 did not consider tow vessels in their analytical, numerical, or experimental model.

In the field of dry transportation of offshore structures such as jackets, they also usually do not include the tow and towed vessels in their models - they consider towlines only with prescribed displacements at the ends of the towlines to calculate tension (Inoue et al., 1991).

Milgram et al. (1988) have proposed a more reasonable scheme to predict the statistics of extreme towline tension when one ship tows another through ocean

waves. The theory of seakeeping of a single ship was used as a basis to develop a twelve-degree-of-freedom theory for a tow system consisting of a tug coupled to a towed vessel through a towline. Since surge motion plays an important role in towing dynamics, the authors added surge terms to a well-established five-degree-of-freedom system for one ship. After development of the surge theory, they coupled the two vessels together with the towline to arrive at the full twelve-degree-of-freedom theory which was used for calculation of ship motions and towline dynamic tensions. Since the extension of the towline is due to the ship motions, which themselves are influenced by the tension, the exact situation is a twelve-degree-of-freedom nonlinear feedback system which is quite complicated. A simplification was made such that the calculation of all twelve ship motions was performed using the theory of equivalent linearisation of towline spring and damping constants, followed by a nonlinear calculation of extreme tension resulting from these ship motions. Figure 2.8 shows a block diagram of this procedure. This procedure worked well and in this specific case demonstrated the importance of including the tow vessel in the overall dynamics.

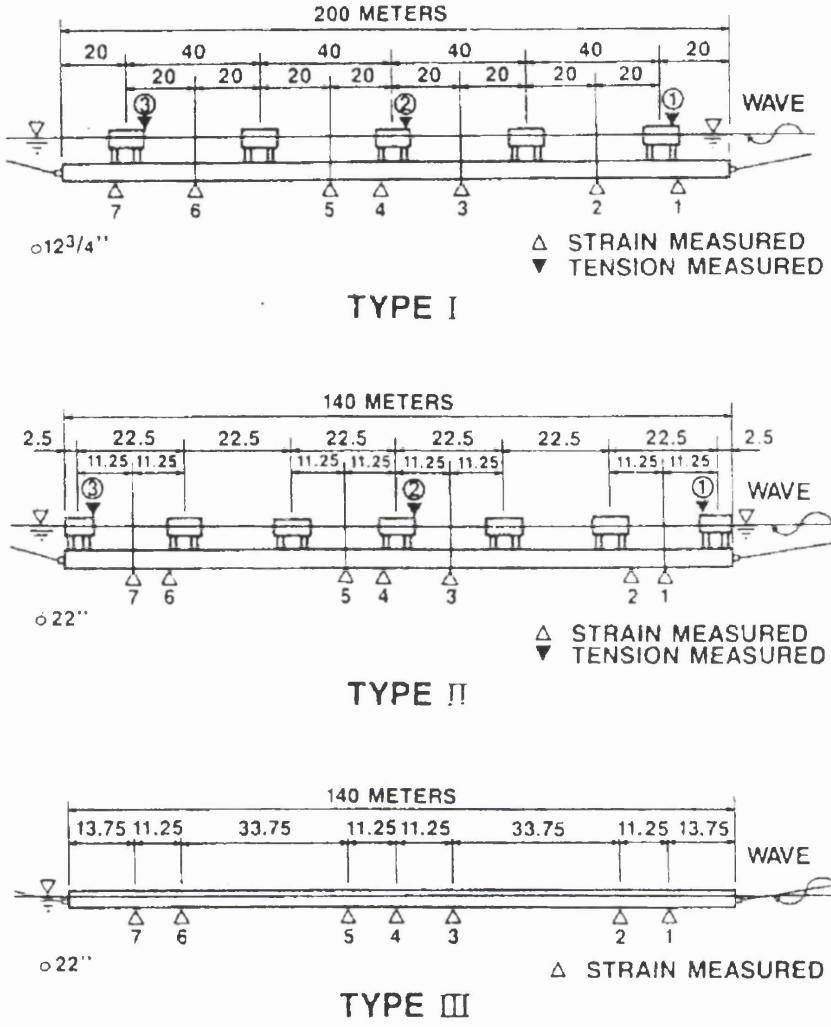

(a) Test set-up of a pipeline

Figure 2.1 Model test of a pipeline in sub-surface tow (Tatsuta and Kimura, 1986)

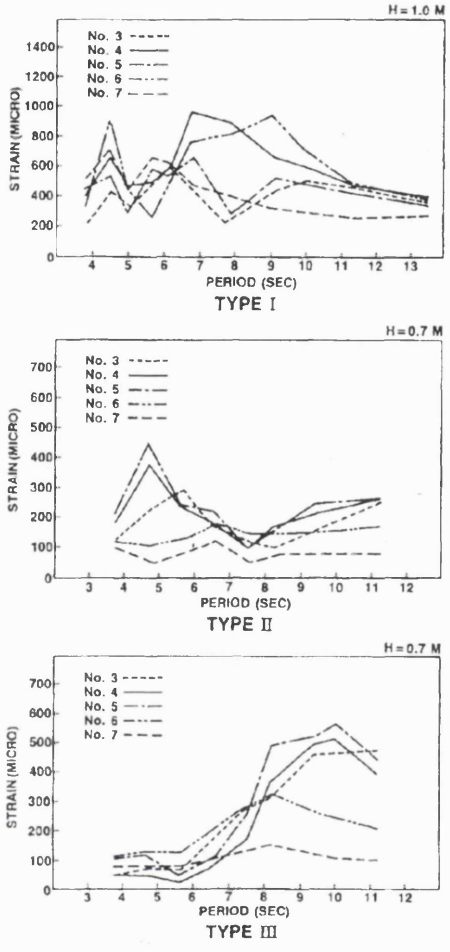

(b) Strain response to regular waves

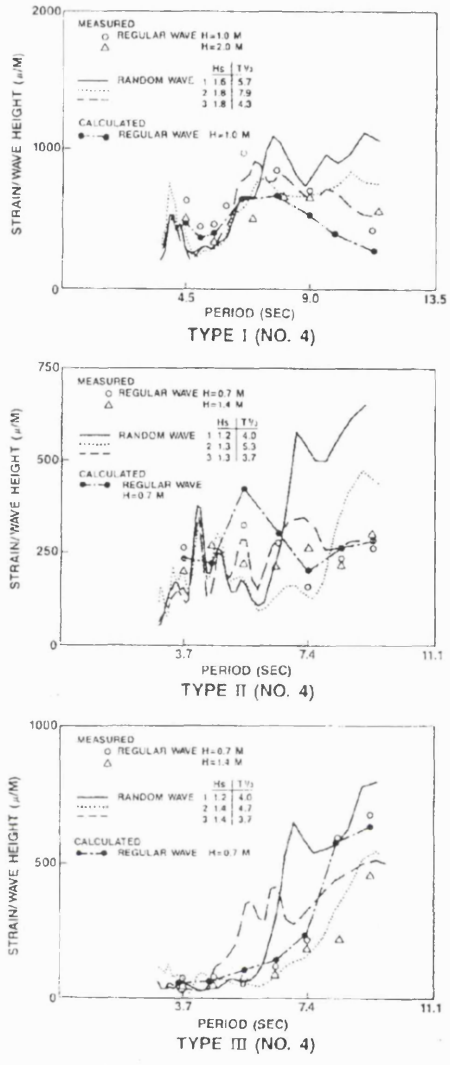

(c) Strain response characteristics

Figure 2.1 Model test of a pipeline in sub-surface tow (Tatsuta and Kimura, 1986)

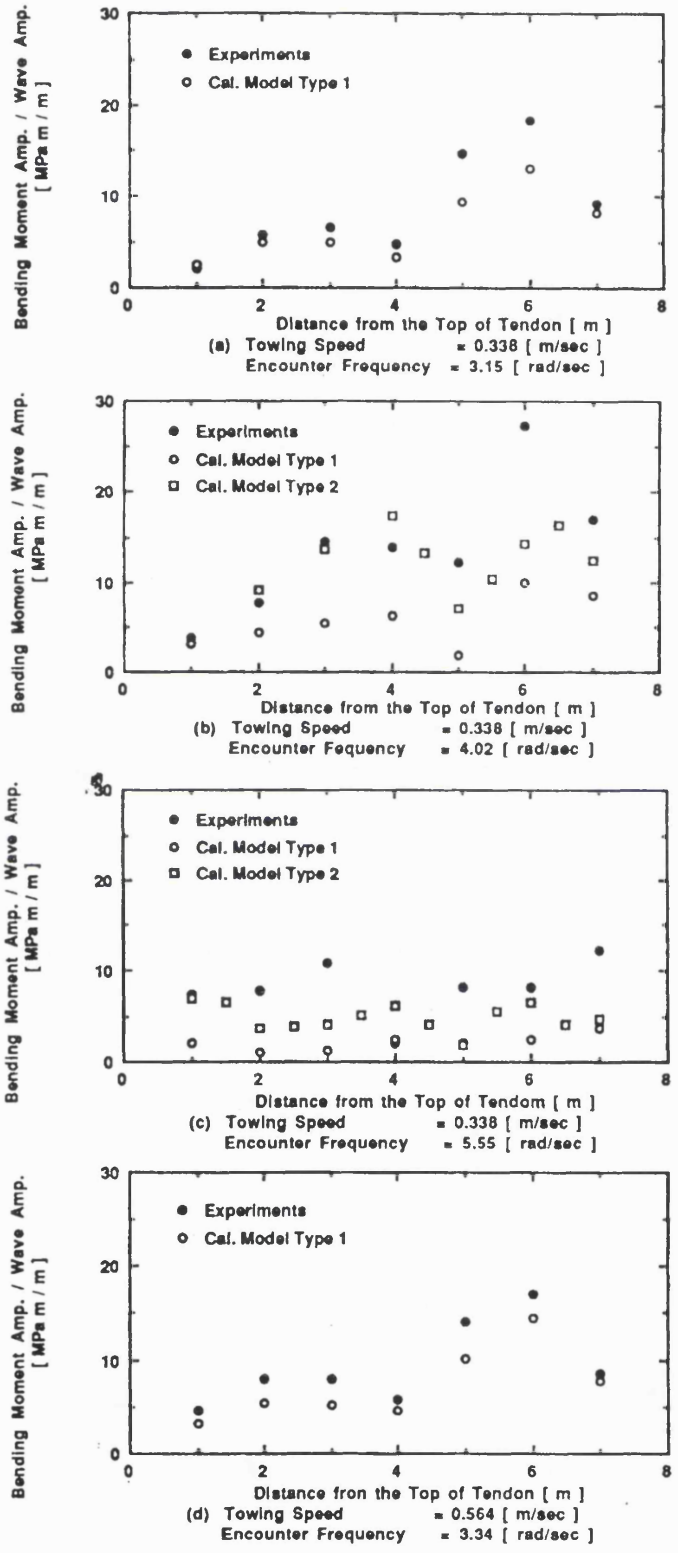

Figure 2.2 Bending moment distribution of a TLP tether (Ishikawa et al., 1992)

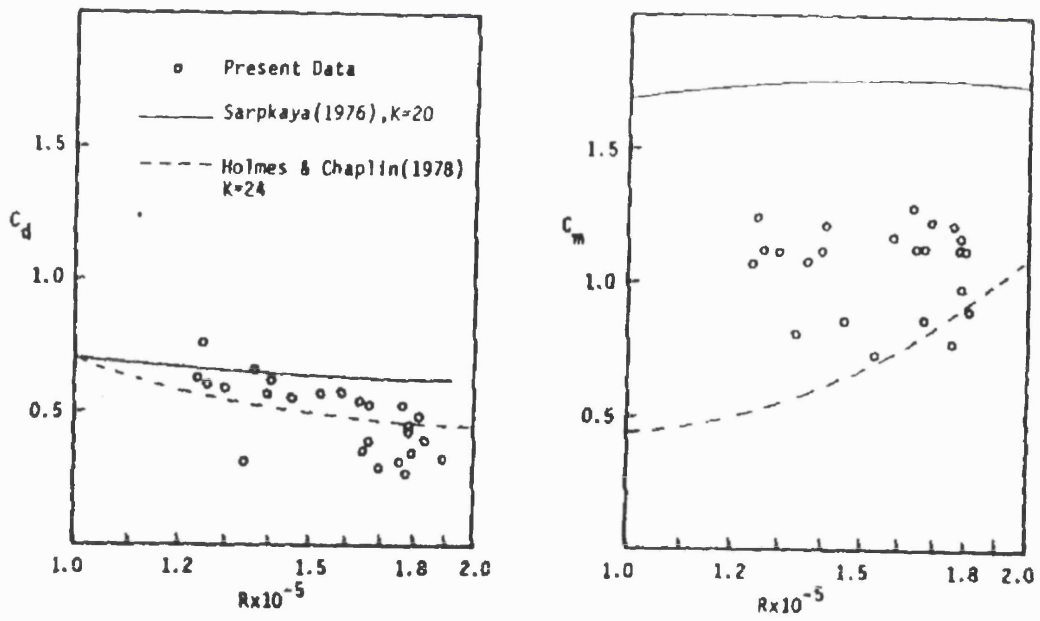

Figure 2.3 Damping and added mass coefficients in waves (Teng and Nach, 1985)

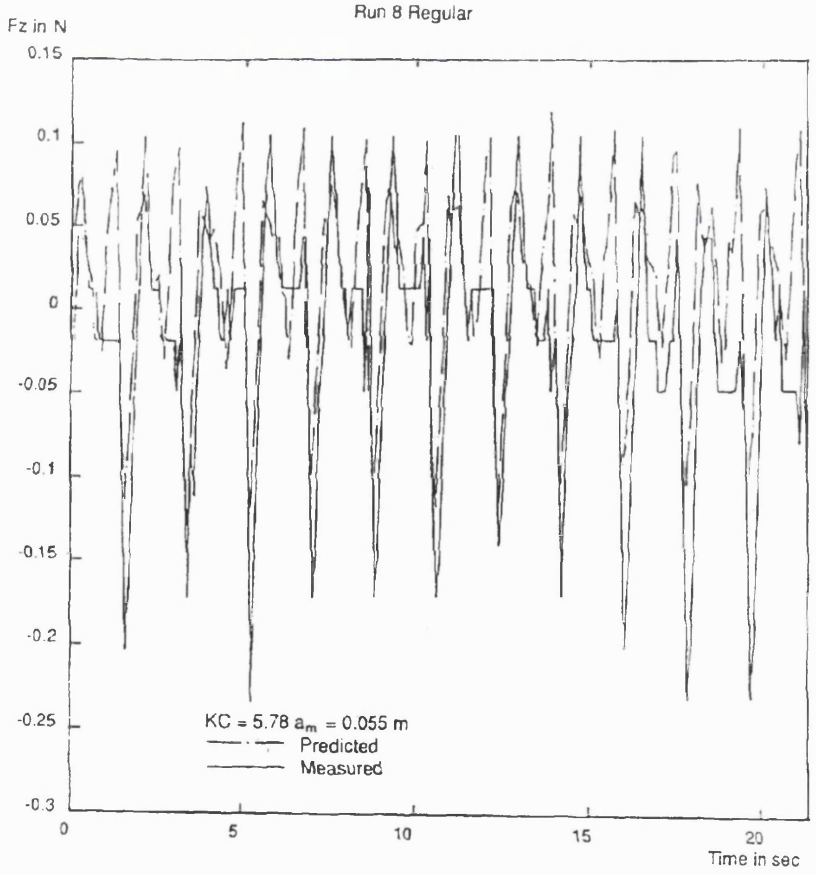

Figure 2.4 Local force trace in regular waves (Moe et al., 1990)

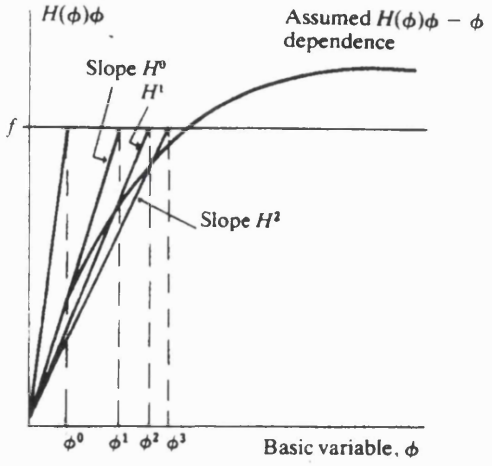

(a) Direct iteration method

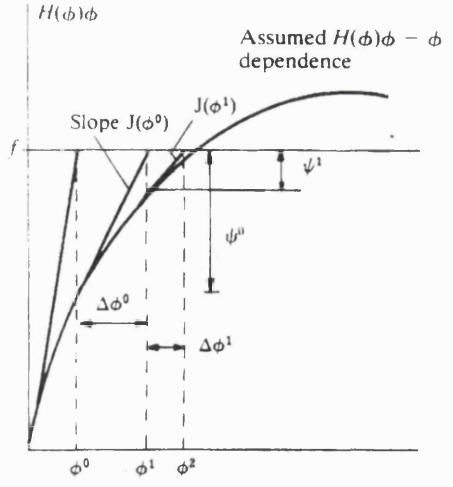

(b) Newton-Raphson method

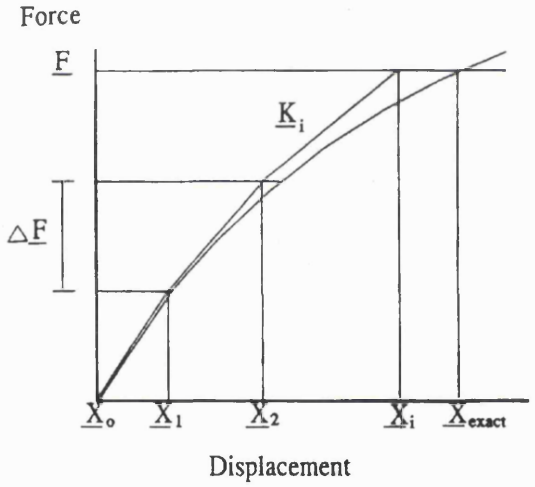

$\underline{F}$ - Total Force Vector
$\underline{K}_i$ - Tangent Stiffness Matrix at Step (i)
$\underline{X}_o$- Starting Nodal Geometry Array
$\underline{X}_i$ - Displacement Array at Step (i)
$\triangle\underline{F}$ - Force Increment
$\underline{X}_{exact}$- Exact Displacement Vector Solution

(c) Incremental method

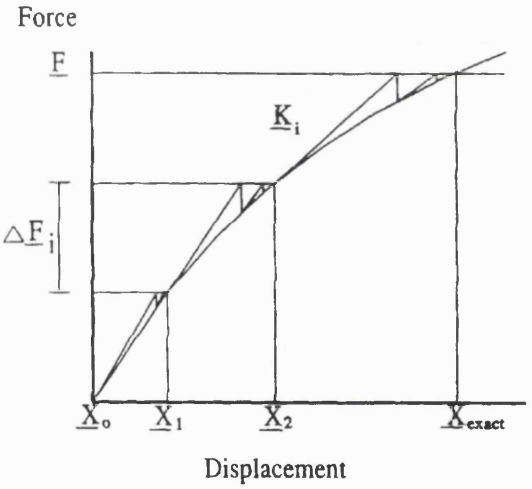

$\underline{F}$ - Total Force Vector
$\underline{K}_i$ - Tangent Stiffness Matrix at Step (i)
$\underline{X}_o$- Starting Nodal Geometry Array
$\underline{X}_i$ - Displacement Array at Step (i)
$\triangle\underline{F}$ - Force Increment
$\underline{X}_{exact}$- Exact Displacement Vector Solution

(d) Hybrid method

Figure 2.5 Solution methods of nonlinear static problems

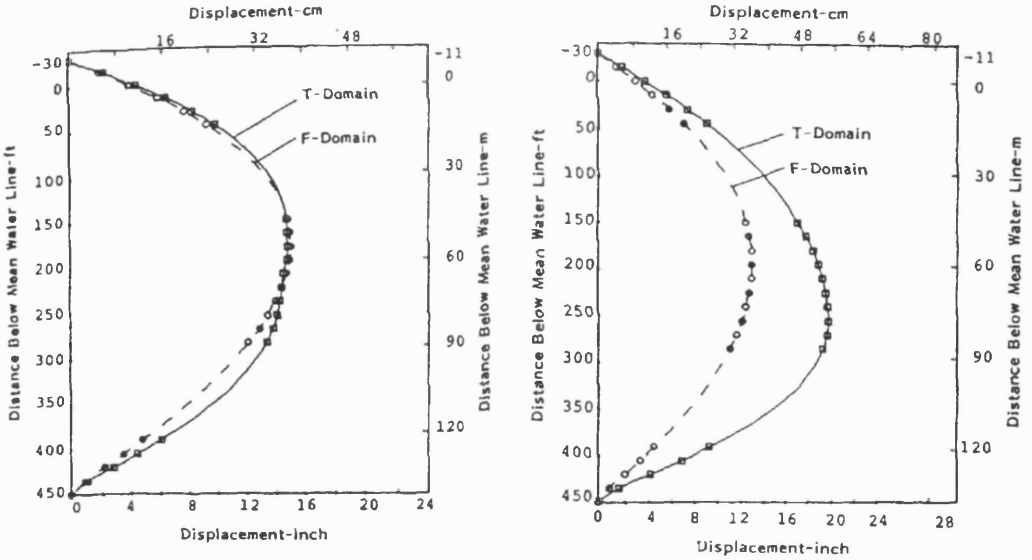

Current = 0.6 knots
Wave height = 20 feet
Wave period = 12 sec

Current = 1.0 knots
Wave height = 10 feet
Wave period = 12 sec

Figure 2.6 Comparison between frequency and time domain results
(Ertos and Kozik, 1987)

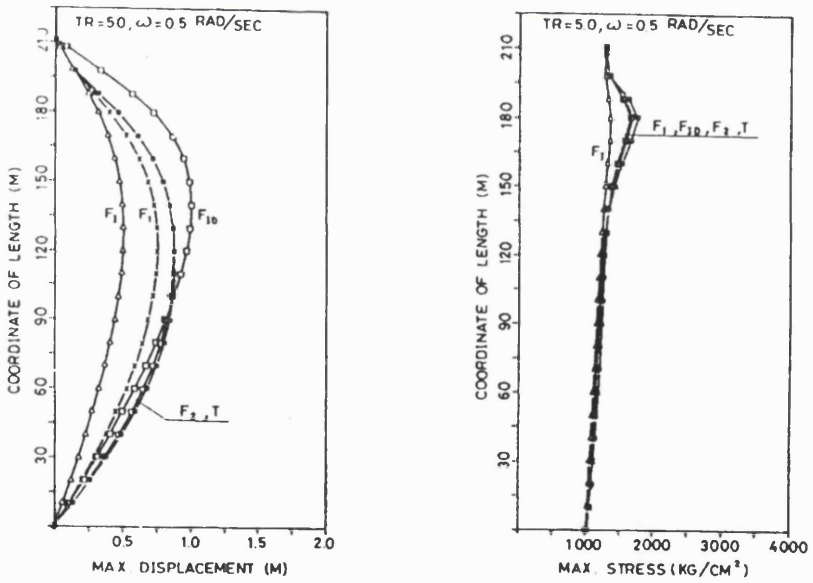

F_1 : First order linearisation
F_2 : Second order linearisation
T : Time domain

Figure 2.7 Comparison between first order and second order linearisation
(Chen and Lin, 1989)

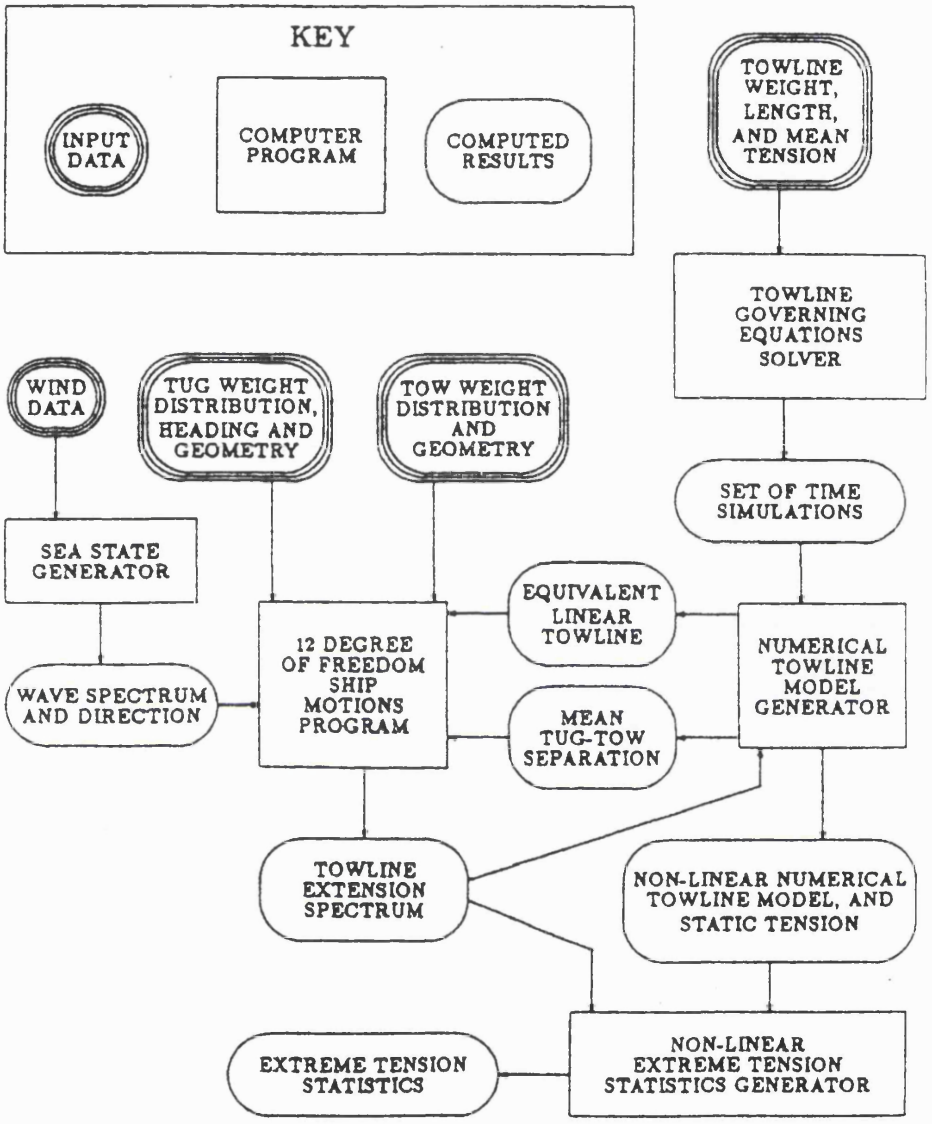

Figure 2.8 Information flow for computation of nonlinear extreme tension statistics of towlines (Milgram et al., 1988)

3. GOVERNING EQUATIONS

A tow system consists of a pipeline, chains, towlines, and tow vessels as described in detail in Section 1.4. The success of a tow operation depends on careful and accurate consideration of the behaviour of each component and its interaction with others under expected environmental conditions.

Towed pipelines are generally very long and exposed to high risk of damage because they are directly exposed to environmental action. The physical problem of towed pipelines in currents and waves is extremely complex. The static component of the problem has a significant structural nonlinearity and the dynamic component is compounded by the quadratic nonlinearity of the hydrodynamic drag force and the unusual nature of the inertia force under a high near-tangential flow. This is further complicated by the axial dynamic interaction of the pipeline, towlines and tow vessels.

Although the usual analysis scheme of towed pipelines evolved originally from vertical riser analysis, there are significant differences in physics between towed pipelines and risers. From a structural point of view, the behaviour of towed pipelines is quite different to that of risers because of the very different configuration of each structure, that is, the near-horizontal configuration of towed pipelines compared to the near-vertical one of risers. Also the tow vessels may have an influence on the behaviour of the pipeline via very flexible towlines because, in the case of long pipelines, the mass of the tow vessel is comparable with that of the pipeline. From a hydrodynamic point of view, the Morison equation originally developed for fluid loading on vertical piles has a fundamental flaw for towed pipelines which are exposed to a relatively high speed incident flow due to towing at small angles between tow direction and pipe centerline.

Towed pipelines are slightly negatively buoyant in a normal mid-depth tow and may be subjected to large displacements due to various types of loads such as self-weights,

buoyancy forces, chain forces, current forces, wave loads, and vessel forces. In this chapter, the governing equations for the analysis of towed pipelines are presented.

At first, conventional and elastic catenary equations and nonlinear equilibrium equations of slender beams are presented in Section 3.1. The catenary equations will be used later to improve a convergence problem of nonlinear finite element solutions. External and internal static pressure forces on pipelines effect their governing equilibrium equations and these forces control the curvature in a way similar to the tensile forces in the wall of the pipeline. The derivation of this static pressure force for a straight and a curved beam in two dimensions is presented in Section 3.2. Since the static tow configuration of pipelines mainly depends on the current forces on chains and pipelines, the accurate estimation of these forces is essential for a successful tow operation. The scheme to calculate forces on chains and pipelines are presented in Section 3.3. Wave kinematics with and without tow speed and wave-induced loads on a tow system with linear wave theory are presented in Section 3.4. The Morison equation and an improvement of its inertia force term under high near-tangential flow are discussed. A simplified method to calculate wave-induced forces on tow vessels are also described. Finally, analytical solutions for static and dynamic tow conditions are presented in Section 3.5.

3.1 Equilibrium Equations of Pipelines

A towed pipeline is usually in a shallow catenary shape with its own slightly negative buoyancy although this initial configuration changes significantly with other static forces due to currents and tow speed. In the case of very long pipelines, it is very difficult to obtain a stable static equilibrium configuration even with a finite element method due to the significant influences of tow speed combined with the high level of inherent geometric nonlinearity. Several special techniques have been developed to improve this problem and the utilisation of a catenary equation is one of them. Initially, conventional and elastic catenary equations are derived and, subsequently,

the full nonlinear equations of a slender beam are derived for general loading conditions.

3.1.1 The Catenary Equation

The catenary equation was originally devised to calculate the deflected configuration of a uniform inextensible cable, or chain, that hangs between two fixed points. The elements of the cable are assumed to be perfectly flexible and it is further assumed that the cable can sustain only tensile forces (Irvine, 1992). This classical catenary approach led also to the elastic catenary equation that is able to consider elastic elongation (O'Brien and Francis, 1964).

Although these catenary equations are in a compact form, they provide an accurate configuration for slender structures under their self-weight, that is, without external and internal loads. Moreover considering that convergence problems are frequent for slender structures even with a nonlinear finite element method, the utilisation of this configuration as an input for a rigorous finite element analysis improves ill-conditioning problems significantly and provides rapid convergence of results.

At first we consider a uniform inextensible cable that hangs between two fixed points, *(0,0)* and *(a,b)*, that are at different levels (see Figure 3.1 for the configuration and definitions of variables).

Vertical equilibrium of the isolated element of the cable at *(x,y)* requires that

$$\frac{d}{ds}\left(T\frac{dy}{ds}\right) = -w \tag{3.1}$$

where T is line tension and w is weight per unit length in water.

Horizontal equilibrium of the element yields

$$\frac{d}{ds}\left(T\frac{dx}{ds}\right) = 0 \tag{3.2}$$

Equation (3.2) may be integrated directly to

$$T\frac{dx}{ds} = X \tag{3.3}$$

where X is the horizontal component of cable tension.

Consequently Equation (3.1) may be reduced to the following governing differential equation of the catenary after replacing T from Equation (3.3)

$$\begin{aligned} X\frac{d^2y}{dx^2} &= -w\frac{ds}{dx} \\ &= -w\left[1+\left(\frac{dy}{dx}\right)^2\right]^{1/2} \end{aligned} \tag{3.4}$$

The Equation (3.4) may be integrated twice to give

$$y = -\frac{X}{w}\cosh\left(\frac{w}{X}x - \phi\right) + C \tag{3.5}$$

where the constants of integration ϕ and C are obtained by using boundary conditions which constrain the cable at $(0,0)$ and (a,b)

$$\begin{aligned} \phi &= \lambda + \sinh^{-1}\left[\frac{wb}{2X}\frac{1}{\sinh\lambda}\right] \\ C &= \frac{X}{w}\cosh(-\phi) \end{aligned} \tag{3.6}$$

where

$$\lambda = \frac{wa}{2X} \tag{3.7}$$

Inserting the above constants to Equation (3.5) gives

$$y = \frac{X}{w}\left[\cosh\phi - \cosh\left(\frac{2\lambda x}{a} - \phi\right)\right] \tag{3.8}$$

The unstretched length L_u of a segment OA can be obtained as

$$\begin{aligned} L_u &= \int_0^a \frac{ds}{dx}dx \\ &= \frac{2X}{w}\sinh\lambda\ \cosh(\phi - \lambda) \end{aligned} \tag{3.9}$$

Also the vertical elevation b is from Equation (3.8)

$$b = \frac{2X}{w}\sinh\lambda\ \sinh(\phi - \lambda) \tag{3.10}$$

Equations (3.9) and (3.10) are now squared and added, giving the well known expression

$$L_u{}^2 - b^2 = \frac{X^2}{\lambda^2}\sinh^2\lambda \tag{3.11}$$

The vertical component of cable tension at the left-hand end of the cable is

$$\begin{aligned} Y_O &= X\left(\frac{dy}{dx}\right)_{x=0} \\ &= X\ \sinh\phi \\ &= \frac{w}{2}\left(b\coth\lambda + L_u\right) \end{aligned} \tag{3.12}$$

Similarly, the tension at the left-hand end of the cable is

$$\begin{aligned} T_O &= X\left(\frac{ds}{dx}\right)_{x=0} \\ &= X\ cosh\phi \\ &= \frac{w}{2}\left(L_u\ coth\lambda\ +\ b\right) \end{aligned} \tag{3.13}$$

O'Brien and Francis (1964) and Jennings (1965) presented an alternative set of equations describing the free hanging catenary with elastic stiffness which are much more suitable for automated calculations. Peyrot and Goulois (1979) converted these mathematical details into a computer algorithm to determine end forces and the tension distribution in a catenary from a knowledge of its end coordinates, line elasticity and unstretched length. To account for its elastic stiffness, the following catenary relationships modified from Equations (3.11) and (3.12) with different sign convention (see Figure 3.2) are used for each cable element.

$$L^2 = b^2 + \frac{X^2}{\lambda^2} sinh^2\ \lambda \tag{3.14}$$

$$Y_O = \frac{w}{2}\left(-b\ coth\lambda + L\right) \tag{3.15}$$

where L is the stretched length of a segment.

Cable end forces and tensions are related by the following equations.

$$\begin{aligned} Y_A &= -Y_O + wL_u \\ X_A &= -X_O \\ T_O &= \left(X_O^{\ 2} + Y_O^{\ 2}\right)^{1/2} \\ T_A &= \left(X_A^{\ 2} + Y_A^{\ 2}\right)^{1/2} \end{aligned} \tag{3.16}$$

By integrating along the cable length, three additional geometric relationships are obtained.

$$
\begin{aligned}
a &= -X_O\left(\frac{L_u}{EA}+\frac{1}{w}ln\frac{T_A+Y_A}{T_O-Y_O}\right)\\
b &= \frac{1}{2EAw}\left(T_A{}^2-T_O{}^2\right)+\frac{T_A-T_O}{w}\\
L &= L_u+\frac{1}{2EAw}\left(Y_AT_A+Y_OT_O+X_O{}^2\,ln\frac{T_A+Y_A}{T_O-Y_O}\right)
\end{aligned}
\tag{3.17}
$$

The line coordinates can be determined by replacing L_u by any fraction of L_u in Equation (3.17). As can be seen from this set of equations, a, b and L can be written as a function of X_O and Y_O alone. An iteration procedure is then set up with the starting values of X_O and Y_O with the first and second terms in an expansion of $[sinh^2\lambda/\lambda^2]$ being used. Hence initial values of a a and b are found, and linear corrections δa and δb are then applied to X_O and Y_O until δa and δb are less than a tolerance. Hence the forces X_O, Y_O, X_A, Y_A and cable tensions are found for any catenary.

3.1.2 Equilibrium Equations for Slender Pipes

Pipelines are generally made of a steel pipe with concrete coating for a conventional pipeline or multi steel pipes for a bundle as shown in Figure 1.2. Towed pipelines are generally very long and these slender structures require analyses during a design stage to ensure that they have acceptable levels of deformations, stresses and fatigue lives due to forces induced by self-weight, buoyancy, currents, waves, and tow vessel motions. Towed pipelines usually experience large deformation compared to their diameters due to these loads and, consequently, their governing equations introduce nonlinearities. Moreover, the presence of internal and external hydrostatic pressure

as well as axial and lateral loading makes the problem more complicated. In this section, governing equations of slender pipes under general loadings are derived.

At first we consider the slender beam segment with static loading as shown in Figure 3.3. The equilibrium of forces in x and y directions yields

$$\sum F_x = (T+dT)\cos(\theta+d\theta) - T\cos\theta + (V+dV)\sin(\theta+d\theta) + V\sin\theta + f_x ds = 0 \tag{3.18}$$

$$\sum F_y = (T+dT)\sin(\theta+d\theta) + T\sin\theta - (V+dV)\cos(\theta+d\theta) + V\cos\theta + f_y ds = 0 \tag{3.19}$$

where V is a shear force, and f_x and f_y are forces per unit length to x and y axis respectively.

For small values of $d\theta$, the following approximations are valid.

$$\cos(\theta+d\theta) = \cos\theta - d\theta\sin\theta$$
$$\sin(\theta+d\theta) = \sin\theta + d\theta\cos\theta$$

Expanding Equations (3.18) and (3.19) using the above approximations and the summation of two resultant equations after multiplying by $(-\sin\theta)$ and $\cos\theta$ respectively gives

$$Td\theta - dV - f_x \sin\theta\, ds + f_y \cos\theta\, ds = 0$$
$$T\frac{d\theta}{ds} - \frac{dV}{ds} - f_x \sin\theta + f_y \cos\theta = 0 \tag{3.20}$$

Equation (3.20) is converted to Equation (3.21) in a Cartesian coordinate system using the following relations

$$\frac{d\theta}{ds} = \frac{1}{r} = y''\left(1+y'^2\right)^{-3/2}$$

$$\sin\theta = y'\left(1+y'^2\right)^{-1/2}$$

$$\cos\theta = \left(1+y'^2\right)^{-1/2}$$

$$\frac{dV}{ds} = \frac{dV}{dx}\frac{dx}{ds} = \frac{dV}{dx}\cos\theta = \frac{dV}{dx}\left(1+y'^2\right)^{-1/2}$$

$$Ty''\left(1+y'^2\right)^{-1} - \frac{dV}{dx} - f_x y' + f_y = 0 \qquad (3.21)$$

where y' and y'' respectively denote the first and second derivatives of y with respect to x.

The relation between shear force V and bending moment M gives

$$\frac{dV}{dx} = \frac{d}{dx}\frac{dM}{dx} = \frac{d^2}{dx^2}\left(EI\frac{d\theta}{ds}\right) = \frac{d^2}{dx^2}\left[EIy''\left(1+y'^2\right)^{-3/2}\right]$$

where EI is a bending rigidity.

Finally, the governing equation of the slender beam element with large deformation is

$$\frac{d^2}{dx^2}\left[EIy''\left(1+y'^2\right)^{-3/2}\right] - Ty''\left(1+y'^2\right)^{-1} + f_x y' - f_y = 0 \qquad (3.22)$$

As can be seen, Equation (3.22) introduces nonlinearities in geometric sense and due to the product of tension and curvature. If the pipe is assumed to be not exposed to hydrostatic pressure forces, then f_x and f_y are simply due to self-weight and current forces in a static case. If, however, that is not the case, we obtain a slightly different

equation. The components of total hydrostatic pressure forces on curved pipes are derived in Section 3.2.2 and these are (for definitions of variables, see Section 3.2)

$$F_x = \left[(P_i A_i - P_o A_o) + r(\gamma_i A_i - \gamma_o A_o)(\cos\theta - \sin\theta\, d\theta)\right] \cdot \sin\theta\, d\theta$$
$$F_y = \left[(P_o A_o - P_i A_i) + r(\gamma_o A_o - \gamma_i A_i)(\cos\theta - \sin\theta\, d\theta)\right] \cdot \cos\theta\, d\theta$$

After replacing f_x and f_y in Equation (3.22) by the uniform distribution of these components to their corresponding directions, the governing equation becomes

$$\frac{d^2}{dx^2}\left[EIy''\left(1+y'^2\right)^{-3/2}\right] - \left(T + P_o A_o - P_i A_i\right)y''\left(1+y'^2\right)^{-1} - \left(\gamma_o A_o - \gamma_i A_i\right) = 0 \qquad (3.23)$$

The effects of hydrostatic pressure forces on the pipeline can be clearly deduced from the second term in the above equation. That is, their effects are similar to that of the actual tension in the pipeline wall.

Although a towed pipeline experiences large deformation compared to its diameter, this deformation can be assumed to be small compared to its global dimensions like length or maximum sagging. Under this small deflection assumption, that is, small y', the governing equation becomes

$$\frac{d^2}{dx^2}(EIy'') - \left(T + P_o A_o - P_i A_i\right)y'' = \left(\gamma_o A_o - \gamma_i A_i\right) + f_y' \qquad (3.24)$$

where f_y' is the static force except hydrostatic pressure forces.

In the case of dynamic force $f_y(x,t)$, inertia force and damping force are introduced.

$$m\frac{d^2y}{dt^2}+c\frac{dy}{dt}+\frac{d^2}{dx^2}(EIy'')-Ty''=f_y(x,t) \tag{3.25}$$

where m is a mass per unit length and c is a damping coefficient of the pipe.

If we neglect bending rigidity EI and a horizontal force component f_x, Equation (3.22) becomes

$$Ty''\left(1+y'^2\right)^{-1}-f_y=0$$

If we consider self-weight only and use the sign convention used during the derivation of the catenary relationships, f_y equals to $(-w)$ and the above equation becomes

$$Ty''\left(1+y'^2\right)^{-1}=-w$$
$$Xy''=-w\left(1+y'^2\right)^{1/2}$$

This final equation is exactly same as the catenary equation, Equation (3.4).

3.2 Hydrostatic Pressure Forces on Pipelines

Towed pipelines are subjected to high external hydrostatic pressure during tow since they are generally placed well below a wave-active zone. To prevent ingress of water in the event of leaking at that depth, they are filled with pressurised nitrogen. This external and internal pressure has an influence on the governing equation of pipelines as shown in Section 3.1.2. Also the very small submerged weight of towed pipelines means that these pressure-induced forces could significantly influence the pipeline's behaviour.

As Sparks (1984) pointed out, the effects of pressure forces on the pipe behaviour have caused a great deal of confusion. Equation (3.24) in Section 3.1.2 clearly shows

that the pressure force controls pipe curvatures in a way similar to the tensile forces in the wall of the pipe. Conventionally these forces are calculated using Archimedes' law with modifications to exclude the effects of end cap pressures, thereby allowing pipe continuity as discussed in detail by Sparks (1979). This approach is, however, based on the assumption of small curvatures and it requires more elements in finite element models to secure accuracy of analysis. In order to improve this drawback, more accurate expressions are needed to accommodate larger element sizes and, consequently, to reduce computer resources.

This section summarises the derivation of pressure forces for a straight pipe and a curved pipe of a constant curvature in two dimensions respectively originated from Seyed (1989) and Patel (1989).

The definitions of variables are as follows (also see Figure 3.4 and 3.5):

R : radius of the pressure bearing surface, that is, outer radius

s : length measured from the centre of a pipe

ℓ : length of a pipe

θ : angle from x axis to the axis of a pipe

ϕ : angle around the circumference of a pipe from z axis

P_i : internal hydrostatic pressure around a pipe

P_o : external hydrostatic pressure around a pipe

γ : specific weight of fluid

γ_i : specific weight of fluid inside of a pipe

γ_o : specific weight of fluid outside of a pipe

A_i : inner cross sectional area of a pipe

A_o : outer cross sectional area of a pipe

3.2.1 Straight Pipes

At first, we consider the forces due to external pressure for the pipe element shown in Figure 3.4. The area of the differential element on the surface of the pipe is given by

$$dA = R\, d\phi\, ds \tag{3.26}$$

If the pressure at the lower end A on on the axis of the pipe is P_A, the pressure P_s at distance s from point A along the axis of the pipe is

$$P_s = P_A - \gamma s \sin\theta \tag{3.27}$$

For this position, pressure on the element of surface area is given by

$$\begin{aligned} P(s,\phi) &= P_s + \gamma R \sin\phi \cos\theta \\ &= P_A - \gamma s \sin\theta + \gamma R \sin\phi \cos\theta \end{aligned} \tag{3.28}$$

The force which acts on the element of differential area dA is then

$$dF = P\, dA \tag{3.29}$$

The differential force dF may be resolved into its three dimensional components - F_x, F_y and F_z along the x, y and z axes respectively - using following relationships.

$$\begin{aligned} dF_x &= (-dF \sin\phi)\sin\theta = -PR \sin\phi \sin\theta\, d\phi\, ds \\ dF_y &= dF \sin\phi \cos\theta = PR \sin\phi \cos\theta\, d\phi\, ds \\ dF_z &= -dF \cos\phi = -PR \cos\phi\, d\phi\, ds \end{aligned} \tag{3.30}$$

The total force in each direction is obtained by integration of the above equations.

$$
\begin{aligned}
F_x &= \int dF_x = -R\sin\theta \int_0^{\ell}\int_0^{2\pi} P\sin\phi \, d\phi \, ds \\
&= -\pi R^2 \gamma \ell \sin\theta\cos\theta \\
&= -\gamma A \ell \sin\theta\cos\theta
\end{aligned}
$$

$$
\begin{aligned}
F_y &= \int dF_y = R\cos\theta \int_0^{\ell}\int_0^{2\pi} P\sin\phi \, d\phi \, ds \\
&= \pi R^2 \gamma \ell \cos^2\theta \\
&= \gamma A \ell \cos^2\theta
\end{aligned}
\qquad (3.31)
$$

$$
\begin{aligned}
F_z &= \int dF_z = -\int_0^{\ell}\int_0^{2\pi} PR\cos\phi \, d\phi \, ds \\
&= 0
\end{aligned}
$$

When the force due to internal pressure is considered, its form will be the same but of opposite sign. Combining the effects of internal and external pressure, the final expression for the resultant pressure forces in the x and y axes becomes

$$
\begin{aligned}
F_x &= \left(\gamma_i A_i - \gamma_o A_o\right) \ell \sin\theta\cos\theta \\
F_y &= \left(\gamma_o A_o - \gamma_i A_i\right) \ell \cos^2\theta
\end{aligned}
\qquad (3.32)
$$

The above derivations are equivalents to a mathematical restatement of Archimedes' law for a continuous and straight pipe. Note that the resulting expressions are independent of fluid pressures and hence independent of depth. Instead they are frame-dependent since the positive y axis is chosen as the axis of pressure gradient. The effect of cap pressure at the ends of a pipe is separately considered.

3.2.2 Curved Pipes

At first, we consider the forces due to external pressure for the pipe element shown in Figure 3.5. The arc length *ds* of any strip on the pipe circumference parallel to its axis is given by

$$ds = (r + R\sin\phi)d\theta \tag{3.33}$$

where r is the radius of curvature.

The area of the section of element described by arc $d\phi$ is given by

$$dA = Rd\phi\, ds \tag{3.34}$$

If the hydrostatic pressure at the lower end A on the center line of the element is P, then the pressure P_a at various levels along the bottom surface is given by

$$P_a = P + \gamma R\sin\phi\cos\theta \tag{3.35}$$

Also the corresponding hydrostatic pressure P_b at the top of the element is given by

$$P_b = P_a - \gamma\, \sin\theta\, ds \tag{3.36}$$

The force which acts on this section of the element dA is then

$$\begin{aligned} dF &= \frac{1}{2}(P_a + P_b)dA \\ &= \left(P + \gamma R\sin\phi\, \cos\theta - \frac{1}{2}\gamma\, \sin\theta\, ds\right) Rd\phi\, ds \end{aligned} \tag{3.37}$$

Replacing Equation (3.33) for ds leads to

$$\begin{aligned} dF = &\left[P + \gamma R\sin\phi\, \cos\theta - \frac{1}{2}\gamma\, \sin\theta(r + R\sin\phi)d\theta\right] \\ &\cdot Rd\phi(r + R\sin\phi)d\theta \end{aligned} \tag{3.38}$$

Expanding the individual terms gives

$$\begin{aligned} dF = &\left[PRr\,d\theta - \frac{1}{2}\gamma Rr^2 \sin\theta (d\theta)^2 \right] d\phi \\ &+ \left[PR^2 d\theta + \gamma R^2 r \cos\theta\, d\theta - \gamma R^2 r \sin\theta (d\theta)^2 \right] \sin\phi\, d\phi \\ &+ \left[\gamma R^3 \cos\theta\, d\theta - \frac{1}{2}\gamma R^3 \sin\theta (d\theta)^2 \right] \sin^2\phi\, d\phi \end{aligned} \tag{3.39}$$

The differential force dF may be resolved into its three dimensional components - F_x, F_y and F_z along the x, y and z axes respectively - using following relationships.

$$\begin{aligned} dF_x &= (-dF \sin\phi)\sin\theta \\ dF_y &= dF \sin\phi \cos\theta \\ dF_z &= -dF \cos\theta \end{aligned} \tag{3.40}$$

The total force in each axis is obtained by integration of the above equations.

$$\begin{aligned} F_x &= \int_{\phi=0}^{2\pi} (-dF \sin\phi)\sin\theta \\ &= -\pi R^2 \left[P + \gamma r (\cos\theta - \sin\theta\, d\theta) \right] \sin\theta\, d\theta \\ &= -\left[PA + \gamma rA (\cos\theta - \sin\theta\, d\theta) \right] \sin\theta\, d\theta \end{aligned}$$

$$\begin{aligned} F_y &= \int_{\phi=0}^{2\pi} dF \sin\phi \cos\theta \\ &= \pi R^2 \left[P + \gamma r (\cos\theta - \sin\theta\, d\theta) \right] \cos\theta\, d\theta \\ &= \left[PA + \gamma rA (\cos\theta - \sin\theta\, d\theta) \right] \cos\theta\, d\theta \end{aligned} \tag{3.41}$$

$$\begin{aligned} F_z &= \int_{\phi=0}^{2\pi} -dF \cos\phi \\ &= 0 \end{aligned}$$

When the force due to internal pressure is considered, its form will be the same but of opposite sign. Combining the effects of internal and external pressure, the final expression for the resultant pressure forces in the x and y axes becomes

$$\begin{aligned} F_x &= \left[(P_i A_i - P_o A_o) + r(\gamma_i A_i - \gamma_o A_o)(\cos\theta - \sin\theta\, d\theta)\right]\sin\theta\, d\theta \\ F_y &= \left[(P_o A_o - P_i A_i) + r(\gamma_o A_o - \gamma_i A_i)(\cos\theta - \sin\theta\, d\theta)\right]\cos\theta\, d\theta \end{aligned} \tag{3.42}$$

3.3 Current Forces on Chains and Pipelines

A tow system is highly influenced by the relative fluid flow arising from current and tow speed. At rest or low tow speed, chains attached to the pipeline are in contact with the seabed. As the tow speed increases, the resultant flow around the system generates a net lift force and it allows the entire system to be towed free of the seabed. Therefore, expected tow configuration mainly depends on the careful control and accurate estimation of current forces on the system, especially those on chains. This section is concerned with calculation of these forces. The current also has an influence on the fluid field and encounter frequency, and consequently the pipe's dynamic responses. This will be discussed later in Section 3.4.1.

3.3.1 Current Forces on Chains

The forces on chains arising from towing and current play a key role in the mid-depth tow. The condition of a tow operation - parking on the seabed, taking off from the seabed, and towing free of the seabed - totally depends on this force and an accurate estimation of this force is essential for a successful operation.

If the fluid has a relative velocity U with respect to the chain, this can be decomposed into a velocity normal to the chain, U_n, and tangential to the chain, U_t (see Figure 3.6.a).

$$U_n = U\cos\theta$$
$$U_t = U\sin\theta \tag{3.43}$$

where θ is the angle where chains are in equilibrium condition under current force and self-weight.

These components generate respectively a normal drag force, F_n, and a tangential drag force, F_t, per length of chains.

$$F_n = \frac{1}{2}\rho U_n^2 C_n \ell_c$$
$$F_t = \frac{1}{2}\rho U_t^2 C_t \pi \ell_c \tag{3.44}$$

where ρ is seawater density, C_n and C_t are appropriate coefficients, and ℓ_c is length of chains.

We can compose a vertical and a horizontal force out of these forces (see Figure 3.6.b) and the resultant vertical component of these forces is called a lift force, F_L. This lift force reduces the chain weight as the tow speed increases, and this is the basic driving mechanism of the mid-depth tow.

$$\begin{aligned} F_L &= F_{ny} - F_{ty} \\ &= F_n \sin\theta - F_t \cos\theta \end{aligned} \tag{3.45}$$

The corresponding horizontal component is called a drag force, F_D, and may be written as

$$\begin{aligned} F_D &= F_{nx} + F_{tx} \\ &= F_n \cos\theta + F_t \sin\theta \end{aligned} \tag{3.46}$$

As can be seen from the above equations, both lift force and drag force depend on the fluid speed U and coefficients C_n and C_t which depend on the specific chain type and fluid velocity. Since an accurate estimation of these forces is essential for a successful mid-depth tow and little data is available for free hanging chains, full scale tests of chains are usually performed in a towing tank. In the present work, the data and formulae originated from full scale tests by MARIN (Maritime Research Institute of Netherlands) are used. Measured lift forces and drag forces on various chains under different current velocities are shown in Figures 3.7 and 3.8 with detailed data for the tested chains.

To derive a proper formula for lift forces and drag forces, following forms of formula were proposed.

$$\begin{aligned} F_L &= A_L U^{B_L} \ell_c d_c \quad (N) \\ F_D &= A_D U^{B_D} \ell_c d_c \quad (N) \end{aligned} \tag{3.47}$$

where A_L, B_L, A_D, and B_D are appropriate coefficients. U is resultant current velocity in metres per second. d_c and ℓ_c are respectively diameter and length of chains in metres.

With the aid of a power regression method, the coefficients A_L, B_L, A_D, and B_D are obtained for each type of chains and the resultant values are presented in Tables 3.1 and 3.2. These resulting coefficients show that there is wide difference of coefficients with different types of chains. The coefficients for other chains not listed in the present tables may be obtained from linear interpolation of the available data for the two nearest diameters.

3.3.2 Current Forces on Pipelines

Offshore engineers usually consider only the component of current normal to the pipeline for the calculation of drag forces. This approach is quite reasonable for most

common offshore structures such as fixed platform legs and risers since the forces due to a tangential component are negligible compared to those due to a normal one. In the case of towed pipelines, however, circumstances are totally different and this approach leads to wrong results. Towed pipelines are generally long and experience high tow speeds with a small angle of attack. In this case, the total frictional drag force due to the tangential component of a current is quite large and it directly influences the structural behaviour of the pipeline through its tension. Also the resultant tensions at the ends of the pipeline provide a good guideline to select the leading and trailing tow vessels with proper tug capabilities.

The normal drag force, F_{dn}, and tangential frictional drag force, F_{dt}, per unit length are calculated from the following formulae.

$$F_{dn} = \frac{1}{2}\rho C_{dn} D U_n^2$$
$$F_{dt} = \frac{1}{2}\rho C_{dt} \pi D U_t^2 \qquad (3.48)$$

where C_{dn} and C_{dt} are respectively coefficients of normal and tangential drag forces and Figure 3.9 (Wilson, 1960) shows proper values of these coefficients for different types of pipes and cables.

3.4 Wave Kinematics and Hydrodynamic Forces

In the case of towed pipelines the influence of waves is equally important all along the length since they are in a near-horizontal configuration and placed close to the free surface.

This section is concerned with the wave kinematics and wave-induced forces on pipelines and tow vessels. Linear wave theory is used throughout this work and the wave kinematics from this theory are modified to consider tow speed. Traditionally, the Morison equation has been used by offshore engineers to predict wave forces on

pipes. In the case of towed pipelines, however, the Morison equation needs some improvements due to the presence of high near-tangential flow. The improvement of its inertia term using the Lighthill's approach is presented. The consideration of axial interaction of a pipeline, towlines, and tow vessels is essential in dynamic analyses. For this, wave forces on tow vessels must be considered instead of the usual approach of using vessel displacements as boundary conditions. The simplified scheme used to calculate the wave forces on tow vessels is also described.

3.4.1 Wave Kinematics with Tow Speed

In order to calculate the wave-induced forces acting on a tow system, we must know its surrounding hydrodynamic flow field under waves and currents, and use an appropriate wave theory. The linear (Airy) wave theory is used throughout this work. It is a small amplitude theory which assumes that a sinusoidal wave amplitude a is small compared to wave length λ and water depth h (see Figure 3.10). This theory is widely used by offshore engineers because it provides a powerful and simple solution that describes the basic characteristics of wave-induced water motion and forms the basis for the probabilistic spectral description of waves. Initially, classical equations from the linear wave theory (Dean and Dalrymple, 1984) are presented and they are later modified to consider the effects of tow speed.

Velocity potential ϕ for a progressive gravity wave is

$$\phi = -a\frac{g}{\omega}\frac{\cosh k(y+h)}{\sinh kh}\cos(kx-\omega t) \tag{3.49}$$

with a space-time representation of surface elevation η as

$$\eta = a\sin(kx-\omega t) \tag{3.50}$$

where g denotes the acceleration of gravity. k and ω denote respectively wave number and wave frequency and they can be defined in terms of the wave length λ and period T.

$$k = \frac{2\pi}{\lambda} \tag{3.51}$$

$$\omega = \frac{2\pi}{T} \tag{3.52}$$

The above wave number and wave frequency can be related by the following so-called dispersion relationship.

$$\omega^2 = gk \tanh kh \tag{3.53}$$

The horizontal velocity u and vertical velocity v of water particles at space (x,y) and time t are

$$\begin{aligned} u &= -\frac{\partial \phi}{\partial x} = a\omega \frac{\cosh k(y+h)}{\sinh kh} \sin(kx - \omega t) \\ v &= -\frac{\partial \phi}{\partial y} = -a\omega \frac{\sinh k(y+h)}{\sinh kh} \cos(kx - \omega t) \end{aligned} \tag{3.54}$$

The corresponding local acceleration $\dot{u}$ and $\dot{v}$ are then

$$\begin{aligned} \dot{u} &= \frac{\partial u}{\partial t} = -a\omega^2 \frac{\cosh k(y+h)}{\sinh kh} \cos(kx - \omega t) \\ \dot{v} &= \frac{\partial v}{\partial t} = -a\omega^2 \frac{\sinh k(y+h)}{\sinh kh} \sin(kx - \omega t) \end{aligned} \tag{3.55}$$

In the case of deep water, the corresponding equations are

$$\begin{aligned}
\phi &= -a\frac{g}{\omega}e^{ky}\cos(kx-\omega t)\\
u &= a\omega e^{ky}\sin(kx-\omega t)\\
v &= -a\omega e^{ky}\cos(kx-\omega t)\\
\dot{u} &= -a\omega^2 e^{ky}\cos(kx-\omega t)\\
\dot{v} &= -a\omega^2 e^{ky}\sin(kx-\omega t)
\end{aligned} \tag{3.56}$$

The wave length at shallow water is determined iteratively from

$$\lambda = \frac{gT^2}{2\pi}\tanh\left(\frac{2\pi h}{\lambda}\right) \tag{3.57}$$

whilst that at deep water is given analytically by

$$\lambda = \frac{gT^2}{2\pi} \tag{3.58}$$

The propagation speed of the wave profile, c, in deep water is

$$c = \frac{\lambda}{T} = \frac{1}{T}\frac{gT^2}{2\pi} = \frac{gT}{2\pi} = \frac{g}{\omega} \tag{3.59}$$

In the case of towed pipelines, we must consider the effects of tow speed because it significantly modifies wave kinematics. In order to do this, it is necessary to define additional frames of reference (Price and Bishop, 1974, see Figure 3.11). The coordinate system *OXYZ* is fixed with *OZX* in the mean sea surface and with the axis *OY* pointing vertically upwards. At any point *(X,Z)*, the elevation of waves travelling with velocity c at an angle μ to the axis *OZ* is given by

$$\eta(X,Z,t) = a\ \sin(kX\sin\mu + k\,Z\cos\mu - \omega t) \tag{3.60}$$

The fixed frame of reference $OX'Y'Z'$ also has $OZ'X'$ in the mean sea surface, but the axis OZ' points in the direction of the towing. The tow is assumed to have velocity U and a heading that is inclined at an angle ξ to the axis OZ as shown in Figure 3.11. From a transformation of coordinates

$$\begin{aligned} X &= X'\cos\xi + Z'\sin\xi \\ Y &= Y' \\ Z &= -X'\sin\xi + Z'\cos\xi \end{aligned} \tag{3.61}$$

The system $c'x'y'z'$ is a moving frame of reference and this frame always remains parallel to $OX'Y'Z'$. At the instant $t=0$, the origins O and c' coincide so that, at time t, the coordinates when measured with respect to $OX'Y'Z'$ are

$$X' = x', \qquad Y' = y', \qquad Z' = z' + Ut \tag{3.62}$$

or when measured with respect to $OXYZ$

$$\begin{aligned} X &= x'\cos\xi + z'\sin\xi + Ut\sin\xi \\ Y &= y' \\ Z &= -x'\sin\xi + z'\cos\xi + Ut\cos\xi \end{aligned} \tag{3.63}$$

Now the wave elevation at any point, measured with respect to the moving frame $c'x'y'z'$ is given by

$$\begin{aligned} \eta(x',z',t) &= a\ \sin\big[k\ \sin\mu(x'\cos\xi + z'\sin\xi + Ut\ \sin\xi) \\ &\qquad + k\ \cos\mu(-x'\sin\xi + z'\cos\xi + Ut\ \cos\xi) - \omega t\big] \\ &= a\ \sin\big[kx'\sin(\mu-\xi) + k\,z'\cos(\mu-\xi) - \{\omega - Uk\cos(\mu-\xi)\}t\big] \end{aligned} \tag{3.64}$$

With $\chi = \mu - \xi$, this becomes

$$\eta(x',z',t) = a\ sin(kx'\ sin\chi + kz'\ cos\chi - \omega_e t) \tag{3.65}$$

where the frequency of encounter ω_e can be written as

$$\omega_e = \omega - Uk\ cos\chi \tag{3.66}$$

For waves in deep water, it can be written using the dispersion relationship

$$\begin{aligned} \omega_e &= \omega - \frac{U\omega^2}{g}cos(\mu - \xi) \\ &= \omega - \frac{U\omega^2}{g}cos\chi \end{aligned} \tag{3.67}$$

If the tow angle is same as the wave angle, that is, $\chi = \mu - \xi = 0$, then the velocity potential, the velocities and accelerations of the wave particles can be written as following since the wave length is unchanged whereas the frequency of encounter is changed due to the tow speed.

$$\begin{aligned} \phi &= -a\frac{g}{\omega}e^{ky}\ cos(kz' - \omega_e t) \\ u &= a\omega e^{ky}\ sin(kz' - \omega_e t) \\ v &= -a\omega e^{ky}\ cos(kz' - \omega_e t) \\ \dot{u} &= -a\omega\omega_e e^{ky}\ cos(kz' - \omega_e t) \\ \dot{v} &= -a\omega\omega_e e^{ky}\ sin(kz' - \omega_e t) \end{aligned} \tag{3.68}$$

3.4.2 The Morison Formulation

Towed pipelines are subjected to several types of loading arising from waves and currents during towing. These loadings are:

- Inertia forces due to the basic need for the water to move aside as the pipeline passes.

- Non-linear drag forces reflecting the size of the wake left behind.
- Oscillatory lift forces due to the resonance of the pipeline and vortex shedding.

The principle involved in the concept of the inertia force is that a water particle moving in a wave carries a momentum with it. As the water particle passes around the circular cylinder it accelerates and decelerates. This requires that work be done through the application of a force on the cylinder to increase this momentum. The incremental force on a small segment of the cylinder, *ds*, needed to accomplish this is proportional to the water particle acceleration at the centre of the cylinder. More details about this force will be given in the next section. The principal cause of the drag force component is the presence of the wake region on the downstream side of the cylinder. The wake is a region of low pressure compared to the pressure on the upstream side and thus a pressure differential is created by the wake between upstream and downstream of the cylinder at a given instant of time.

Usually most of the hydrodynamic modelling of cylinders which have a relatively small diameter compared with wave length and water depth has been based on Morison equation. The central concept in the analysis of hydrodynamic phenomena is the classical division of the flow field into the above two components and the total hydrodynamic load as the sum of the hydrodynamic loads felt in the two flows considered separately. Although the Morison equation was originally developed for vertical stiff piles in shallow water (Morison et. al., 1950), for engineering purposes it is assumed to be valid for cylinders of arbitrary orientation in deep and shallow water. In the case of relatively stiff structures, the velocities of the structure are negligible compared to the fluid velocities, and the fluid forces acting on the structure can be calculated from

$$dF = \frac{1}{4}\rho\pi D^2 C_M \dot{u}_n ds + \frac{1}{2}\rho D C_d u_n |u_n| ds \qquad (3.69)$$

where dF is the normal force on a strip of length ds of a rigid circular cylinder. u_n and $\dot{u}_n$ are respectively normal components of velocity and acceleration of a wave particle. C_M is an inertia coefficient and can be written $C_M=1+C_m$, where C_m is an added mass coefficient. C_d is a drag coefficient.

In the case of compliant structures like towed pipelines and flexible risers, the dynamic responses y caused by waves may become much more significant and, therefore, the loadings are a function of the relative velocities between structure and fluid. In this case original Morison equation can be modified and can be written as

$$\begin{aligned} dF = & \frac{1}{4}\rho\pi D^2 C_M \dot{u}_n ds - \frac{1}{4}\rho\pi D^2 (C_M - 1)\ddot{y} ds \\ & + \frac{1}{2}\rho D C_d (u_n - \dot{y})|u_n - \dot{y}| ds \end{aligned} \tag{3.70}$$

where $\dot{y}$ and $\ddot{y}$ are respectively normal components of velocity and acceleration of the structure.

If the added mass term of the above equation is taken to the left hand side of the equation of motion, Equation (3.25) in Section 3.1.2, and combined with the physical mass term, the resulting governing equation becomes for a constant bending rigidity EI

$$\begin{aligned} & (m + m_a)\ddot{y} + c\dot{y} + EIy^{(4)} - Ty'' \\ & = \frac{1}{4}\rho\pi D^2 C_M \dot{u}_n + \frac{1}{2}\rho D C_d (u_n - \dot{y})|u_n - \dot{y}| \end{aligned} \tag{3.71}$$

where $m_a = \frac{1}{4}\rho\pi D^2$.

3.4.3 The Lighthill Approach

The Morison equation is primarily concerned with pipes and piles that are essentially normal to a flow, and its accuracy for a near-tangential flow is questionable. In the case of inertia forces, they can be checked and improved analytically whilst drag forces must be checked experimentally due to the complexity of handling wakes. This section is concerned with improvement of the accuracy of the inertia force term for near-tangential flow.

The inertia force on a pipeline is produced by two mechanisms. First, if a flow accelerates, a pressure gradient is generated in the flow field and this pressure gradient exerts a force, the so-called Froude-Krylov force, on a structure just as a buoyancy force is exerted on a structure immersed in a still fluid. This force is simply equal to the mass of the fluid displaced by the structure multiplied by the acceleration of the flow. The second component of the inertia force is an added mass force which accounts for fluid entrained by an accelerating structure. The added mass force depends on section shape and is proportional to the relative accelerations between the structure and the fluid. The analytical derivation of this force is possible for simple cases such as a two dimensional flow normal to a circular cylinder. In the case of slender pipes experiencing a lateral displacement and a high near-tangential flow, Lighthill (1960) showed using potential theory and a momentum method that there exist other terms contributing to the added mass force. At first, we derive these additional terms in two dimensions using the momentum method and later extend this to three dimensions.

If we assume that a towed pipeline experiences a lateral displacement $y(x,t)$ from a stretched straight position, the displacement is at right angles to the direction of towing and varies both with position and time. Then the flow around the pipeline can be regarded as made up of

(i) the steady flow around a stretched straight pipeline, and

(ii) the flow arising from the displacements of the pipeline, $y(x,t)$.

The flow component (ii) needs more attention for near-tangential flow whereas component (i) can be directly calculated in the absence of the pipeline. Component (ii), the resultant relative flow between the pipeline and the fluid, can be obtained by deriving the flow observed from the moving frame on the water particle. Using a total (sometimes called material or convective) derivative, we obtain the velocity, $v_f(x,t)$, relative to the fluid flowing with a tangential velocity v_t

$$\begin{aligned} v_f(x,t) &= \frac{d}{dt}[y(x,t)] \\ &= \frac{\partial y}{\partial t} + \frac{\partial y}{\partial x}\frac{\partial x}{\partial t} \\ &= \frac{\partial y}{\partial t} + v_t \frac{\partial y}{\partial x} \end{aligned} \tag{3.72}$$

where $y(x,t)$ is the lateral displacements of the pipeline.

The section shape and area of the pipeline differ little with that of an infinite cylinder and they are assumed to be same along the length. Accordingly, flow component (ii) is identical to the two-dimensional potential flow that would result from the motion of the pipeline with velocity $v_f(x,t)$ through a still fluid. Now we suppose that this resultant flow has momentum $\rho A v_f(x,t)$ per unit length of the pipeline, where ρA is the virtual mass of the pipeline per unit length for motion in the lateral direction. Lighthill's work (1960) shows that the resultant force F_a due to this flow is equal and opposite to the rate of change of momentum as seen by the water particle, that is,

$$
\begin{aligned}
F_a(x,t) &= -\frac{d}{dt}\left[\rho A v_f(x,t)\right] \\
&= -\rho A \frac{d}{dt}\left(\frac{\partial y(x,t)}{\partial t} + v_t \frac{\partial y(x,t)}{\partial x}\right) \\
&= -\rho A\left(\frac{\partial}{\partial t} + v_t \frac{\partial}{\partial x}\right)^2 \left[y(x,t)\right] \\
&= -\rho A\ddot{y} - 2\rho A v_t \frac{\partial^2 y}{\partial x \partial t} - \rho A v_t^{\,2} y''
\end{aligned}
\tag{3.73}
$$

The first term of the above resultant equation is exactly equivalent to a Morison inertia term and the second term has no equivalent in the Morison formulation. If this resultant added mass force is combined with the external force term in the equation of motion, Equation (3.25) in Section 3.1.2, and for constant bending rigidity *EI*, the resulting equation of motion becomes

$$
\left(m + m_a\right)\ddot{y} + 2m_a v_t \frac{\partial^2 y}{\partial x \partial t} + c\dot{y} + EIy^{(4)} - \left(T - m_a v_t^{\,2}\right)y'' = 0 \tag{3.74}
$$

where $m_a = \rho A$ and $y^{(4)}$ is the fourth derivative of y with respect to x.

The above equation clearly shows that the third term of Equation (3.73), $-\rho A v_t^{\,2} y''$, is exactly equivalent to the mechanical effect of an axial tension, *T*, and this term tends to induce larger lateral deformation. Therefore consideration of this additional term from the Lighthill's approach is important for the analysis of towed pipelines which are subjected to high tangential flow arising from tow speed.

Quiggin and Carsen (1994) extended the above approach to three dimensions. They considered a short element of the pipeline in general motion in a moving fluid. Allowing for body motion, the fluid momentum is $\rho A C_a\left(\boldsymbol{v}_b - \boldsymbol{v}_f\right)$ and, consequently, the resultant force is

$$\boldsymbol{F}_a = -\frac{d}{dt}\left[\rho A \boldsymbol{C}_a \left(\boldsymbol{v}_b - \boldsymbol{v}_f\right)\right] \tag{3.75}$$

where $\boldsymbol{C}_a$ is added mass matrix as will be explained later in detail. $\boldsymbol{v}_b$ and $\boldsymbol{v}_f$ are velocity vectors of the element and the fluid, respectively.

This expression will include extra terms that do not arise in the simple Morison case as described earlier. Specifically, $\boldsymbol{C}_a$ varies in time if the pipeline rotates relative to the fluid since the pipeline has different added mass coefficients in different directions. Secondly, the total derivative $d\left(\boldsymbol{v}_b - \boldsymbol{v}_f\right)/dt$ does not generally equal $\left(\boldsymbol{a}_b - \boldsymbol{a}_f\right)$ since $\left(\boldsymbol{v}_b - \boldsymbol{v}_f\right)$ is not just a function of time t but also of arc length s along the pipeline.

In order to calculate the rate of change of momentum, we work with the components of the added mass matrix with respect to two different right handed orthogonal frames of reference. Let $OXYZ$ be a non-rotating global frame having the axis OY pointing vertically upwards and axis OX and OZ horizontal. And $cxyz$ is a frame fixed on the element with axis cy and cz normal to its axis connecting ends, i.e., cx. The added mass matrix $\boldsymbol{C}_a$ in the expression has different components with respect to different axis systems whereas the terms ρ and A are scalars. In order to consider the added mass matrix systematically, we introduce another constant added mass matrix $\boldsymbol{C}$ whose components are with respect to body axes.

$$\boldsymbol{C} = \begin{bmatrix} 0 & 0 & 0 \\ 0 & C_m & 0 \\ 0 & 0 & C_m \end{bmatrix} \tag{3.76}$$

where C_m is an added mass coefficient of pipes in a normal flow.

Now the added mass matrix with respect to global axes can be written as

$$C_a = \boldsymbol{R}^T \boldsymbol{C} \boldsymbol{R} \tag{3.77}$$

where the transformation matrix $\boldsymbol{R}$ is the 3 by 3 matrix whose *(i,j)* entry is *cos*(angle between *i*-th body axis and *j*-th global axis).

The advantage of the above expression is that its variation with time is now contained purely in the transformation matrix $\boldsymbol{R}$ and the way that orientation changes. Therefore the momentum with respect to the global axes is $\rho A \boldsymbol{R}^T \boldsymbol{C} \boldsymbol{R}\left(\boldsymbol{v}_b - \boldsymbol{v}_f\right)$ and we can now find its rate of change, as seen by the fluid, by calculating the rate of change of these global components. Following the same procedure of Equation (3.72), the added mass force vector $\boldsymbol{F}_a$ is

$$\begin{aligned} \boldsymbol{F}_a &= -\frac{d}{dt}\left[\rho A \boldsymbol{C}_a\left(\boldsymbol{v}_b - \boldsymbol{v}_f\right)\right] \\ &= \rho A \frac{\partial}{\partial t}\left[\boldsymbol{R}^T \boldsymbol{C} \boldsymbol{R}\left(\boldsymbol{v}_f - \boldsymbol{v}_b\right)\right] + \rho A v_t \frac{\partial}{\partial x}\left[\boldsymbol{R}^T \boldsymbol{C} \boldsymbol{R}\left(\boldsymbol{v}_f - \boldsymbol{v}_b\right)\right] \end{aligned} \tag{3.78}$$

The second term here is the rate of change due to passage of the pipeline axially through the fluid. The first term can be calculated by simply differentiating term by term noting that,

- $\boldsymbol{C}$ is the added mass matrix with respect to body axes and so does not change with time.
- $\frac{\partial \boldsymbol{v}_b}{\partial t} = \boldsymbol{a}_b$
- The term $\frac{\partial \boldsymbol{v}_f}{\partial t}$ is the rate of change of fluid velocity with x fixed, i.e. as seen by the pipeline. This is the sum of the rate of change as time varies but with position p fixed, i.e. $\boldsymbol{a}_f$, and the rate of change with time fixed but position p varying as rate $\boldsymbol{v}_b$, i.e. $\left(\partial \boldsymbol{v}_f / \partial p\right)\boldsymbol{v}_b$. Therefore

$$\frac{\partial \boldsymbol{v}_f}{\partial t} = \boldsymbol{a}_f + \left(\frac{\partial \boldsymbol{v}_f}{\partial p}\right)\boldsymbol{v}_b \tag{3.79}$$

Using the above information and relationships, the force vector $\boldsymbol{F}_a$ can be written

$$\begin{aligned}\boldsymbol{F}_a = {} & \rho A\left(\frac{\partial \boldsymbol{R}^T}{\partial t}\right)\boldsymbol{C}\boldsymbol{R}\left(\boldsymbol{v}_f - \boldsymbol{v}_b\right) \\ & + \rho A\boldsymbol{R}^T\boldsymbol{C}\left(\frac{\partial \boldsymbol{R}}{\partial t}\right)\left(\boldsymbol{v}_f - \boldsymbol{v}_b\right) \\ & + \rho A\boldsymbol{R}^T\boldsymbol{C}\boldsymbol{R}\left[\boldsymbol{a}_f + \left(\frac{\partial \boldsymbol{v}_f}{\partial p}\right)\boldsymbol{v}_b - \boldsymbol{a}_b\right] \\ & + \rho A v_t \frac{\partial}{\partial x}\left[\boldsymbol{R}^T\boldsymbol{C}\boldsymbol{R}\left(\boldsymbol{v}_f - \boldsymbol{v}_b\right)\right]\end{aligned} \tag{3.80}$$

We can simplify these terms further using the following two relationships. Firstly, for any vector $\boldsymbol{u}$ (for details, see Bedford and Fowler (1995) and Love (1944))

$$\begin{aligned}\left(\frac{\partial \boldsymbol{R}}{\partial t}\right)\boldsymbol{u} &= \boldsymbol{R}\left(\boldsymbol{u} \times \boldsymbol{w}_b\right) \\ \left(\frac{\partial \boldsymbol{R}^T}{\partial t}\right)\boldsymbol{u} &= \boldsymbol{w}_b \times \left(\boldsymbol{R}^T\boldsymbol{u}\right)\end{aligned} \tag{3.81}$$

where $\boldsymbol{w}_b$ is the angular velocity vector of the body axes relative to the global axes.

And secondly, from the diagonal form of $\boldsymbol{C}$ and the symmetric property of $\boldsymbol{R}$

$$\boldsymbol{R}^T\boldsymbol{C}\boldsymbol{R}\boldsymbol{u} = C_m\left(\textit{normal component of}\ \boldsymbol{u}\right) \tag{3.82}$$

After applying these relationships and rearranging, we obtain the following equation for the added mass force vector $\boldsymbol{F}_a$

$$
\begin{aligned}
\boldsymbol{F}_a = {} & \rho A C_m \left[\textit{normal component of} \left(\boldsymbol{a}_f - \boldsymbol{a}_b \right) \right] \\
& + \rho A C_m \boldsymbol{w}_b \times \left[\textit{normal component of} \left(\boldsymbol{v}_f - \boldsymbol{v}_b \right) \right] \\
& + \rho A C_m \left[\textit{normal component of} \left\{ \left(\boldsymbol{v}_f - \boldsymbol{v}_b \right) \times \boldsymbol{w}_b \right\} \right] \\
& + \rho A C_m v_t \frac{\partial}{\partial x} \left[\textit{normal component of} \left(\boldsymbol{v}_f - \boldsymbol{v}_b \right) \right] \\
& + \rho A C_m \left[\textit{normal component of} \left(\frac{\partial \boldsymbol{v}_f}{\partial p} \right) \boldsymbol{v}_b \right]
\end{aligned}
\tag{3.83}
$$

3.4.4 Hydrodynamic Forces on Vessels

Consideration of the axial interaction of a pipeline, towlines, and tow vessels is essential in dynamic analyses since the mass of the tow vessel is comparable with that of the long pipeline. In this case, it is important that wave forces on the tow vessels are considered rather than the usual approach of prescribing vessel displacements. Hydrodynamic forces on pipelines can be calculated using the Morison equation with the assumption that wave properties are not influenced by the presence of the structure. The vessels, however, interact with incident waves in a complex manner depending on the hull shape. Surface pressures on the hull induced by wave and vessel motion can only be deduced from a solution of the linearised wave problem with no flow boundary conditions satisfied at the free surface, the seabed and the vessel hull. Numerical solutions of the problem are obtained using source distributions on a discretised body surface and a Green's function for a unit source satisfying the linearised free surface and seabed boundary conditions. This approach is, however, quite complex and not within the aims of the work in this thesis. Instead a simplified scheme (Patel, 1986) is used to calculate wave-induced forces on tow vessels. This scheme considers the most significant features of the governing physics and provides reasonable results despite the following simplifying assumptions.

- Wave diffraction is ignored, including linear damping due to gravity wave radiation from the hull.
- Drag forces due to wave velocities are also neglected.

- Deep-water linear gravity wave theory is used.
- The hull is simplified to a rectangular box (see Figure 3.12).

The hydrodynamic forces on the vessels are assumed to be composed of a pressure force, F_p, and an inertia force, F_i. In the case of a heave component, these can be written as

$$\begin{aligned} F_p &= \int_A -\gamma \frac{\partial \phi}{\partial t} dA \\ F_i &= \int_V \gamma (C_{mh} + 1) \frac{\partial^2 \phi}{\partial y \partial t} dV \end{aligned} \tag{3.84}$$

where γ, A, V, and C_{mh} are respectively seawater density, waterplane area of vessel, submerged volume of vessel, and added mass coefficient. ϕ is the velocity potential with the effect of tow speed included and from Equation (3.56), $\phi = -ag / \omega e^{ky} \cos(kx - \omega_e t)$. ω_e is the frequency of encounter.

After simple mathematical manipulation with the fluid acceleration calculated at mid-draft, the heave force on the vessel shown in Figure 3.12 is

$$\begin{aligned} F_{heave} &= \int_{-\frac{L}{2}}^{\frac{L}{2}} -\gamma \frac{\partial \phi}{\partial t} B\, dx + \int_{-\frac{L}{2}}^{\frac{L}{2}} \gamma (C_{mh} + 1) \frac{\partial^2 \phi}{\partial y \partial t} B d\, dx \\ &= 2a\gamma B \frac{g}{\omega} \omega_e \sin \frac{kL}{2} \left[-\frac{1}{k} e^{-kd} + (C_{mh} + 1) d e^{-\frac{k}{2}d} \right] \sin \omega_e t \end{aligned} \tag{3.85}$$

where B, L, and d are respectively breadth, length, and draft of the vessel.

Following the same procedure, the surge force is

$$F_{surge} = -\gamma Bd\frac{\partial \phi}{\partial t}\bigg|_{x=-\frac{L}{2},y=-\frac{d}{2}} - \gamma Bd\frac{\partial \phi}{\partial t}\bigg|_{x=\frac{L}{2},y=-\frac{d}{2}} + \int_{-\frac{L}{2}}^{\frac{L}{2}} \gamma(C_{ms}+1)\frac{\partial^2 \phi}{\partial x \partial t} Bd\,dx$$
$$= 2a\gamma Bd\frac{g}{\omega}\omega_e e^{-\frac{k}{2}d}\left[-\cos\frac{kL}{2} + (C_{ms}+1)\sin\frac{kL}{2}\right]\sin\omega_e t \qquad (3.86)$$

where C_{ms} is the added mass coefficient in the longitudinal direction.

3.5 Analytical Solutions for Towed Pipelines

The static and dynamic behaviour of towed pipelines is very complicated due to structural and hydrodynamic nonlinearities as described in the previous sections. Moreover, the dynamic response becomes further complicated due to the interactions between the tow vessels and pipeline. In the past, computer analyses with finite element or finite difference formulation have been used to give results that include consideration of all major important structural and hydrodynamic aspects. This approach, however, needs specially written softwares and is quite expensive, especially for the early stage of design. The derivation of exact analytical solutions of the static and dynamic governing equations, Equations (3.24) and (3.25) is, however, almost impossible and consequently needs many simplifications to successfully obtain reasonable solutions. This section presents the derivation of static and dynamic analytical solutions for towed pipelines experiencing only vertical deformation in two dimensions. Results from this work will be compared later with those from finite element analyses.

3.5.1 Analytical Solutions for Static Conditions

Towed pipelines are subjected to various types of static loadings such as self-weight, drag forces and hydrostatic pressure forces, and their structural behaviour under these loadings is highly nonlinear as described in the previous sections. Consequently it is almost impossible to derive an analytical solution of the governing equation of towed pipelines, analogous to Equation (3.24), even for simple models. Although catenary

equations provide an exact solution for submerged weight only, the results are not sufficient for the preliminary estimation of key data such as maximum sagging, tension of the pipeline, tow capacities of leading and trailing tow vessels, and so on.

To derive a useful analytical solution, many simplifications are inevitable. The following simplifications and assumptions have been used.

- The position and force components of a trailing tow vessel are known.
- Deformation from a stretched straight configuration is small compared to the length of the pipeline, that is, a small deflection theory is used throughout the development. This assumption is reasonable considering that the maximum sagging is usually less than 100 metres even for pipe lengths of many kilo metres.
- Bending rigidity of the pipeline is ignored.
- The pipeline experiences no axial elongation.
- Submerged weight and longitudinal components of drag forces on the pipeline are considered. Both forces are assumed to be equal all along the pipeline.
- Chain forces are distributed equally all along the pipeline.

Consider the force equilibrium in x and y directions for the pipe segment shown in Figure 3.13.

$$\begin{aligned} \Sigma F_x &= \frac{\partial X}{\partial x}dx - w_x dx = 0 \\ \Sigma F_y &= \frac{\partial Y}{\partial x}dx - w_y dx = 0 \end{aligned} \tag{3.87}$$

where w_x and w_y are external forces per unit length in the x and y directions respectively, and $X(x)$ and $Y(x)$ are horizontal and vertical member forces respectively at x.

From integration of the above equations, we obtain the following relationships.

$$X(x) = w_x x + C_1$$
$$Y(x) = w_y x + C_2 \tag{3.88}$$

Since the bending stiffness, *EI*, is neglected, the pipeline experiences tension only and the following relationship is obtained:

$$\frac{dy}{dx} = \frac{Y(x)}{X(x)} \tag{3.89}$$

Integration after replacing X and Y by Equation (3.88) gives the configuration of the pipeline as:

$$y = \int \frac{Y}{X}\, dx = \int \frac{w_y x + C_2}{w_x x + C_1} dx = \int \left(\frac{w_y}{w_x} - \frac{\frac{w_y}{w_x} C_1 - C_2}{w_x x + C_1} \right) dx$$
$$= \frac{w_y}{w_x} x - \left(\frac{w_y}{w_x} C_1 - C_2 \right) \frac{1}{w_x} \ln\left(w_x x + C_1\right) + C_3 \tag{3.90}$$

This equation has three unknowns, C_1, C_2, and C_3, and they can be obtained from the following assumed boundary conditions for the trailing tow vessel, that is, at $x=0$.

$$y(0) = 0$$
$$X(0) = X_O$$
$$Y(0) = -Y_O \tag{3.91}$$

where X_O and Y_O represent respectively horizontal and vertical components of the force excited by the trailing tow vessel.

The resultant integration constants are

$$
\begin{aligned}
C_1 &= X_O \\
C_2 &= -Y_O \\
C_3 &= \left(X_O \frac{w_y}{w_x} + Y_O \right) \frac{1}{w_x} ln\, X_O
\end{aligned}
\tag{3.92}
$$

Finally, we obtain the analytical solution of deflection under submerged weight, longitudinal current force, and chain forces.

$$
y = \frac{w_y}{w_x} x - \frac{w_y X_O + w_x Y_O}{{w_x}^2} ln\left(\frac{w_x x}{X_O} + 1 \right) \tag{3.93}
$$

Many valuable initial estimations can be obtained from the above equations such as maximum sagging and tension of the pipeline, required tug capacity of a leading tow vessel, and so on. It's accuracy, however, decreases if hydrostatic pressure forces significantly influence on pipe's behaviour and it will be discussed in Section 5.3.1.

3.5.2 Analytical Solutions for Dynamic Conditions

Towed pipelines are subjected to wave loadings and interact dynamically with the tow vessels via towlines. Deriving an exact analytical solution to model these phenomena is impossible mainly due to the structural and hydrodynamic nonlinearities involved and their variations in space. Langley (1989) and Nihous (1995) have proposed approximate solutions respectively for towed pipelines and pipes used for ocean thermal energy conversion. Both assumed that these pipes are very long, horizontal and straight. The procedure proposed by Langley is more compact and reasonable compared to that by Nihous. It neglects tow speed, assumes very stiff pipes, and unfortunately requires prior knowledge of the tensioned pipe eigenvalues with free-free boundary conditions.

This section presents the derivation of an approximate solution of an infinite and straight pipeline under a regular wave, tow speed and prescribed forces at ends of the

pipeline based on the work of Langley (1985). The basic scheme is that initially the response of an infinite pipeline is calculated and the results obtained are then modified to account for the relevant boundary conditions. The following simplifications and assumptions are used:

- Consider the pipeline only, that is, ignore tow vessels and towlines.
- The pipeline is infinitely long, horizontal and straight.
- Properties of the pipeline such as bending stiffness and mass distribution are uniform along its length.
- Tension T is equal along the length and an average value is used.
- The resultant forces exerted by the tow vessels on the ends of the pipeline are known.
- Linear wave theory is used.
- Structural damping is ignored.

At first we consider the response of a pipeline due to a regular wave propagating to the positive direction of the pipeline axis (see Figure 3.14). Assuming that the pipeline is horizontal and straight, the governing equation of motion in the vertical direction is

$$\begin{aligned} &m\ddot{y} + m_a\left(\frac{\partial}{\partial t} + U\frac{\partial}{\partial x}\right)^2 y + EIy^{(4)} - Ty'' \\ &= \frac{1}{4}\pi\rho D^2 C_M \dot{v} + \frac{1}{2}\rho C_d D(v - \dot{y})|v - \dot{y}| \end{aligned} \tag{3.94}$$

where m and m_a are respectively the mass and added mass per unit length of the pipeline and U is the relative forward velocity of the pipeline. Note that U is ignored in the drag force term because it has no normal component to the horizontal pipeline. v and $\dot{v}$ are respectively vertical components of fluid velocity and acceleration from the wave.

After linearising a nonlinear drag force term and neglecting the term from Lighthill's approach, Equation (3.94) becomes

$$B\dot{y} + (m + m_a)\ddot{y} + EIy^{(4)} - Ty'' = C\dot{v} + Bv \tag{3.95}$$

where B is a linearisation term, which is same along the length, and assumed to be known (for details see Section 4.6). $C = 1/4\pi\rho D^2 C_M$.

Using the linear wave theory and allowing for the effect of forward speed U, the vertical components of fluid velocity and acceleration at a point x on the pipeline may be written as

$$\begin{aligned} v &= -\omega a f e^{ikx} e^{-i\omega_e t} \\ \dot{v} &= i\omega\omega_e a f e^{ikx} e^{-i\omega_e t} \end{aligned} \tag{3.96}$$

where real terms are used. a, k, ω, and ω_e are wave amplitude, wave number, wave frequency and encounter frequency respectively. $f = \dfrac{\sinh k(-y_o + h)}{\sinh kh}$, where h is water depth and y_o is the depth of tow (see Figure 3.14).

The forced dynamic response $y(x,t)$ can be written as

$$y(x,t) = aH_\omega(\omega)e^{ikx}e^{-i\omega_e t} \tag{3.97}$$

Substituting Equations (3.96) and (3.97) into Equation (3.95) yields the response of the pipeline in the form

$$y(x,t) = aH(x,\omega)e^{-i\omega_e t} \tag{3.98}$$

where

$$H(x,\omega) = H_{\omega}(\omega)e^{ikx}$$
$$= \left[\frac{iC\omega\omega_e f - B\omega f}{EIk^4 + Tk^2 - iB\omega_e - (m+m_a)\omega_e^2} \right] e^{ikx} \qquad (3.99)$$

This equation is not in its final form since the linearisation term B itself depends on the response $y(x,t)$. Therefore, an iteration process is performed until convergence is achieved. This convergent result is, however, expected to provide rough estimates of the response only around the middle region of a long pipeline, that is, it does not provide reasonable estimates near the ends of the pipeline since compatible boundary conditions are not considered during the above derivation. The boundary conditions can be matched by adding to Equation (3.98) a suitable homogeneous solution of Equation (3.95). The homogeneous form of the equation of motion is

$$EIy^{(4)} - Ty'' + B\dot{y} + (m+m_a)\ddot{y} = 0 \qquad (3.100)$$

This equation generally has four complex roots and its solutions, which are harmonic with frequency ω_e, may be found assuming that $y(x,t)$ has the form

$$y(x,t) = aAe^{sx}e^{-i\omega_e t} \qquad (3.101)$$

where A is an arbitrary complex amplitude scaled by a to simplify the ensuing algebra.

Substituting Equation (3.101) into Equation (3.100) gives

$$EIs^4 - Ts^2 - i\omega_e B - \omega_e^2(m+m_a) = 0 \qquad (3.102)$$

Solving the above equation as a quadratic in s^2 yields

$$s^2 = T' \pm \sqrt{G^2(1+iQ)} \qquad (3.103)$$

where

$$T' = \frac{T}{2EI}$$

$$G^2 = \left(\frac{1}{2EI}\right)^2 \left[T^2 + 4EI\omega_e{}^2 (m + m_a)\right]$$

$$Q = \frac{B\omega_e}{G^2 EI}$$

The form of the solution, Equation (3.103), will depend on the sign of G^2 and solutions can be obtained using the following relationships of complex numbers.

$$\begin{aligned} \sqrt{Z_r + iZ_i} &= \sqrt{R_z e^{i\theta}} \\ &= \sqrt{R_z}\left(cos\frac{\theta}{2} + i\, sin\frac{\theta}{2}\right) \end{aligned} \tag{3.104}$$

where $R_z = \sqrt{Z_r{}^2 + Z_i{}^2}$, $\theta = tan^{-1}\frac{Z_i}{Z_r}$.

For $G^2>0$, the four solutions for s are

$$\begin{aligned} s_1 &= -\frac{1}{\sqrt{2}}\left[\left(p + \sqrt{p^2+q^2}\right)^{1/2} + i\left(-p + \sqrt{p^2+q^2}\right)^{1/2}\right] \\ s_2 &= -\frac{1}{\sqrt{2}}\left[\left(r + \sqrt{r^2+q^2}\right)^{1/2} - i\left(-r + \sqrt{r^2+q^2}\right)^{1/2}\right] \\ s_3 &= -s_1 \\ s_4 &= -s_2 \end{aligned} \tag{3.105}$$

where

$$p = T' + \frac{G}{\sqrt{2}}(1+Q')^{1/2}$$
$$q = \frac{G}{\sqrt{2}}(Q'-1)^{1/2}$$
$$r = T' - \frac{G}{\sqrt{2}}(1+Q')^{1/2}$$
$$Q' = \sqrt{1+Q^2}$$

For $G^2<0$, the four solutions for s have the same form of Equation (3.105), but in this case

$$p = T' - \frac{G'}{\sqrt{2}}(Q'-1)^{1/2}$$
$$q = \frac{G'}{\sqrt{2}}(Q'+1)^{1/2}$$
$$r = T' + \frac{G'}{\sqrt{2}}(Q'-1)^{1/2}$$

where $G'^2 = -G^2$

The solutions of s_1 and s_2 have negative real parts, which means that they represent damped free waves which decay to the right whereas those of s_3 and s_4 have positive real parts and therefore represent damped free waves which decay to the left. The four independent homogeneous solutions are now written as

$$y_j = aA_j e^{s_j x} e^{-i\omega_e t} \tag{3.106}$$

The boundary conditions at the ends of the pipeline can be established considering shear forces V and bending moments M.

$$\begin{aligned} V &= EIy''' - Ty' = F_{vsl} \\ M &= EIy'' = 0 \end{aligned} \tag{3.107}$$

where F_{vsl} represents the external forces from vessels and can be written

$$F_{vsl} = aV_i e^{i\omega_e t} \tag{3.108}$$

where V_i is the complex force amplitude at the left end of the pipeline ($x=0$) for $i=1$ and that at the right end of the pipeline ($x=L$) for $i=2$.

The boundary conditions at the left hand end of the pipeline, $x=0$, may be matched by adding y_1 and y_2 to the solution given by Equation (3.98) and then imposing Equation (3.107). This leads to the following equations and complex amplitudes A_1 and A_2 can be solved.

$$\begin{aligned} &\left(EIs_1^3 - Ts_1\right)A_1 + \left(EIs_2^3 - Ts_2\right)A_2 = i\left(EIk^3 + Tk\right)H(0,\omega) + V_1 \\ &EIs_1^2 A_1 + EIs_2^2 A_2 = EIk^2 H(0,\omega) \end{aligned} \tag{3.109}$$

The boundary conditions at the right hand end of the pipeline, $x=L$, may be matched by adding y_3 and y_4 to the solution given by Equation (3.98) and then imposing Equation (3.107). This leads to the following equations which can be solved for the complex amplitudes A_3 and A_4.

$$\begin{aligned} &\left(EIs_3^3 - Ts_3\right)A_3 e^{s_3 L} + \left(EIs_4^3 - Ts_4\right)A_4 e^{s_4 L} = i\left(EIk^3 + Tk\right)H(L,\omega) + V_2 \\ &EIs_3^2 A_3 e^{s_3 L} + EIs_4^2 A_4 e^{s_4 L} = EIk^2 H(L,\omega) \end{aligned} \tag{3.110}$$

Finally, the complete response of the pipeline is

$$y(x,t) = a\left[H(x,\omega) + \sum_{j=1}^{4} A_j e^{s_j x}\right] e^{-i\omega_e t} \tag{3.111}$$

As can be seen from the above procedure, it is quite difficult to obtain a final solution. Moreover, considering that the end forces of the pipeline are available only after

rigorous consideration of the interaction of the pipeline, towlines, and tow vessels, the applicability of the above solution is very limited.

Table 3.1 Coefficients for the calculation of lift forces on chains

$$F_L = A_L U^{B_L} \ell_c d_c$$

Chain Diameter (m)	A_L	B_L
0.0340	139.254	2.661
0.0450	145.796	2.735
0.0530	157.360	2.708
0.0785	97.917	3.240
0.0800	77.386	3.122

Table 3.2 Coefficients for the calculation of drag forces on chains

$$F_D = A_D U^{B_D} \ell_c d_c$$

Chain Diameter (m)	A_D	B_D
0.0340	868.618	1.347
0.0450	985.120	1.596
0.0530	973.682	1.453
0.0785	927.370	1.715
0.0800	863.983	1.599

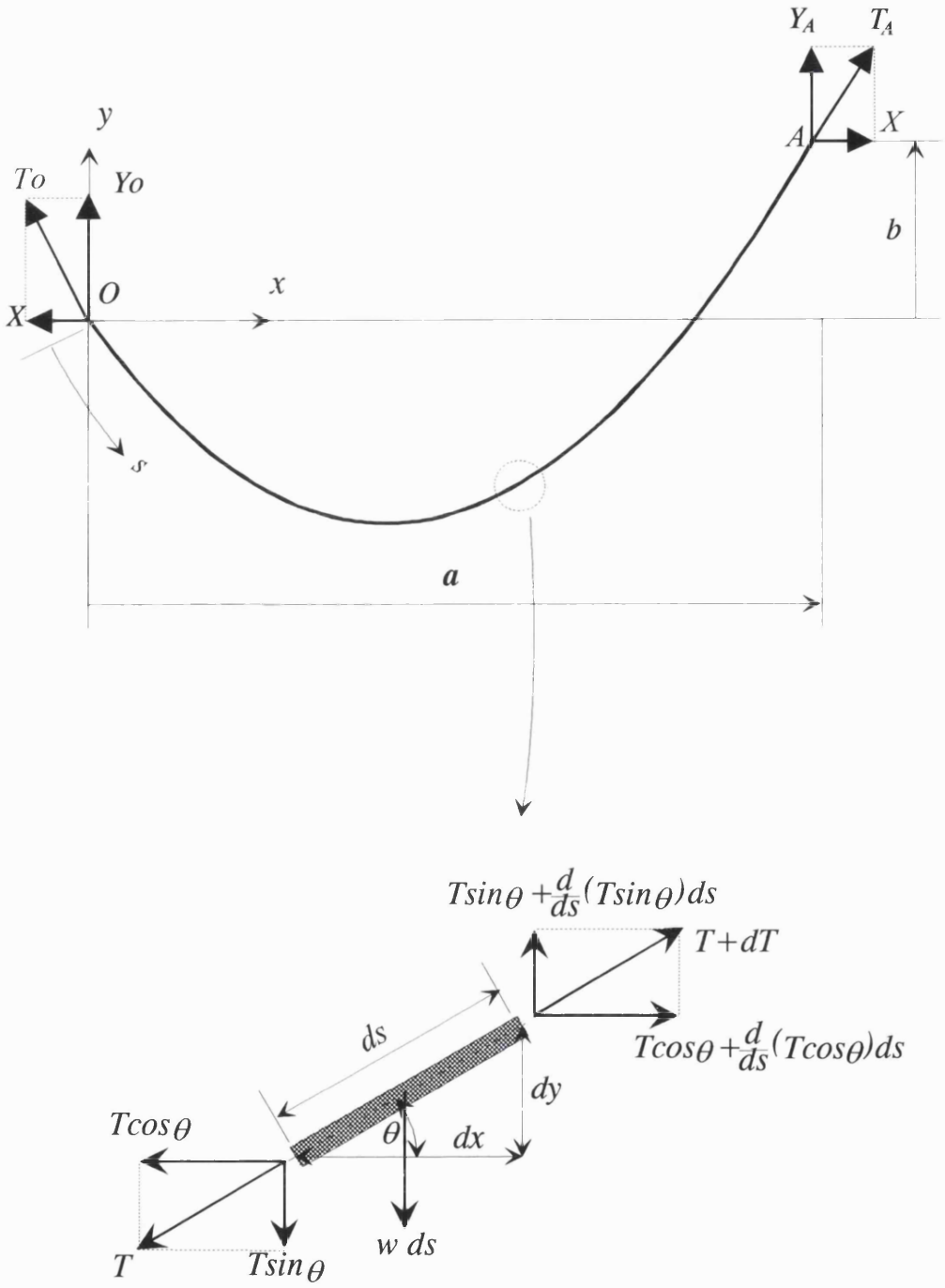

Figure 3.1 Catenary line and its free body diagram

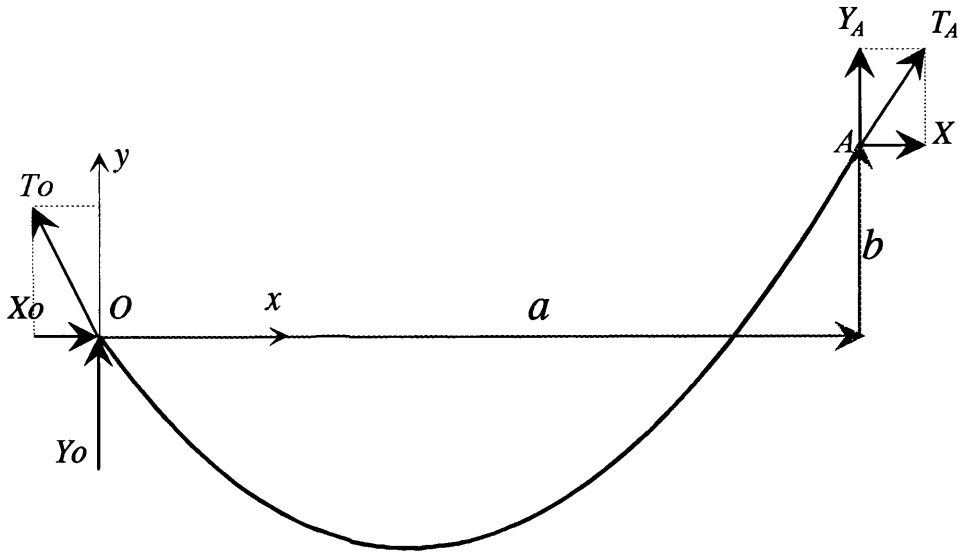

Figure 3.2 Variables of catenary line element for automated calculation

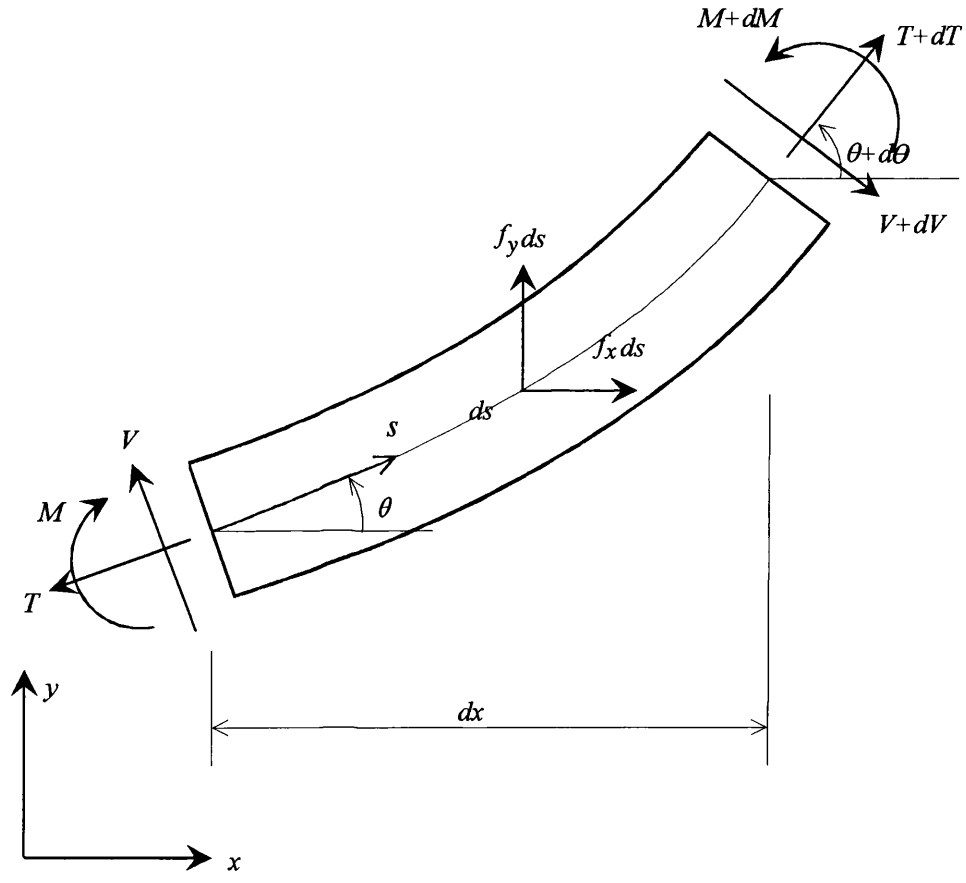

Figure 3.3 Free body diagram of slender beam element

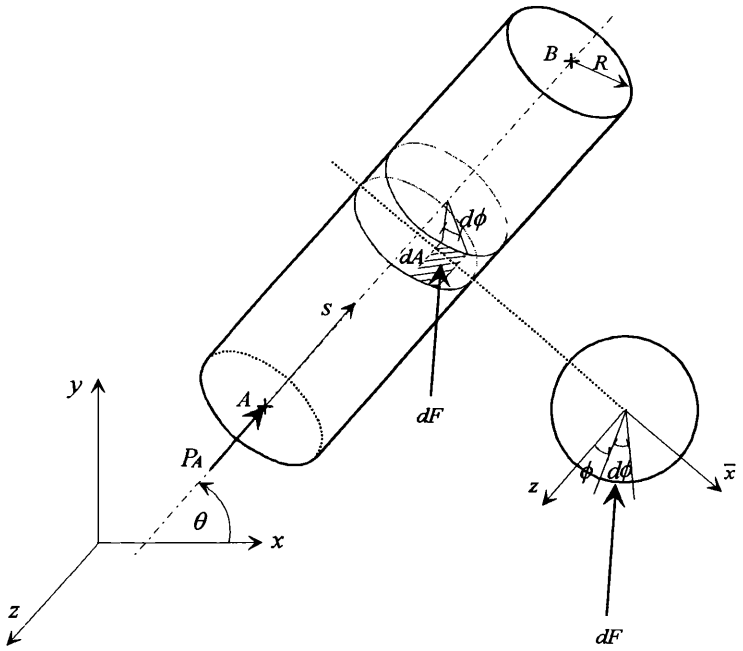

Figure 3.4 Hydrostatic pressure force on straight pipe

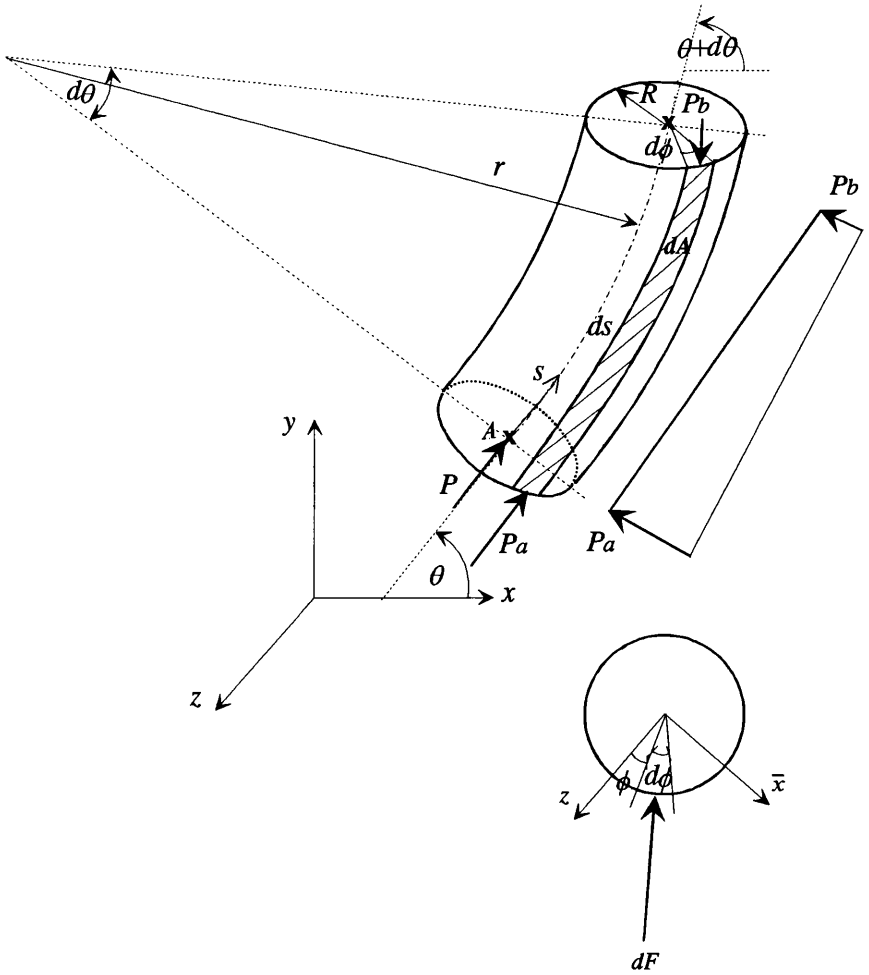

Figure 3.5 Hydrostatic pressure force on curved pipe

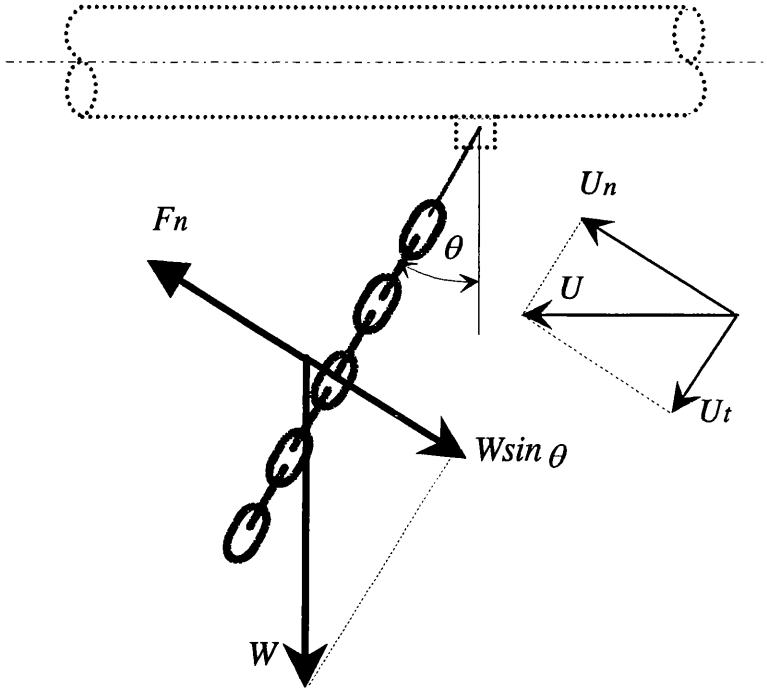

(a) Equilibrium condition of chains under currents

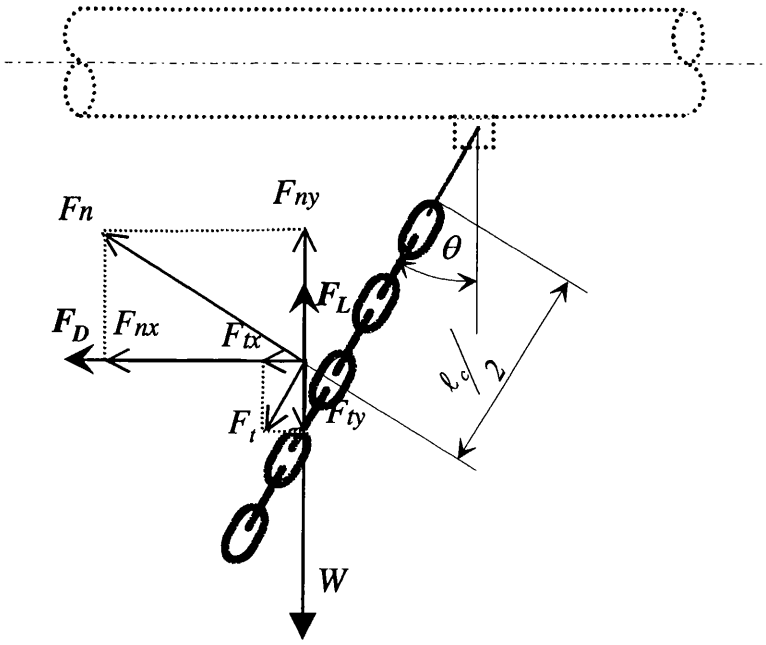

(b) Lift and drag forces on chains

Figure 3.6 Current forces on chains

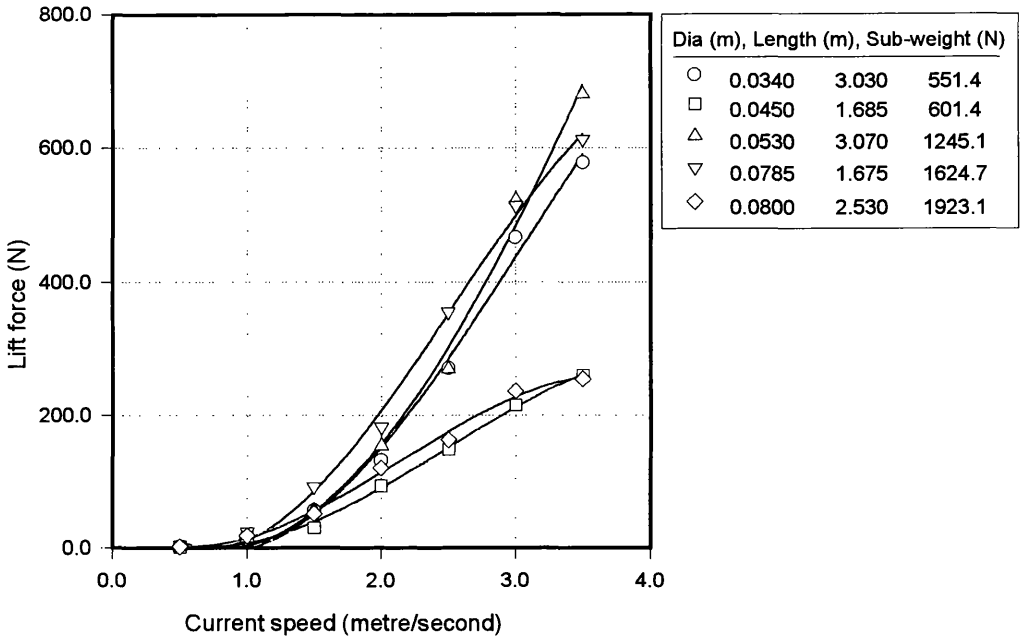

Figure 3.7 Lift forces on various chains (Source : MARIN)

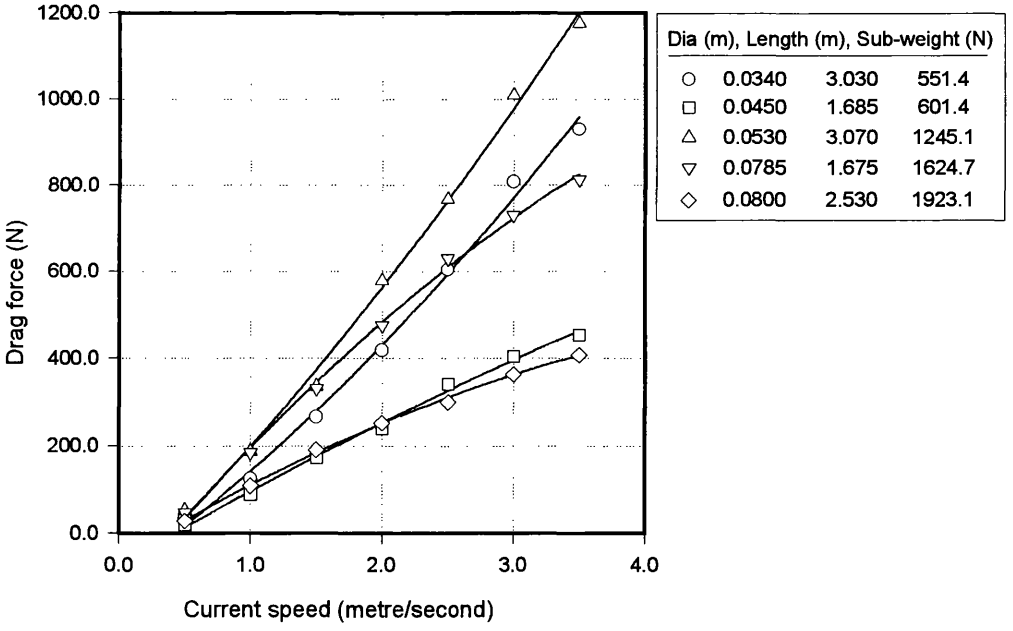

Figure 3.8 Drag forces on various chains (Source : MARIN)

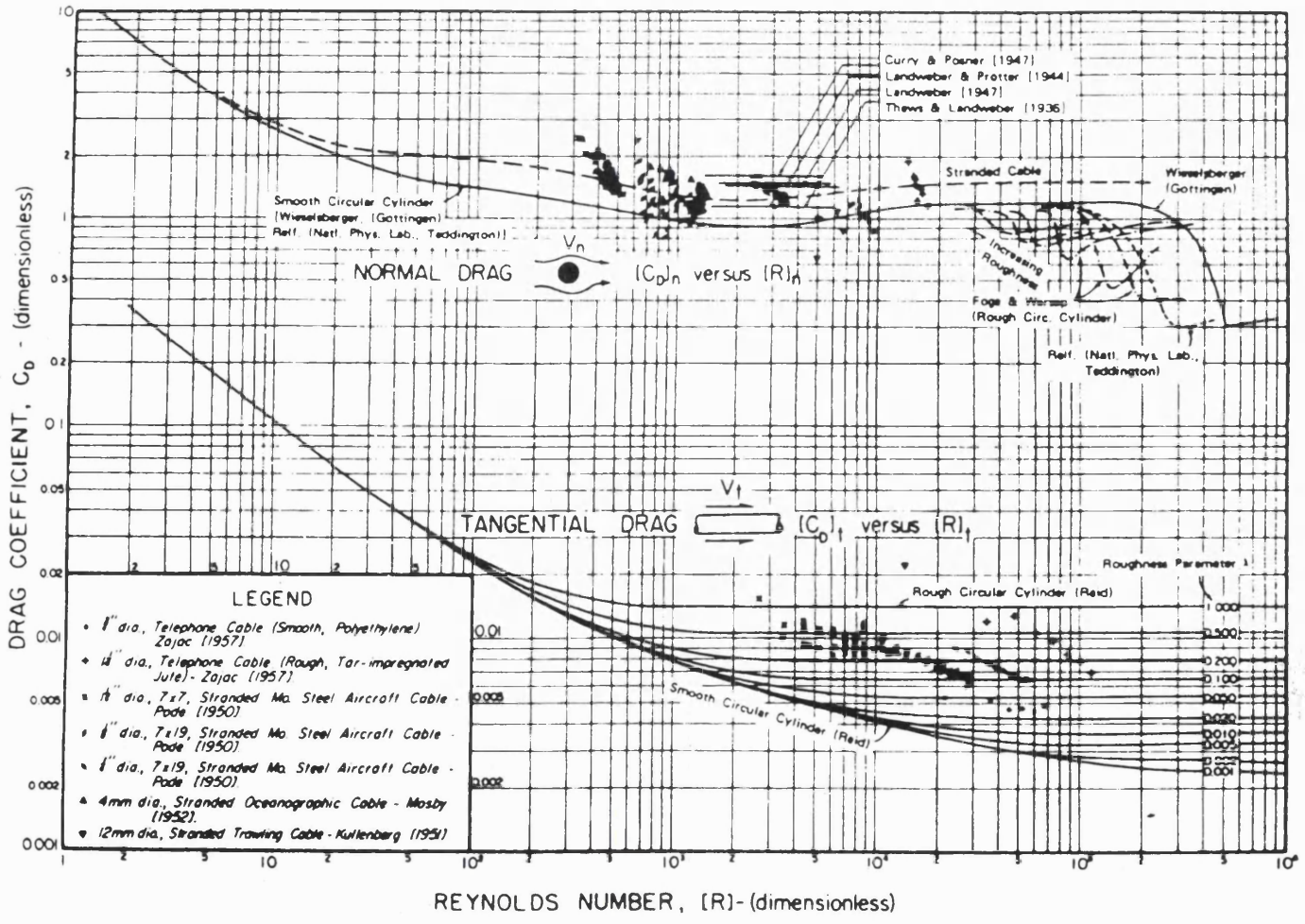

Figure 3.9 Drag coefficients for flow normal and tangential to circular cylinders (Wilson, 1960)

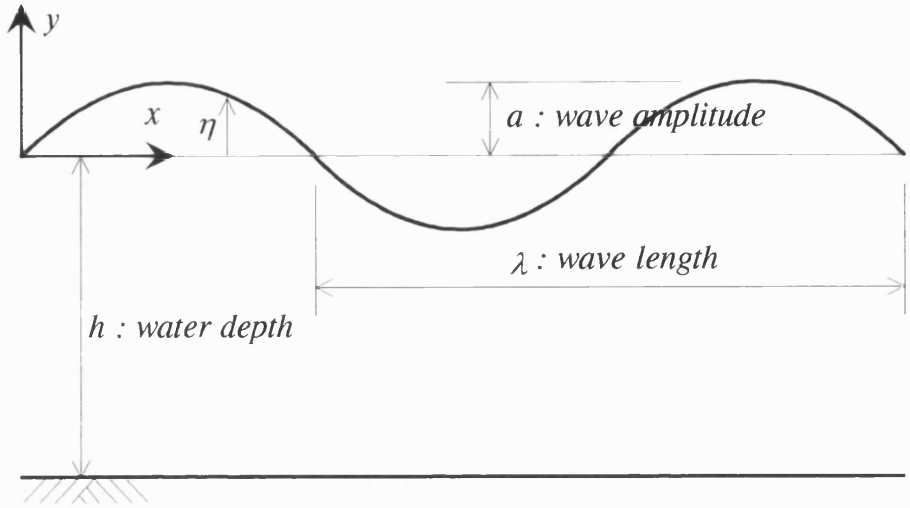

Figure 3.10 Definition of linear wave parameters

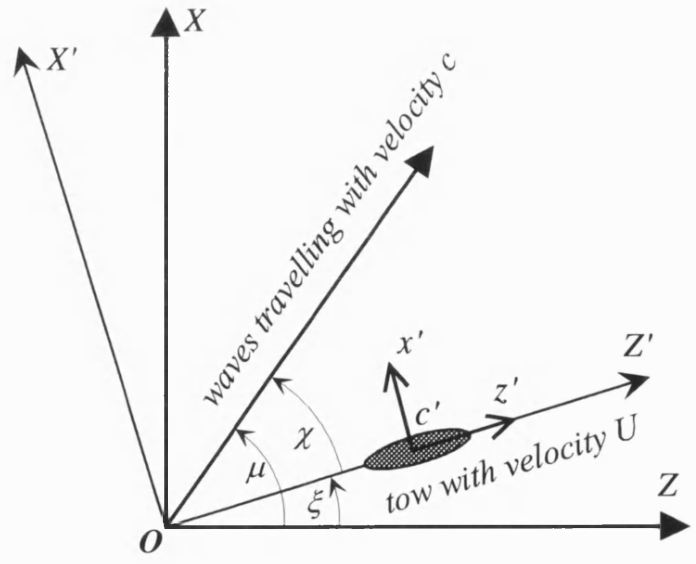

Figure 3.11 Frames of reference to consider tow speed in waves

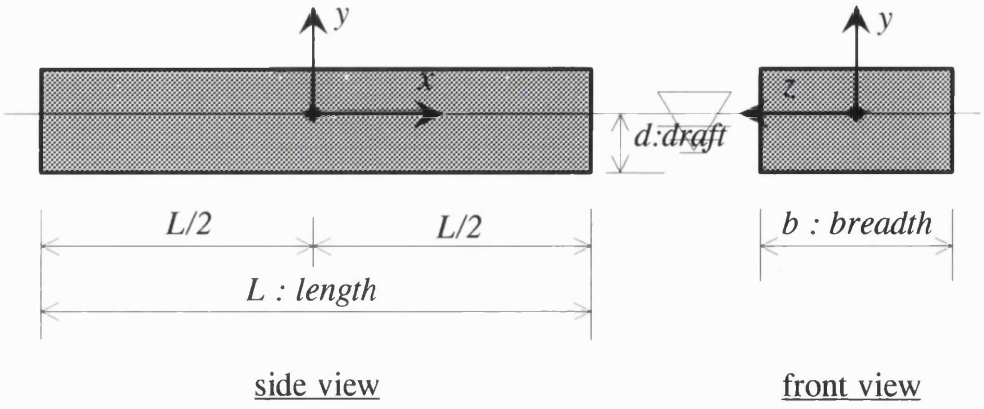

Figure 3.12 Dimension and coordinate system of simplified vessel

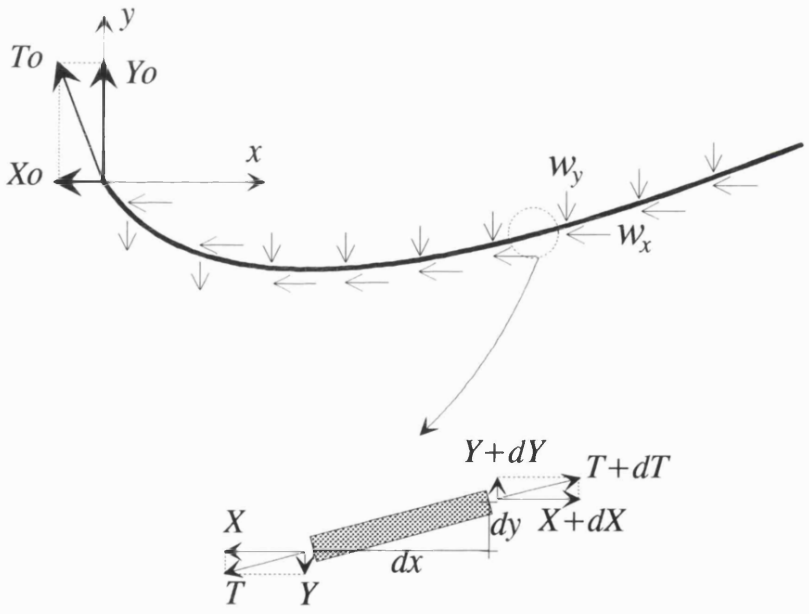

Figure 3.13 Definition of variables and free body diagram
for static analytical solution

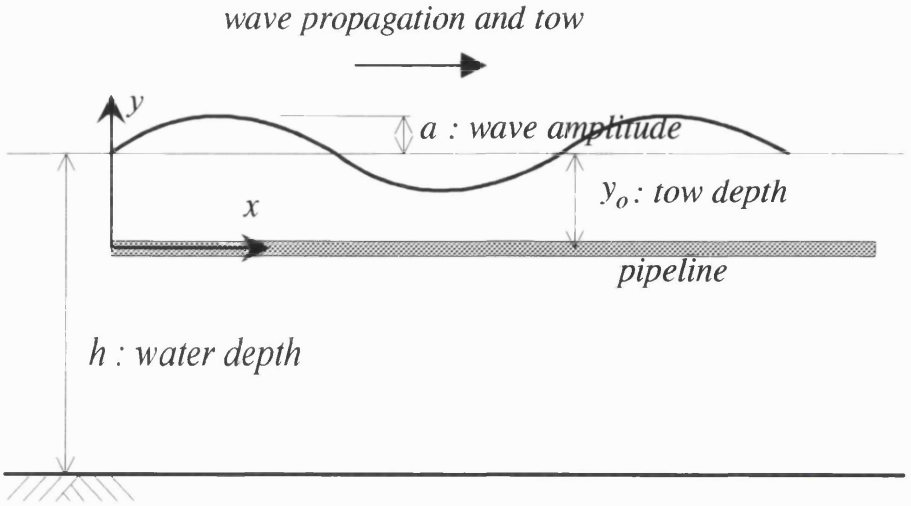

Figure 3.14 Definition of variables for dynamic analytical solution

4. FINITE ELEMENT FORMULATION AND SOLUTION

The structural response of towed pipelines in currents and waves is very complex. The static component of the problem has a significant structural nonlinearity with the dynamic analysis further complicated by the quadratic nonlinearity of the drag force and unusual inertia forces under high near-tangential flow. Moreover, the horizontal dynamics of the pipeline, towlines and tow vessels makes the problem difficult to tackle. Although an analytical solution of the governing equilibrium equations of the pipeline is possible if many simplifications are made, as a result of these simplifications, the solution lacks accuracy and practical applicability. All of this leads to the utilisation of numerical techniques and the finite element method (FEM) is one feasible way of tackling the problem. The present work uses FEM for both static and dynamic analysis with the main issues discussed in previous chapters fully accommodated in the FEM computer package. Typical features of the package are summarised as follows:

Static Analysis:

- Non-linear analysis with direct iteration method to account for non-linear geometric stiffness.
- Enhanced elastic catenary equation to improve convergence performance.
- Deformation-dependent loading to guarantee an accurate static equilibrium configuration.
- Internal and external pressure forces on pipelines.
- Tangential drag forces on pipelines.
- Modeling of chains to consider drag and lift forces accurately.

Dynamic Analysis:

- Frequency or time domain analysis with Newmark's method.
- Non-linear analysis in time domain using initial stiffness method.
- Forward speed of tow vessels.
- Deformation-dependent loading at each time step.
- Force input of tow vessels to consider interaction.
- Improved calculation of hydrodynamic loading for near-tangential flow.

While the FEM is widely used and accepted as one of the standard tools for structural analysis, it frequently experiences ill-conditioning problems and slow convergence for slender structures. Therefore, several specialised techniques and careful choice of a solution algorithm are required to obtain accurate results. This chapter is concerned with these issues for static and dynamic analyses. At first, Section 4.1 presents schemes to simulate efficient and accurate computer models. A FE formulation for the pipeline element with Galerkin method and the procedure to form global system matrices are summarised in Section 4.2. To obtain stable and accurate results for the static condition, the starting geometry from an enhanced catenary analysis and the improved form of direct iteration method are used. Details of these are described in Section 4.3. Finally Section 4.4 presents the procedures of frequency domain analysis for linearised systems and time domain analysis for nonlinear systems.

4.1 Setup of Analysis Models

A tow system consists of a pipeline, tow vessels, towlines, chains and so on. In order to establish a proper analysis model and procedure, an accurate understanding of the physics of a tow system is essential. The governing equations for motion and loads described in Chapter 3 provide a mathematical background for understanding the behaviour of tow systems as well as the basis of the computer models.

Towed pipelines are usually very long - of the order of kilo metres - and slightly negatively-buoyant with chains in a normal tow condition. The sagging of the pipeline in static cases is mainly controlled by the lift forces on chains arising from tow speed and the tensions supplied by tow vessels via towlines. In dynamic cases, high modes of vibration give a dominant influence on the dynamic responses of the pipeline due to its long and near-horizontal configuration. Moreover, the pipeline interacts with tow vessels via towlines since the mass of the long pipeline is comparable with that of the tow vessel. In both static and dynamic cases, the

response of the pipeline is very sensitive to the longitudinal, or surge, component of excitations due to its geometric characteristics mentioned earlier - very long with small sag. For example, the slight prescribed displacements at the ends of the pipeline induce very large sagging for static cases and very large axial forces for dynamic cases. In order to reduce the effects of these phenomena, flexible towlines are used. These towlines significantly reduce dynamic loadings by absorbing a significant proportion of the excitation from the tow vessels. Also, due to their small inclination angles, the pipeline is not significantly influenced by other components of vessel excitation such as those in transverse (yaw) and vertical (heave) directions.

From the governing equations of pipelines and the mechanical property of towlines, four principal nonlinearities can be identified:

- The deformation (curvature)-dependent tension of pipelines.
- The nonlinear drag force on pipelines, proportional to the square of the relative velocity between a pipeline and fluid.
- The nonlinear inertia force on pipelines, when the equations are formulated from Lighthill's approach.
- The nonlinear tension-axial deformation of towlines.

Although the FEM usually provides accurate results for most structural problems, its reliability totally depends on the reasonable modelling of the problem, that is, a model which lacks the important physics of the system being modelled leads to wrong results. Also considering that FEM frequently experiences ill-conditioning problems and slow convergence for slender structures, the analysis models must be examined and tested to ensure that they are delivering accurate results efficiently. The following sections describe the computer models for static analysis and dynamic analysis.

4.1.1 Computer Model for Static Analysis

Tow systems are subjected to various kinds of static load listed below and they experience large deformation from these loads.

- Self-weight of the pipeline itself and attached chains.
- Lift and drag forces on chains due to tow and current.
- Normal and tangential drag forces on the pipeline.
- Tug forces.
- Hydrostatic pressure forces on the pipeline.
- Drag forces on towlines.

The static analysis has three principal objectives:

- To evaluate the stress level in the pipeline.
- To help setup a manoeuvring plan (see Figure 4.1) which includes tow speed, tow heading, tug forces, maximum vertical and lateral sags, maximum clearance between a pipeline and seabed, and so on.
- To provide an initial equilibrium condition for a subsequent dynamic analysis.

To accomplish these objectives, two types of models are considered - the first *'Model A'* includes the pipeline and towlines and the second *'Model B'* includes the pipeline only. Both models introduce strong ill-conditioning problems since the ratio of tensile to flexural rigidity of the pipeline is very large. Moreover, the analysis becomes more unstable and slow for *Model A* due to the inherent highly nonlinear and flexible properties of the towlines (see Table 1.1 and Figure 1.7). On the other hand, the possible ill-conditioning problem with *Model B* can be significantly improved by using the results from a catenary analysis as the input to the FE model (for details, see Section 4.3.1). Also the results from *Model B* provide enough information to setup a maneuvering plan and the static model for dynamic analysis. Therefore, the model which includes a pipeline only (*Model B*) is used for static analyses and simple support conditions are applied to both ends of the pipeline (see Figure 4.2.a).

4.1.2 Computer Model for Dynamic Analysis

Tow systems need to be designed to maintain an acceptable safety margin when subjected to the dynamic wave-induced loads listed below.

- Normal and tangential drag forces on the pipeline.
- Inertia forces on the pipeline.
- Wave forces on tow vessels.
- Wave forces on chains
- Wave forces on towlines.

Among these force components, tangential drag forces on the pipeline and forces on chains and towlines are ignored in the model since they cancel out each other along the length of the pipeline or give little influence on the dynamic behaviour of the tow system.

The review of previous literature (see Section 2.4) reveals that all the physics and the analysis scheme of towed pipeline behaviour in waves has not been firmly established. Usually the analysis scheme was imported from riser analysis, that is, vessels are not included in the model and motion RAO's of the vessel are prescribed at the ends of the pipeline. In the case of Langley's work (Langley, 1989), he imposed the force RAO's from vessels at the ends of the pipeline instead of motion RAO's. These conventional approaches, however, fail to provide accurate results for towed pipelines. Considering that the mass of a tow vessel is generally small and consequently comparable with that of a long pipeline, the dynamic interaction between tow vessels and the pipeline is significant. To illustrate this phenomenon and the importance of the inclusion of tow vessels in the model, simple spring-mass models with different vessel masses are presented (see Figure 4.3.a). The tow system is simulated by a model with two degrees of freedom with the following assumptions.

- The far-end vessel (*M3* in the Figure) is not influenced by the excitation of the other vessel (*M2*), that is, the far-end vessel remains stationary.

- The pipeline is rigid enough compared with towlines.
- Structural damping is ignored.
- Wave forces on the pipeline and towlines are ignored.

Although this model is approximate, it is sufficiently good to check the influence of tow vessel masses on the dynamic response. The result is shown in Figure 4.3.b and it clearly shows that the dynamic responses obtained are significantly influenced by changes in vessel mass. Therefore, the dynamic model for tow analysis should include tow vessels with associated mass and wave exciting forces to obtain accurate results.

The dynamic model (see Figure 4.2.b) is constructed from the result of a static analysis. This process is systematically and easily accomplished by the following procedure.

- Start with the static equilibrium geometry of the pipeline.
- Calculate orientation angles of towlines from the reaction forces at the ends of the pipeline.
- Calculate vessel positions from these angles and the depth of towheads. Towlines are assumed to be straight.
- Include tow vessels with associated mass using representative hydrodynamic coefficients.
- Add towlines between the tow vessel and the end of the pipeline
- Linear translational springs are provided to simulate boundary conditions at the ends of the model, that is, at the vessels. The spring constant in a vertical direction is equal to the change of vessel's buoyancy due to unit displacement while that in other directions are kept very small sufficient only to prevent rigid body motion.

4.2 Finite Element Formulation and System Matrices

The FEM is one computer-aided mathematical technique available for obtaining approximate numerical solutions to the governing equations that predict the response of physical systems subjected to external influences. The main procedure in a FE formulation is the transformation of analytically unsolvable governing equations into approximately equivalent but solvable algebraic equations. In the FEM, the structure is divided into an appropriate number of elements connected by points, called nodes. The response of each such node then becomes the generalised coordinate of the structure. The response of the complete structure can then be expressed in terms of these generalised coordinates by means of an appropriate set of shape functions. This section presents the FE formulation of the problem using the Galerkin method. It also describes the calculation of system matrices for stiffness, mass, damping, and exciting forces.

4.2.1 Finite Element Formulation

The governing differential equation of an element provides a framework to develop a FE procedure. In the case of towed pipelines, the governing equations with lateral loads are (from Section 3.1.2)

$$EI_z y^{(4)} - Ty'' = f_y(x) \tag{4.1.a}$$

$$(m+m_a)\ddot{y} + c\dot{y} + EI_z y^{(4)} - Ty'' = f_y(x,t) \tag{4.1.b}$$

In this section, an element stiffness matrix in a local coordinate system is derived using the Galerkin method. If we denote its trial solution as $\bar{u}$, it can be written as

$$\bar{u}(x;a) = \sum_{j=1}^{n} a_j N_j(x) \tag{4.2}$$

where a_j are undetermined parameters at nodes and N_j are shape functions.

Since $\bar{u}(x;a)$ is an approximate solution, it does not exactly satisfy the governing equation and so produces a residual $R(x;a)$ given by:

$$R(x;a) = EI_z \bar{u}^{(4)} - T\bar{u}'' - f_y \tag{4.3}$$

A more accurate trial solution can be obtained as the residual approaches to zero. Many optimisation schemes were proposed for this process and the Galerkin method became the most popular because of its wider applicability compared to the variational method (Burnett, 1987). Thus the following formulation is based on the Galerkin method.

Galerkin residual equation is written as

$$\int_0^\ell R(x;a)N_i(x)\,dx = 0 \qquad i=1,\ 2,\ldots,\ n \tag{4.4}$$

where ℓ is the length of the considered element. After substituting Equation (4.3), it becomes

$$\int_0^\ell \left(EI_z \bar{u}^{(4)} - T\bar{u}'' - f_y\right)N_i(x)\,dx = 0 \qquad i=1,\ 2,\ldots,\ n \tag{4.5}$$

Integrating the first term of Equation (4.5) twice by parts and the second term once gives:

$$\begin{aligned}\int_0^\ell EI_z \bar{u}^{(4)} N_i(x)\,dx &= \left(EI_z \bar{u}^{(3)} N_i\right)\Big|_0^\ell - \int_0^\ell EI_z \bar{u}^{(3)} N_i'\,dx \\ &= \int_0^\ell EI_z \bar{u}''\, N_i''\,dx + \left(EI_z \bar{u}^{(3)} N_i\right)\Big|_0^\ell - \left(EI_z \bar{u}''\, N_i'\right)\Big|_0^\ell\end{aligned} \tag{4.6}$$

$$-\int_0^\ell T\bar{u}''\,N_i(x)dx=\int_0^\ell T\bar{u}'N_i'\,dx-\left(T\bar{u}'N_i\right)\Big|_0^\ell \tag{4.7}$$

From Equation (4.2), the derivatives of the trial solution can be written as

$$\begin{aligned}\frac{d\bar{u}(x;a)}{dx}&=\sum_{j=1}^{n}a_j\frac{dN_j(x)}{dx}\\ \frac{d^2\bar{u}(x;a)}{dx^2}&=\sum_{j=1}^{n}a_j\frac{d^2N_j(x)}{dx^2}\end{aligned} \tag{4.8}$$

Also the expressions for moment M and shear force V are respectively

$$\begin{aligned}EI_z\bar{u}''&=-M\\ \frac{d}{dx}\left(EI_z\bar{u}''\right)-T\bar{u}'&=-V\end{aligned} \tag{4.9}$$

Substituting Equations (4.6)~(4.9) into Equation (4.5) yields the following expression for the element equation.

$$\begin{aligned}&\int_0^\ell EI_z\sum_{j=1}^{n}a_jN_j''\,N_i''\,dx+\int_0^\ell T\sum_{j=1}^{n}a_jN_j'\,N_i'\,dx\\ &=\int_0^\ell f_y\,N_i dx+\left(V_ON_i\right)\Big|_0^\ell-\left(M_ON_i'\right)\Big|_0^\ell\end{aligned} \tag{4.10}$$

where V_O and M_O are natural boundary conditions. The above equation may be written more compactly as

$$\bar{\boldsymbol{k}}\bar{\boldsymbol{a}}=\bar{\boldsymbol{f}} \tag{4.11}$$

where the element stiffness matrix $\bar{k}$ is the sum of a flexural stiffness matrix $\bar{k}_F$ and a geometric stiffness matrix $\bar{k}_G$ and the element load matrix $\bar{f}$ is the sum of an interior load matrix $\bar{f}_I$ and a boundary load matrix $\bar{f}_B$, that is

$$\begin{aligned}\bar{k} &= \bar{k}_F + \bar{k}_G \\ &= \int_0^\ell EI_z N_i'' N_j'' dx + \int_0^\ell T N_i' N_j' dx\end{aligned} \tag{4.12}$$

and

$$\begin{aligned}\bar{f} &= \bar{f}_I + \bar{f}_B \\ &= \int_0^\ell f_y N_i dx + \left[\left(V_O N_i\right)\Big|_0^\ell - \left(M_O N_i'\right)\Big|_0^\ell \right]\end{aligned} \tag{4.13}$$

As can be seen from Equation (4.11), the FEM can be viewed as the procedure that transforms unsolvable governing differential equation, Equation (4.1), into approximately equivalent but solvable algebraic equation which can be easily automated on computers.

Now to develop the shape function $N_j(x)$. Before proceeding with the usual well-established scheme with polynomials, consider the analytical solution $y(x)$ of the static governing Equation (4.1.a). The form of analytical solutions with and without tension T are respectively

$$y(x) = c_1 + c_2 x + c_3 x^2 + c_4 x^3 \qquad \textit{for } T=0$$

$$\begin{aligned}y(x) &= d_1 \sinh(\alpha x) + d_2 \cosh(\alpha x) + d_3 x + d_4 \\ &= d_1 \left\{ \alpha x + \frac{(\alpha x)^3}{3!} + \frac{(\alpha x)^5}{5!} + \ldots \right\} + d_2 \left\{ 1 + \frac{(\alpha x)^2}{2!} + \frac{(\alpha x)^4}{4!} + \ldots \right\} + d_3 x + d_4\end{aligned} \qquad \textit{for } T>0$$

where $\alpha = \sqrt{T/EI}$ and the c's and d's are constants to be determined from boundary conditions. From the above analytical solutions, it can be seen that both solutions

are basically the same polynomial form with different orders and that the difference between the two solutions is negligible if αx is less than 1.0. Considering that α is less that 10^{-2} for conventional towed pipelines, the polynomial of order three gives sufficiently accurate results if the element length is less than 100 metres. If this is not the case, the shape functions with higher order should be used. In the present work, however, the element lengths will be kept below 100 metres to enable the influence of waves to be considered and, consequently, the polynomial with order of three is accurate enough to express the approximate solution.

The consistent (sometimes also called compatible) shape functions which satisfy both completeness and continuity requirements are used for the present problem to ensure convergence. Since the governing equation is a fourth order differential equation, the trial solution $\bar{u}$ and its first derivative should be continuous. This requires two unknown parameters at each boundary node, hence a total of four for a one dimensional element. Four parameters require a cubic polynomial and the element trial solution takes the following form (for graphic presentation of $\bar{u}$, a_j and $N_j(x)$, see Figure 4.4).

$$\bar{u}(x;a) = \sum_{j=1}^{4} a_j N_j(x) \tag{4.14}$$

where

$$\begin{aligned} N_1(x) &= 1 - 3\left(\frac{x}{\ell}\right)^2 + 2\left(\frac{x}{\ell}\right)^3 \\ N_2(x) &= x\left(1 - \frac{x}{\ell}\right)^2 \\ N_3(x) &= 3\left(\frac{x}{\ell}\right)^2 - 2\left(\frac{x}{\ell}\right)^3 \\ N_4(x) &= \frac{x^2}{\ell}\left(\frac{x}{\ell} - 1\right) \end{aligned} \tag{4.15}$$

After substituting these shape functions into Equations (4.12) and (4.13), finally we obtain element property matrices. If we assume E, I_z, f_y, and T to be constant within an element, then these matrices are written as

$$\bar{k}_F = \frac{2EI_z}{\ell^3}\begin{bmatrix} 6 & 3\ell & -6 & 3\ell \\ & 2\ell^2 & -3\ell & \ell^2 \\ & & 6 & -3\ell \\ sym. & & & 2\ell^2 \end{bmatrix} \tag{4.16}$$

$$\bar{k}_G = \frac{T}{30\ell}\begin{bmatrix} 36 & 3\ell & -36 & 3\ell \\ & 4\ell^2 & -3\ell & -\ell^2 \\ & & 36 & -3\ell \\ sym. & & & 4\ell^2 \end{bmatrix} \tag{4.17}$$

$$\begin{aligned} \bar{f} &= \bar{f}_I + \bar{f}_B \\ &= \frac{f_y \ell}{12}\begin{Bmatrix} 6 \\ \ell \\ 6 \\ -\ell \end{Bmatrix} + \begin{Bmatrix} -V_O(0) \\ M_O(0) \\ V_O(\ell) \\ -M_O(\ell) \end{Bmatrix} \end{aligned} \tag{4.18}$$

Note that the boundary load matrix $\bar{f}_B$ is canceled whilst applying essential inter-element and natural boundary conditions.

Following the same procedure with different governing equations, that is, different shape functions, an axial stiffness matrix $\bar{k}_A$ and a torsional stiffness matrix $\bar{k}_T$ of the beam element are respectively

$$\begin{aligned} N_1(x) &= \left(1 - \frac{x}{\ell}\right) \\ N_2(x) &= \frac{x}{\ell} \end{aligned} \tag{4.19}$$

$$\bar{k}_A = \int_0^\ell EA\, N_i' N_j' dx = \frac{AE}{\ell}\begin{bmatrix} 1 & -1 \\ -1 & 1 \end{bmatrix} \tag{4.20}$$

$$\bar{k}_T = \int_0^\ell GI_x N_i' N_j' dx = \frac{GI_x}{\ell}\begin{bmatrix} 1 & -1 \\ -1 & 1 \end{bmatrix} \tag{4.21}$$

A resulting element stiffness matrix $\bar{k}$ is

$$\bar{k} = \bar{k}_F + \bar{k}_G + \bar{k}_A + \bar{k}_T \tag{4.22}$$

where adjustment of the matrix size and superposing the components of common degrees of freedom are implicitly assumed.

4.2.2 Calculation of System Matrices

The element stiffness matrix derived in the previous section is based on the local coordinate system and, therefore, must be transformed to a global system to form a total stiffness matrix. Besides of the stiffness matrix, mass and damping matrices are also required for dynamic analysis. This section is concerned with the derivation of these matrices and the procedure for forming total property matrices.

Making use of the above finite element procedure, it is also possible to evaluate a mass matrix for each element of a structure. In the case of towed pipelines, an element mass matrix $\bar{m}$ consists of a structural mass matrix $\bar{m}_S$ and an added mass matrix $\bar{m}_A$. Again the structural mass matrix consists of matrices in the flexural $\bar{m}_{Sf}$, axial $\bar{m}_{Sa}$, and torsional degrees of freedom $\bar{m}_{St}$, and these can be written as follows using related consistent shape functions.

$$\overline{m}_S = \overline{m}_{Sf} + \overline{m}_{Sa} + \overline{m}_{St} \tag{4.23}$$

where each matrix is written as follows for uniform structural mass per unit length m.

$$\begin{aligned}\overline{m}_{Sf} &= \int_0^\ell m(x)N_i(x)N_j(x)\,dx \\ &= \frac{m\ell}{420}\begin{bmatrix} 156 & 22\ell & 54 & -13\ell \\ & 4\ell^2 & 13\ell & -3\ell^2 \\ & & 156 & -22\ell \\ sym. & & & 4\ell^2 \end{bmatrix}\end{aligned} \tag{4.24}$$

$$\begin{aligned}\overline{m}_{Sa} &= \int_0^\ell m(x)N_i(x)N_j(x)\,dx \\ &= \frac{m\ell}{420}\begin{bmatrix} 140 & 70 \\ 70 & 140 \end{bmatrix}\end{aligned} \tag{4.25}$$

$$\begin{aligned}\overline{m}_{St} &= \int_0^\ell \frac{m}{A} I_p N_i(x)N_j(x)\,dx \\ &= \frac{mI_p}{A}\begin{bmatrix} 140 & 70 \\ 70 & 140 \end{bmatrix}\end{aligned} \tag{4.26}$$

The element added mass matrix, however, only consists of the matrix in the flexural degrees of freedom and can be obtained by replacing m in Equation (4.24) by the added mass per unit length, m_a.

Although the above formulations are for deformation in the local y-direction only, the inclusion of deformation in the local z-direction is possible by following the same procedure with additional parameters (for definition, see Figure 4.5). The complete element stiffness and mass matrices for this case are shown in Tables 4.1~4.3.

In the case of damping, the FE procedure could be used again to define an element damping matrix, $\overline{c}$.

$$\bar{c} = \int_0^{\ell} c(x) N_i(x) N_j(x)\, dx \tag{4.27}$$

In practice, however, evaluation of the damping property *c(x)* is impracticable. For this reason, the damping is generally expressed in terms of damping ratios and the explicit damping matrix can be computed from these damping ratios as described later in this section.

The distributed load on the pipeline is assumed to be linearly varying within an element. In this case the consistent nodal load matrix $\bar{\boldsymbol{f}}_I$ under axial and lateral loads is shown in Table 4.4.

All the previous formulations for an element are based on the local coordinate system which is specific for each element. Therefore, all related matrices of each element must be transformed to a common global coordinate system to form a total system matrix. This process is carried out using a transformation matrix $\boldsymbol{R}$ whose component r_{ij} is a directional cosine between a local *i*-axis and a global *j*-axis, i.e.,

$$\bar{P}_i = \sum_{j=1}^{3} r_{ij} P_j \tag{4.28}$$

where $\bar{P}_i$ is a component in a local *i*-axis and P_j is that in a global *j*-axis.

To transform the element property matrices in a local coordinate system which are *12* by *12* or *12* by *1* to those in a global system, another transformation matrix $\boldsymbol{T}$ is used.

$$\boldsymbol{T} = \begin{bmatrix} \boldsymbol{R} & \boldsymbol{0} & \boldsymbol{0} & \boldsymbol{0} \\ & \boldsymbol{R} & \boldsymbol{0} & \boldsymbol{0} \\ & & \boldsymbol{R} & \boldsymbol{0} \\ sym. & & & \boldsymbol{R} \end{bmatrix} \tag{4.29}$$

The element property matrices $\boldsymbol{k}$, $\boldsymbol{c}$, $\boldsymbol{m}$ and $\boldsymbol{f}$ in a global coordinate system are respectively

$$\begin{aligned} \boldsymbol{k} &= \boldsymbol{T}^t \bar{\boldsymbol{k}} \boldsymbol{T} \\ \boldsymbol{c} &= \boldsymbol{T}^t \bar{\boldsymbol{c}} \boldsymbol{T} \\ \boldsymbol{m} &= \boldsymbol{T}^t \bar{\boldsymbol{m}} \boldsymbol{T} \\ \boldsymbol{f} &= \boldsymbol{T}^t \bar{\boldsymbol{f}} \end{aligned} \tag{4.30}$$

The stiffness matrix $\boldsymbol{K}$, mass matrix $\boldsymbol{M}$, and force matrix $\boldsymbol{F}$ of the complete element assemblage are effectively obtained from the element property matrices by direct superposition.

$$\begin{aligned} \boldsymbol{K} &= \sum_i \boldsymbol{k}_i \\ \boldsymbol{M} &= \sum_i \boldsymbol{m}_i \\ \boldsymbol{F} &= \sum_i \boldsymbol{f}_i \end{aligned} \tag{4.31}$$

where the summation i includes all elements.

There is no need to express damping by means of a damping matrix for frequency domain analysis because it is represented more conveniently in terms of the modal damping ratios ξ_n. In the case of time domain analysis, however, the damping cannot be expressed by the damping ratio and instead an explicit damping matrix is needed. The most effective way to determine the required damping matrix is to use Rayleigh damping - Clough and Penzien (1993) presented a detailed procedure to calculate it. Rayleigh damping is assumed to be proportional to a combination of the mass and the stiffness matrices.

$$\boldsymbol{C} = a_0 \boldsymbol{M} + a_1 \boldsymbol{K} \tag{4.32}$$

Rayleigh damping leads to the following relation between damping ratio ξ_n and frequency ω_n.

$$\xi_n = \frac{a_0}{2\omega_n} + \frac{a_1 \omega_n}{2} \tag{4.33}$$

This relationship is shown graphically in Figure 4.6. The two factors a_0 and a_1 can be evaluated by the solution of a pair of simultaneous equations if damping ratios ξ_m and ξ_n associated with two specific frequencies ω_m and ω_n are known. Writing Equation (4.33) for each of these two cases and expressing the two equations in matrix form leads to

$$\begin{Bmatrix} \xi_m \\ \xi_n \end{Bmatrix} = \frac{1}{2} \begin{bmatrix} 1/\omega_m & \omega_m \\ 1/\omega_n & \omega_n \end{bmatrix} \begin{Bmatrix} a_0 \\ a_1 \end{Bmatrix} \tag{4.34}$$

The factors resulting from the simultaneous solutions are

$$\begin{Bmatrix} a_0 \\ a_1 \end{Bmatrix} = 2 \frac{\omega_m \omega_n}{\omega_n^2 - \omega_m^2} \begin{bmatrix} \omega_n & -\omega_m \\ -1/\omega_n & 1/\omega_m \end{bmatrix} \begin{Bmatrix} \xi_m \\ \xi_n \end{Bmatrix} \tag{4.35}$$

Once these two factors are calculated, the damping matrix $\boldsymbol{C}$ is readily available from Equation (4.32).

4.3 Nonlinear Static Solution

The application of the FEM to a continuous pipeline with static load results in the following system of simultaneous equation

$$\boldsymbol{KU} = \boldsymbol{F} \tag{4.36}$$

Since the coefficients of both the stiffness matrix $\boldsymbol{K}$ and the force matrix $\boldsymbol{F}$ depend on unknowns $\boldsymbol{U}$ or their derivatives, the problem clearly becomes nonlinear. In this case, the direct solution of the above equation is generally impossible and an iterative scheme must be adopted. Among many iterative schemes (Owen and Hinton, 1980), the direct iteration method is employed for the present problem. In this method, an initial estimation for the unknown vector $\boldsymbol{U}$ is required to calculate a starting stiffness matrix and the result from catenary analysis is used for this. Once equilibrium with constant loading is achieved, additional iteration is done to guarantee the equilibrium with deformation-dependent loading.

4.3.1 Starting Geometry from Catenary Analysis

The nonlinear FE analysis for towed pipelines experiences frequent ill-conditioning problems and poor convergence performance due to the following reasons.

- Pipelines are usually very long and their ratio of tensile to flexural rigidity is very large.
- The deformation-dependent tensile forces contribute to the pipeline stiffness.
- Pipelines experience large deformation and, consequently, external static forces depend on the deformed geometry.

Usually these problems can be significantly improved by using the result from catenary analysis as the starting condition of the direct iteration method. This scheme, however, cannot be applicable to the model with side current because

- The catenary equation takes into account the submerged weight of a pipeline including chains and, therefore, provides equilibrium in the vertical plane (see Figure 4.7).
- This equilibrium condition with simple support conditions at both ends of the pipeline provides little stiffness to resist lateral loading.
- If there is side current, the lateral component of the drag force on the pipeline easily exceeds the vertical component from submerged weight since the submerged weight is usually very small.

- Consequently, this lateral load induces unrealistically large rigid body rotation about the axis on the two supporting nodes and prohibits obtaining convergent results.

To overcome this critical problem with side current, an enhanced form of catenary equation is employed - hereinafter it is called enhanced catenary method. The idea behind this method is simple. If we assume that lateral loads as well as vertical loads are distributed uniformly all along the pipeline, we can identify the equilibrium plane from these loads and proceed with the usual catenary analysis at this plane with a modified force term. This scheme is briefly illustrated in Figure 4.7. The angle α between the equilibrium plane and a horizontal plane is

$$\alpha = tan^{-1} \frac{w_y}{w_z} \tag{4.37}$$

where w_y is the intensity of the submerged weight of a pipeline including chains, and w_z is that of the lateral component of drag force at the mid span of the pipeline. The corresponding force w for enhanced catenary analysis is

$$w = \left(w_y^{\,2} + w_z^{\,2} \right)^{1/2} \tag{4.38}$$

This force is, however, far from the real one and the resulting difference of loads needs to be systematically corrected for during the FE analysis.

4.3.2 Method of Direct Iteration

In the direct iteration method, successive solutions are performed and in each iteration the previous solutions for the unknowns $\boldsymbol{U}$ is used to calculate the changing stiffness matrix $\boldsymbol{K(U)}$. If we rewrite equation (4.36) as

$$\boldsymbol{U} = \left[\boldsymbol{K}(\boldsymbol{U})\right]^{-1}\boldsymbol{F} \tag{4.39}$$

then the iterative process yields the *(r+1)-th* approximation to be

$$\boldsymbol{U}^{r+1} = \left[\boldsymbol{K}(\boldsymbol{U}^{r})\right]^{-1}\boldsymbol{F} \tag{4.40}$$

If the process is convergent then $\boldsymbol{U}^{r}$ tends to the true solution as r tends to infinity. It is seen from Equation (4.40) that it is necessary to recalculate the stiffness matrix $\boldsymbol{K}$ for each iteration. To commence the process, the tangent stiffness matrix based on the geometry vector $\boldsymbol{U}_0$ and tensile force vector $\boldsymbol{T}_0$ from the enhanced catenary analysis are used. From the tangent stiffness $\boldsymbol{K}_0$, Equation (4.40) is solved to give $\boldsymbol{U}_1$. The new stiffness $\boldsymbol{K}_1$ corresponding to $\boldsymbol{U}_1$ is calculated and then solved to obtain $\boldsymbol{U}_2$. This cycling process is continued until $\boldsymbol{U}_{n-1}$ and $\boldsymbol{U}_n$ are deemed to be sufficiently close, indicating that convergence has achieved. Usually the norm of nodal displacements between successive iterations is used to check the convergence. This process is illustrated graphically in Figure 4.8 for a single variable.

Towed pipelines experience large deformations from the starting geometry from catenary analysis due to drag forces on the pipeline and drag and lift forces on chains. In this case, external loads depend on the deformation and this feature must be considered during analysis. The shortcoming of the conventional direct iteration method is that it can not allow for this deformation-dependence of loading. Seyed (1989) proposed an improved version with two nested iterations and this scheme is used in the present work. With this method, the inner iteration is the conventional direct iteration approach with constant external load and the outer one is to ensure the residual forces resulting from the deformation-dependent loading are equilibrated. This process is illustrated in Figure 4.9 for a single variable. Starting from a known equilibrium geometry vector $\boldsymbol{U}_0$, the full force vector $\boldsymbol{F}_0$ is applied and the deformed geometry vector $\boldsymbol{U}_1$ is calculated using the conventional iteration method. The geometry is then updated and the full loading for the new geometry is calculated.

The difference of force vector ΔF_1 between two successive iterations are applied to the system and the basic iteration method is again employed to obtain a new equilibrium position U_2. This cycling process is continued until convergence has occurred. Paths OA and AB represent the results from first and second force iterations respectively. The flow chart for the nonlinear analysis with this scheme is presented in Figure 4.10.

4.4 Dynamic Solution

The application of the FEM to a tow system with dynamic load results in the following system of simultaneous equations:

$$\boldsymbol{M\ddot{U} + C\dot{U} + KU = F} \tag{4.41}$$

Two approaches may be used to calculate dynamic responses - they are frequency domain and time domain analysis. In frequency domain analysis, it is assumed that the system behaviour is linear and that all time-dependent terms are harmonic thus eliminating time variables from the equation and giving only the steady state response. Since this method works only for linear equation, it requires a linearisation process for a nonlinear term. The time domain analysis requires no such process. Instead, numerical integration of Equation (4.41) using a numerical step-by-step procedure leads to the time history solution. This analysis provides more accurate results than the frequency domain analysis although it needs considerable amounts of computer time in the computation of transient response, which is generally of little interest. To improve this drawback, an initial stiffness method is applied.

4.4.1 Frequency Domain Analysis

Since the frequency domain analysis operates only on linear equations of motion, the quadratic hydrodynamic drag force and geometric stiffness nonlinearities in the towed

pipeline equations of motion need to be linearised using a reasonable scheme. In spite of this shortcoming, this method has been widely used because it is much faster than the direct integration method and is suitable for obtaining irregular response statistics.

The stiffness matrix which depends on tensile forces can be easily linearised by using the tangent stiffness matrix about a static configuration with the assumption of small dynamic responses. The linearisation of drag force needs special care and will be described later in this section. Once these linearisations are made, a frequency domain solution offers readily usable transfer functions of structure displacements, internal forces and stresses which can be applied to evaluate member strength or to derive statistical response results.

In the frequency domain solution of equation (4.41), the vector of dynamic nodal displacement $\boldsymbol{U}$ is written as

$$\boldsymbol{U} = \boldsymbol{U}_0 e^{-i\omega t} \tag{4.42}$$

where $\boldsymbol{U}_0$ is the vector of complex amplitudes and ω is the frequency of an incident wave. Similarly, it is assumed that the nodal load vector $\boldsymbol{F}$ may be expressed as

$$\boldsymbol{F} = \boldsymbol{F}_0 e^{-i\omega t} \tag{4.43}$$

Substituting Equations (4.42) and (4.43) into Equation (4.41) results in the following equation that may be solved for the complex amplitudes $\boldsymbol{U}_0$.

$$\left[\boldsymbol{K} - i\omega \boldsymbol{C} - \omega^2 \boldsymbol{M}\right]\boldsymbol{U}_0 = \boldsymbol{F}_0 \tag{4.44}$$

Solution of Equation (4.44) requires the inversion of a matrix with complex number elements and the above process is repeated until a convergent solution is reached. If

the dynamic response is limited to only a few low modes of vibration, the modal superposition technique can be used to reduce computer time and obtain results that are simple to understand. This method, however, offers little advantage to towed pipelines since long and near-horizontal towed pipelines are usually influenced by many high modes of vibration - consequently requiring long computer runs for eigenvalue analysis.

In order to apply the frequency domain approach, the quadratic drag force on the pipeline must be linearised. Previously the linearisation for a wave plus current was obtained by summing the results from the wave only and the current only cases and it is referenced to as the superposition method. This method, however, introduces a substantial error into the frequency domain method. Krolikowski and Gay (1980) have presented an improved linearisation procedure for regular waves and for regular and irregular waves with current and this is adopted for the present work. This method is a form of quasi-linearisation which minimises the mean-square error between the output of the original non-linearity and the linear replacement. The mean squared approximation error is minimised by expanding the non-linear output in a Fourier series and neglecting higher harmonics. Although Chen and Lin (1989) have proposed the expansion up to *n-th* order, neglecting the higher harmonics can be justified by noting that the higher harmonics have less amplitude than the fundamental. In addition, higher harmonics in the drag forces are filtered by the pipeline dynamics.

The linearised form of the drag force per unit length can be written as

$$\begin{aligned} F &= \frac{1}{2}\rho D C_d \left(u_w + u_c - \dot{y}\right) \left|u_w + u_c - \dot{y}\right| \\ &= \frac{1}{2}\rho D C_d \left\{\left(u_0 - i\omega y_0\right)e^{-i\omega t} + u_c\right\} \left|\left(u_0 - i\omega y_0\right)e^{-i\omega t} + u_c\right| \\ &\cong \frac{1}{2}\rho D C_d B_1 \left(u_0 - i\omega y_0\right)e^{-i\omega t} + \frac{1}{2}\rho D C_d B_2 u_c \end{aligned} \qquad (4.45)$$

where u_c is current velocity. Wave particle velocity u_w and structural response y are expressed respectively as

$$\begin{aligned} u_w(x,t) &= u_0(x)e^{-i\omega t} \\ y(x,t) &= y_0(x)e^{-i\omega t} + y_c(x) \end{aligned} \tag{4.46}$$

The term y_c is the mean displacement and the variables u_0 and y_0 are complex amplitudes. After expanding the nonlinear drag force in a Fourier series, it gives the following linearisation coefficients B_1 and B_2.

$$B_1 = \begin{cases} 2u_c & for\ u_c \geq A \\ \dfrac{8}{3\pi}A\left[\left\{1+\dfrac{1}{2}\left(\dfrac{u_c}{A}\right)^2\right\}\sqrt{1-\left(\dfrac{u_c}{A}\right)^2}+\dfrac{3}{2}\dfrac{u_c}{A}sin^{-1}\left(\dfrac{u_c}{A}\right)\right] & for\ u_c < A \end{cases}$$

$$B_2 = \begin{cases} \dfrac{A^2}{2u_c}u_c & for\ u_c \geq A \\ \dfrac{A^2}{\pi u_c}\left[\left\{1+2\left(\dfrac{u_c}{A}\right)^2\right\}sin^{-1}\left(\dfrac{u_c}{A}\right)+3\dfrac{u_c}{A}\sqrt{1-\left(\dfrac{u_c}{A}\right)^2}\right] & for\ u_c < A \end{cases} \tag{4.47}$$

where $A^2 = u_0^{\,2} + \omega^2 y_0^{\,2}$.

4.4.2 Nonlinear Time Domain Analysis

Frequency domain analysis requires that the system remains linear during the response. Any nonlinearity indicated by a change in the coefficients of the system matrices would reduce the reliability of results. However, in the case of towed pipelines the coefficients usually do not remain constant. For example, changes in the member axial forces may cause appreciable changes in the geometric stiffness and the mass or damping coefficients will undergo changes during dynamic response. The only generally applicable procedure for analysis of an arbitrary set of nonlinear response equations is by numerical step-by-step integration. Although the

application of this method is discouraged due to limited computer resources, it has become popular nowadays with advances in computer technology enabling faster processing and greater memory availability.

The direct integration method is based on two ideas as described clearly by Bathe (1982). First, instead of trying to satisfy the governing equilibrium Equation (4.41) at any time t, it is aimed to satisfy it only at discrete time intervals Δt apart. Second, a variation of displacements, velocities, and accelerations within each time interval Δt is assumed and it is the form of this assumption that determines the accuracy, stability, and cost of the solution procedure. In the direct integration method, the response history is divided into a sequence of short time steps, and during each step, the response is calculated for a linear system having the physical properties from the end of a previous step. In the case of the full Newton-Raphson method, the properties are modified at the end of the interval to conform to the state of deformation and stress at that time for use during the subsequent time step. So the nonlinear analysis is approximated as a sequence of analysis of successively changing linear systems. Wilson, etc. (1973) and Bathe (1982) have described this procedure in detail for nonlinear systems. Among the many possible methods available, Newmark's method is used in this work.

The Newmark integration scheme is an extension of the linear acceleration method, in which a linear variation of acceleration from time t to time $t+\Delta t$ is assumed. That is, the following assumptions are used in the linear acceleration method.

$$\dot{\boldsymbol{U}}_{t+\Delta t} = \dot{\boldsymbol{U}}_t + \left\{(1-\delta)\ddot{\boldsymbol{U}}_t + \delta\ddot{\boldsymbol{U}}_{t+\Delta t}\right\}\Delta t \tag{4.48}$$

$$\boldsymbol{U}_{t+\Delta t} = \boldsymbol{U}_t + \dot{\boldsymbol{U}}_t\Delta t + \left\{\left(\frac{1}{2}-\alpha\right)\ddot{\boldsymbol{U}}_t + \alpha\ddot{\boldsymbol{U}}_{t+\Delta t}\right\}\Delta t^2 \tag{4.49}$$

where α and δ are parameters that can be determined to obtain integration accuracy and stability. Newmark proposed the constant-average-acceleration method as an

unconditionally stable scheme, in which case $\alpha=1/4$ and $\delta=1/2$. In this case Equations (4.48) and (4.49) become respectively,

$$\dot{\boldsymbol{U}}_{t+\Delta t} = \dot{\boldsymbol{U}}_t + \frac{\Delta t}{2}\left(\ddot{\boldsymbol{U}}_t + \ddot{\boldsymbol{U}}_{t+\Delta t}\right) \tag{4.50}$$

$$\boldsymbol{U}_{t+\Delta t} = \boldsymbol{U}_t + \frac{\Delta t}{2}\left(\dot{\boldsymbol{U}}_t + \dot{\boldsymbol{U}}_{t+\Delta t}\right) \tag{4.51}$$

Using Newmark's implicit integration method, the equilibrium of the system is considered at time $t+\Delta t$. In case of linear analysis, the equilibrium equation is written as

$$\boldsymbol{M}\ddot{\boldsymbol{U}}_{t+\Delta t} + \boldsymbol{C}\dot{\boldsymbol{U}}_{t+\Delta t} + \boldsymbol{K}\boldsymbol{U}_{t+\Delta t} = \boldsymbol{F}_{t+\Delta t} \tag{4.52}$$

Solving for $\ddot{\boldsymbol{U}}_{t+\Delta t}$ and $\dot{\boldsymbol{U}}_{t+\Delta t}$ in terms of $\boldsymbol{U}_{t+\Delta t}$ from Equations (4.50) and (4.51) and then substituting into Equation (4.52) yield the equation which is ready to solve for $\boldsymbol{U}_{t+\Delta t}$. $\ddot{\boldsymbol{U}}_{t+\Delta t}$ and $\dot{\boldsymbol{U}}_{t+\Delta t}$ can be then calculated using Equations (4.50) and (4.51).

For nonlinear analysis, the situation is somewhat complicated although the major basic procedures used in the linear analysis are still applicable. As in linear analysis, we consider the equilibrium of the system at time $t+\Delta t$ using an iteration process for solution. Although the Newton-Raphson or direct iteration method is widely applied to highly nonlinear systems, they require much computing time for the continuous modification and inversion of system matrices. In the case of towed pipelines, which do not experience dramatic changes in global deformation due to dynamic forces, there is no significant change in the system matrices. Also considering that the Newton-Raphson method or its modified version is unstable for very long and flexible structures, the initial stiffness method remains an economic and feasible choice. The initial stiffness method uses constant system matrices throughout the time domain analysis with constant time interval - these matrices being based on the static equilibrium case. Since the same system matrices are employed at each step, the

reduced equations can be stored in their reduced or factored form and a subsequent solution merely necessitates the reduction of the force terms, together with a backsubstitution. This has the immediate advantage of significant reducing the computer storage whilst reducing the convergence rate. Using the initial stiffness method with initial system matrices $\boldsymbol{K}_0$, $\boldsymbol{C}_0$ and $\boldsymbol{M}_0$, the governing incremental equilibrium equations are written as

$$\boldsymbol{M}_0\ddot{\boldsymbol{U}}^{(k)}_{t+\Delta t} + \boldsymbol{C}_0\dot{\boldsymbol{U}}^{(k)}_{t+\Delta t} + \boldsymbol{K}_0\Delta\boldsymbol{U}^{(k)} = \boldsymbol{F}_{t+\Delta t} - \boldsymbol{R}^{(k-1)}_{t+\Delta t} \tag{4.53}$$

where $\boldsymbol{R}^{(k-1)}_{t+\Delta t}$ denotes the internal resisting force vector from *(k-1)-th* iteration. The nodal displacement vector $\boldsymbol{U}^{(k)}_{t+\Delta t}$ can be expressed as follows with the displacement increment vector $\Delta\boldsymbol{U}^{(k)}$.

$$\boldsymbol{U}^{(k)}_{t+\Delta t} = \boldsymbol{U}^{(k-1)}_{t+\Delta t} + \Delta\boldsymbol{U}^{(k)} \tag{4.54}$$

Using the constant-average-acceleration method the following assumptions are employed.

$$\boldsymbol{U}^{(k)}_{t+\Delta t} = \boldsymbol{U}_t + \frac{\Delta t}{2}\left(\dot{\boldsymbol{U}}_t + \dot{\boldsymbol{U}}^{(k)}_{t+\Delta t}\right) \tag{4.55}$$

$$\dot{\boldsymbol{U}}^{(k)}_{t+\Delta t} = \dot{\boldsymbol{U}}_t + \frac{\Delta t}{2}\left(\ddot{\boldsymbol{U}}_t + \ddot{\boldsymbol{U}}^{(k)}_{t+\Delta t}\right) \tag{4.56}$$

Using Equations (4.54), (4.55) and (4.56), we thus obtain $\ddot{\boldsymbol{U}}^{(k)}_{t+\Delta t}$ and $\dot{\boldsymbol{U}}^{(k)}_{t+\Delta t}$ in terms of and $\Delta\boldsymbol{U}^{(k)}$.

$$\begin{aligned}\dot{\boldsymbol{U}}^{(k)}_{t+\Delta t} &= \frac{2}{\Delta t}\left(\boldsymbol{U}^{(k)}_{t+\Delta t} - \boldsymbol{U}_t\right) - \dot{\boldsymbol{U}}_t \\ &= \frac{2}{\Delta t}\left(\boldsymbol{U}^{(k-1)}_{t+\Delta t} + \Delta\boldsymbol{U}^{(k)} - \boldsymbol{U}_t\right) - \dot{\boldsymbol{U}}_t\end{aligned} \tag{4.57}$$

$$\begin{aligned}\ddot{\boldsymbol{U}}_{t+\Delta t}^{(k)} &= \frac{2}{\Delta t}\left(\dot{\boldsymbol{U}}_{t+\Delta t}^{(k)} - \dot{\boldsymbol{U}}_t\right) - \ddot{\boldsymbol{U}}_t \\ &= \frac{4}{\Delta t^2}\left(\boldsymbol{U}_{t+\Delta t}^{(k-1)} + \Delta \boldsymbol{U}^{(k)} - \boldsymbol{U}_t\right) - \frac{4}{\Delta t}\dot{\boldsymbol{U}}_t - \ddot{\boldsymbol{U}}_t\end{aligned} \tag{4.58}$$

Substituting the above two equations into Equation (4.53) gives the following incremental equilibrium equation.

$$\hat{\boldsymbol{K}}\Delta \boldsymbol{U}^{(k)} = \Delta \hat{\boldsymbol{F}}_{t+\Delta t}^{(k)} \tag{4.59}$$

where effective stiffness matrix $\hat{\boldsymbol{K}}$ and effective incremental load matrix $\Delta \hat{\boldsymbol{F}}_{t+\Delta t}^{(k)}$ are respectively written as

$$\hat{\boldsymbol{K}} = \boldsymbol{K}_0 + \frac{2}{\Delta t}\boldsymbol{C}_0 + \frac{4}{\Delta t^2}\boldsymbol{M}_0 \tag{4.60}$$

$$\begin{aligned}\Delta \hat{\boldsymbol{F}}_{t+\Delta t}^{(k)} = \boldsymbol{F}_{t+\Delta t} - \boldsymbol{R}_{t+\Delta t}^{(k-1)} &+ \boldsymbol{M}_0\left\{\frac{4}{\Delta t^2}\left(\boldsymbol{U}_t - \boldsymbol{U}_{t+\Delta t}^{(k-1)}\right) + \frac{4}{\Delta t}\dot{\boldsymbol{U}}_t + \ddot{\boldsymbol{U}}_t\right\} \\ &+ \boldsymbol{C}_0\left\{\frac{2}{\Delta t}\left(\boldsymbol{U}_t - \boldsymbol{U}_{t+\Delta t}^{(k-1)}\right) + \dot{\boldsymbol{U}}_t\right\}\end{aligned} \tag{4.61}$$

The final form of the incremental equilibrium Equation (4.59) is the same as that considered in the static analysis, Equation (4.36). We can, therefore, see that all iterative solution techniques for static analysis are also directly applicable here. The iteration with the initial stiffness matrix method is continued until convergence has occurred. Because nonlinear dynamic response is highly path-dependent, the convergence criterion used is more stringent at each step than in the static analysis. In order to provide some indication when both displacement and forces are near equilibrium, the following convergence criterion with energy is used, in which the increment in internal energy during each iteration is compared to the initial internal energy increment.

$$\frac{\Delta \boldsymbol{U}^{(k)^t}\left(\boldsymbol{F}_{t+\Delta t} - \boldsymbol{R}_{t+\Delta t}^{(k-1)} - \boldsymbol{C}_0\dot{\boldsymbol{U}}_{t+\Delta t}^{(k-1)} - \boldsymbol{M}_0\ddot{\boldsymbol{U}}_{t+\Delta t}^{(k-1)}\right)}{\Delta \boldsymbol{U}^{(1)^t}\left(\boldsymbol{F}_{t+\Delta t} - \boldsymbol{R}_t - \boldsymbol{C}_0\dot{\boldsymbol{U}}_t - \boldsymbol{M}_0\ddot{\boldsymbol{U}}_t\right)} \leq ETOL \tag{4.62}$$

where $ETOL$ is an energy tolerance. After arriving at the expected convergence, the integration process proceeds to the next step with modified initial conditions. The complete algorithm used in the present work is given in Table 4.5.

Table 4.1 Element Stiffness Matrix

1	2	3	4	5	6	7	8	9	10	11	12	dof
$\frac{EA}{\ell}$	0	0	0	0	0	$-\frac{EA}{\ell}$	0	0	0	0	0	1
	$\frac{12EI_z}{\ell^3}+\frac{6T}{5\ell}$	0	0	0	$\frac{6EI_z}{\ell^2}+\frac{T}{10}$	0	$-\frac{12EI_z}{\ell^3}-\frac{6T}{5\ell}$	0	0	0	$\frac{6EI_z}{\ell^2}+\frac{T}{10}$	2
		$\frac{12EI_y}{\ell^3}+\frac{6T}{5\ell}$	0	$-\frac{6EI_y}{\ell^2}-\frac{T}{10}$	0	0	0	$-\frac{12EI_y}{\ell^3}-\frac{6T}{5\ell}$	0	$-\frac{6EI_y}{\ell^2}-\frac{T}{10}$	0	3
			$\frac{GI_x}{\ell}$	0	0	0	0	0	$-\frac{GI_x}{\ell}$	0	0	4
				$\frac{4EI_y}{\ell}+\frac{2T\ell}{15}$	0	0	0	$\frac{6EI_y}{\ell^2}+\frac{T}{10}$	0	$\frac{2EI_y}{\ell}-\frac{T\ell}{30}$	0	5
					$\frac{4EI_z}{\ell}+\frac{2T\ell}{15}$	0	$-\frac{6EI_z}{\ell^2}-\frac{T}{10}$	0	0	0	$\frac{2EI_z}{\ell}-\frac{T\ell}{30}$	6
						$\frac{EA}{\ell}$	0	0	0	0	0	7
							$\frac{12EI_z}{\ell^3}+\frac{6T}{5\ell}$	0	0	0	$-\frac{6EI_z}{\ell^2}-\frac{T}{10}$	8
			symmetric					$\frac{12EI_y}{\ell^3}+\frac{6T}{5\ell}$	0	$\frac{6EI_y}{\ell^2}+\frac{T}{10}$	0	9
									$\frac{GI_x}{\ell}$	0	0	10
										$\frac{4EI_y}{\ell}+\frac{2T\ell}{15}$	0	11
											$\frac{4EI_z}{\ell}+\frac{2T\ell}{15}$	12

Table 4.2 Element structural mass matrix

$$\frac{m\ell}{420}\begin{bmatrix}
1 & 2 & 3 & 4 & 5 & 6 & 7 & 8 & 9 & 10 & 11 & 12 & dof \\
\hline
140 & 0 & 0 & 0 & 0 & 0 & 70 & 0 & 0 & 0 & 0 & 0 & 1 \\
 & 156 & 0 & 0 & 0 & 22\ell & 0 & 54 & 0 & 0 & 0 & -13\ell & 2 \\
 & & 156 & 0 & -22\ell & 0 & 0 & 0 & 54 & 0 & 13\ell & 0 & 3 \\
 & & & \frac{140I_p}{A} & 0 & 0 & 0 & 0 & 0 & \frac{70I_p}{A} & 0 & 0 & 4 \\
 & & & & 4\ell^2 & 0 & 0 & 0 & -13\ell & 0 & -3\ell^2 & 0 & 5 \\
 & & & & & 4\ell^2 & 0 & 13\ell & 0 & 0 & 0 & -3\ell^2 & 6 \\
\hline
 & & & & & & 140 & 0 & 0 & 0 & 0 & 0 & 7 \\
 & & & & & & & 156 & 0 & 0 & 0 & -22\ell & 8 \\
 & & & sym. & & & & & 156 & 0 & 22\ell & 0 & 9 \\
 & & & & & & & & & \frac{140I_p}{A} & 0 & 0 & 10 \\
 & & & & & & & & & & 4\ell^2 & 0 & 11 \\
 & & & & & & & & & & & 4\ell^2 & 12
\end{bmatrix}$$

Table 4.3 Element added mass matrix

$$\frac{m_a\ell}{420}\begin{bmatrix}
1 & 2 & 3 & 4 & 5 & 6 & 7 & 8 & 9 & 10 & 11 & 12 & dof \\
\hline
0 & 0 & 0 & 0 & 0 & 0 & 0 & 0 & 0 & 0 & 0 & 0 & 1 \\
 & 156 & 0 & 0 & 0 & 22\ell & 0 & 54 & 0 & 0 & 0 & -13\ell & 2 \\
 & & 156 & 0 & -22\ell & 0 & 0 & 0 & 54 & 0 & 13\ell & 0 & 3 \\
 & & & 0 & 0 & 0 & 0 & 0 & 0 & 0 & 0 & 0 & 4 \\
 & & & & 4\ell^2 & 0 & 0 & 0 & -13\ell & 0 & -3\ell^2 & 0 & 5 \\
 & & & & & 4\ell^2 & 0 & 13\ell & 0 & 0 & 0 & -3\ell^2 & 6 \\
\hline
 & & & & & & 0 & 0 & 0 & 0 & 0 & 0 & 7 \\
 & & & & & & & 156 & 0 & 0 & 0 & -22\ell & 8 \\
 & & & symmetric & & & & & 156 & 0 & 22\ell & 0 & 9 \\
 & & & & & & & & & 0 & 0 & 0 & 10 \\
 & & & & & & & & & & 4\ell^2 & 0 & 11 \\
 & & & & & & & & & & & 4\ell^2 & 12
\end{bmatrix}$$

Table 4.4 Consistent nodal load matrix for linearly varying load

nodal force	*dof*
$(2f_{x1}+f_{x2})\ell/6$	*1*
$(7f_{y1}+3f_{y2})\ell/20$	*2*
$(7f_{z1}+3f_{z2})\ell/20$	*3*
0	*4*
$-(3f_{z1}+2f_{z2})\ell^2/60$	*5*
$(3f_{y1}+2f_{y2})\ell^2/60$	*6*
$(f_{x1}+2f_{x2})\ell/6$	*7*
$(3f_{y1}+7f_{y2})\ell/20$	*8*
$(3f_{z1}+7f_{z2})\ell/20$	*9*
0	*10*
$(2f_{z1}+3f_{z2})\ell^2/60$	*11*
$-(2f_{z1}+3f_{z2})\ell^2/60$	*12*

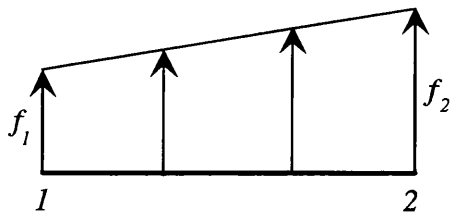

Table 4.5 Step-by-step solution procedure for nonlinear system

A. Initial Calculations:

1. Form stiffness matrix $\boldsymbol{K}_0$, mass matrix $\boldsymbol{M}_0$, and damping matrix $\boldsymbol{C}_0$.
2. Initialise $\boldsymbol{U}_0$, $\dot{\boldsymbol{U}}_0$, and $\ddot{\boldsymbol{U}}_0$.
3. Select time step size Δt, parameters α and δ, and calculate integration constants:

$$\delta \geq 0.50; \qquad \alpha \geq 0.25\,(0.5+\delta)^2$$

$$a_0 = \frac{1}{\alpha\,\Delta t^2}\;; \qquad a_1 = \frac{\delta}{\alpha\,\Delta t}\;; \qquad a_2 = \frac{1}{\alpha\,\Delta t}\;; \qquad a_3 = \frac{1}{2\alpha} - 1\;;$$

$$a_4 = \frac{\delta}{\alpha} - 1\;; \qquad a_5 = \frac{\Delta t}{2}\left(\frac{\delta}{\alpha} - 2\right)\;; \qquad a_6 = \Delta t(1-\delta)\;; \qquad a_7 = \delta\Delta t$$

4. Form effective stiffness matrix $\hat{\boldsymbol{K}}$: $\hat{\boldsymbol{K}} = \boldsymbol{K}_0 + a_0\boldsymbol{M}_0 + a_1\boldsymbol{C}_0$
5. Triangularise $\hat{\boldsymbol{K}}$: $\hat{\boldsymbol{K}} = \boldsymbol{L}\boldsymbol{D}\boldsymbol{L}^t$.

B. For Each Time Step:

1. Form effective incremental load vector:

$$\Delta\hat{\boldsymbol{F}}_{t+\Delta t}^{(k)} = \boldsymbol{F}_{t+\Delta t} - \boldsymbol{R}_{t+\Delta t}^{(k-1)} + \boldsymbol{M}_0\left\{a_0\left(\boldsymbol{U}_t - \boldsymbol{U}_{t+\Delta t}^{(k-1)}\right) + a_2\dot{\boldsymbol{U}}_t + a_3\ddot{\boldsymbol{U}}_t\right\}$$
$$+ \boldsymbol{C}_0\left\{a_1\left(\boldsymbol{U}_t - \boldsymbol{U}_{t+\Delta t}^{(k-1)}\right) + a_4\dot{\boldsymbol{U}}_t + a_5\ddot{\boldsymbol{U}}_t\right\}$$

2. Solve incremental displacement vector:

$$\boldsymbol{L}\boldsymbol{D}\boldsymbol{L}^t\Delta\boldsymbol{U}^{(k)} = \Delta\hat{\boldsymbol{F}}_{t+\Delta t}^{(k)}$$

3. Calculate new acceleration and velocity vectors:

$$\ddot{\boldsymbol{U}}_{t+\Delta t}^{(k)} = a_0\left(\boldsymbol{U}_{t+\Delta t}^{(k-1)} + \Delta\boldsymbol{U}^{(k)} - \boldsymbol{U}_t\right) - a_2\dot{\boldsymbol{U}}_t - a_3\ddot{\boldsymbol{U}}_t$$

$$\dot{\boldsymbol{U}}_{t+\Delta t}^{(k)} = a_1\left(\boldsymbol{U}_{t+\Delta t}^{(k-1)} + \Delta\boldsymbol{U}^{(k)} - \boldsymbol{U}_t\right) - \dot{\boldsymbol{U}}_t$$

4. Calculate internal force vector $\boldsymbol{R}_{t+\Delta t}^{(k)}$.
5 Check convergence. If not converged, iterate again. If converged, proceed with next step.

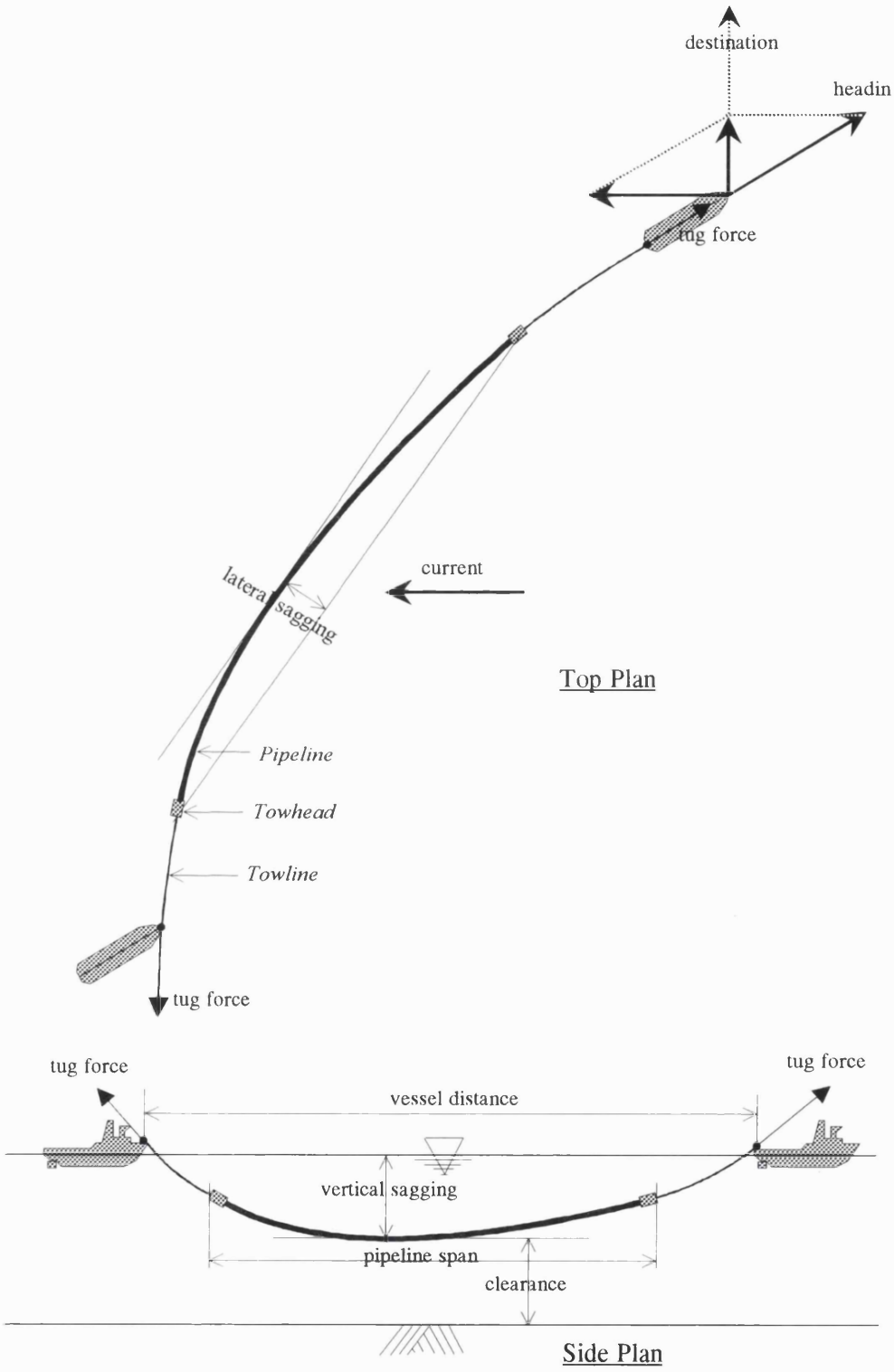

Figure 4.1 Parameters for manoeuvring plan

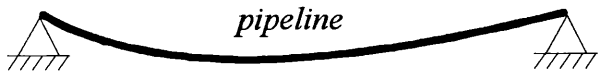

(a) Model for static analysis

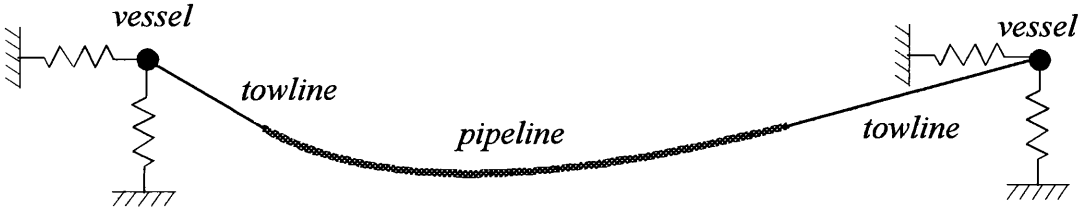

(b) Model for dynamic analysis

Figure 4.2 Computer models for static and dynamic analyses

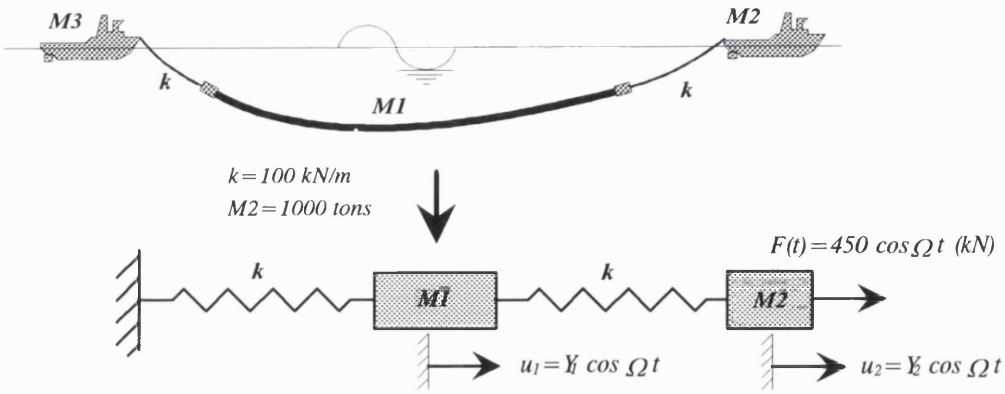

(a) Idealisation of a tow system

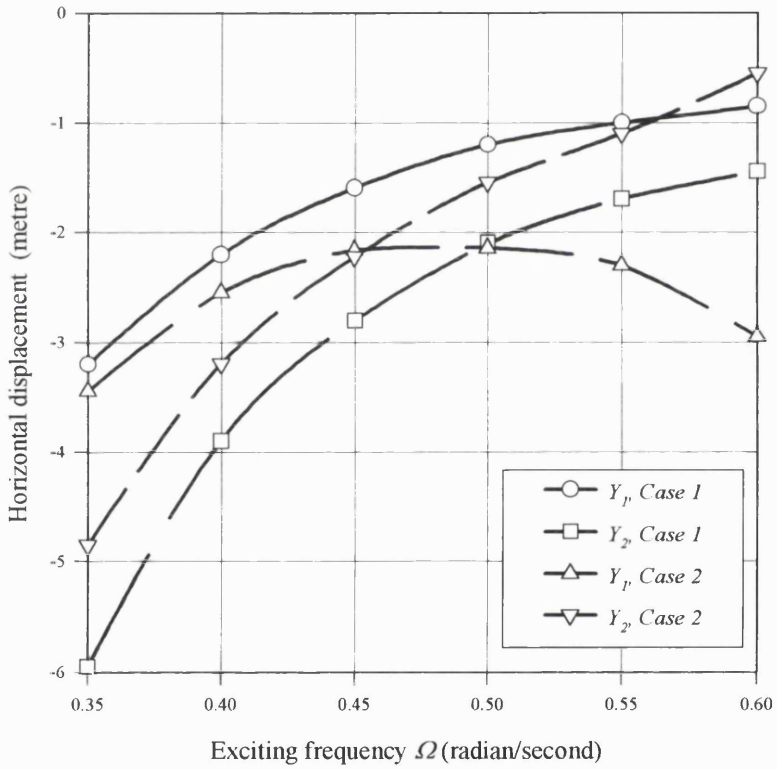

	Mass, *M1* (ton)	ω_1 (rad/sec)	ω_2 (rad/sec)
Case 1	100	0.221	1.432
Case 2	500	0.209	0.674

(b) Dynamic response

Figure 4.3 Simplified check of the influence of vessel mass on dynamic responses

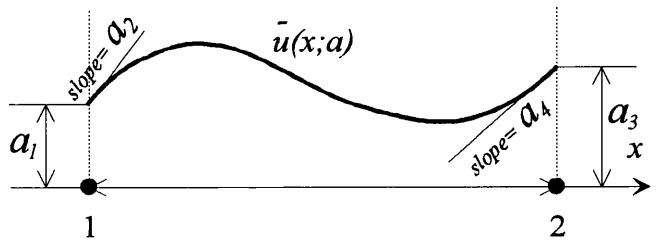

(a) Trial Solution

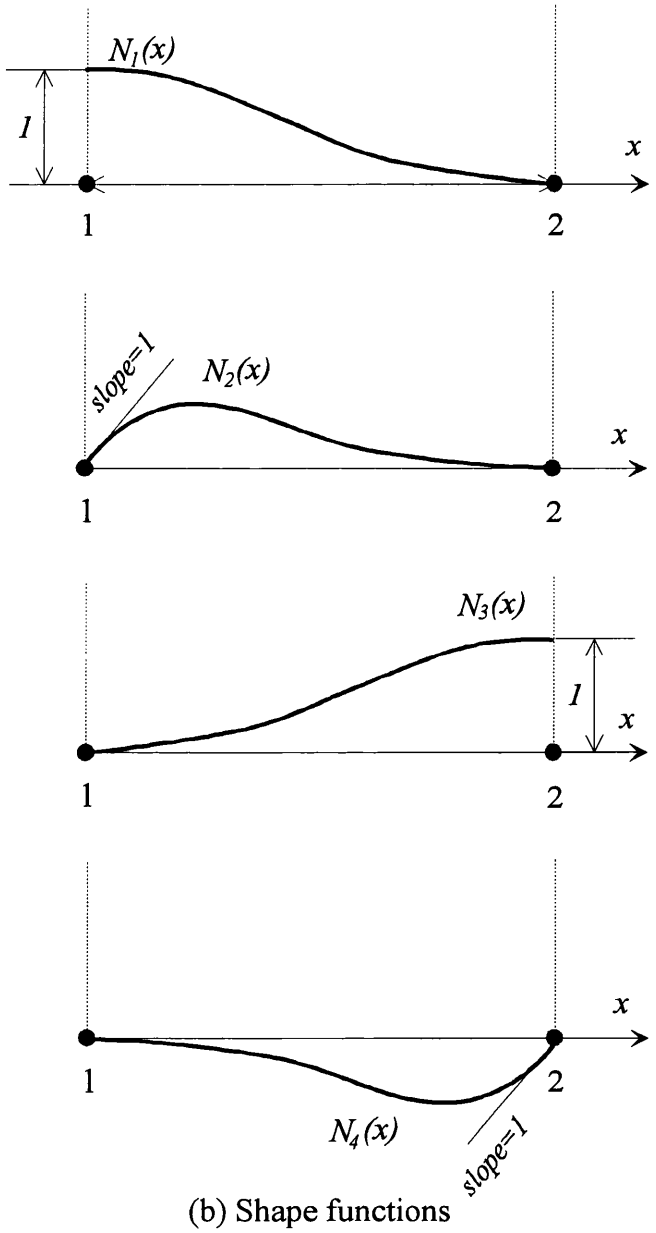

(b) Shape functions

Figure 4.4 Trial solution and shape functions for a one dimensional cubic element

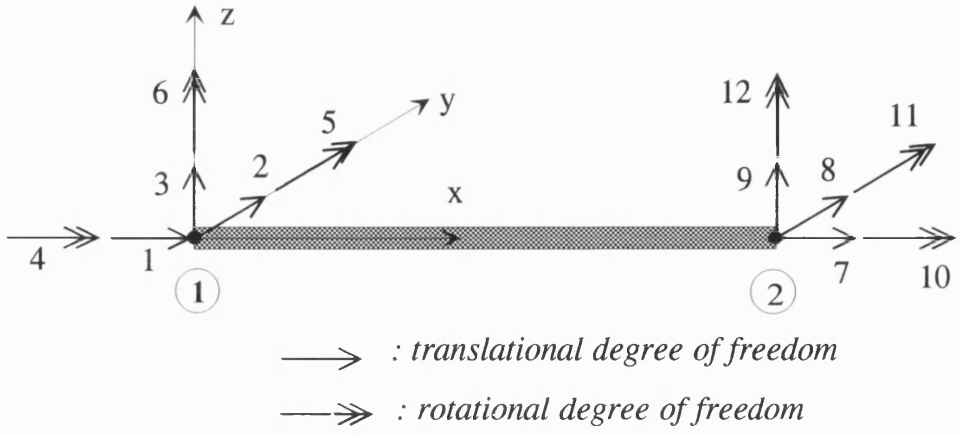

Figure 4.5 Definition of degrees of freedom for a beam element

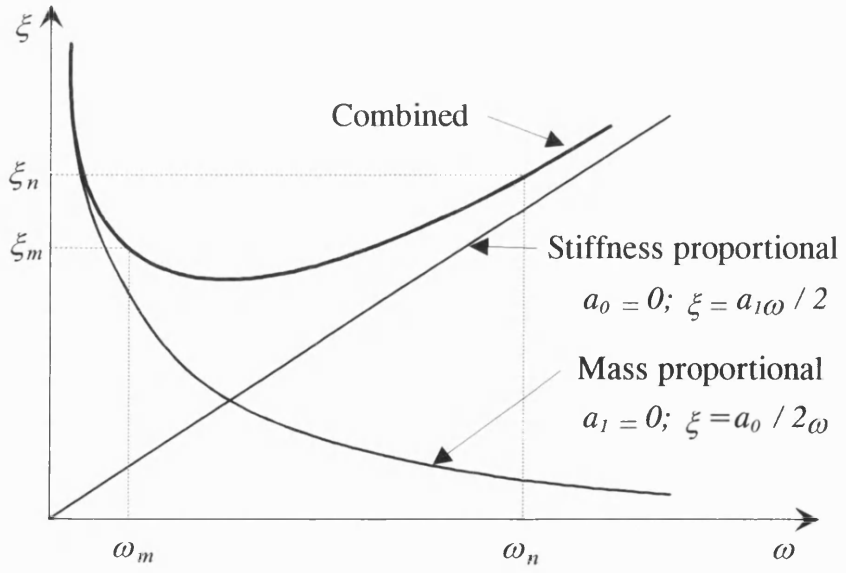

Figure 4.6 Relationship between damping ratio and frequency for Rayleigh damping

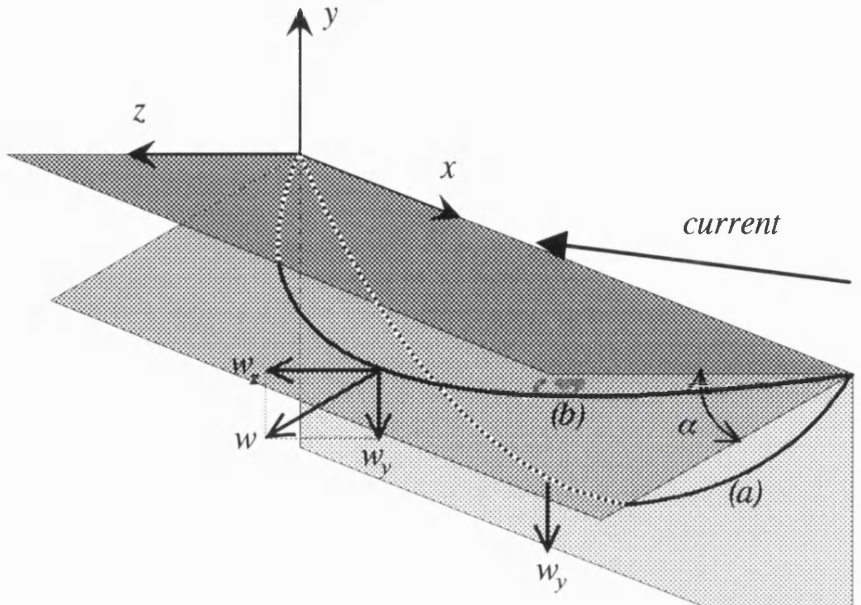

(a) : from conventional catenary analysis
(b) : from enhanced catenary analysis

Figure 4.7 Starting geometry from conventional and enhanced catenary analyses

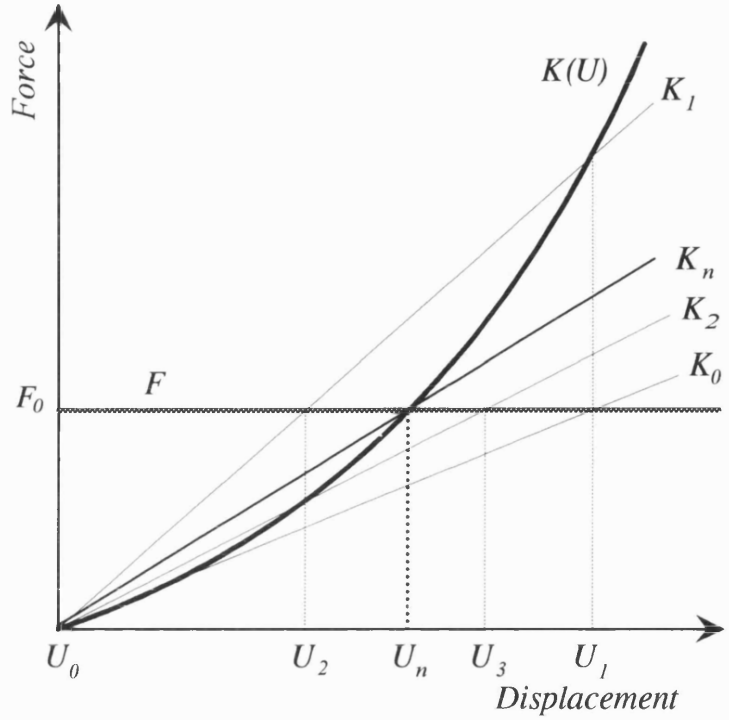

Figure 4.8 Direct iteration method with deformation-independent load

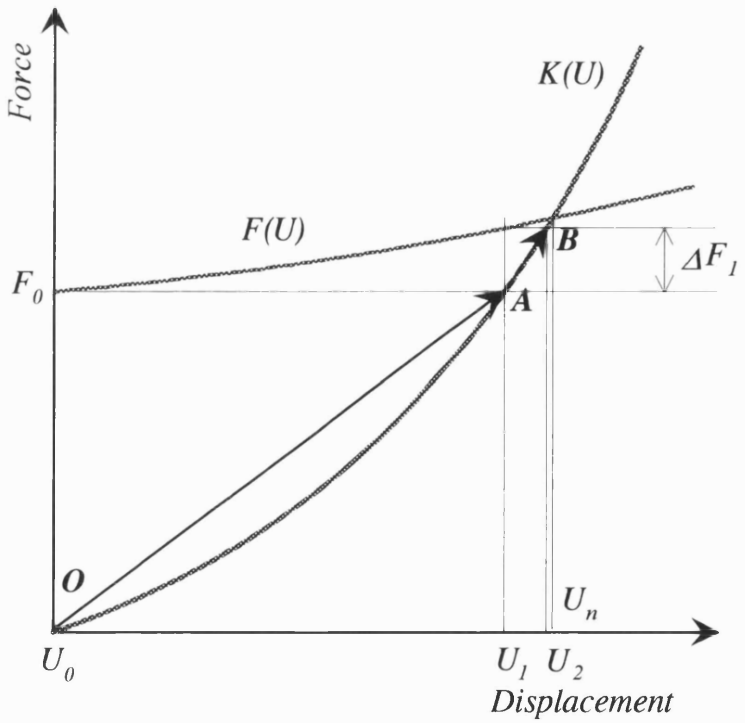

Figure 4.9 Direct iteration method with deformation-dependent load

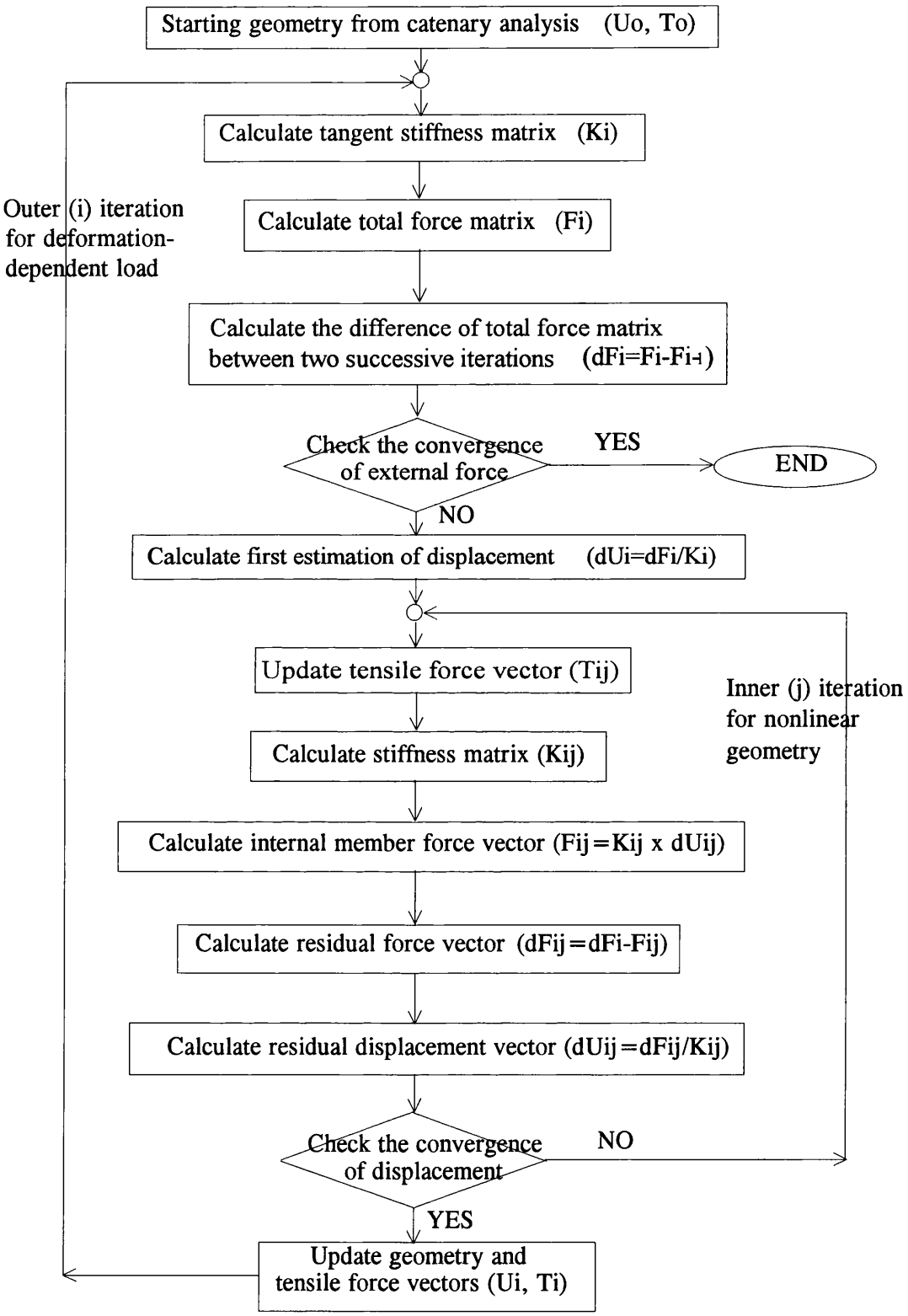

Figure 4.10 Procedure for nonlinear static analysis

5. APPLICATION STUDIES

The theories and finite element techniques described in Chapters 3 and 4 are implemented by the author in a finite element based computer package (hereafter called REFLEX).

The main objectives of any tow analysis are to confirm its feasibility and to prepare the operation manual for the considered tow condition. Among many analysis conditions of interest, such as a normal mid-depth tow, transition from off-bottom tow to mid-depth tow and vice versa, a change of heading and so on, only the normal mid-depth condition is considered in the present study. The definition of terms including sign convention and coordinate system is summarised in Figure 5.1.

Firstly in Section 5.1, the static and dynamic results from REFLEX are verified by comparison with those from ABAQUS (1995), a general purpose FE package. Although the mid-depth tow is becoming popular, the physics and analysis method for this tow condition have not yet been fully understood and established. Therefore, the remaining sections are concerned with investigating the related physics by examining the sensitivity of the tow system to variations in key parameters and establishing a reasonable analysis method using the theories and techniques presented in the previous chapters. Section 5.2 lists the properties of the considered bundle including structural properties and load distribution on the bundle and chains. Static structural behaviour due to the application of different hydrostatic pressure forces and the change in heading angle and offset is considered in Section 5.3. Dynamic responses with change in key parameters such as vessel mass, towline stiffness and towhead depth are checked in Section 5.4. This also includes the influence from applying the Lighthill formulation of loading in near-tangential flow.

5.1 Verification of REFLEX Results

The reliability of REFLEX is verified by comparing its results with those from ABAQUS. ABAQUS offers many powerful analysis options for linear and nonlinear problems. Many of the problems to which ABAQUS will be applied are history dependent, so the solution is developed by a series of small increments. In the case of nonlinear systems, ABAQUS generally uses Newton-Raphson method as a numerical technique for solving nonlinear equilibrium equations. The motivation for this choice is its excellent convergence rate compared to the convergence rates exhibited by alternative methods such as a modified Newton-Raphson method or an initial stiffness method. For beam structures immersed in fluid, that is, offshore piping and riser problems, ABAQUS provides a capability for introducing hydrodynamic forces using the Morison equation. Although ABAQUS usually provides stable and reliable results for most problems, it is unstable during handling towed pipelines due to their unusual properties - it experiences serious ill-conditioning problems or slow convergence in tow analysis. For example, it fails to handle a pipeline with very small submerged weight in static analysis. Therefore, only the most important issues are compared where possible. Somewhat large submerged weight is applied and chains are not included in the model. Currents are not considered during the dynamic analysis.

The properties of the pipeline considered are as follows:

Pipeline length = 400 *m*

Outer diameter = 0.6 *m*

Wall thickness = 15.0 *mm*

Young's modulus = 2.06×10^{11} N/m^2

Submerged weight per unit length = 500 *N/m*

Mass per unit length = 324.57 *kg/m*

The pipeline is modeled by 20 elements, each with a length of 20 metres. Water depth is assumed to be 500 metres and both leading and trailing towheads are kept 7.5 metres below still water surface.

5.1.1 Verification of Static Analysis Results

The considered pipeline is subjected to all or part of following loads for related analysis methods, FEM or the catenary equation.

- Uniformly distributed effective submerged weight of 500 *N/m*.
- Normal and tangential drag forces on the pipeline arising from the tow speed of 3 knots (1.542 *m*/second). The following hydrodynamic coefficients are applied.

  Normal drag coefficient, $C_{dn} = 1.0$

  Tangential drag coefficient, $C_{dt} = 0.2$ (an unrealistically large coefficient is applied to clearly check the reliability of REFLEX with tangential loads)

At first, the condition with submerged weight only is considered. In this case, REFLEX is expected to provide an exact solution because the catenary equation is accommodated within REFLEX (for details, see Sections 3.1.1 and 4.3.1). Tensile forces from both REFLEX and ABAQUS show good agreement as shown in Figure 5.2. Figures 5.3 and 5.4 also show reasonable agreement of bending moments and element rotations along most part of the pipeline except around both boundary nodes. The reason for this difference around the boundary nodes can be explained by the fact that the pipeline does not have negligible bending stiffness, which contradicts the catenary concept. It also explains why the axial forces from REFLEX are slightly higher than those from ABAQUS - only tensile energy is considered in the catenary equation instead of both tensile energy and bending energy. The difference in bending moments is, however, a localised problem just around the boundary nodes and does not have a significant influence on the evaluation of structural safety and subsequent dynamic analysis because all other results, especially axial forces, show

good agreement. Moreover, as the pipeline becomes longer, this problem becomes negligible in the global sense.

Next, the results with submerged weight and drag forces are compared. Two headings, 0° and 30° respectively, are considered and the results are shown in Figures 5.5 to 5.11. The analytical results in these figures are obtained using Equations (3.88) and (3.93). The results show the same trend as the previous case - good agreement in deformed shapes, axial forces and bending moments, with some difference of bending moment around the boundary nodes. Due to drag loads on the pipeline, there is a large change in axial force along the length (Figures 5.6 and 5.10) and maximum bending moments occurs around the aft of the pipeline (Figures 5.7 and 5.11).

5.1.2 Verification of Dynamic Analysis Results

The dynamic analysis models of REFLEX and ABAQUS include a pipeline, tow vessels, and towlines as shown in Figure 5.12. The properties of the pipeline are the same as those used for the static case described in Section 5.1.1. Additional data for the dynamic analysis are as follows:

Tow vessel

Mass of each vessel, M = 1025 tons

Longitudinal position of trailing vessel = –9.2 m

leading vessel = 509.2 m

Vertical spring stiffness, k_y = 2,510 kN/m

Longitudinal spring stiffness, k_x = 25.1 N/m

Amplitude of surge force, F_v = 300 kN

Towline

Axial rigidity, EA = 4368 kN

Length = 60.1 m

Wave

Height = 6.0 m

Period = 10.0 seconds

Position = phase of 0° at the origin of the coordinate system at time 0

Drag coefficient, $C_d = 1.0$

Inertia coefficient, $C_M = 2.0$

The positions of the tow vessels and the length of towlines are taken as those at static equilibrium with static loads. Rayleigh damping with a damping ratio of 0.05 is used. The model is subjected to dynamic loads from a linear wave propagating in the positive x direction. Surge force on the trailing vessel is applied in-phase with the wave, whilst that on the leading vessel is out-of-phase. The same computational time interval, Δt, of 0.25 second and energy tolerance, *ETOL* (for details, see Section 4.4.2), of 1.0×10^{-9} are applied throughout the considered time range of 100 seconds.

Both REFLEX and ABAQUS provide convergent results after four or five cycles of the wave. Figures 5.13 and 5.14 show the vertical component of dynamic displacement at 90 seconds and half cycle later, that is 95 seconds, respectively. Both figures reveal that the response patterns are similar with the ABAQUS result apparently showing larger responses than REFLEX. Despite this difference in displacements, Figures 5.15 and 5.16 show excellent agreement for dynamic axial forces and bending moments. The reason for the above results large difference in displacements good agreement of member forces can be found by considering the pure dynamic response components which do not include non-varying components. Figure 5.17 shows the envelope of vertical displacements from static equilibrium from one cycle of the excitation. It clearly shows larger deviation of the mean configuration of ABAQUS results compared to the REFLEX results. Although the deviation of mean configuration is frequent in nonlinear analysis, the present deviation from ABAQUS is quite large. It may be due to the combined reasons of very flexible towlines and different analysis methods, the full nonlinear method in ABAQUS and an initial stiffness method in REFLEX. After removing the deviated component from dynamic responses, both results show a relatively good match as

presented in Figure 5.18. Figures 5.19 to 5.21 show envelopes of longitudinal components of dynamic displacements, dynamic bending moments and dynamic axial forces respectively, and all show good agreement.

5.2 Bundle for Application Studies

For the following application studies, a realistic bundle, the bundle for the Britannia Field, is chosen. The Britannia Field is approximately 200 *km* northeast of Aberdeen in the UK sector of the North Sea. The water depth ranges from approximately 150 metres in the west of the Field to 135 metres in the eastern region. The flowline bundle system comprises two off 7.5 *km* nominal length bundles which, once connected in line, will provide the 15 *km* connection between the Britannia Manifold and the Britannia Platform. In the present work, a bundle of 1.0 *km* in length is used instead of 7.5 *km*. Each bundle consists of four flowlines contained within a carrier pipe whose outer diameter is 946.2 *mm*. The detailed section with related dimensions is shown in Figure 5.22. The detailed data of the bundle used for this work are as follows:

Bundle

Total length = 1000 *m*, Leading towhead = 20 *m*
Trailing towhead = 20 *m*
Bundle itself = 960 *m*

Towhead position = 30 *m* below still water surface unless otherwise mentioned

Offset = 2.0 *m* unless otherwise specified

Outer diameter = 0.9462 *m*

Cross sectional area, A = $0.0846\ m^2$

Moment of inertia, I_y and I_z = $5.253\times10^{-3}\ m^4$

Torsional moment of inertia, J = $8.299\times10^{-3}\ m^4$

Young's modulus, E = $2.06\times10^{11}\ N/m^2$

Dry weight per unit length without chains = 6801.5 *N/m*

Buoyancy per unit length = 7070.5 *N/m*

Mass per unit length = 693.3 *kg/m*

Normal drag coefficient, $C_{dn} = 1.2$

Tangential drag coefficient, $C_{dt} = 0.005$

Chain

Size = 78.5 *mm*

Spacing = 20 *m*, from 30 *m* to 970 *m* (actually chains will be attached every ten metres. However, two chains are lumped at one node during analysis to reduce problem size)

Length = 3.22 *m* × 2

Submerged weight = 3116 *N* × 2

Mass = 364.28 *kg* × 2

Tow

Speed = 3.0 knots unless otherwise specified

Heading = 0° unless otherwise specified

Allowable forces of the considered bundle which is made of mild steel are as follows :

Axial force,	Static case	$= 1.25\times10^7$ *N*
	Dynamic case	$= 1.66\times10^7$ *N*
Bending moment,	Static case	$= 1.63\times10^6$ *N-m*
	Dynamic case	$= 2.17\times10^6$ *N-m*

The weight summary of the bundle with chains in water is given below:

Total dry weight	= –6801.5 × 1000	= –6,801,500 *N*
Total buoyancy	= 7070.5 × 1000	= 7,070,500 *N*
Total submerged weight of chains	= –3116 × 2 × 48	= –299,136 *N*

⇒ Total submerged weight = –30,136 *N*

Submerged weight per length = –30.136 *N/m*

The above weight summary shows how small the total submerged weight is under real tow conditions. Therefore this long bundle may become unstable to other external loads unless enough tension, that is geometric stiffness, is developed. If the tow speed exceeds 4.26 knots, the bundle will float to surface due to the lift forces on chains. For the planned tow speed, three knots, the chain forces from equation (3.47) and their distributed loads along the bundle are:

Lift force = 201.38 *N*/chain = 9.666 *N/m*

Drag force = 985.30 *N*/chain = 47.295 *N/m*

Assuming that the bundle is parallel to the tow direction with a speed of three knots, total tangential drag force per unit length is 18.112 *N/m* from Equation (3.48). This tangential drag force, along with the drag forces on the chains, will produce a difference in axial forces at the ends of the bundle. In the present case, the difference is about 65.4 *kN* and it will increase proportionally with increase in the bundle length.

The axial forces, bending moments and vertical coordinates from REFLEX, the catenary solution, and the analytical solution (for details, see Section 3.5.1) for the above condition are respectively shown in Figures 5.23 to 5.25. REFLEX models an exact distribution of the loads while the analytical solution uses uniformly distributed weight and current loads. Figure 5.23 shows good agreement between the FEM and catenary solution with the difference in axial forces at both ends, 65.4 *kN*, as explained previously. Since chains are attached along the length from 30 metres to 970 metres at every 20 metres, the bundle is negatively buoyant in this range and positively buoyant outside this range. Bending moments from REFLEX in Figure 5.24 show the effect from this pattern of weight distribution. Also vertical coordinates from the analytical solution, that is with uniformly distributed loads, show large deviation from REFLEX results. Therefore, from now on the REFLEX model with its exact modeling of loads will be considered.

For FE element analysis the first 30 metres and the last 30 metres of the bundle are respectively modeled by three elements of equal length, each of 10 metres. The rest of the bundle, 940 metres, is modeled by 47 elements of equal length, 20 metres. So the FE model consists of 53 elements and 54 nodes.

5.3 Application Studies for Static Condition

Accurate estimation of the bundle behaviour with static load is important for a manoeuvring plan as well as for structural safety. Since bundles are very flexible due to their inherent section properties, very small submerged weight and limited tensile forces, their behaviour may be highly influenced by slight external disturbances. This section is concerned with the structural behaviour with change in key parameters such as heading angle and offset, including the application of accurate hydrostatic pressure forces.

5.3.1 Influence of Hydrostatic Pressure Force

For most offshore structures, little attention has been paid to hydrostatic pressure forces. Conventionally the 'effective weight' from the simple summation of dry weight and classical buoyancy with submerged volume has been used during structural analysis. This approach is quite reasonable if the buoyancy is negligible compared to other load items and/or the structures are stiff enough to be little influenced by their buoyancy. In the case of towed bundles, however, this is totally the opposite - their buoyancy is comparable to other loads, such as dry weight, and these structures are very flexible. As discussed in Section 3.2, hydrostatic pressure forces control pipe curvature in a way similar to the tensile forces in the wall of the pipe. In this section, the effects of hydrostatic pressure forces are studied by comparing these analysis results with those obtained from analysis with effective weight. Since curvatures of the towed bundle are small, the formulae for straight pipes in Section 3.2.1 are used.

Firstly, consider the case without tow speed. Figures 5.26 to 5.28 respectively show vertical coordinates, bending moments and axial forces with and without hydrostatic pressure forces for this condition. The terms 'with' and 'without' pressure forces respectively mean the cases with the application of accurate hydrostatic pressure forces and without it, that is effective weight only. Figure 5.27 clearly shows the so-called curvature reversal due to the hydrostatic pressure forces. Also this force gives rise to a significant change in axial forces along the length of the bundle as shown in Figure 5.28.

Next, consider the case with a tow speed of three knots. Two heading conditions, 0° and 30°, are considered and the axial forces and bending moments are shown in Figures 5.29 and 5.30, respectively. These results show that the application of accurate hydrostatic pressure force is still important for the towing condition with 0° heading while it gives negligible influence to that with 30° heading. The latter is because the current from 30° heading produces normal drag forces which are very large compared to the hydrostatic pressure forces. However, considering that the tow must be performed with a small heading angle (for details, see next section), the application of the accurate hydrostatic pressure force is essential for tow analysis and it is considered in all subsequent analyses.

5.3.2 Influence of Heading Angle

If the bundle is subjected to side current, its lateral load from normal drag easily exceeds the vertical load on it. Therefore the bundle will move near to the horizontal plane. This phenomenon is checked by applying different heading angles and Figures 5.31 and 5.32 clearly show this pattern. In addition to this phenomenon, due to the limited towline length, the bundle will consequently float just near the still water surface for large heading angles. This condition is very dangerous and must be avoided because the bundle is then directly exposed to the severe wave action zone. Also with increase in heading angle, axial forces increase rapidly while bending moments decrease as shown in Figures 5.33 and 5.34 respectively. The

required tug forces for different heading angles and tow speeds are shown in Figure 5.35. In side current the normal drag force is very large compared to the tangential force and therefore tows with large heading angles require very large tug forces and very strong towlines, which are difficult and unrealistic.

Considering the above results, it is very important to keep the heading angle as small as possible except in some special cases, such as the changing of tow direction, which requires careful planning and operation. The following analyses, including dynamic cases, are for the tow with 0° heading angle unless otherwise mentioned.

5.3.3 Influence of Offset

Throughout the analysis and tow operation, the position of towheads, along with tow speed, provides much useful information such as sag, axial forces and bending moments along the bundle. This section is concerned with the structural behaviour to the changes in offset. Due to the special geometric characteristic of the towed bundle, that is very long with shallow sag, a slight disturbance of offset gives rise to large sag of the bundle as shown in Figure 5.36. If the tow is performed in limited water depth, careful planning and operation are necessary to avoid contact between the bundle and seabed. Figure 5.37 shows that as offset increases there is almost a proportional increase in maximum absolute bending moment around 400 metres along the bundle. Although it is well below the allowable bending moment of 1.63×10^6 *N-m*, this increase shows it is very sensitive to offset compared to the variation of other factors as considered in previous sections. The required tug forces with change in offset and tow speed are shown in Figure 5.38. It shows that the larger the offset the higher the tug force that is required, except for offsets between one and two metres. This exception is due to the combined effect of the distribution of the weight and the hydrostatic pressure force. The above trend of the tug force variation is very different or almost contrary to that from the analysis without considering the hydrostatic pressure force, as shown in Figure 5.39.

5.4 Application Studies for Dynamic Condition

Towed bundles experience various kinds of dynamic loads such as waves, currents and vessel forces and the resulting dynamic responses are quite complicated due to the interaction between a bundle and tow vessels. In this section the dynamic response pattern of the bundle is investigated by comparison of results obtained when changing key parameters such as vessel mass, towline stiffness and towhead depth. Also the inertia forces and resulting dynamic responses from the Morison's and Lighthill's approaches are compared to check the accuracy of the Morison's formula in calculating inertia forces for near-tangential flow.

Details of the modeling scheme are explained in Section 4.1.2. The properties of the considered bundle are the same as those used for the static case described in Section 5.2. Additional data for the dynamic analysis are as follows. These are the same for all subsequent analyses unless otherwise mentioned.

Tow vessel

Mass of each vessel, M_o = 1076 tons

Longitudinal position of trailing vessel = –285.8 *m*

leading vessel = 1435.1 *m*

Vertical spring stiffness, k_y = 2,110 *kN/m*

Longitudinal spring stiffness, k_x = 21.1 *N/m*

Amplitude of surge force, F_v = 420 *kN*

Amplitude of heave force, F_h = 4070 *kN*

Towline

Axial rigidity, EA_o = 10,000 *kN*

Length, trailing = 287.4 *m*

, leading = 438.1 *m*

Wave

Height = 6.0 *m*

Period = 10.0 seconds

Position = phase of 0° at the origin of the coordinate system at time 0

Drag coefficient, $C_d = 1.2$

Inertia coefficient, $C_M = 2.0$

The positions of the tow vessels and the length of towlines are automatically calculated from the static equilibrium with static loads. Rayleigh damping with a damping ratio of 0.05 is used. The model is subjected to dynamic loads a linear wave propagating in the negative longitudinal direction. Surge force on the trailing vessel is applied in-phase with the wave, whilst that on the leading vessel is out-of-phase. The same computational time interval, Δt, of 0.25 second and energy tolerance, *ETOL* (for details, see Section 4.4.2), of 1.0×10^{-9} are applied throughout the considered time range of 100 seconds.

5.4.1 General Aspects of Dynamic Responses

Dynamic responses of the tow system with wave, current and vessel forces are investigated for the conditions described previously in Section 5.4.

In the case of displacements, there is large movement in the mean configuration from the starting geometry, that is the static equilibrium geometry, as shown in Figures 5.40 and 5.41. This phenomenon is due to the effect from dynamic current and it must be considered accurately during a dynamic analysis because the fore part of the bundle experiences higher responses as the bundle moves nearer to the water surface. Since the hydrodynamic loading around the surface is highly influenced by the bundle elevation, this large movement requires the application of deformation-dependent hydrodynamic loading. From this new mean geometry, pure dynamic responses can be estimated. Figure 5.40 shows that large vertical dynamic displacements are concentrated around the ends of the bundle and it is mainly due to the soft constraints from towlines. The response of other parts is relatively small due to large hydrodynamic damping in the normal (vertical) direction. In the case of longitudinal

dynamic displacement, their variation along the bundle is relatively uniform as shown in Figure 5.41 due to small tangential (longitudinal) hydrodynamic damping.

The bundle will experience higher dynamic bending moment around its ends than other parts due to their soft constraint and proximity to water surface and the envelope for one cycle of the excitation, Figure 5.42, shows this trend. Under the considered analysis condition, a maximum combined bending moment of 8.078×10^5 *N-m* (static bending moment of 2.222×10^5 plus dynamic bending moment of 5.856×10^5) is obtained at 70 metres from the aft end and it is 37 percent of the allowable bending moment, 2.17×10^6 *N-m*.

The axial force along the bundle is from wave action and the interaction between the bundle and the tow vessels. Figure 5.43 shows that the resulting axial forces are small, about 10 percents, compared to the vessel force, 420 *kN*. It means that most of the vessel force is used for vessel motion and towline deformation. Also the occurrence of the peak axial forces at the ends of the bundle suggests that the interaction decreases due to the hydrodynamic damping on the bundle. The maximum combined axial force of 363 *kN* is only two percent of the allowable axial force, 1.66×10^4 *kN*. Although the dynamic axial force is negligibly small compared to the allowable force, it significantly influences fatigue life and, consequently, the selection of the towline. Therefore, accurate consideration of the interaction between tow vessels and a bundle is essential in tow analysis.

5.4.2 Influence of Tow Vessels

The influence of tow vessels on the dynamic response of the bundle is investigated in this section. For this, dynamic responses for different vessel masses and different phase angles of exciting forces are compared. Other conditions, including amplitude of vessel exciting force, are described in Section 5.4.

Firstly, dynamic responses for surge forces are considered. Figures 5.44 to 5.47 show the comparison of dynamic responses for different vessel masses. The excitations of both vessels are in-phase with the wave. The vertical displacement (Figure 5.44) and the bending moment along the length (Figure 5.46) are almost the same for different vessel masses whilst there are large differences in longitudinal displacement and axial force. This tendency is the same for vessel excitations with different phase angles as shown in Figures 5.48 to 5.51. Moreover, the bending moments along the length are almost identical regardless of the vessel mass and phase angle of the vessel force whilst the axial force shows large difference. It means that the dynamic bending moment is mainly from wave forces on the bundle and the dynamic axial force from the interaction is too small to influence the lateral responses.

In the case of heave force, its influence is much less than the surge force as shown in Figures 5.52 and 5.53 due to the small inclination angles of the towlines. Figure 5.52 shows that the heave force induces less axial force than the surge force even with very large exciting force, 4080 *kN*, compared to the surge force, 420 *kN*.

5.4.3 Influence of Towlines

The interaction between tow vessels and a bundle is highly influenced by the property of connecting members, the towlines. To investigate the influence of towline stiffness, the dynamic force responses with different axial rigidities of the towline, EA_o and $2EA_o$, are compared.

As the towlines become stiffer, the interaction becomes stronger. Figure 5.54 shows a roughly proportional increase in dynamic axial force around the ends of the bundle with the increase in axial rigidity. The peak amplitude of the axial force of 109 *kN* with $2EA_o$ is obtained at the aft end of the bundle and it is 39 percent of the static axial force there, 277 *kN*. Therefore, towlines that are too stiff will induce large dynamic axial forces and, when these are larger than the static force, will lead to

transient compressive axial forces. Because the bundle is very vulnerable to buckling with compressive axial force, the towlines should be designed to avoid this condition. Again the dynamic bending moment is slightly influenced by the change in axial rigidity as shown in Figure 5.55.

5.4.4 Influence of Towhead Depth

Dynamic responses of a bundle are highly influenced by the elevation of a bundle since it is in a near-horizontal configuration and placed close to the free surface. This influence is checked by comparison the results from different depths of towheads. Two conditions, 30 and 20 metres respectively below the still water surface, are considered.

As expected there is a large difference in dynamic displacements as shown in Figures 5.56 and 5.57. Figure 5.58 also shows large increase in bending moment as the towheads are placed from 30 to 20 metres below the surface. Considering this result, careful decision and control of the towhead depth are very important for successful tow. To keep the towheads closer to the surface, shorter towlines are required. For the depth of 20 metres, the lengths of trailing and leading towlines are respectively 191 and 292 metres instead of 287 and 438 metres for the depth of 30 metres. This decrease in towline length means the increase in towline stiffness and, consequently, larger dynamic axial forces as shown in Figure 5.59.

5.4.5 Influence of the Lighthill's Formulation for Fluid Loading

Bundles are subjected to inertia and drag forces arising from waves and currents. Traditionally Morison's formula has been used to predict these loads but this formulation does not include the inertia loads in near-tangential flow. In this section the accuracy of the Morison's formula is checked by comparing its inertia forces and structural responses with those from Lighthill's approach (for details, see Section 3.4.3).

Inertia forces at 90 seconds from these two approaches are compared in Figure 5.60, along with drag forces. In absolute values, the Lighthill's approach provides slightly larger inertia forces than the Morison's formula and this trend is the same over time. These larger forces tend to induce larger lateral deformation in a way similar to compressive axial forces as described in detail in Section 3.4.3. Components of the total inertia force from the Lighthill's approach are presented in Figure 5.61 and the item numbers in the figure represent the term numbers of Equation (3.83) - Item 1 represents the first term of that equation and it is the Morison equation. The main cause of these different inertia forces between two approaches is Item 4 and it represents the effect of the high tow speed. The bundle configurations used to calculate the inertia forces are almost the same as shown in Figure 5.62. The comparison of resulting axial forces and bending moments respectively along the length is shown in Figures 5.63 and 5.64 and they show the above mentioned trend. The envelopes of dynamic axial force and bending moment for one cycle of the excitation are compared and presented in Figures 5.65 and 5.66. There is about 7 percent increase in the peak bending moment with negligible difference in the axial forces.

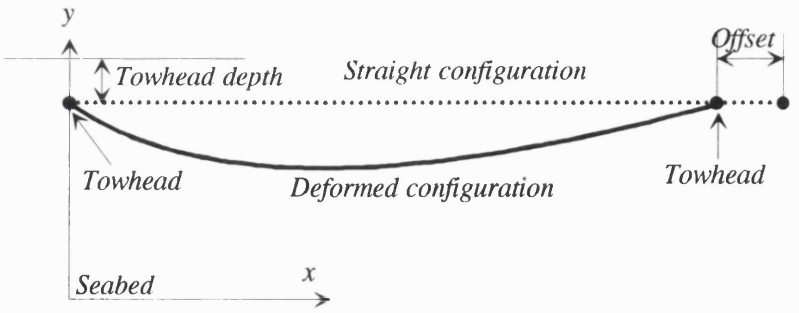

(a) Global coordinate system and offset

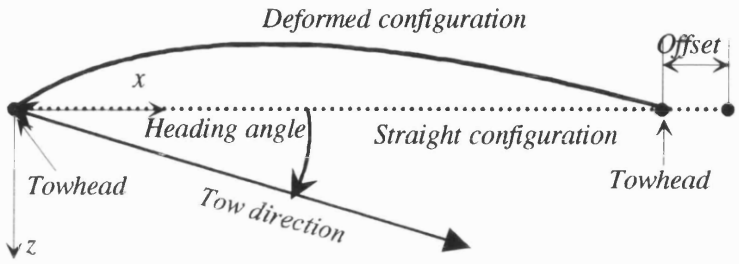

(b) Heading angle

Figure 5.1 Definition of parameters

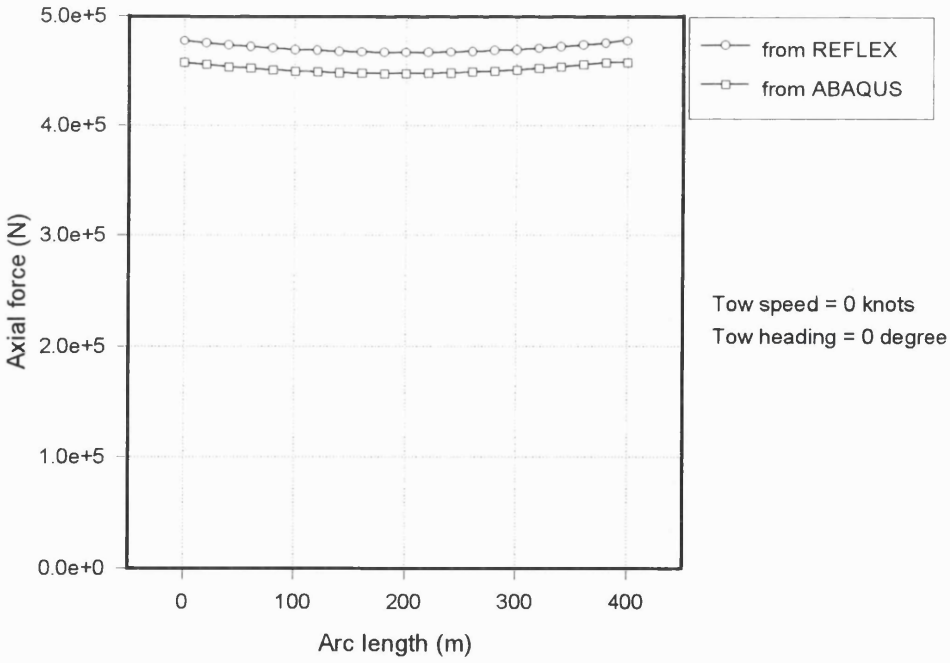

Figure 5.2 Axial forces from REFLEX and ABAQUS without tow speed

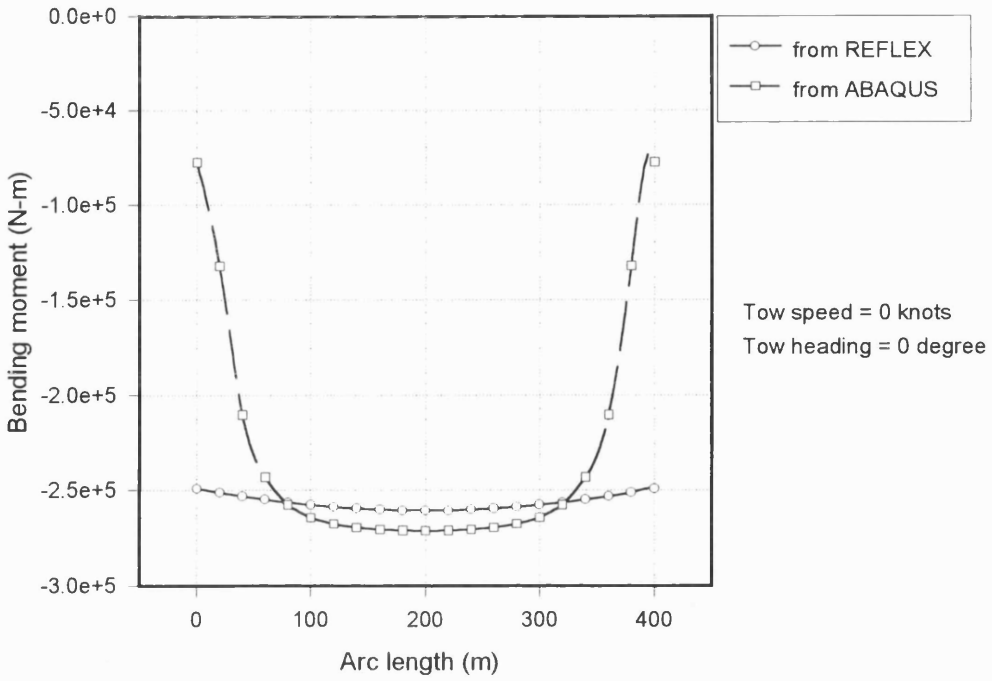

Figure 5.3 Bending moments from REFLEX and ABAQUS without tow speed

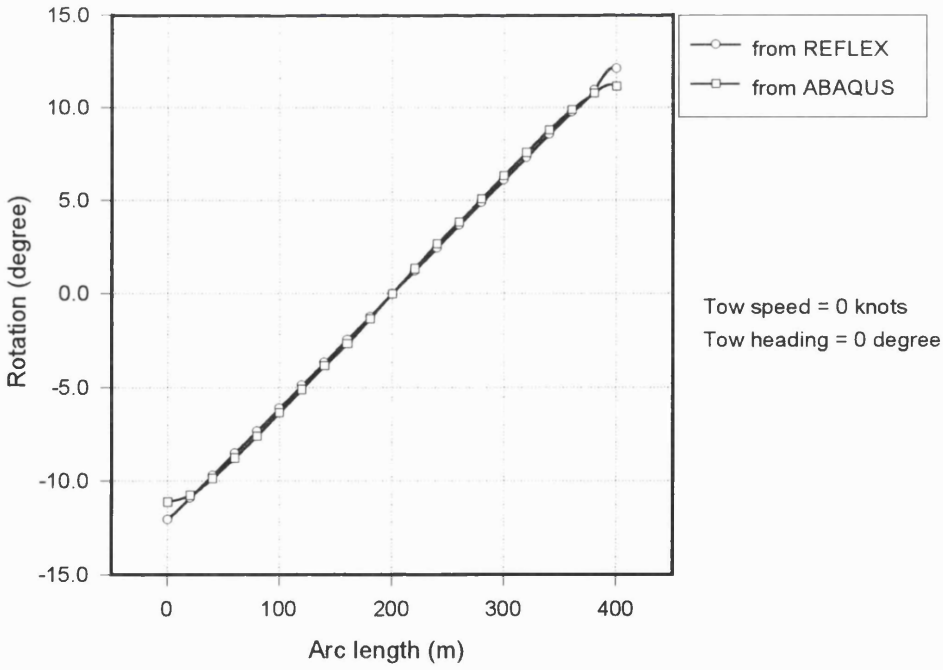

Figure 5.4 Element rotations from REFLEX and ABAQUS without tow speed

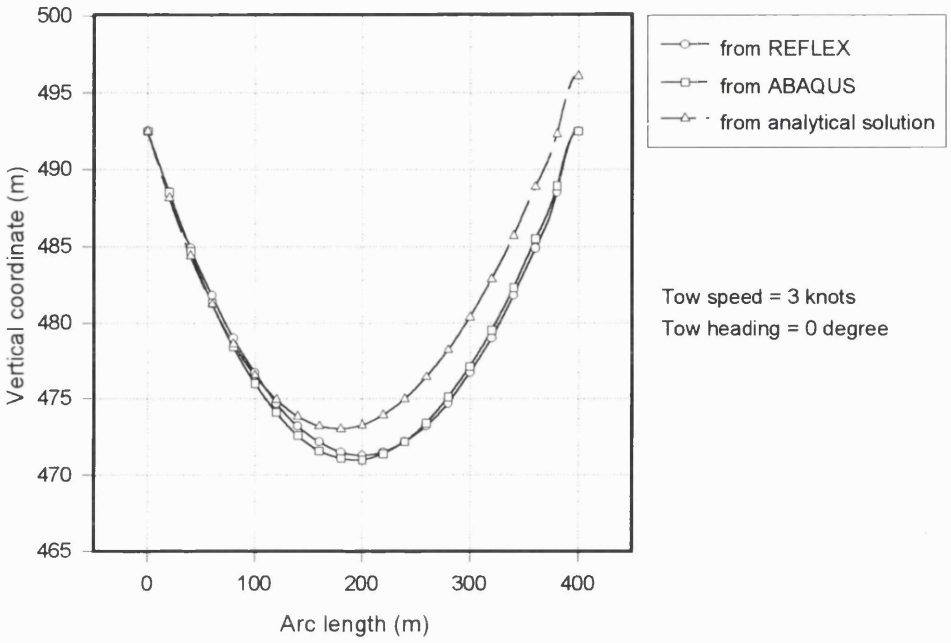

Figure 5.5 Vertical coordinates from REFLEX and ABAQUS with tow speed

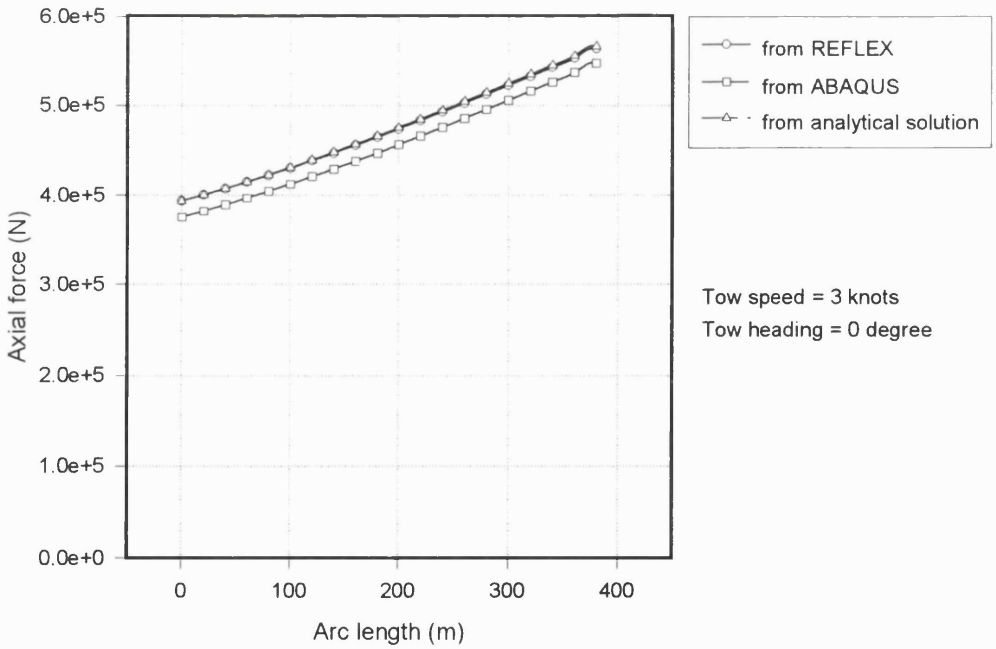

Figure 5.6 Axial forces from REFLEX and ABAQUS with tow speed

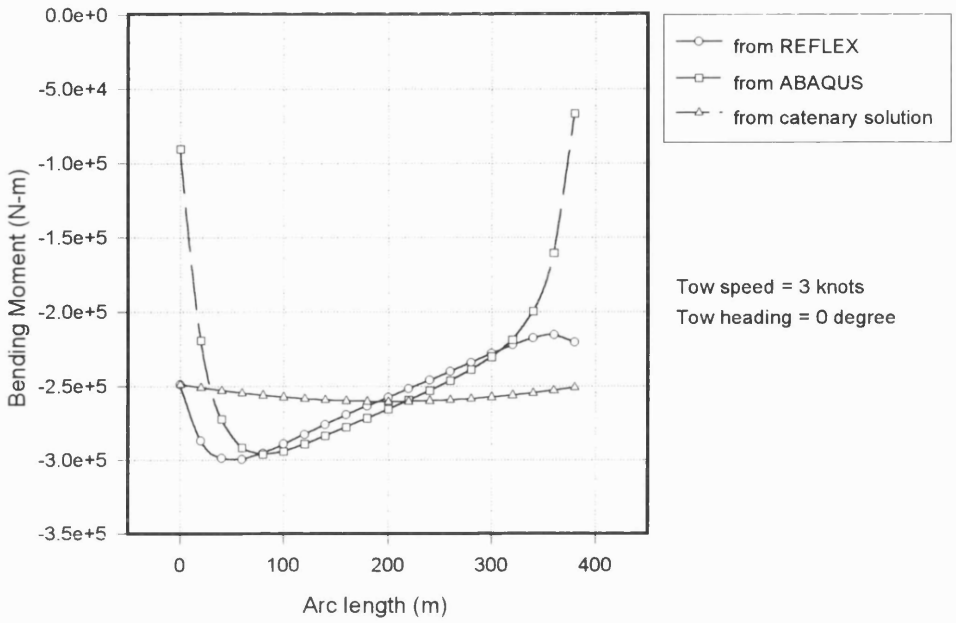

Figure 5.7 Bending moments from REFLEX and ABAQUS with tow speed

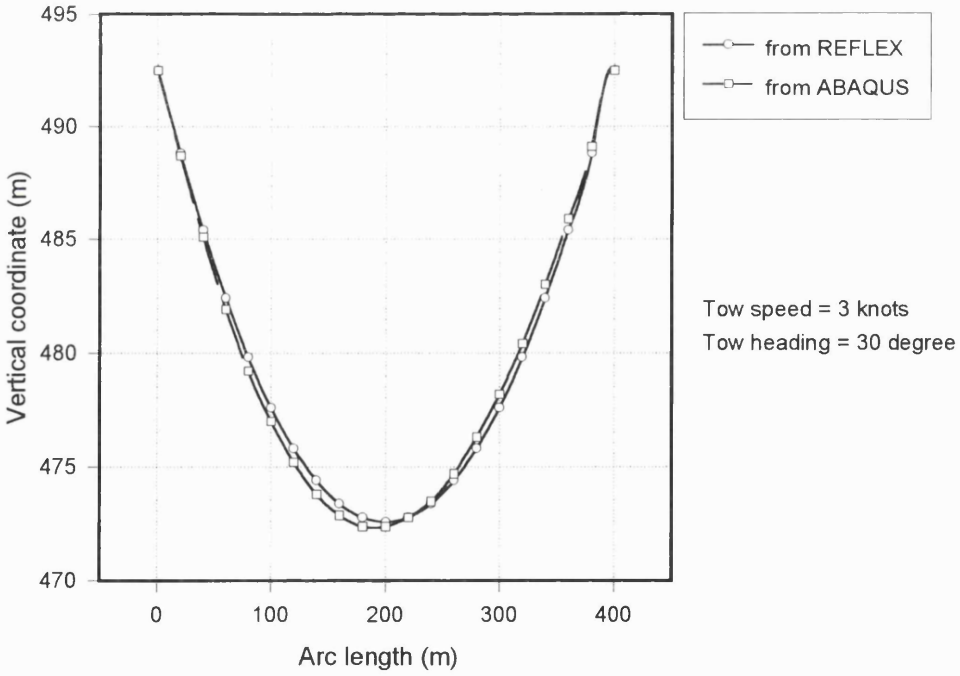

Figure 5.8 Vertical coordinates from REFLEX and ABAQUS with side current

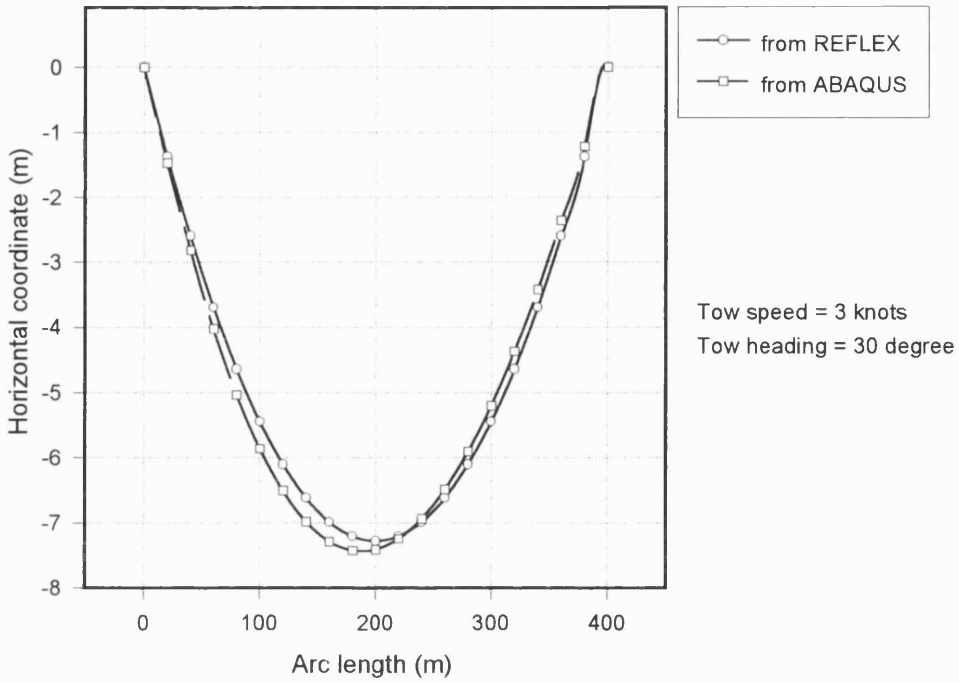

Figure 5.9 Horizontal coordinates from REFLEX and ABAQUS with side current

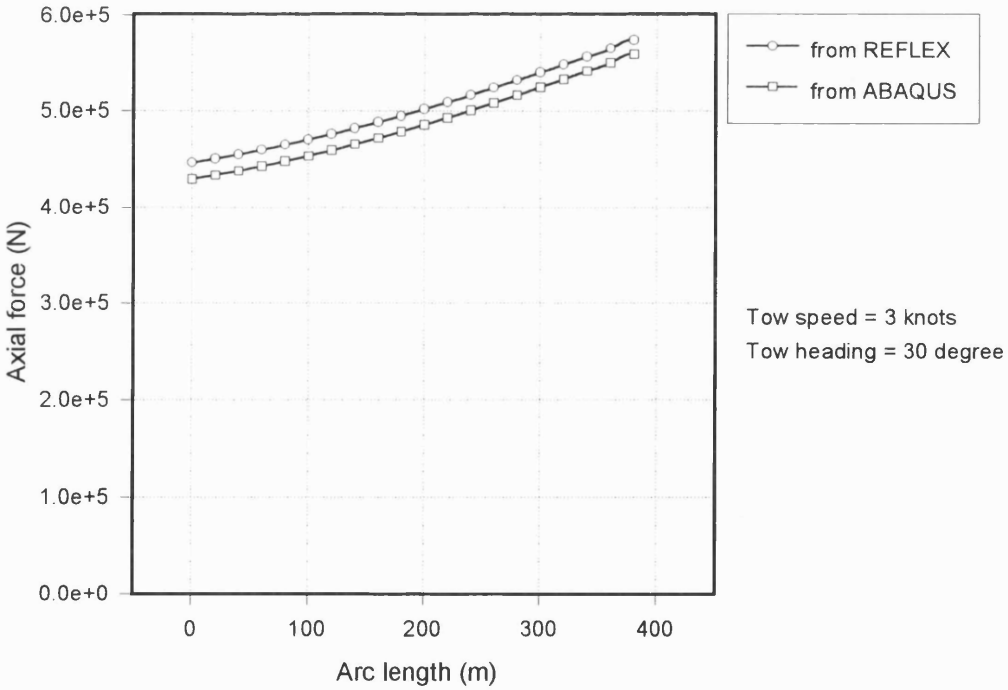

Figure 5.10 Axial forces from REFLEX and ABAQUS with side current

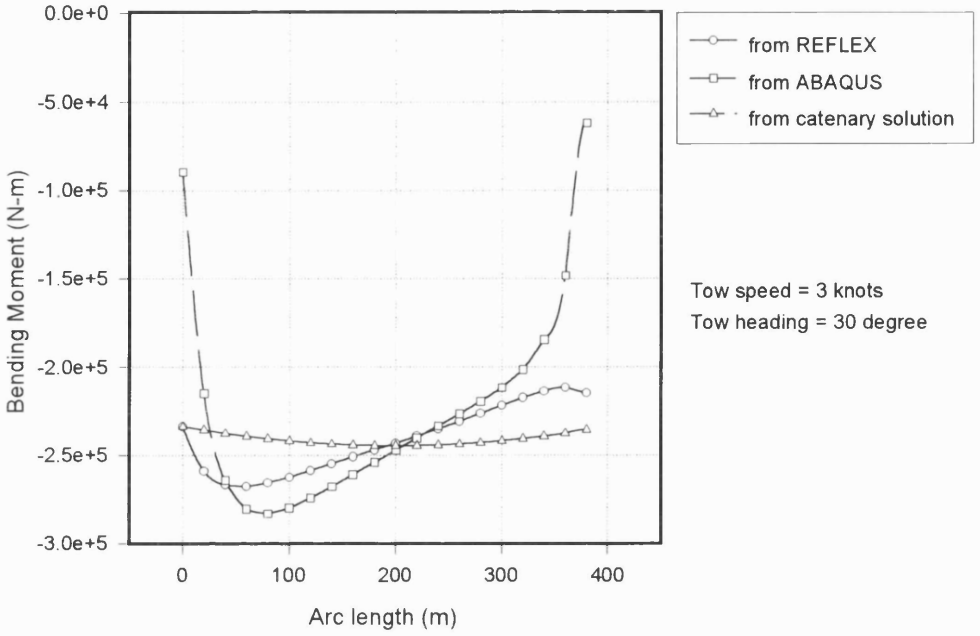

Figure 5.11 Bending moments from REFLEX and ABAQUS with side current

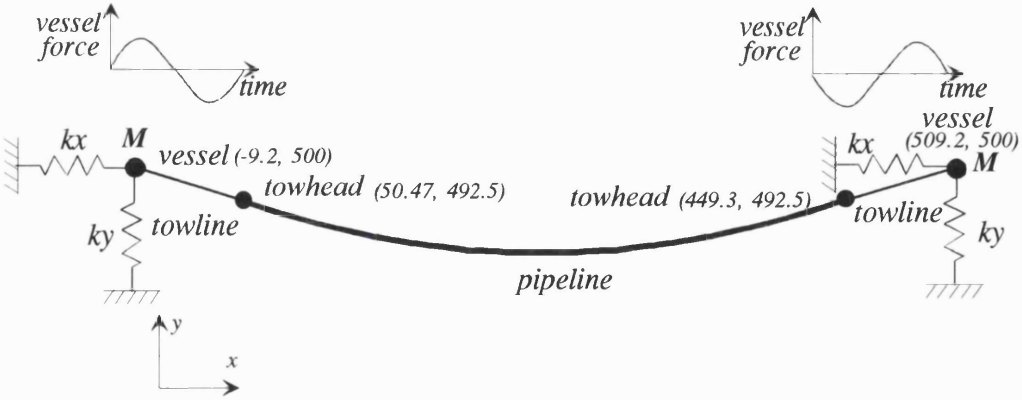

Figure 5.12 Dynamic model for comparison work

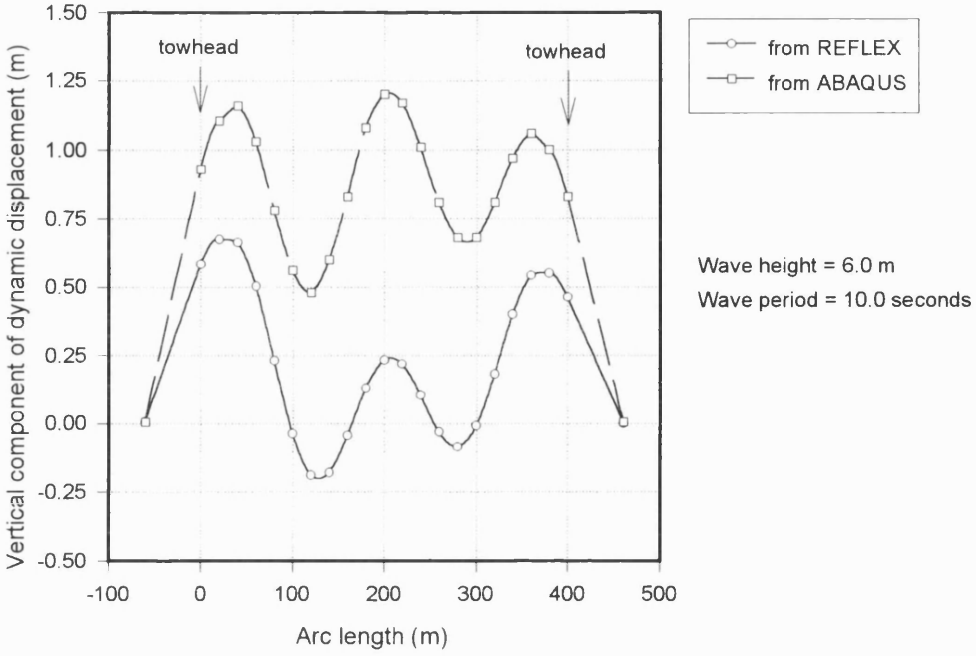

Figure 5.13 Dynamic vertical displacement from REFLEX and ABAQUS at 90 seconds

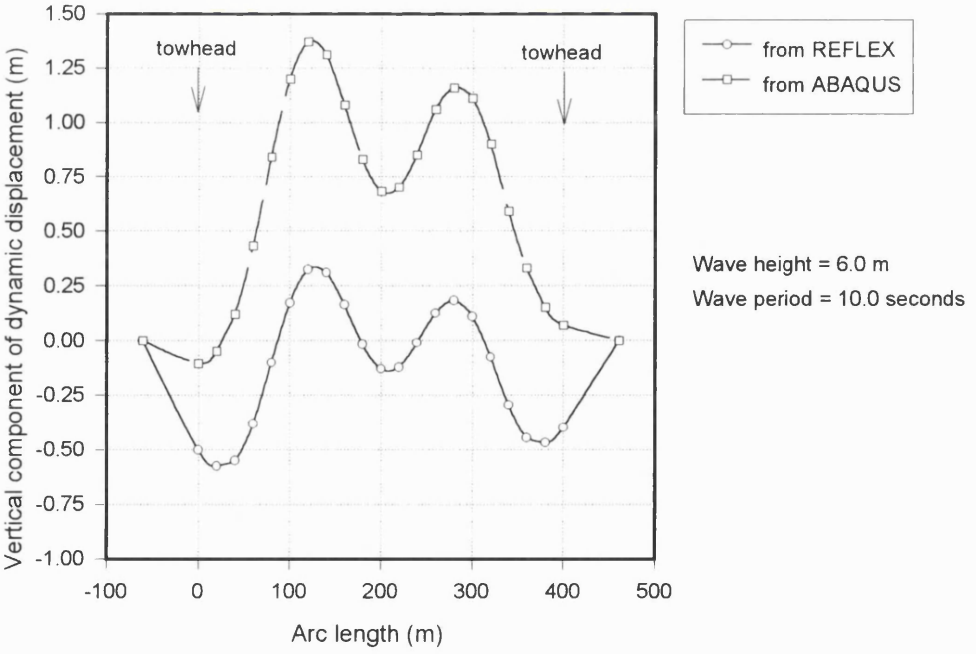

Figure 5.14 Dynamic vertical displacement from REFLEX and ABAQUS at 95 seconds

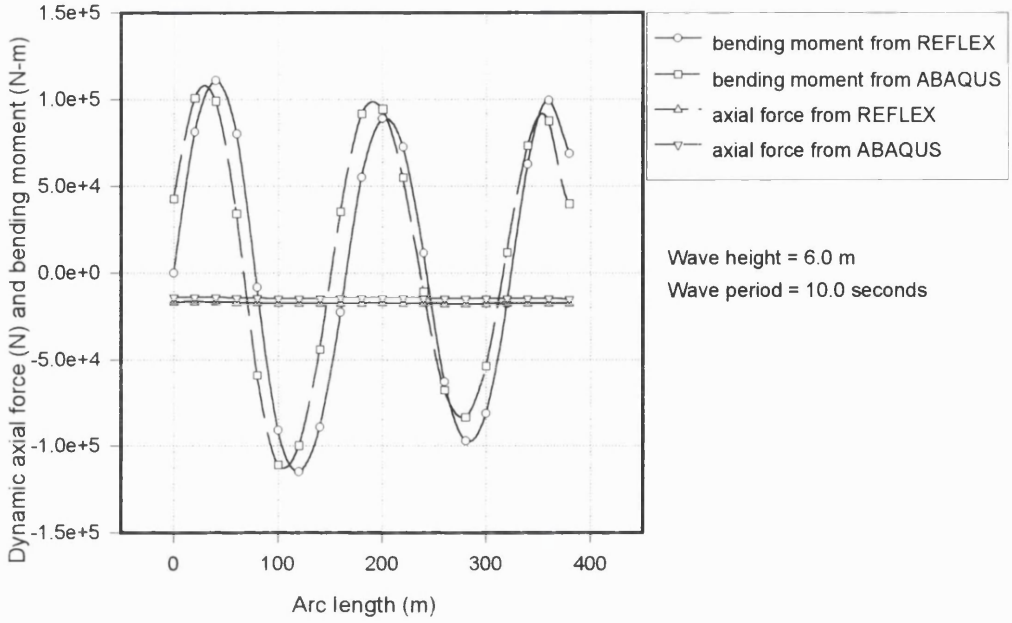

Figure 5.15 Dynamic axial force and bending moment from REFLEX and ABAQUS at 90 seconds

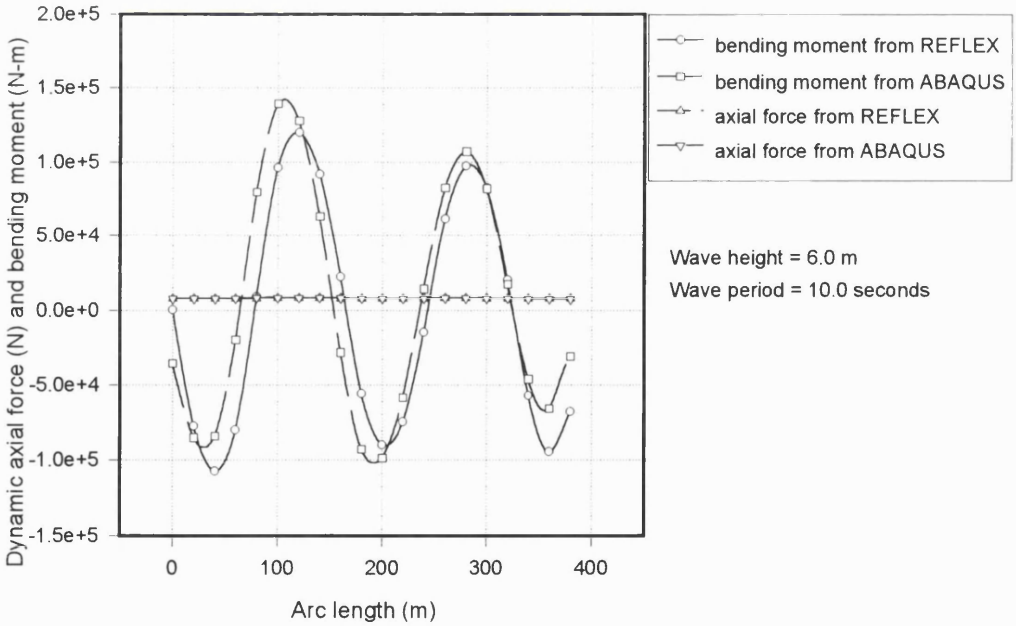

Figure 5.16 Dynamic axial force and bending moment from REFLEX and ABAQUS at 95 seconds

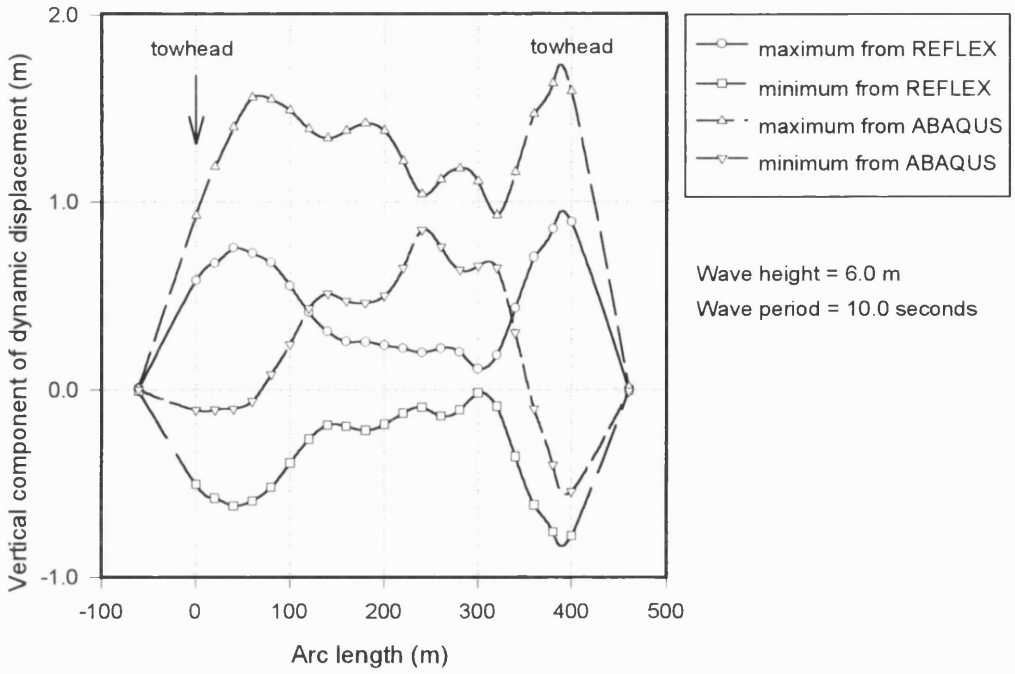

Figure 5.17 Envelope of dynamic vertical displacement from REFLEX and ABAQUS including nonvariant components

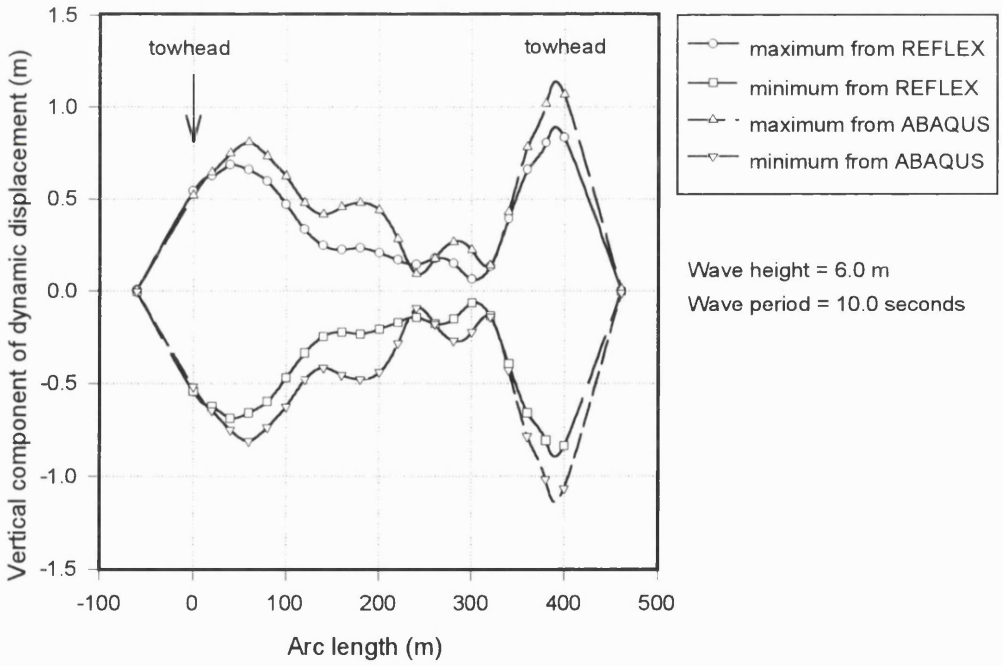

Figure 5.18 Envelope of dynamic vertical displacement from REFLEX and ABAQUS after removing nonvariant components

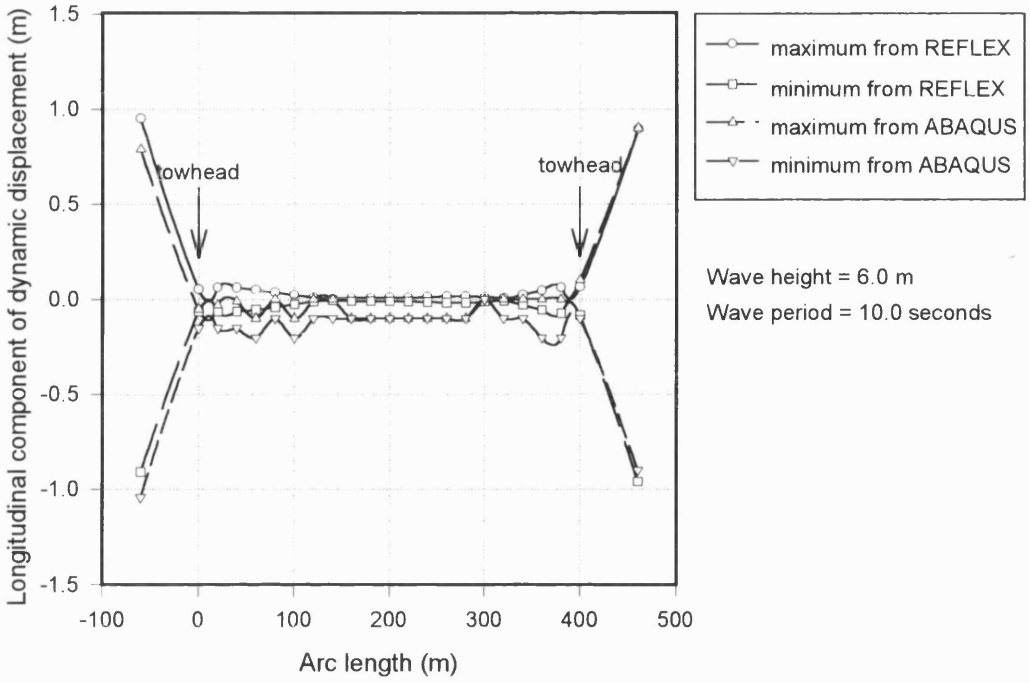

Figure 5.19 Envelope of dynamic longitudinal displacement from REFLEX and ABAQUS

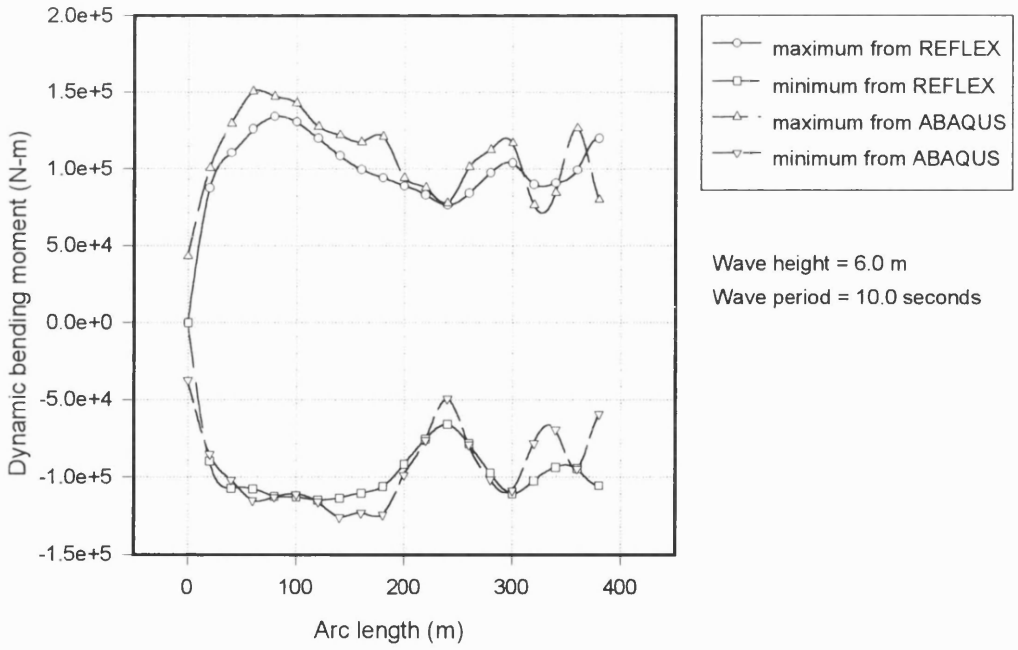

Figure 5.20 Envelope of dynamic bending moment from REFLEX and ABAQUS

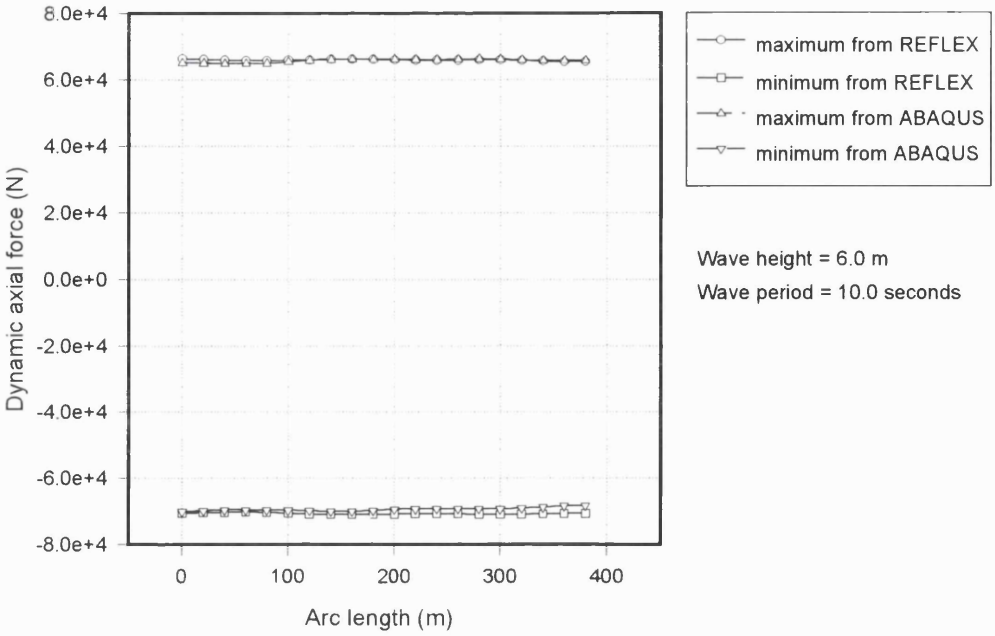

Figure 5.21 Envelope of dynamic axial force from REFLEX and ABAQUS

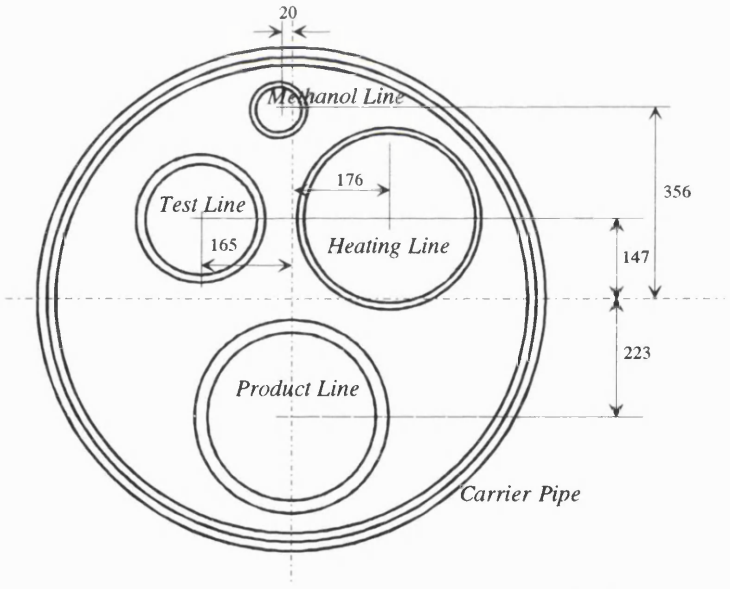

(unit : *mm*)

Type	Outer Dia.	Wall Thickness	Lining	Coat
Carrier	946.2	13.0	0.1	16.3
Product	355.6	22.5	-	-
Test	219.1	17.1	-	-
Heating	323.9	9.8	-	-
Methanol	88.9	9.8	34.7	-

Figure 5.22 Cross section of the Britannia bundle

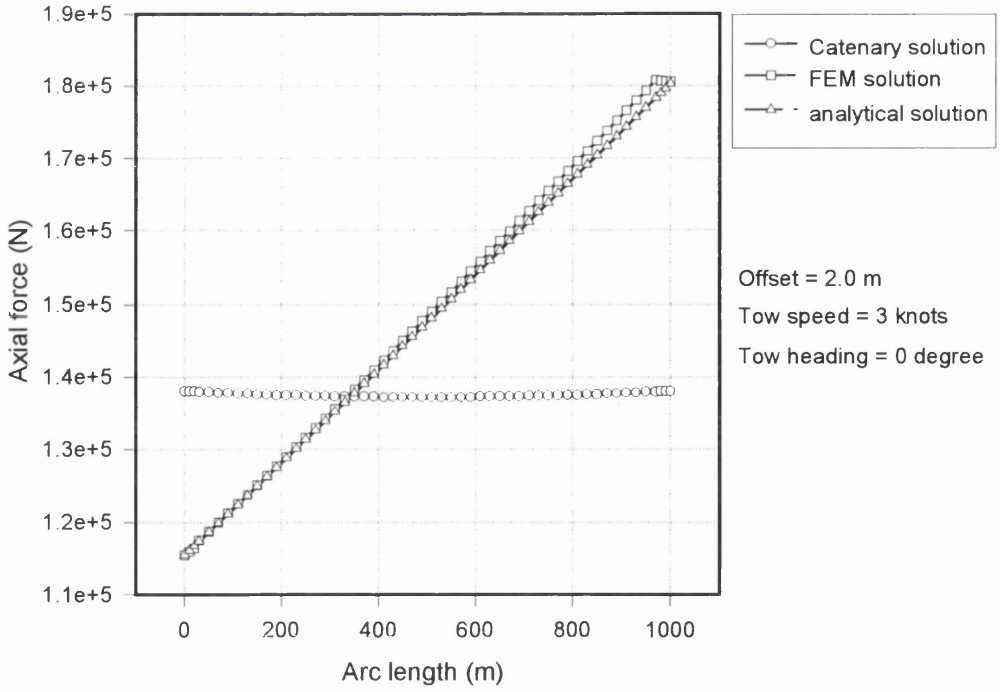

Figure 5.23 Comparison of static axial forces along bundle with tow speed

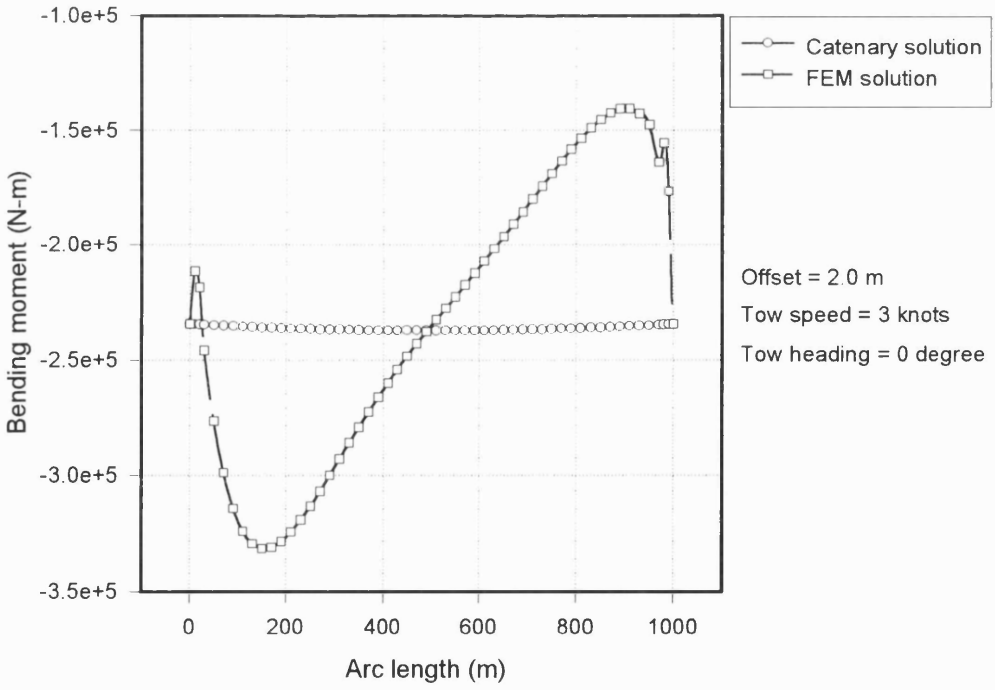

Figure 5.24 Comparison of static bending moments along bundle with tow speed

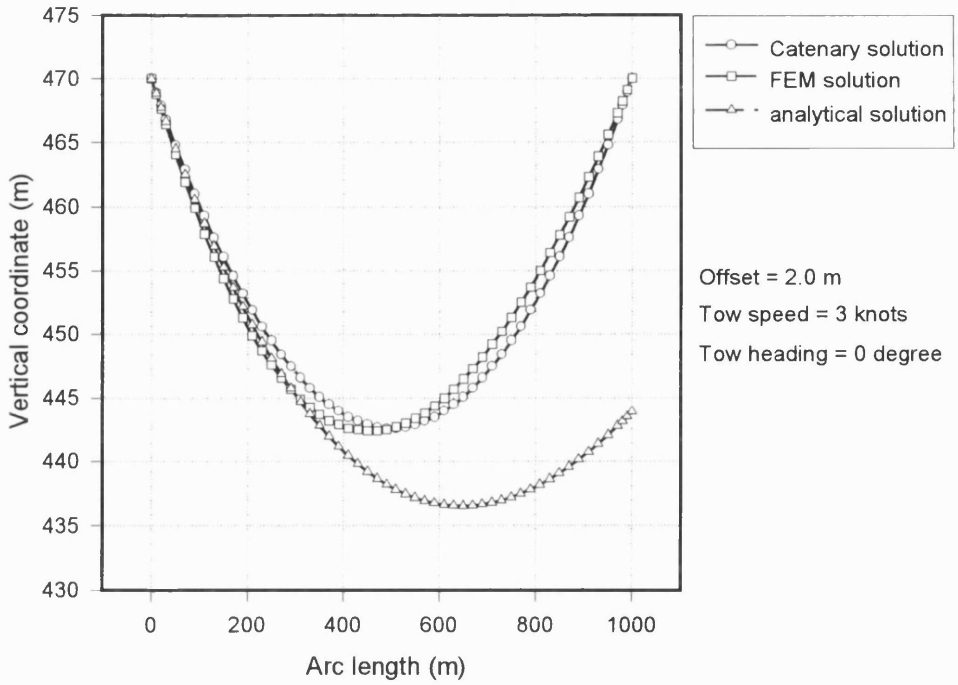

Figure 5.25 Comparison of static vertical displacements of bundle with tow speed

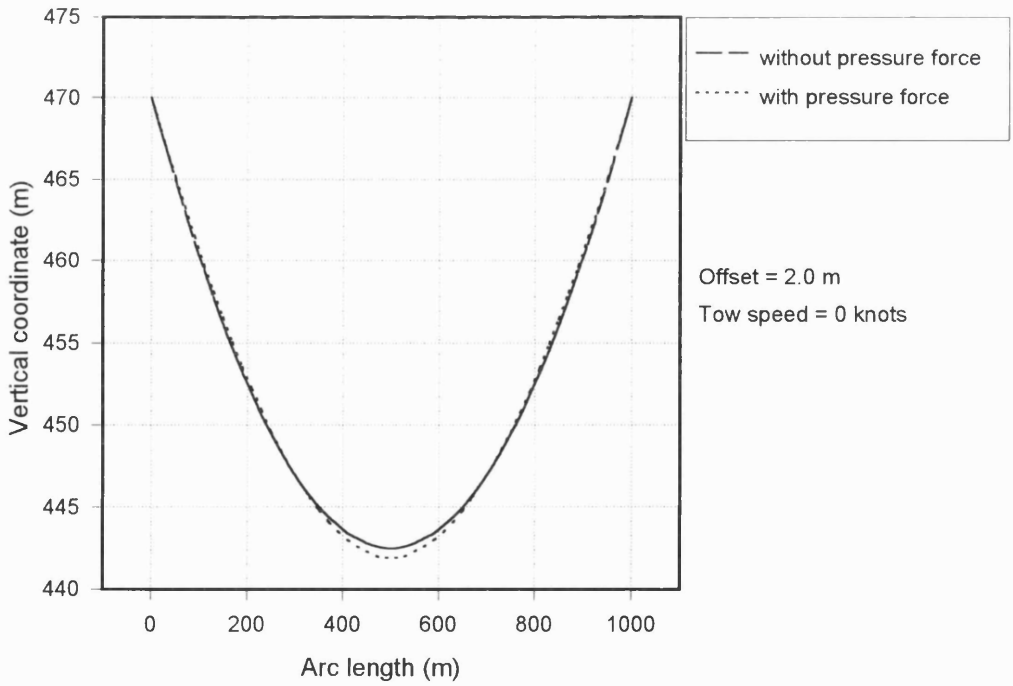

Figure 5.26 Influence of hydrostatic pressure force on vertical displacement for the case without tow speed

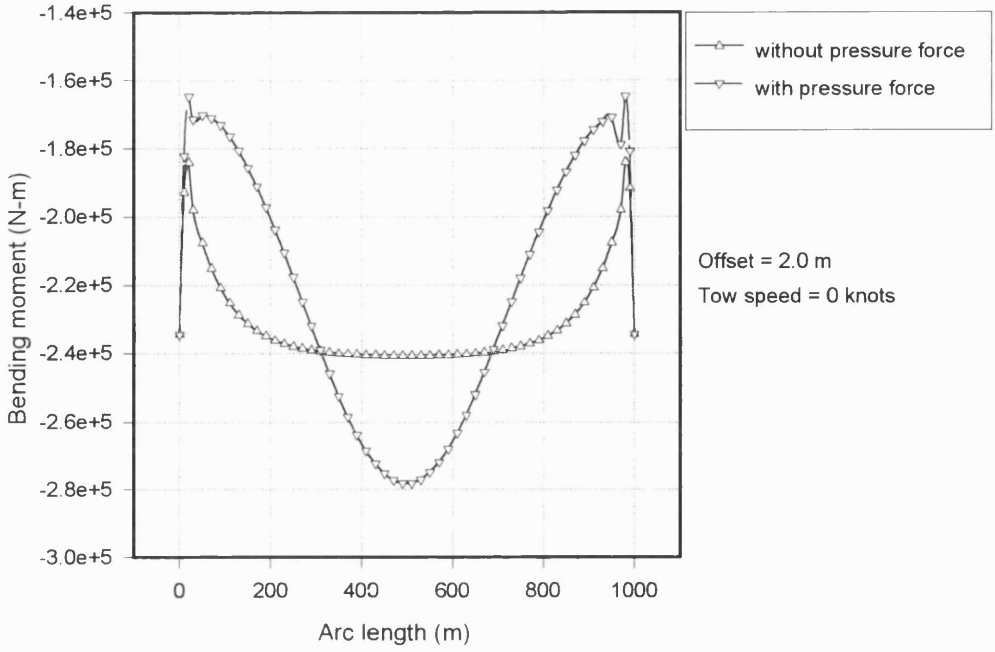

Figure 5.27 Influence of hydrostatic pressure force on bending moments for the case without tow speed

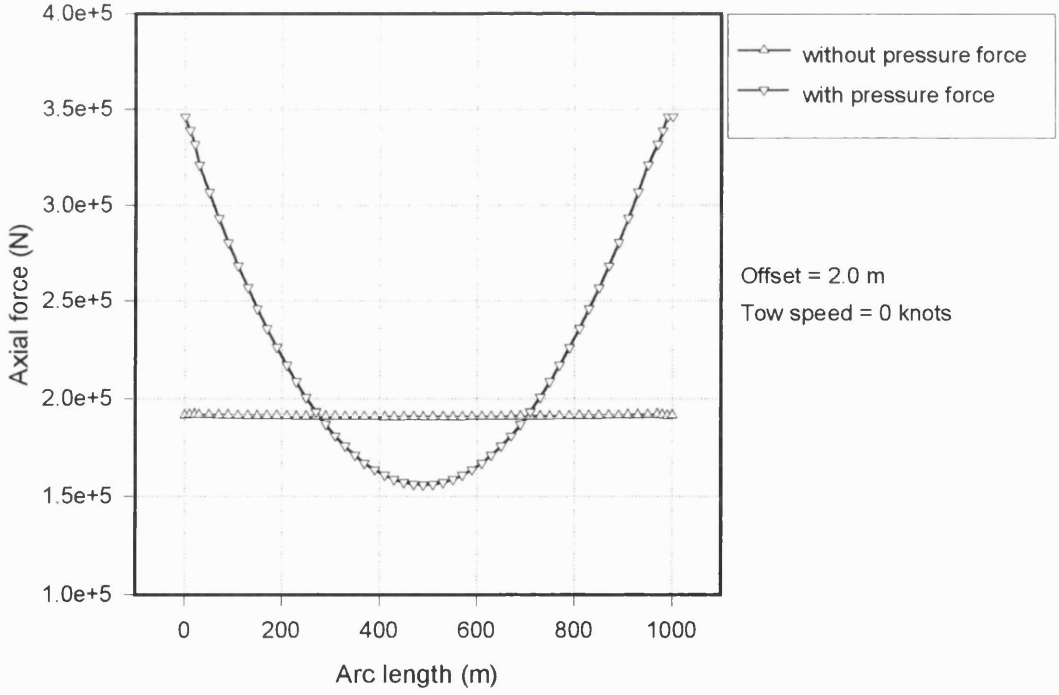

Figure 5.28 Influence of hydrostatic pressure force on axial forces for the case without tow speed

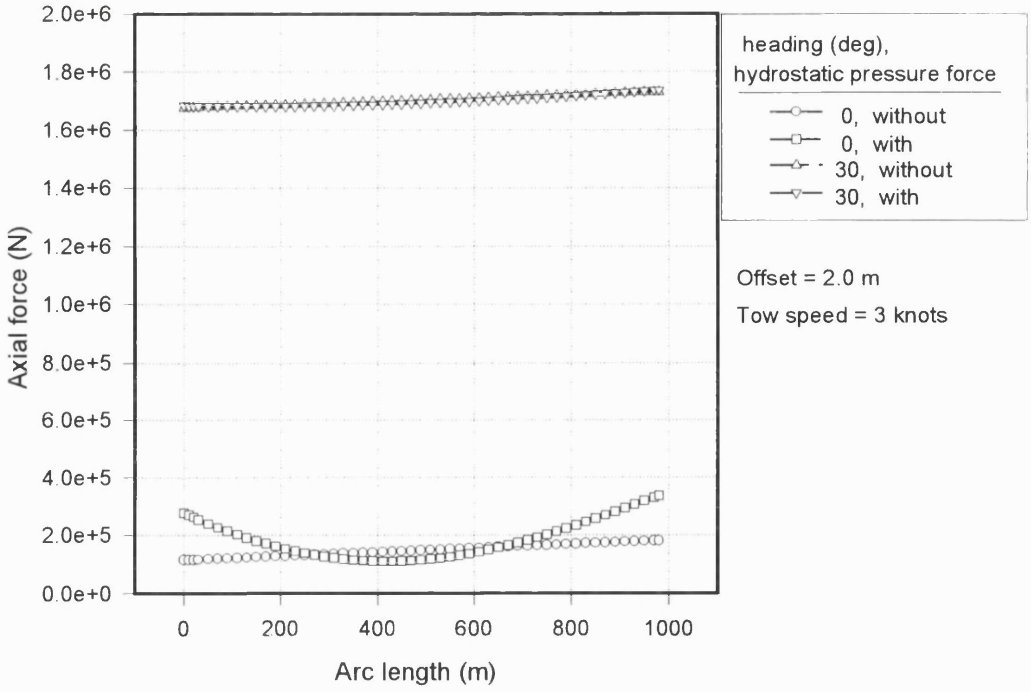

Figure 5.29 Influence of Hydrostatic pressure force on axial forces for the case with tow speed and heading angle

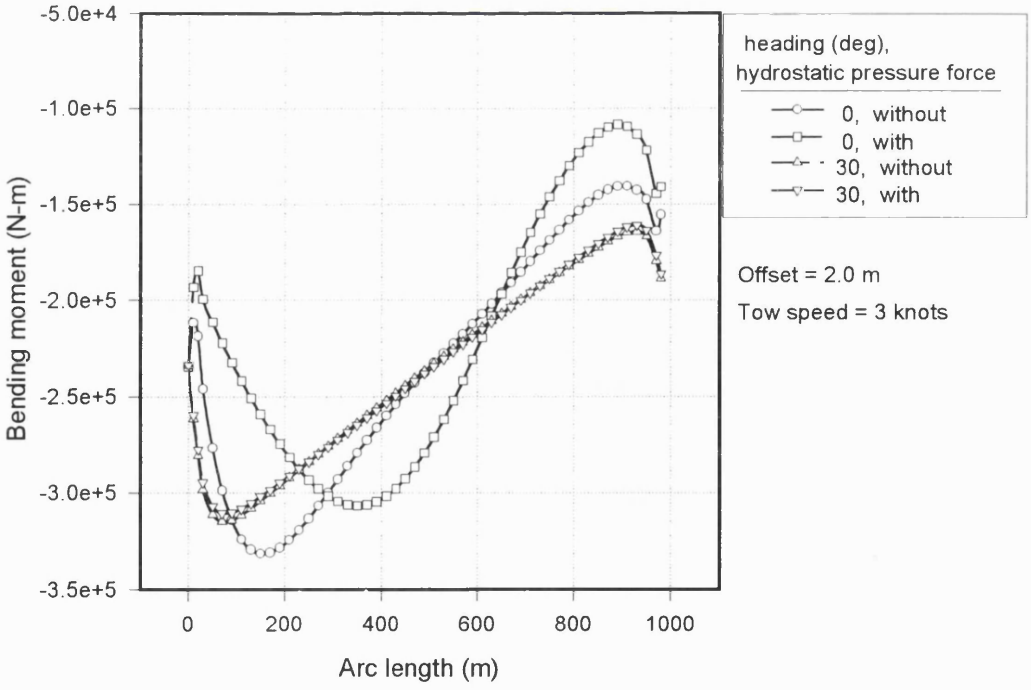

Figure 5.30 Influence of Hydrostatic pressure force on bending moments for the case with tow speed and heading angle

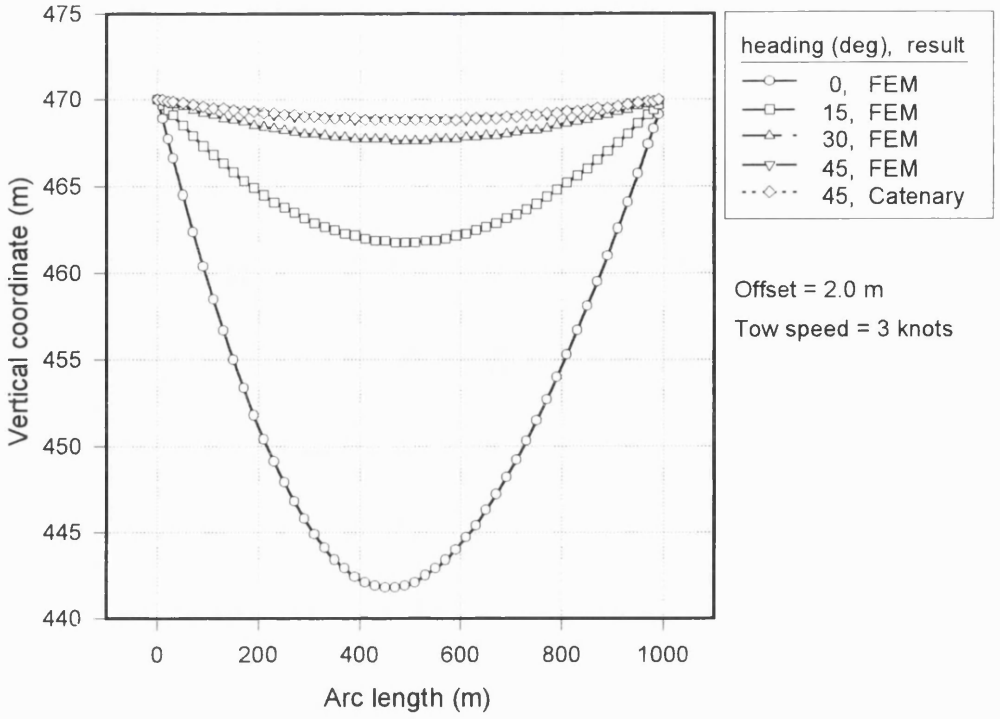

Figure 5.31 Influence of heading angle on vertical displacement

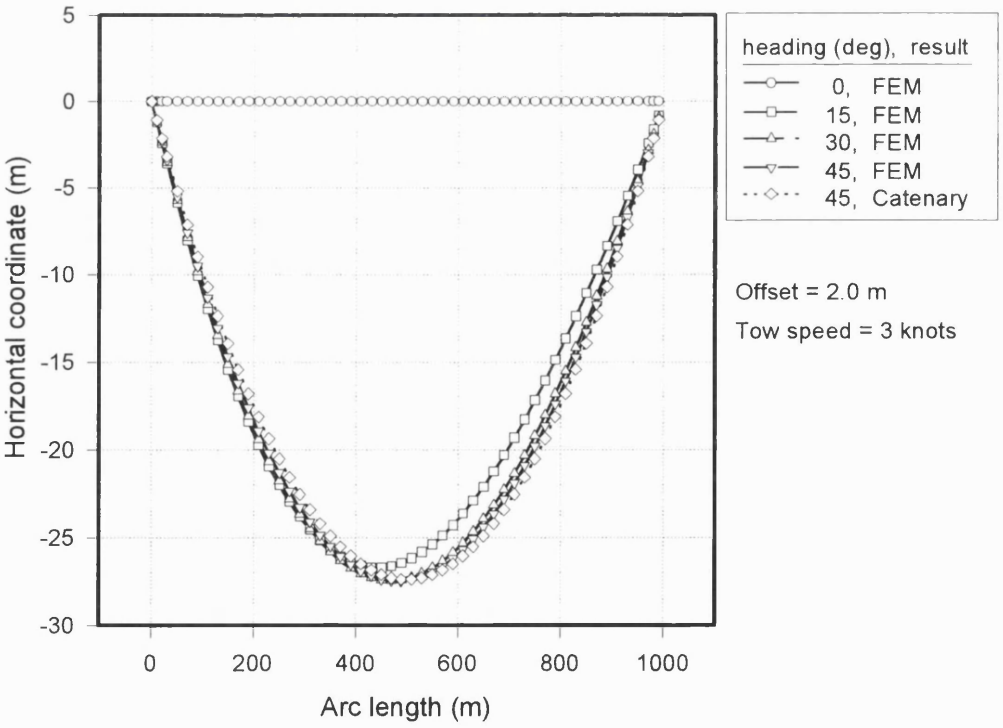

Figure 5.32 Influence of heading angle on horizontal displacement

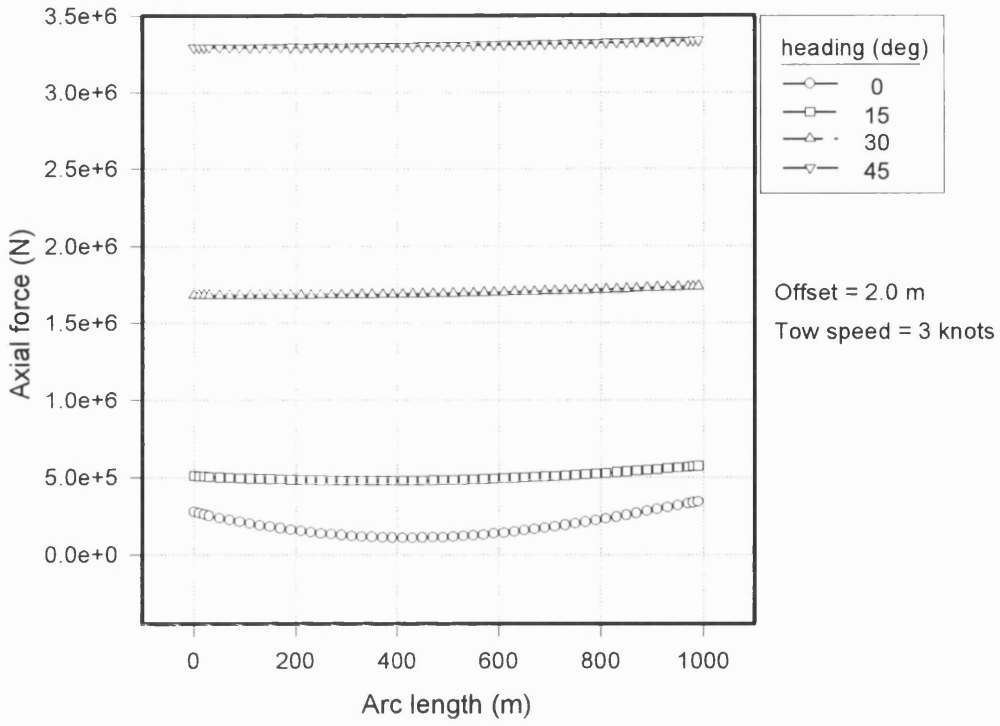

Figure 5.33 Influence of heading angle on axial forces

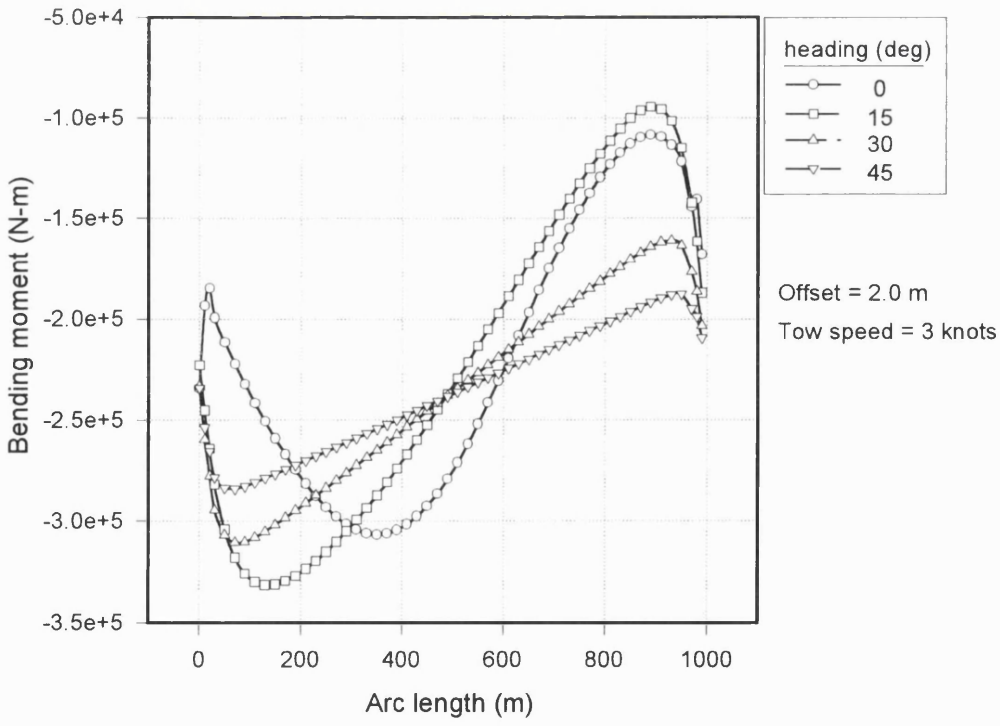

Figure 5.34 Influence of heading angle on bending moments

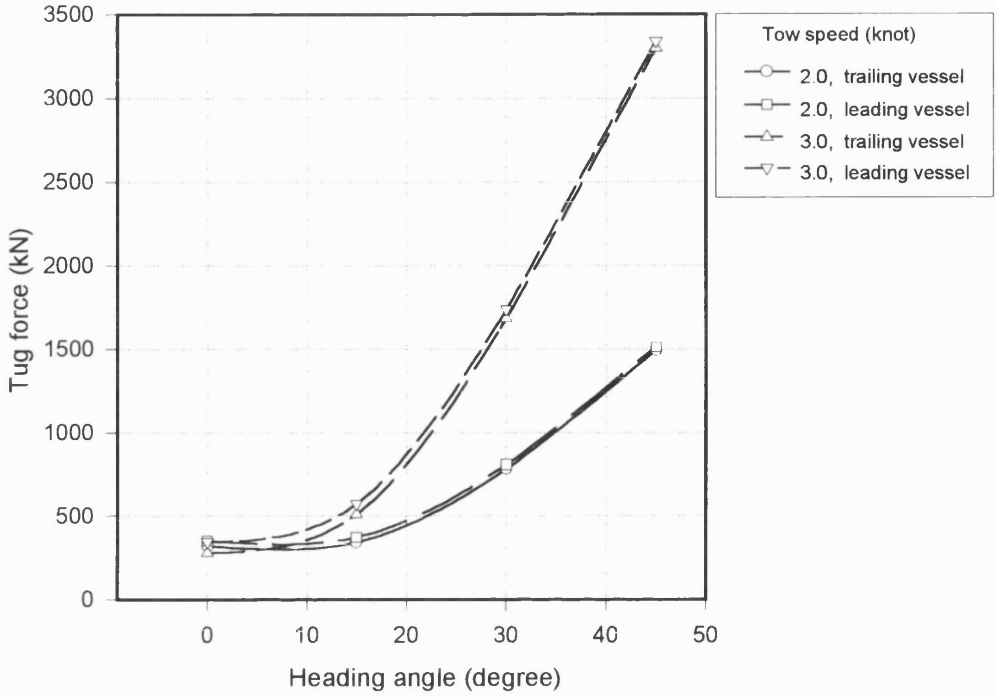

Figure 5.35 Tug forces with change in heading angle and tow speed

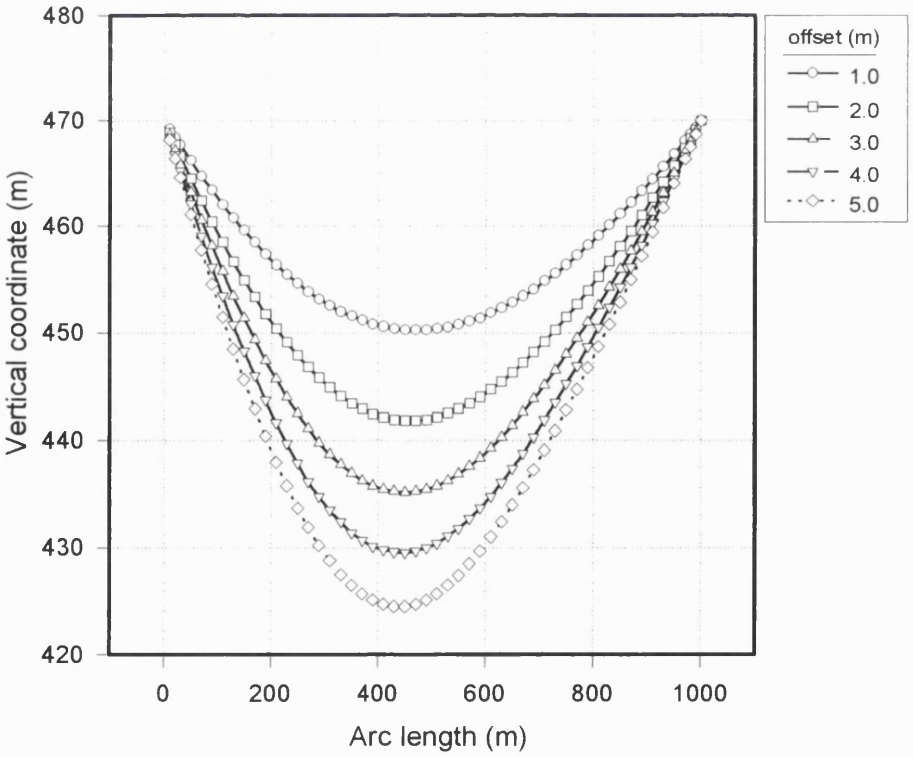

Figure 5.36 Sag with the change in offset

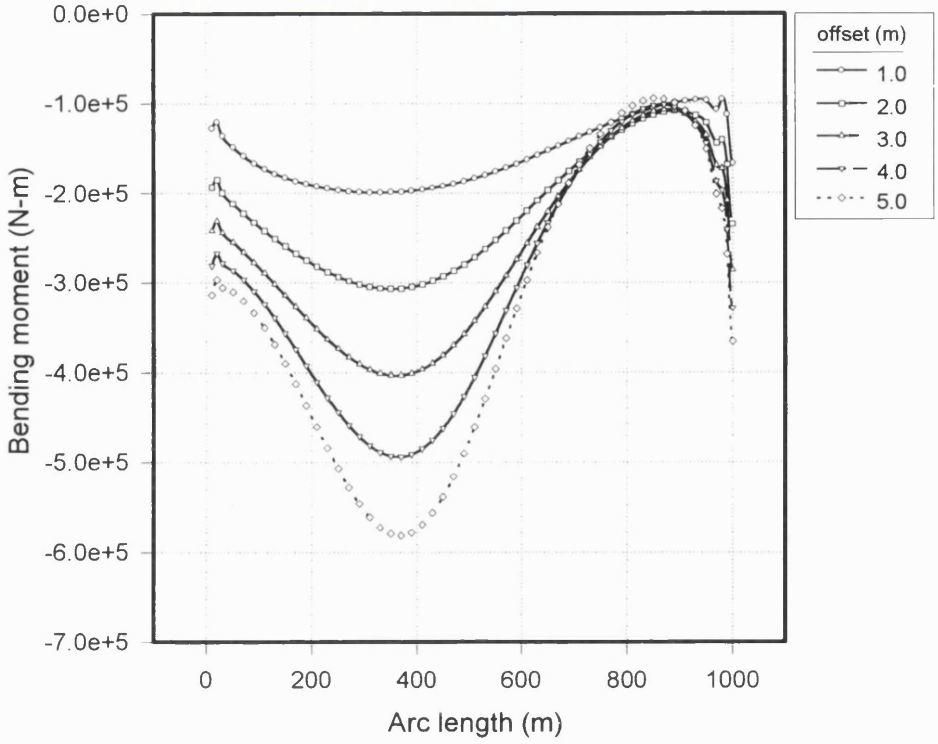

Figure 5.37 Bending moment with change in offset

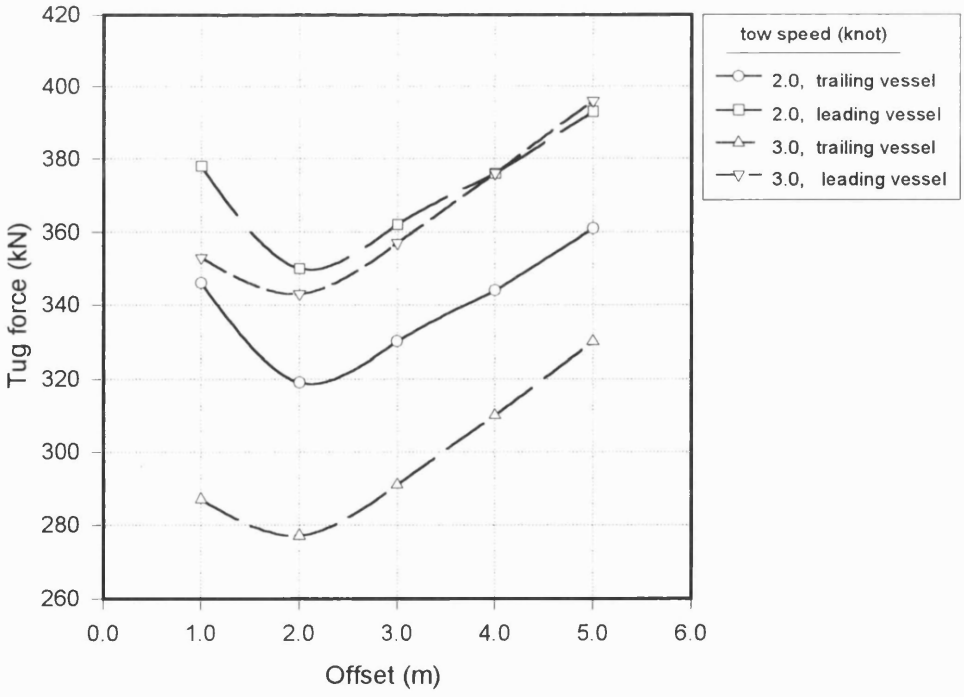

Figure 5.38 Tug force with change in offset - with hydrostatic pressure force

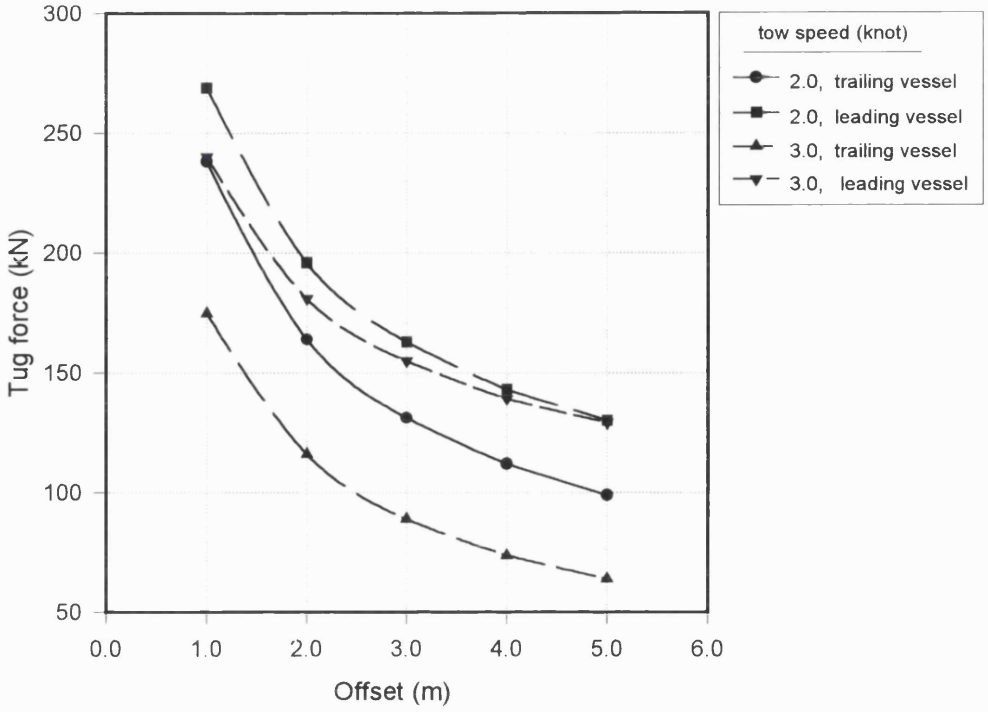

Figure 5.39 Tug force with change in offset - without hydrostatic pressure force

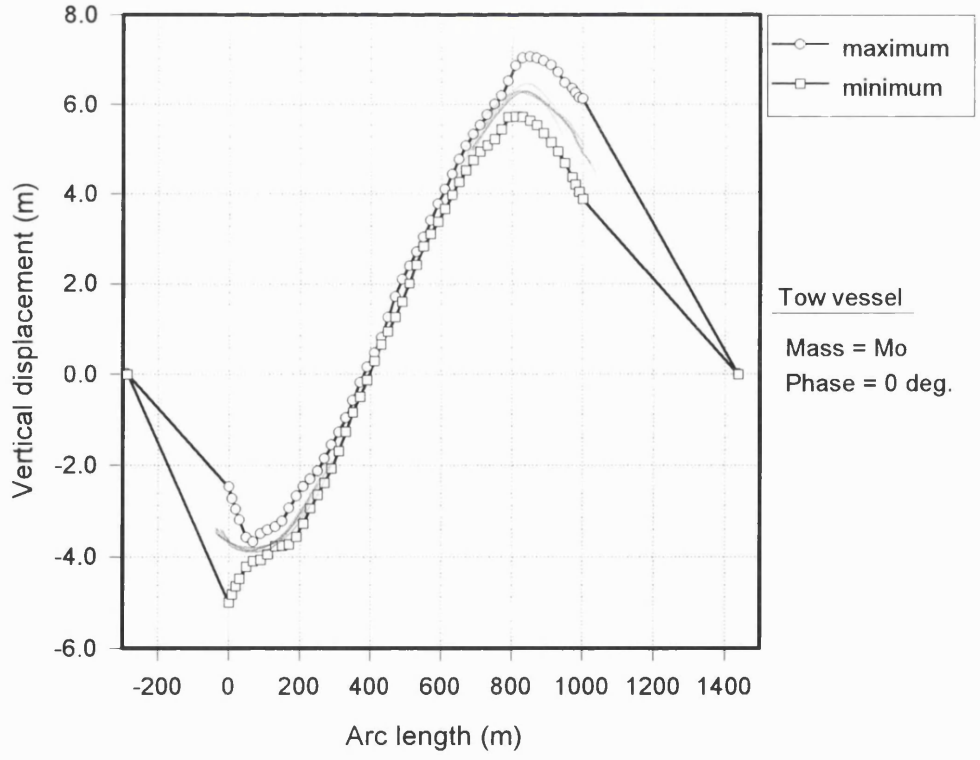

Figure 5.40 Vertical displacements under wave, current and in-phase surge forces

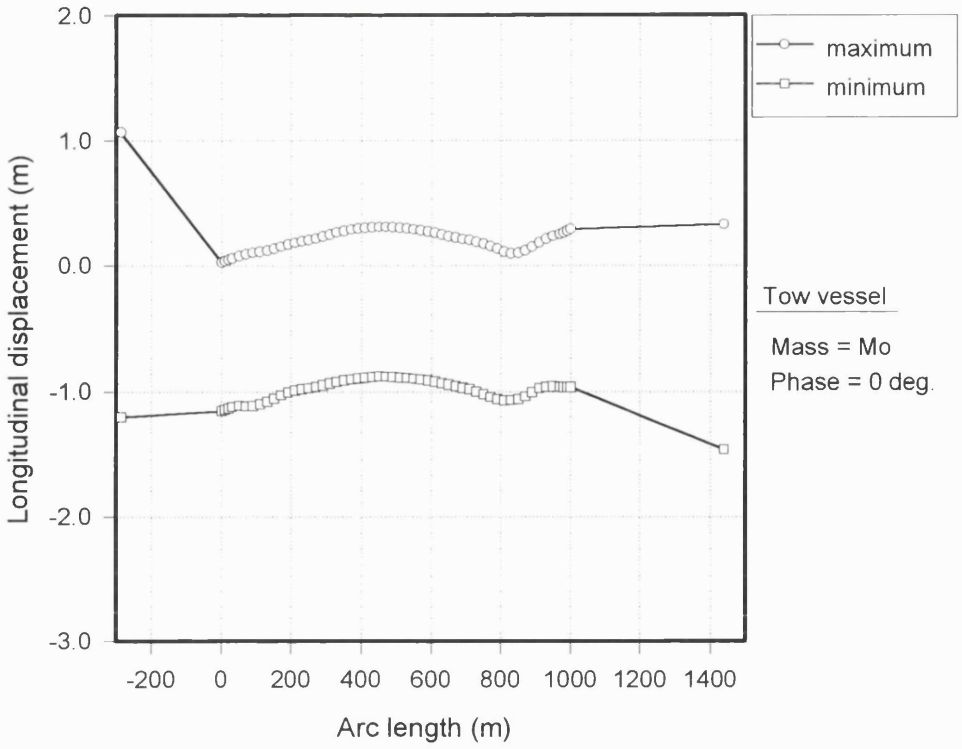

Figure 5.41 Longitudinal displacements under wave, current and in-phase surge forces

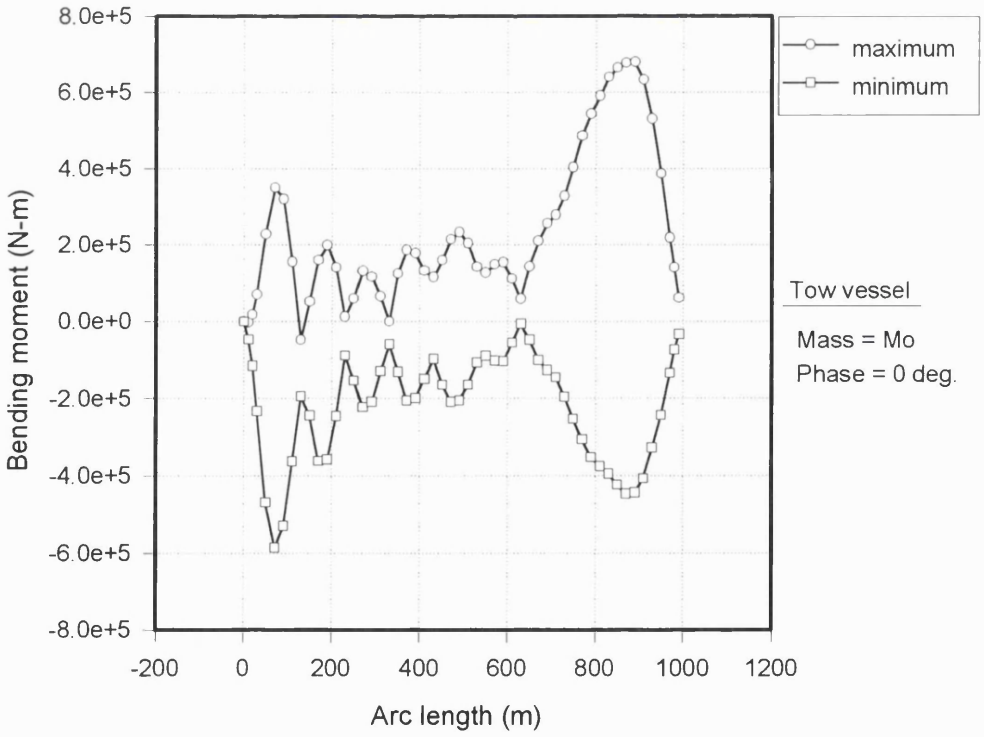

Figure 5.42 Bending moments under wave, current and in-phase surge forces

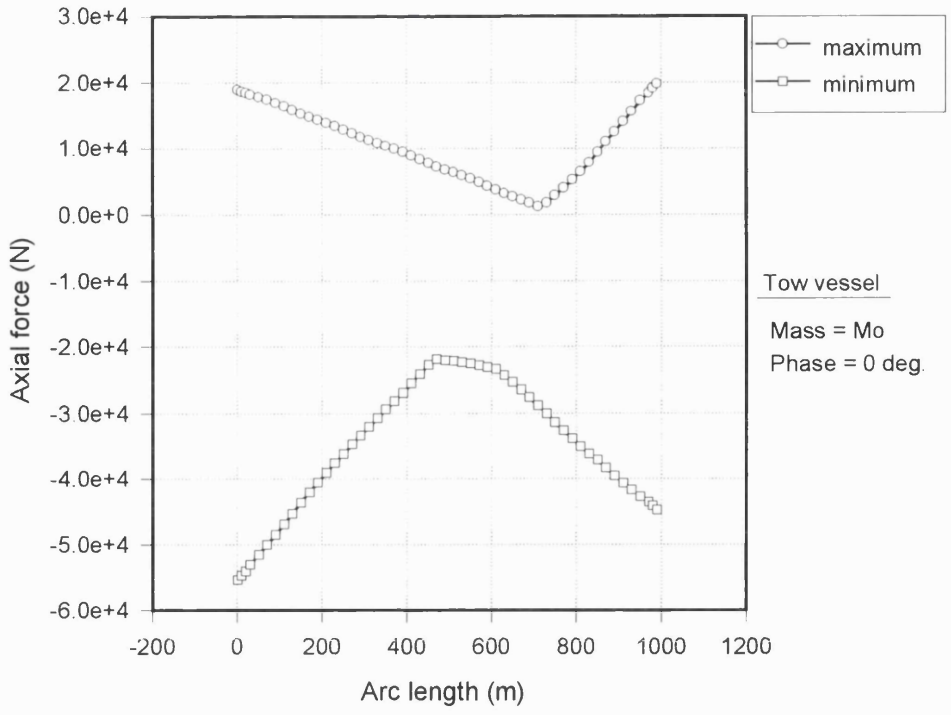

Figure 5.43 Axial forces under wave, current and in-phase surge forces

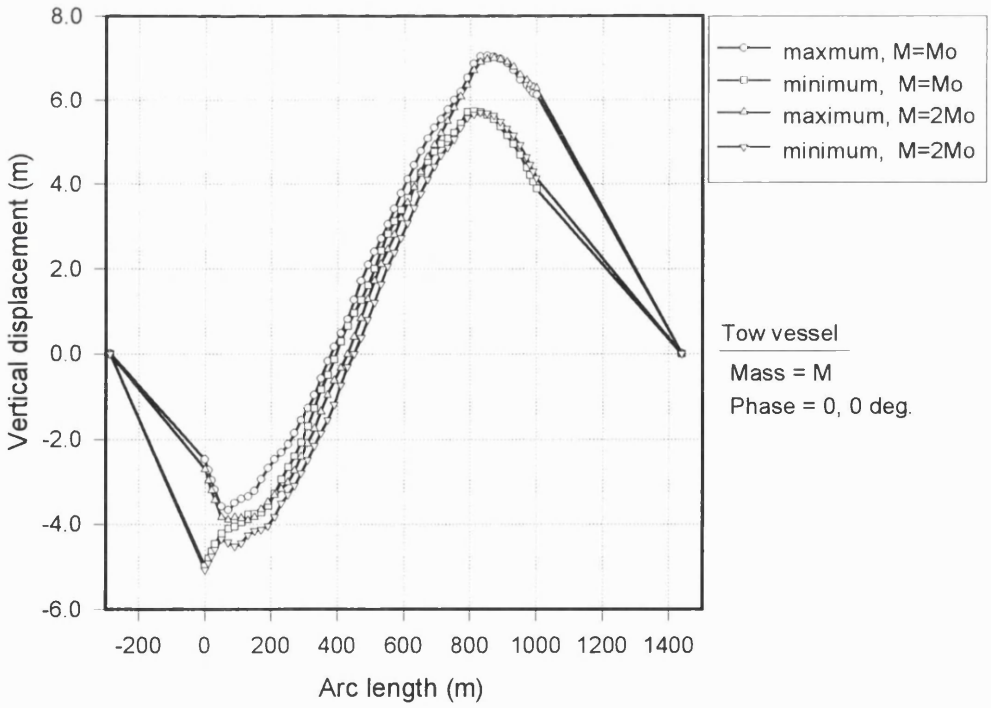

Figure 5.44 Comparison of vertical displacements from different vessel masses - in-phase surge forces

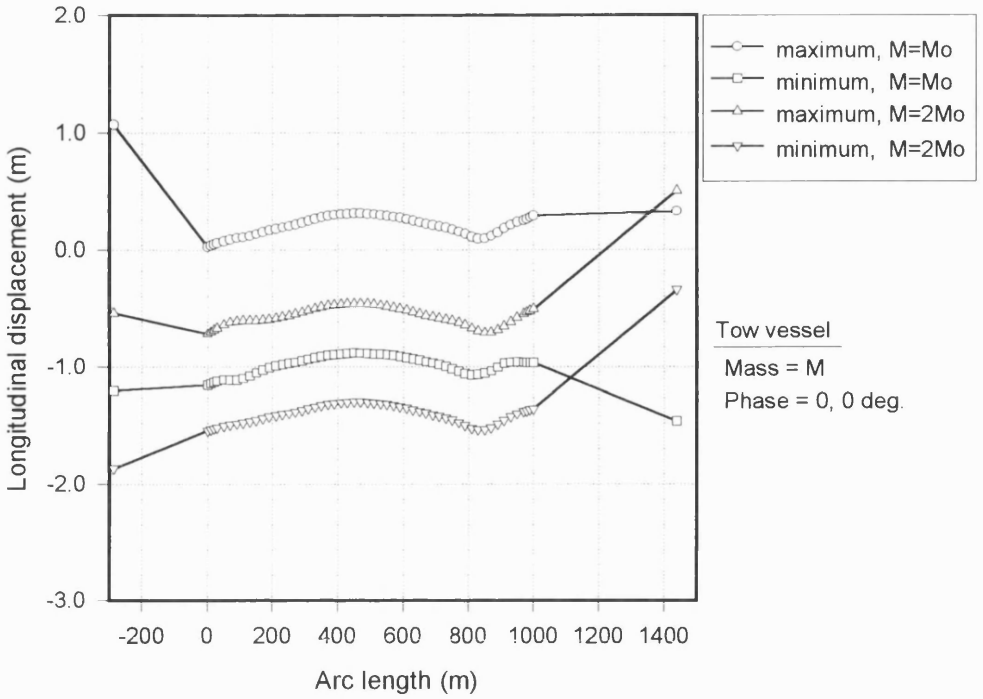

Figure 5.45 Comparison of longitudinal displacements from different vessel masses - in-phase surge forces

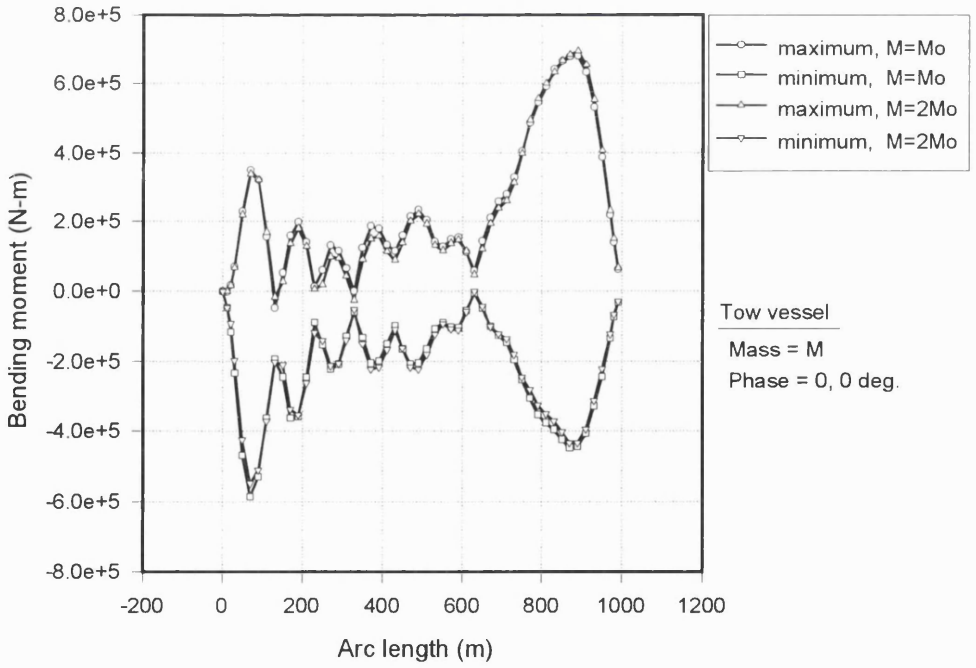

Figure 5.46 Comparison of vertical bending moments from different vessel masses - in-phase surge forces

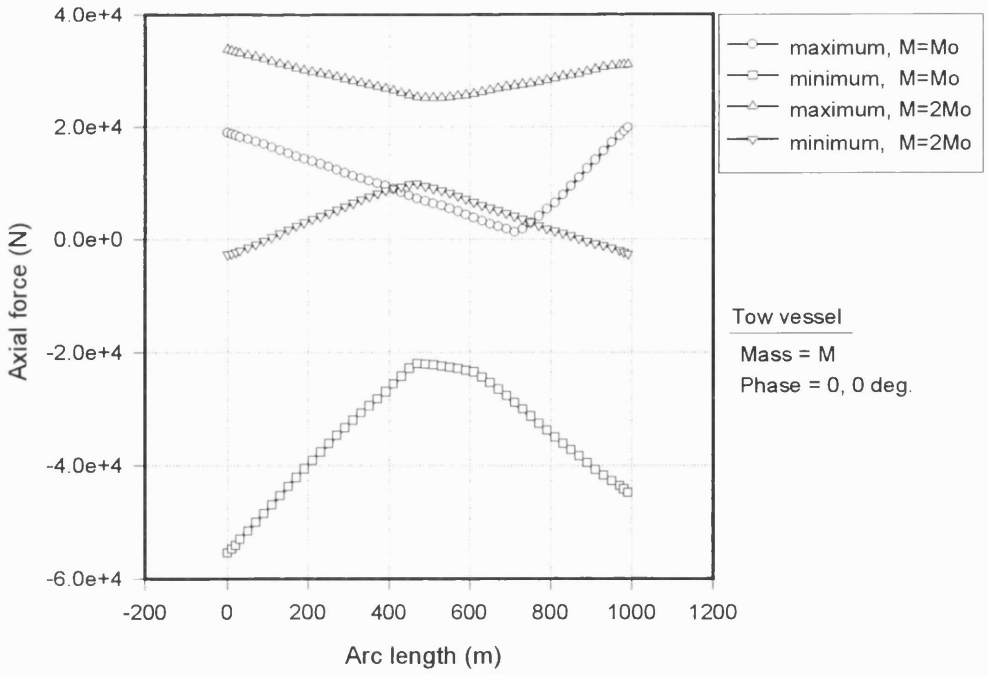

Figure 5.47 Comparison of axial forces from different vessel masses - in-phase surge forces

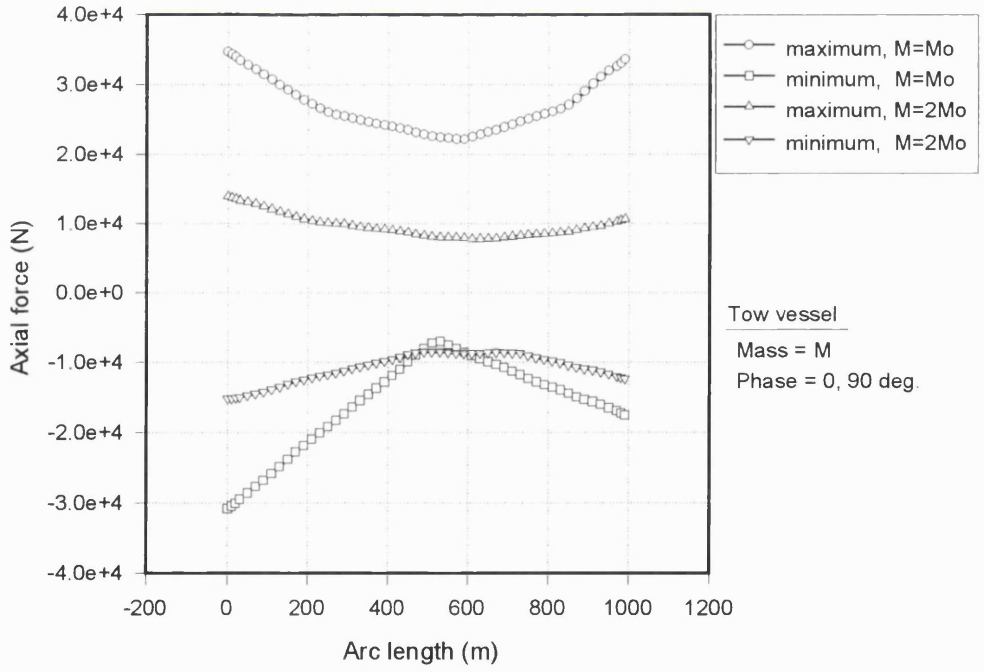

Figure 5.48 Comparison of axial forces from different vessel masses - surge forces with phase angles of 0 and 90 degrees for trailing and leading vessels respectively

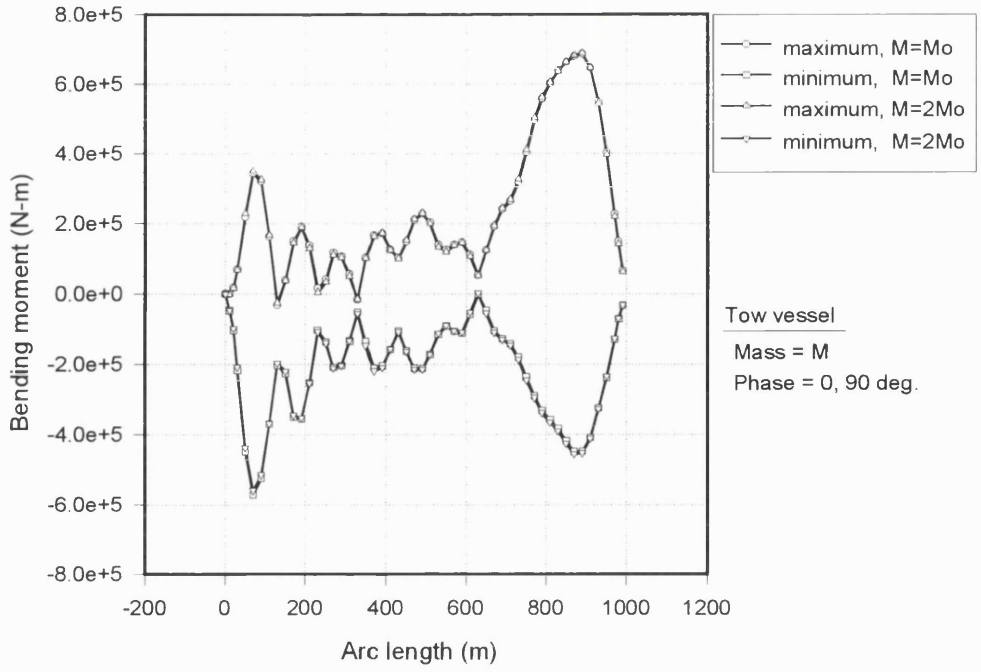

Figure 5.49 Comparison of bending moments from different vessel masses - surge forces with phase angles of 0 and 90 degrees for trailing and leading vessels respectively

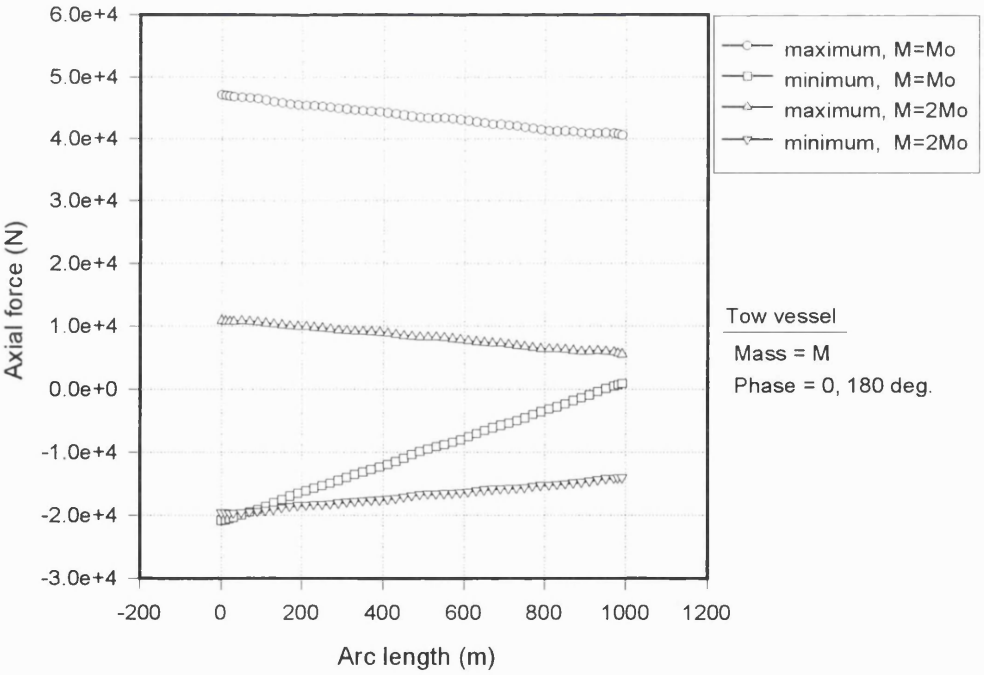

Figure 5.50 Comparison of axial forces from different vessel masses - out-of-phase surge forces

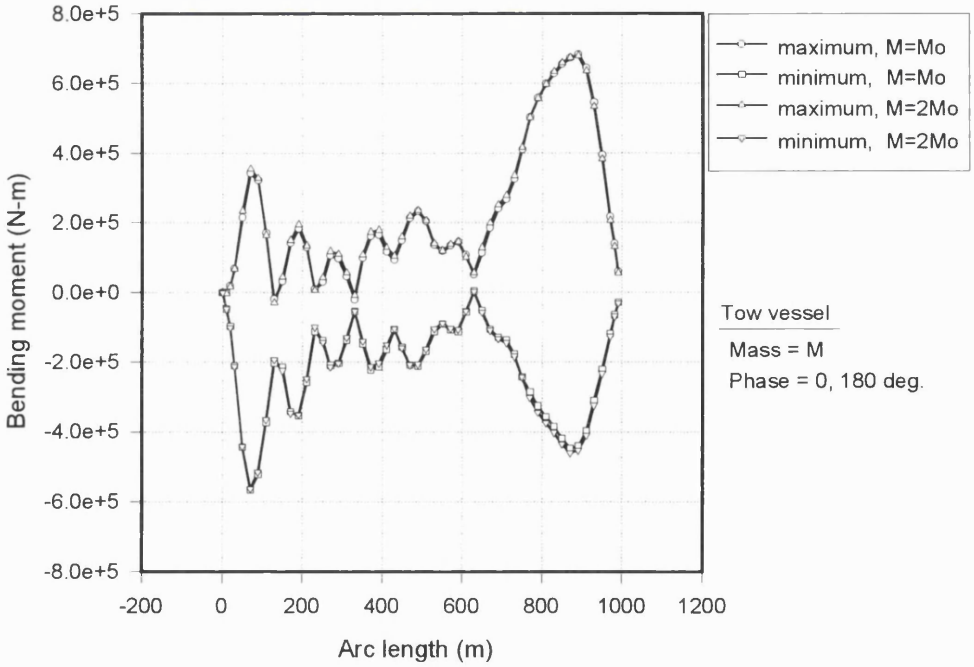

Figure 5.51 Comparison of bending moments from different vessel masses - out-of-phase surge forces

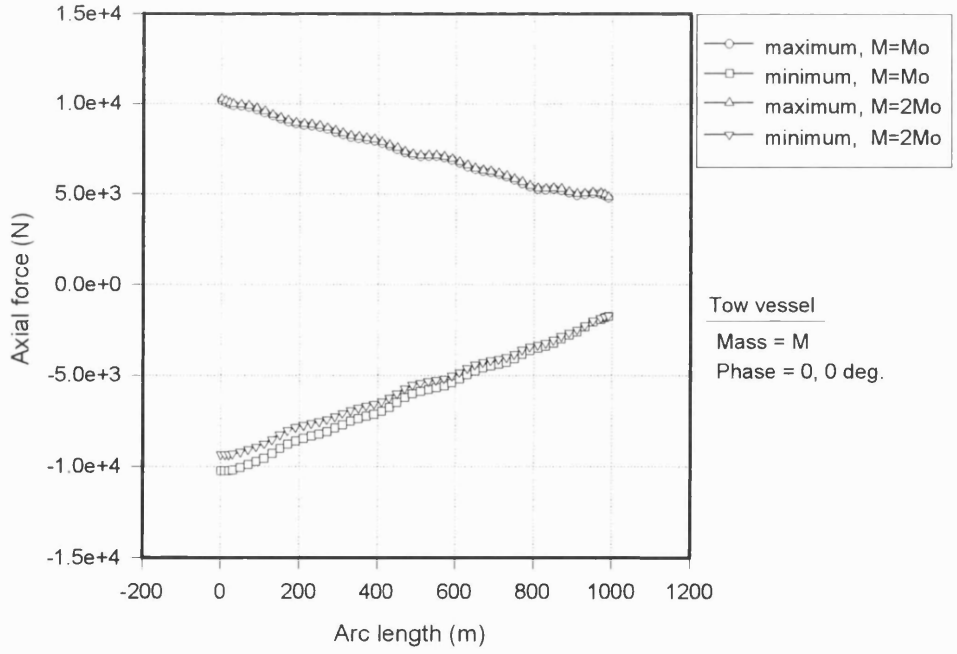

Figure 5.52 Comparison of axial forces from different vessel masses - in-phase heave forces

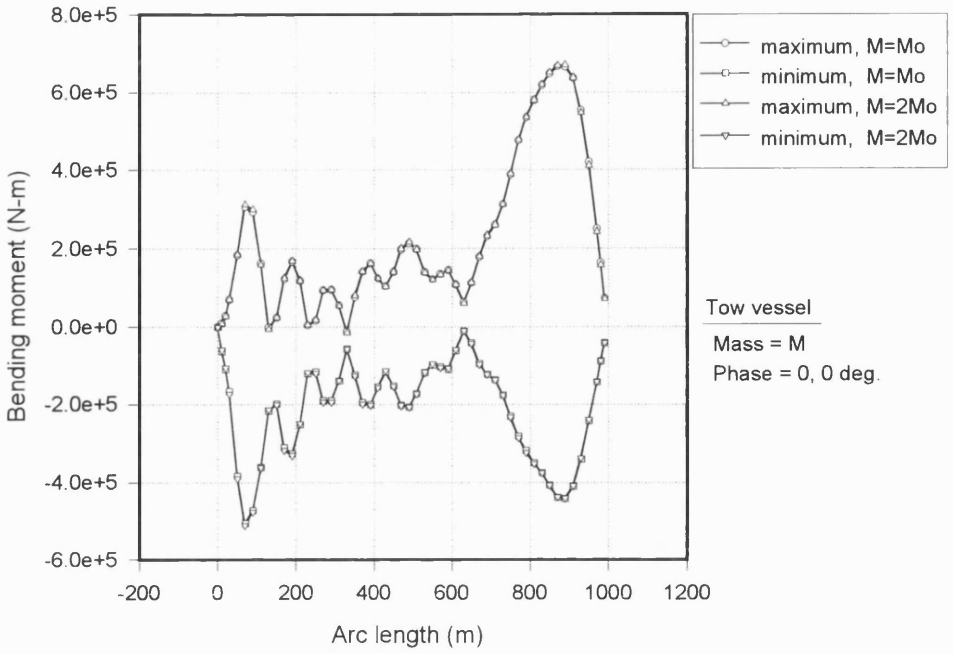

Figure 5.53 Comparison of bending moments from different vessel masses - in-phase heave forces

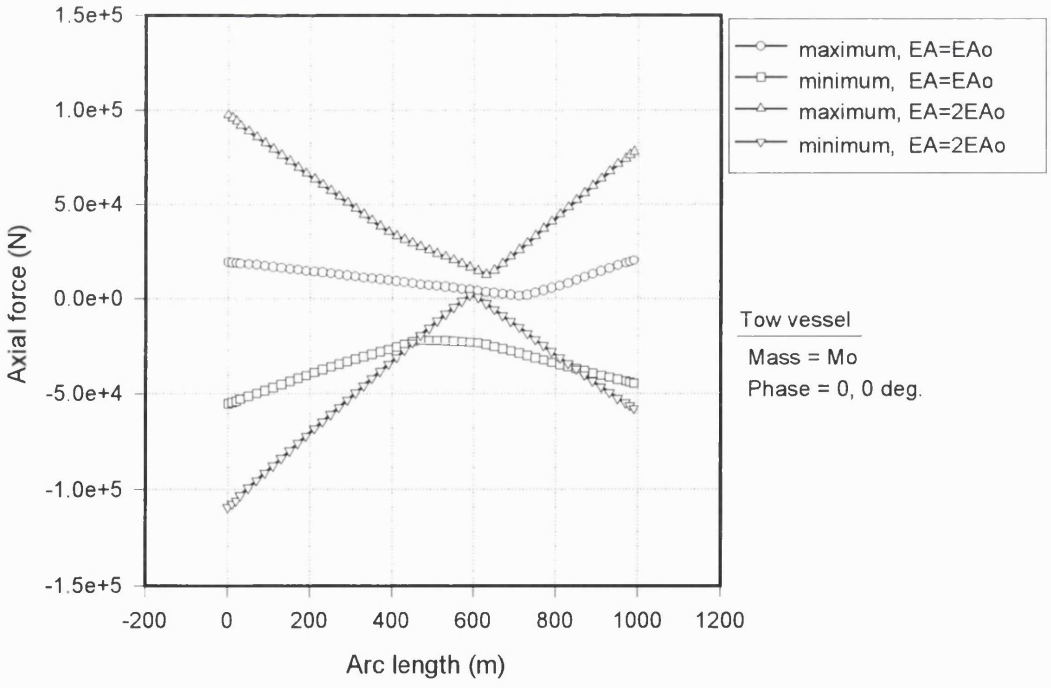

Figure 5.54 Comparison of axial forces from different axial rigidities of towlines - in-phase surge forces

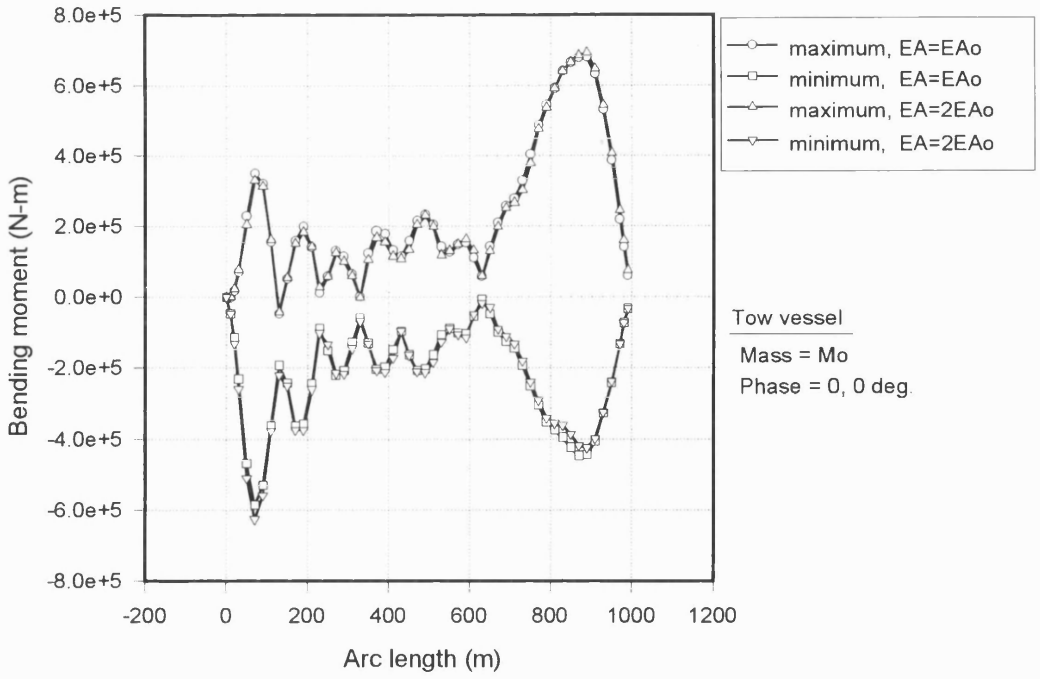

Figure 5.55 Comparison of bending moments from different axial rigidities of towlines - in-phase surge forces

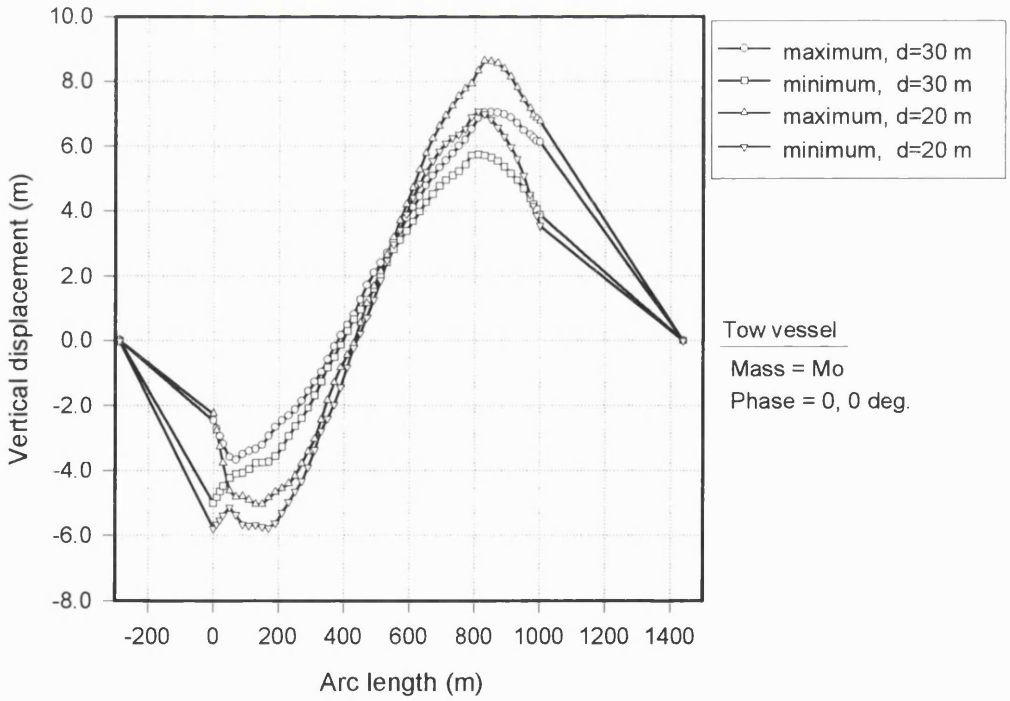

Figure 5.56 Comparison of vertical displacements from different towhead depths

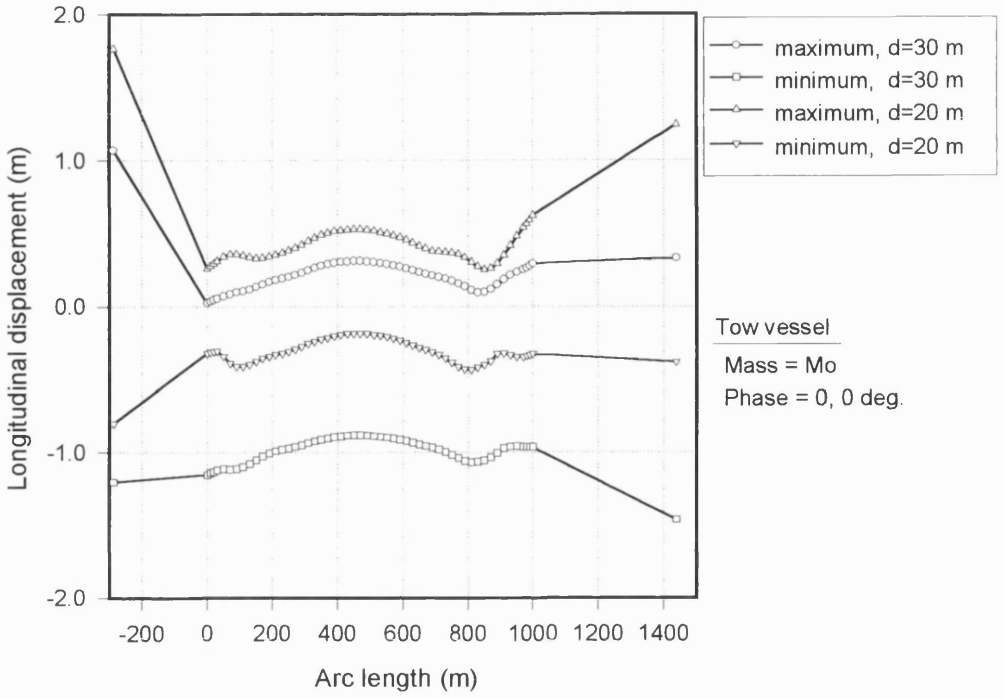

Figure 5.57 Comparison of longitudinal displacements from different towhead depths

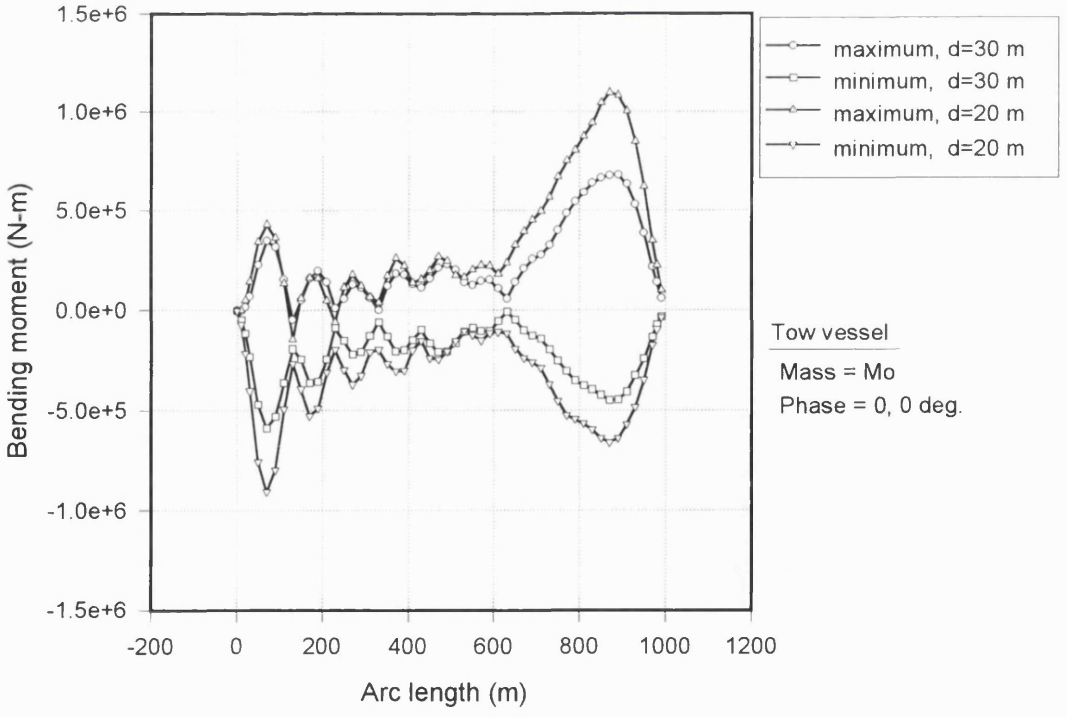

Figure 5.58 Comparison of bending moments from different towhead depths

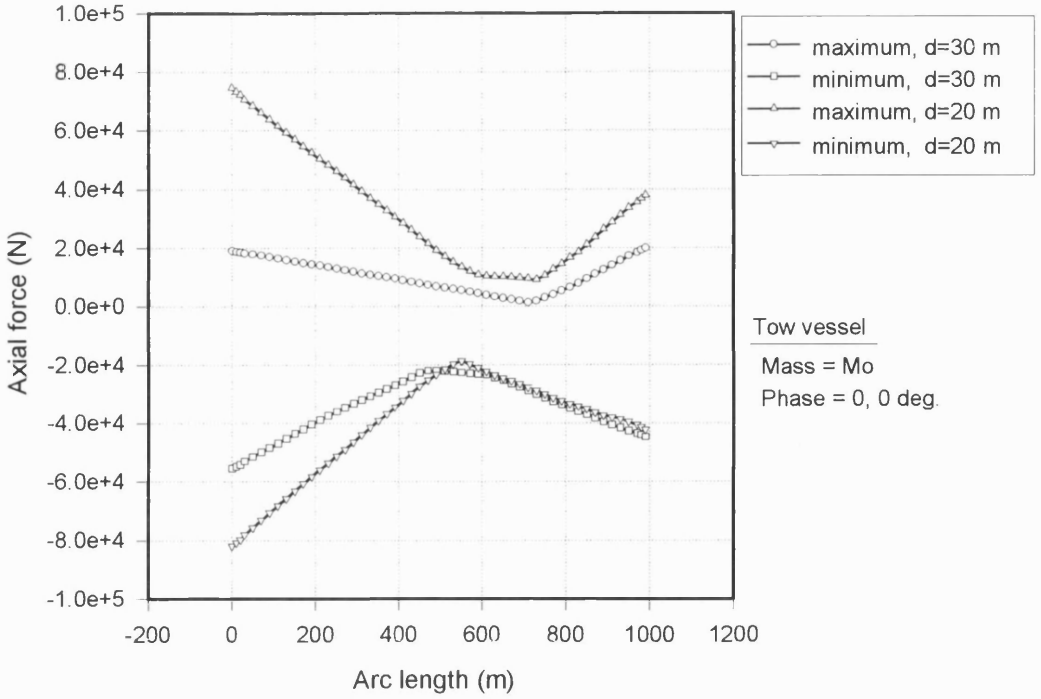

Figure 5.59 Comparison of axial forces from different towhead depths

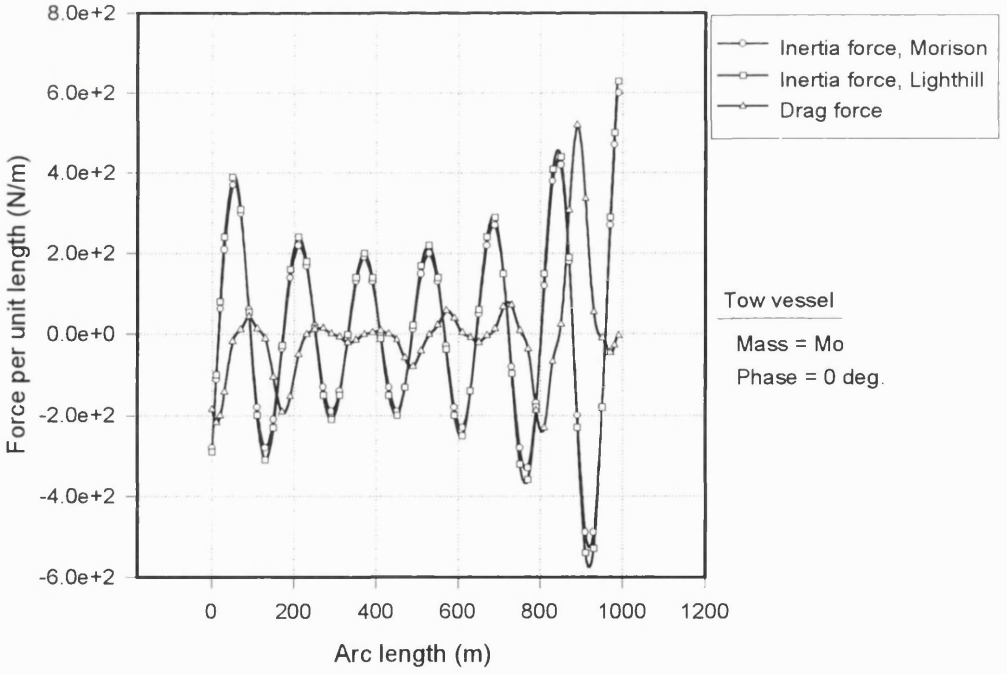

Figure 5.60 Distribution of hydrodynamic forces at 90 seconds

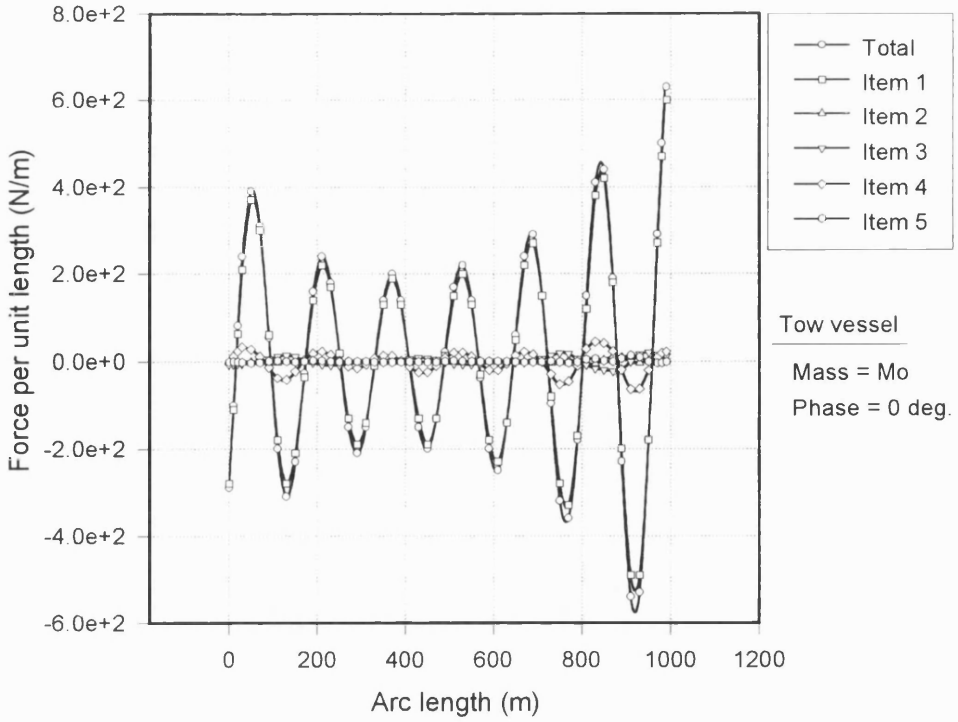

Figure 5.61 Distribution of inertia force components from the Lighthill's approach at 90 seconds

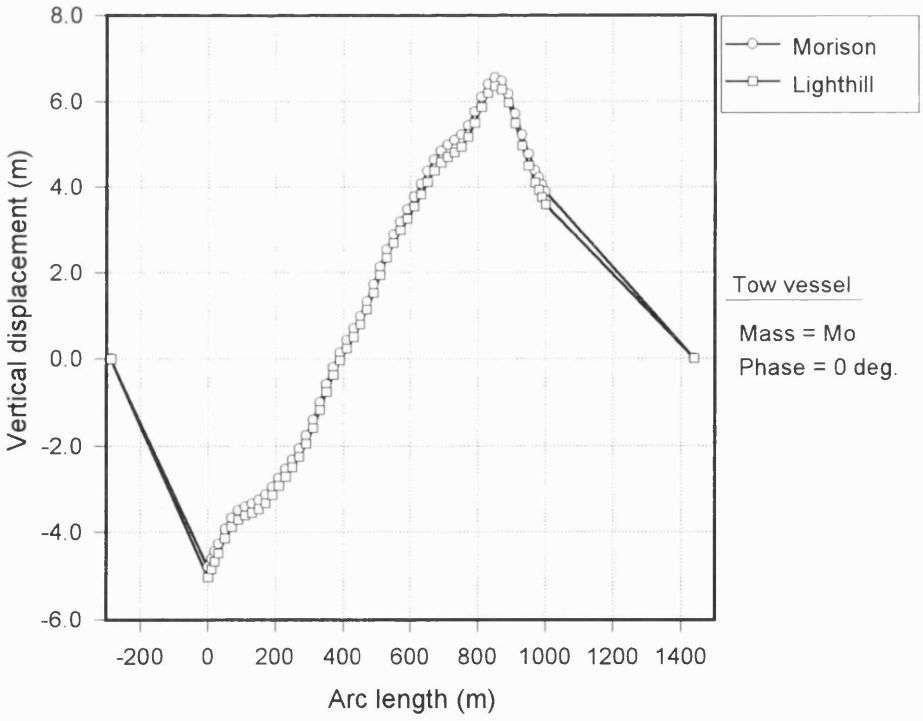

Figure 5.62 Comparison of dynamic vertical displacements from Morison's and Lighthill's approaches at 90 seconds

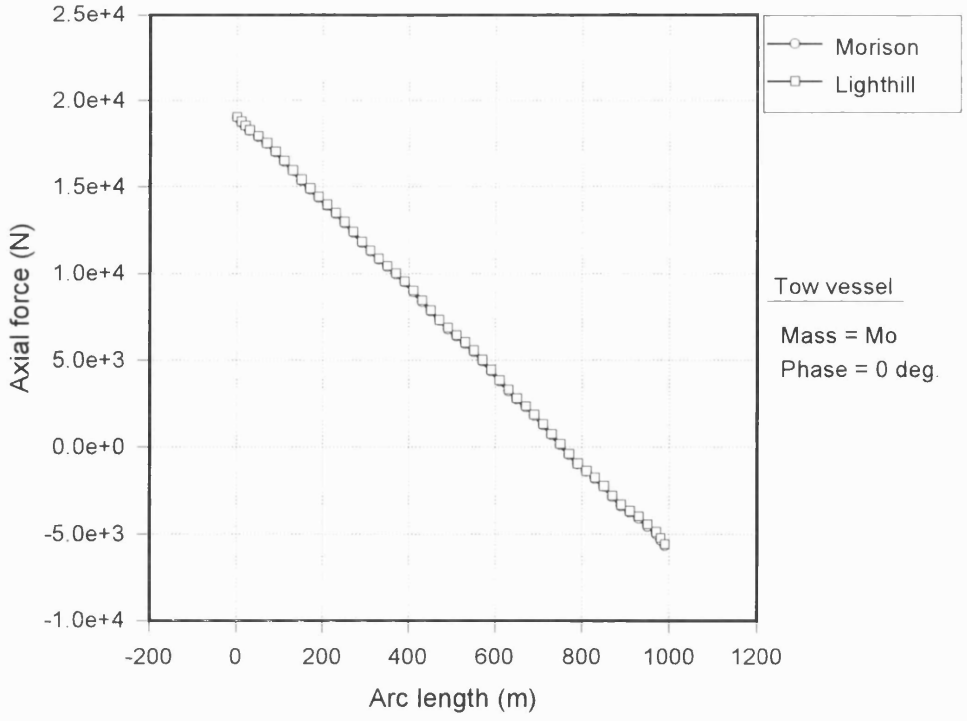

Figure 5.63 Comparison of dynamic axial forces from Morison's and Lighthill's approaches at 90 seconds

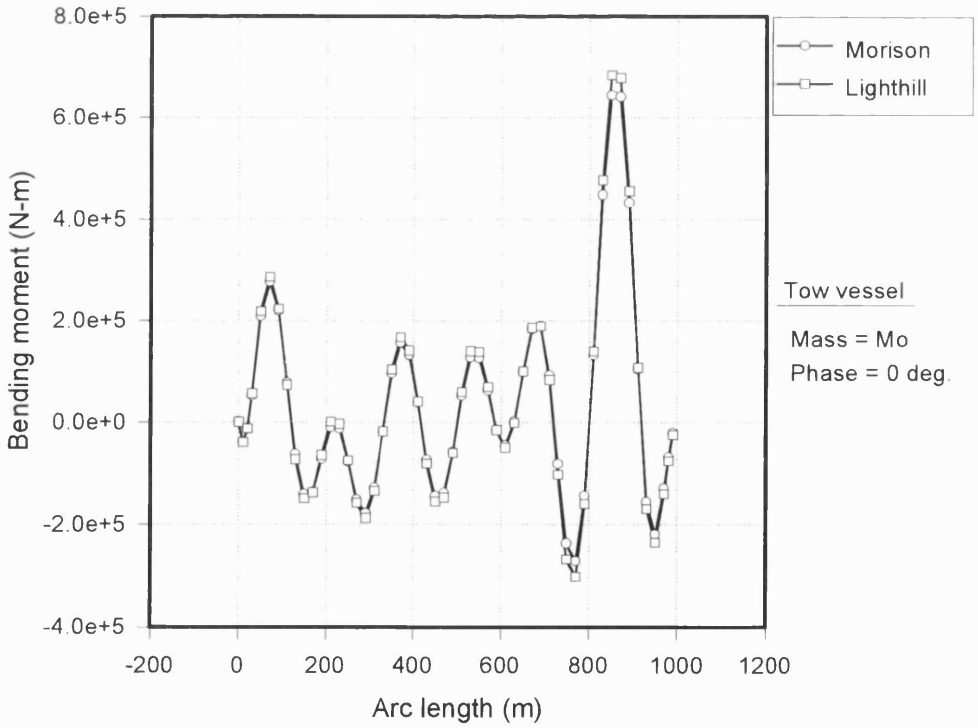

Figure 5.64 Comparison of dynamic bending moments from Morison's and Lighthill's approaches at 90 seconds

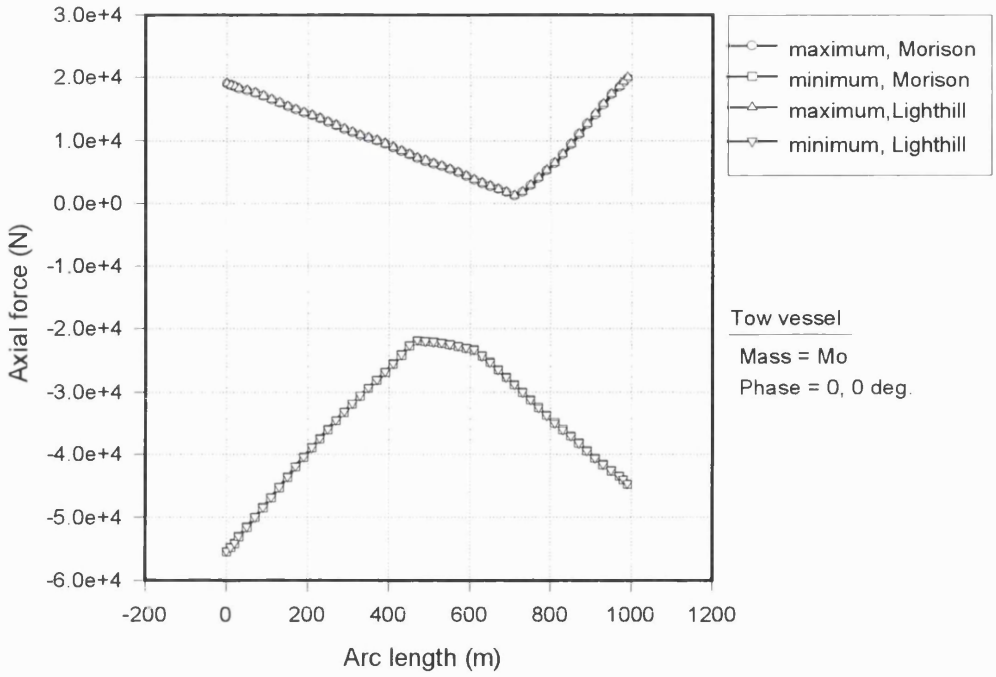

Figure 5.65 Comparison of dynamic axial force envelopes from Morison's and Lighthill's approaches

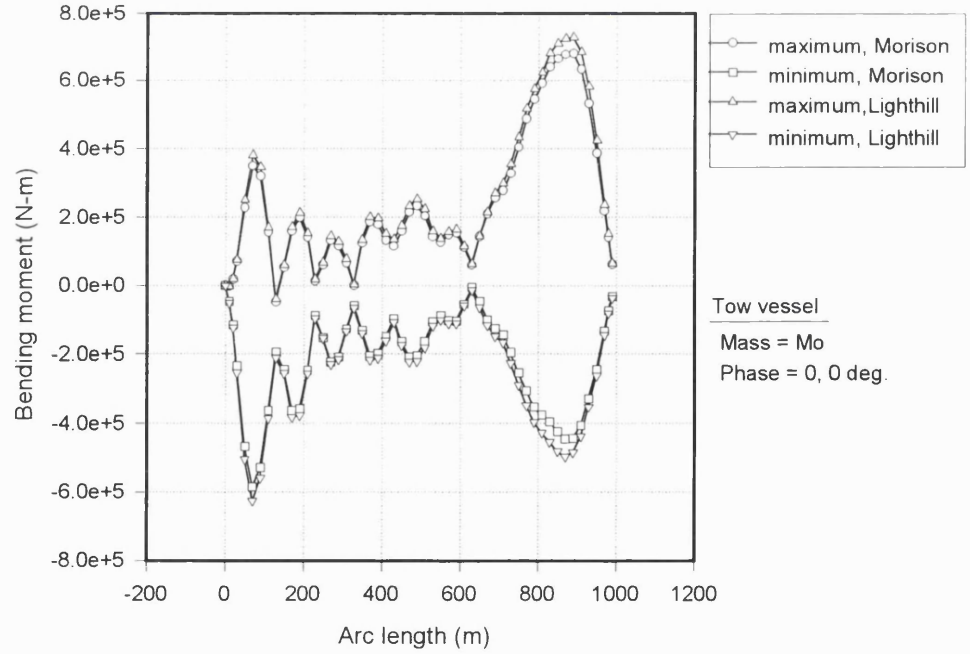

Figure 5.66 Comparison of dynamic bending moment envelopes from Morison's and Lighthill's approaches

6. DISCUSSION AND CONCLUSION

Research aims, response pattern and analysis methods for the tow system are summarised in this chapter based on the previous formulation and analysis results.

6.1 Research Aims

The present work is aimed at investigating the response of a towed pipeline and establishing an efficient and reliable analysis scheme using the FEM. The main research aims are as follows:

- To investigate the axial interaction between tow vessels and a pipeline.
- To apply Lighthill's formulation for inertia loading in near tangential flow and to check the accuracy of this against the Morison equation for typical towed pipeline.
- To investigate the influence of the "effective" tension term included by hydrostatic pressure forces on towed pipes.
- To improve convergence performance and ill-conditioning problems for the numerical analysis involved.
- To obtain a quantitative understanding of towed pipeline response to current and waves.

To achieve these aims, the following typical inherent properties or requirements of the tow system must be kept in mind throughout the formulation and numerical work.

- Geometric property : Towed pipelines are usually very long and their sag must be kept reasonably small enough to avoid contact with the seabed.
- Structural property : The ratio of bending rigidity to axial rigidity is inherently very small. Also the axial rigidity of towlines must be kept reasonably small to reduce the influence from vessels.
- Mass property : The mass of typical long towed pipelines is comparable with that of the tow vessel.

- Weight property : Submerged weight of the pipeline, along with chains, must be reasonably small to satisfy available tug capacity.
- Environmental condition : The influence of waves is equally important all along the length since towed pipelines are in a near-horizontal configuration and placed close to the free surface. Towed pipelines are also exposed to a relatively high near-tangential flow due to towing.

6.2 Physics and Response Pattern

A tow system consists of a pipeline, chains, tow vessels and towlines. Since an accurate understanding of the physics of the tow system is essential for a successful and economic tow operation, the mechanism of the tow system is summarised briefly.

- Towed pipelines are usually very long with small sag obtained from their small submerged weight. Therefore, the system may experience large deformation even with a slight external disturbance. To reduce this drawback, a reasonable amount of tension is supplied along the pipeline by tow vessels via towlines. This tension depends on submerged weight, offset and current forces on the pipeline and chains.
- In dynamic cases, the pipeline lateral motions are predominantly at high modes of vibration due to its long and near-horizontal configuration. The pipeline also interacts longitudinally with its tow vessels via towlines since the mass of typical long towed pipelines is comparable with that of the tow vessel.
- In both static and dynamic cases, the response of the pipeline is very sensitive to the longitudinal, or surge, component of excitation due to its geometric characteristics mentioned earlier - very long with small sag. In order to soften these phenomena, flexible towlines are used. These towlines play a very favourable role in the axial dynamics by absorbing a significant proportion of the dynamic force excitation from the tow vessels.

Most of these issues are accommodated in the FE analysis technique described in this thesis. This analysis is used to investigate the response of the pipeline due to currents and waves. The following points summarise key aspects of the results obtained:

- Towed pipelines are highly influenced by the hydrostatic pressure force and, as a result, experience curvature reversal in the absence of tow speed. Although this influence decreases with increase in tow speed, it is still important in normal tow conditions.
- Since the pipeline experiences rapid increase in normal drag force with increase in heading angle, the heading angle must be kept as small as possible. In the normal tow condition, the resultant tensile forces along the pipeline must be reasonably small to satisfy available vessel and towline capacity.
- High dynamic bending moments and lateral displacements are concentrated around the ends of the pipeline due to their proximity to the water surface and the soft constraints from towlines. The bending moment increases rapidly as the pipeline approaches the water surface.
- The distribution of dynamic bending moment along the length is almost the same regardless of change in vessel mass and phase angle of the vessel force whilst that of axial forces shows large difference. It means that the dynamic bending moment is mainly influenced by wave forces on the pipeline. The dynamic axial force from the axial interaction is not large enough to influence the lateral responses.
- In the case of longitudinal dynamic displacements, their variation along the pipeline is relatively uniform due to small tangential (longitudinal) hydrodynamic damping. Also the occurrence of peak axial forces at the ends of the pipeline suggests that the interaction decreases with distance from the ends. Although the dynamic axial force is negligibly small compared to the allowable axial force, it significantly influences the strength and fatigue life of the towline and, consequently, the selection of the towline.
- The axial interaction between tow vessels and a pipeline is highly influenced by the property of connecting towline members. As the towlines become stiffer, the

interaction becomes stronger. Therefore, towlines that are too stiff may induce larger dynamic axial force than axial force in the static case and induce transient compressive axial forces. Because the bundle is very vulnerable to buckling, towlines need to be designed to avoid this condition.

- This axial interaction is mainly influenced by surge forces from the tow vessel with other components of vessel excitation such as those in transverse (yaw) and vertical (heave) directions having little influence due to small inclination angles and flexibility of the towlines.
- Pipeline analysis can give large changes in the mean configuration of dynamic displacements from the starting geometry, that is the static equilibrium geometry. This is due to the inclusion of currents in dynamic analysis and, along with waves, generating non-zero mean drag forces.

6.3 Analysis Methods

The structural response of a tow system in currents and waves is very complex as described in the previous section. To tackle this complicated problem systematically, the FEM is used for both static and dynamic analysis with efficient treatment of ill-conditioning problems and an attempt to represent all of the physics of the tow operation. The following points summarise the methods and issues considered in this research:

- The enhanced catenary equation, which can consider the effect of a uniform normal component of current load, is proposed and used to provide the starting geometry for nonlinear FE analysis. From this geometry, the direct iteration method is applied to account for the nonlinear geometric stiffness. Although this scheme provides rapidly convergent results for very long pipeline with small sag, it provides slightly higher axial forces along the length and a small but finite difference in bending moments at the ends of the pipeline due to the small bending stiffness of the pipeline, which counteracts the catenary effect.

- Since a typical towed pipeline is designed to have very small submerged weight, other external forces and their distribution along the pipeline significantly influence its structural behaviour. In this case, it is essential to consider deformation-dependent loading. For this, an improved version of the direct iteration method is applied using a conventional inner iteration approach with constant external load and an outer iteration to ensure that the residual forces resulting from the deformation-dependent loading are equilibrated.
- Little attention has been paid by other researchers to the hydrostatic pressure forces on the pipeline with too much attention being paid to conventional loads such as lift and drag on the chains and normal and tangential drag forces on the pipeline. The work presented here shows that the hydrostatic pressure force controls pipe curvature in a way similar to tensile forces. The application of classical buoyancy with submerged volume leads to totally wrong results for this slightly negatively buoyant pipeline. Therefore, an accurate formulation and application of the hydrostatic pressure forces is essential in tow analysis.
- Since the tow system does not experience dramatic changes in global deformation due to dynamic loads, there is no significant change in the system matrices. Also considering that the Newton-Raphson method or its modified version is unstable for this very long and flexible system, the initial stiffness method remains an economic and feasible choice for dynamic analysis. The initial stiffness method uses constant system matrices throughout the time domain analysis with constant time interval. Since the same system matrices are employed at each step, the equations can be stored in their reduced form and a subsequent solution merely necessitates the reduction of the force terms, together with a backsubstitution. This method, however, requires many iterations or fails to provide results if the system experiences large responses.
- Axial forces in the towlines and along the pipeline provide important information for choosing proper towlines. Since the masses of the tow vessels are comparable to that of a long pipeline, consideration of the axial interaction of the pipeline, towlines and tow vessels is essential to obtain a reliable dynamic axial force. For

this, the analysis model must include tow vessels and towlines as well as the pipeline.

- The Lighthill formulation for inertia loads in near-tangential flow is applied to check the accuracy of the Morison formulation in calculating inertia forces. The Morison formulation provides slightly lower inertia forces and responses than Lighthill's approach. Considering this slight difference and the uncertainties in wave kinematics and drag forces, it can be concluded that the Morison formulation still provides reliable results for towed pipelines. Nevertheless, it should be recognised that the Lighthill formulation is physically "more" correct and it may be more properly applicable to cases with higher tow speed and less flexibility, for example towed arrays.

REFERENCES

"ABAQUS/Standard User's Manual", Hibbit, Karlsson & Sorensen, Inc., 1995.

Bathe, K.-J., "Finite Element Procedures in Engineering Analysis", Prentice-Hall, Inc., New Jersey, 1982.

Bedford, A. and Fowler, W., "Engineering Mechanics - Dynamics", Addison-Wesley Publishing Company, 1995.

Bergan, P. G. and Mollestad, E., "An Automatic Time-Stepping Algorithm for Dynamic Problems", Computer Methods in Applied Mechanics and Engineering, Vol. 49, pp. 299~318, Elsevier Science Publishers B.V., 1985.

Bernitsas, M. M. and Vlahopoulos, N., "Three-Dimensional Nonlinear Statics of Pipelaying Using Condensation in an Incremental Finite Element Algorithm", Computers and Structures, Vol. 35, No. 3, pp. 195~214, Pergamon Press plc, 1990.

Bourget, P.-L. and Marichal, D., "Remarks about Variations in the Drag Coefficient of Circular Cylinders Moving through Water", Ocean Engineering, Vol. 17, No. 6, pp. 569~585, Pergamon Press plc, 1990.

Burnett, D. S., "Finite Element Analysis, from Concepts to Applications", pp. 87~89, Addison-Wesley Publishing Company, 1987.

Chen, Y.-H. and Lin, F.-M., "General Drag-Force Linearization for Nonlinear Analysis of Marine Risers", Ocean Engineering, Vol. 16, No. 3, pp. 265~290, Pergamon Press plc, 1989.

Clough, R. W. and Penzien, J., "Dynamics of Structures", 2nd ed., McGraw-Hill, Inc., 1993.

Costello, G. J., Brink, F. I. A., and Henery, D., "Insulated Pipelines between the Underwater Manifold Centre and Cormorant A Platform in the Northern North Sea", Proceedings of Offshore Technology Conference, Vol. 3, pp. 265~274, 1983.

Dean, R. G. and Dalrymple, R. A., "Water Wave Mechanics for Engineers and Scientists", Prentice-Hall, Inc., New Jersey, 1984.

den Boer, A. S., Rooduyn, E. J., and Barber, W. A., "An Integrated Towed Flowline Bundle Production System for Subsea Development", Proceedings of Offshore Technology Conference, Vol. 4, pp. 85~94, 1990.

Ertos, A. and Kozik, T. J., "Numerical Solution Techniques for Dynamic Analysis of Marine Riser", Journal of Energy Resources Technology, Vol. 109, pp. 1~5, American Society of Mechanical Engineers, 1987.

Flory, J. F., Parsey, M. R., and McKenna, H. A., "The Choice between Nylon and Polyester for Large Marine Ropes", Proceedings of Offshore Mechanics and Arctic Engineering, Vol. 1, pp. 517~523, American Society of Mechanical Engineers, 1988.

Huang, T. and Chucheepsakul, S., "Large Displacement Analysis of a Marine Riser", Journal of Energy Resources Technology, Vol. 107, pp. 54~59, American Society of Mechanical Engineers, March 1985.

Inoue, Y., Nakamura, T., and Miyabe, H., "On the Dynamic Tension of Towline in Ocean Towing", Proceedings of Offshore Mechanics and Arctic Engineering, Vol. 1-B, pp. 547~553, American Society of Mechanical Engineers, 1991.

Irvine, M., "Cable Structures", Dover Publications, Inc., New York, 1992.

Ishikawa, K., Morikawa, M., Kodan, N., and Komiya, H., "Towing and Upending Procedure of Pre-Fabricated Tendon of TLP", Proceedings of International Offshore and Polar Engineering Conference, Vol. 1, pp. 213~217, International Society of Offshore and Polar Engineers, 1992.

Jacob, B. P. and Ebecken, N. F. F., "Computational Strategies for the Nonlinear Dynamic Analysis of Compliant Deepwater Structures", Proceedings of International Offshore and Polar Engineering Conference, Vol. 3, pp. 27~34, International Society of Offshore and Polar Engineers, 1992.

Jennings, A., "Cable Movements under Two-Dimensional Loads", Journal of Structural Division, pp. 307~311, American Society of Civil Engineers, Feb. 1965.

Kan, W. C. and Healey, A. J., "Finite Element Analysis with the State Transfer Matrix and Geometric Nonlinearity for Marine Pipelines in Subsurface Tow", Journal of Energy Resources Technology, Vol. 103, pp. 26~31, American Society of Mechanical Engineers, March 1981.

Krolikowski, L. P. and Gay, T. A., "An Improved Linearization Technique for Frequency Domain Riser Analysis", Proceedings of Offshore Technology Conference, Vol. 2, pp. 341~353, 1980.

Langley, R. S., "The Linearisation of Three Dimensional Drag Force in Random Seas with Current", Applied Ocean Research, Vol. 6, No. 3, pp. 126~131, CML Publications, 1984.

Langley, R. S., "Random Dynamic Analysis of Towed Pipelines", Ocean Engineering, Vol. 16, No. 1, pp. 85~98, Pergamon Press plc, 1989.

Leira, B. J. and Remseth, S. N., "A Comparison of Linear and Nonlinear Methods for Dynamic Analysis of Marine Risers", Behaviour of Offshore Structures, pp. 383~394, Elsevier Science Publisher B.V., 1985.

Lighthill, M. J., "Note on the Swimming of Slender Fish", Journal of Fluid Mechanics, Vol. 9, pp. 305~317, 1960.

Love, A. E. H., "A Treatise on the Mathematical Theory of Elasticity", pp. 628~632, Dover Publications, Inc., New York, 1944.

Martin, H. C. and Carey, G. F., "Introduction to Finite Element Analysis", McGraw-Hill, Inc., 1973.

McNamara, J. F. and Lane, M., "Computational Tools for the Time and Frequency Domain Analysis of TLP Tethers and Risers", Proceedings of Offshore Mechanics and Arctic Engineering, Vol. 1-B, pp. 519~526, American Society of Mechanical Engineers, 1991.

Milgram, J. H., Triantafyllou, M. S., Frimm, F. C., and Anagnostou, G., "Seakeeping and Extreme Tensions in Offshore Towing", SNAME Transactions, Vol. 96, pp. 35~70, 1988.

Moe, G., Gryta, O., and Wu, Z. J., "Wave Forces on a Marine Pipeline under Tow", Proceedings of the First European Offshore Mechanics Symposium, pp. 414~423, Trondheim, Norway, 1990.

Morison, J. R., O'Brien, M. P., Johnson, J. W., and Schaaf, S. A., "The Force Exerted by Surface Waves on Piles", Petroleum Transactions, Vol. 189, pp. 149~154, American Institute of Mining, Metallurgical and Petroleum Engineers, 1950.

Morton, A. W., "New Concepts Used in the Murchison Field Submerged Production System", Proceedings of Offshore Technology Conference, Vol. 2, pp. 309~318, 1981.

Nedergaard, H., Jensen, G., Ahlen, C. H., and Hansen, N. -E. O., "Controlled Tow-Out and Laying of Very Long Pipeline Sections", Proceedings of Offshore Mechanics and Arctic Engineering, Vol. 5, pp. 23~31, American Society of Mechanical Engineers, 1989a.

Nedergaard, H. and Hansen, N. -E. O., "Dynamic Response and Positioning of Long Pipeline Sections in the Tow-Out Phase", Proceedings of the Fourth International Symposium on Practical Design of Ships and Mobile Units, pp. 106.1~106.7, 1989b.

Nihous, G. C., "A Prediction of Dynamic Stresses for Long, Large-Diameter Horizontal Pipes at or Near the Ocean Free Surface", Journal of Offshore Mechanics and Arctic Engineering, Vol. 117, pp. 239~244, American Society of Mechanical Engineers, Nov. 1995.

O'Brien, W. T. and Francis, A. J., "Cable Movements under Two-Dimensional Loads", Journal of Structural Division, pp. 89~123, American Society of Civil Engineers, June 1964.

Owen, D. R. J. and Hinton, E., "Finite Elements in Plasticity : Theory and Practice", Pineridge Press Limited, Swansea, 1980.

Patel, M. H., "On the Hydrodynamics of Tandem-Hull Marine Vehicles", Journal of Ship Research, Vol. 30, No. 4, pp. 275~286, 1986.

Patel, M. H., "Dynamics of Offshore Structures", Butterworths, 1989.

Pelleau, R., Rouillon, J., and Fausa, T., "Design, Installation, and Connection of Subsea Lines on East Frigg Field", Proceedings of Offshore Technology Conference, Vol. 3, pp. 219~227, 1988.

Peyrot, A. H. and Goulois, A. M., "Analysis of Cable Structures", Computers and Structures, Vol. 10, pp. 805~813, Pergamon Press Ltd., 1979.

Price, W. G. and Bishop, R. E., "Probabilistic Theory of Ship Dynamics", pp. 222~224, Chapman and Hall Ltd., 1974.

Quiggin, P. P. and Carson, R. M., "Hydrodynamics of Flexibles : Replacing the Morison Inertia Term", Underwater Technology, Vol. 20, No. 4, pp. 22~28, the Society for Underwater Technology, Winter 1994.

Rainey, R. C. T., "Aspects of the Hydrodynamic Loading on Towed Arrays and Flexible Risers", Engineering Structures, Vol. 11, pp. 248~253, Butterworth & Co. Ltd., 1989.

Sarpkaya, T., "In-Line and Transverse Forces on Cylinders in Oscillatory Flow at High Reynolds Numbers", Journal of Ship Research, Vol. 21, pp. 200~216, Dec. 1977.

Seyed, F. B., "On the Dynamics of Flexible Riser and Suspended Pipe Spans", Ph.D. Thesis, University of London, Sept. 1989.

Sparks, C. P., "Mechanical Behavior of Marine Risers Mode of Influence of Principal Parameters", Proceedings of the Winter Annual Meeting of American Society of Mechanical Engineers, OED Vol. 7, pp. 59~81, 1979.

Sparks, C. P., "The Influence of Tension, Pressure and Weight on Pipe and Riser Deformations and Stresses", Journal of Energy Resources Technology, Vol. 106, pp. 46~54, American Society of Mechanical Engineers, March 1984.

Tatsuta, M. and Kimura, H., "Offshore Pipeline Construction by a Near-Surface Tow", Proceedings of Offshore Technology Conference, Vol. 4, pp. 425~432, 1986.

Teng, C-C and Nath, J.H., "Forces on Horizontal Cylinder Towed in Waves", Journal of Waterway, Port, Coastal and Ocean Engineering, Vol. 111, No. 6, pp. 1022~1040, American Society of Civil Engineers, 1985.

Verner, E. A., Cheatham, C. A., Garrett, D. L., and Langner, C. G., "Predicting Motions of Long Towed Pipe Strings", Proceedings of Offshore Technology Conference, Vol. 1, pp. 159~169, 1984.

Vlahopoulos, N. and Bernitsas, M. M., "Three-Dimensional Nonlinear Dynamics of Pipelaying", Applied Ocean Research, Vol. 12, No. 3, pp. 112~125, Computational Mechanics Publications, 1990.

Wilson, B. W., "Characteristics of Anchor Cables in Uniform Ocean Currents", A & M College of Texas, Department of Oceanography and Meteorology, Technical Report No. 204-1, April, 1960.

Wilson, E. L., Farhoomand, I., and Bathe, K. J., "Nonlinear Dynamic Analysis of Complex Structures", Earthquake Engineering and Structural Dynamics, Vol. 1, pp. 241~252, John Wiley & Sons, Ltd., 1973.